# Production and detection of polyhydroxybutyrate (PHB) in the alphaproteobacterial methanotroph *Methylocystis* sp. Rockwell

by

Marina Lazic

A thesis submitted in partial fulfillment of the requirements for the degree of

Doctor of Philosophy

in

Microbiology and Biotechnology

Department of Biological Sciences

University of Alberta

**Abstract**

Anthropogenic agricultural and industrial activities have intensified in the past few decades to satisfy the food and energy demands of a rapidly growing human population. The increase in these activities is causing extremely high emission of greenhouse gases which results in global warming and inevitable climate change. One of the most potent greenhouse gases is methane. From a biological perspective, methane represents a sole carbon source for microorganisms known as methanotrophs. These microbes, which are the only known biotic methane sink, can act as natural barrier to methane emissions. From an industrial perspective, these organisms can be used as microbial factories to produce value-added compounds from methane. Another important feature of methanotrophs is their ability to consume methanol as well as methane, which is immediately available without the need to control gas to liquid mass transfer.

The focus of this thesis is the alphaproteobacterial methanotroph *Methylocystis* sp. Rockwell. Alphaproteobacterial methanotrophs encode the enzymatic machinery for the production of bioplastics while growing on methane and/or methanol. The most important bioplastic produced by alphaproteobacterial methanotrophs is polyhydroxybutyrate (PHB). The overall goal of this study was to optimize production and detection of PHB in *Methylocystis* sp. Rockwell.

To optimize production of PHB, bacterial cultures were grown under different combinations of methane and/or methanol with ammonium or nitrate mineral salts as the source of nitrogen. Growth was monitored along with oxygen and methane consumption, while biomass and PHB were analyzed at the end of growth. Results of this study revealed the importance of methane/methanol combination for PHB production, regardless of nitrogen source, and led to the question of the mechanism of beneficial influence of methanol on PHB synthesis.

In addition, this study established novel, environmentally friendly, cheaper, and faster approach for direct PHB detection in methanotroph cells and confirmed its accuracy with the standard detection approach. In another approach, a molecular tool for detection of novel PHB-producing organisms in the environment was created, and the proof-of-concept principle has been confirmed.

Overall, results of this study offer new perspectives in both, optimization and detection/quantification and serve as the basis for further improvements in designing methanotrophic PHB biofactories.

## Preface

Two chapters of this thesis have been previously published as peer-reviewed scientificarticles, and two chapters will be submitted for publication in next two years.

Chapter 3 was published as Lazic, M., Sugden, S., Sauvageau, D., and Stein, L. (2020) "Metabolome profiles of the alphaproteobacterial methanotroph *Methylocystis* sp. Rockwell in response to carbon and nitrogen source" in FEMS Microbiology Letters, 368. doi: 10.1093/femsle/fnaa219. As the primary author, I was responsible for analyzing metabolomic results, performing PHB analysis and additional biomass and growth analysis, as well as for writing the manuscript. Scott Sugden was an MSc student at University of Alberta, and he was responsible for statistical analysis as well as for editing and conceptual advice. The biomass collection for metabolomic analysis was performed by Melissa Harrison, laboratory technician at the University of Alberta. Dr. Dominic Sauvageau and Dr. Lisa Stein were supervisory authors who contributed to all stages of preparation, conceptualization, data interpretation, advice, and manuscript composition.

Chapter 5 was published as Lazic, M., Gudneppanavar, R., Whiddon, K., Sauvageau, D., Stein, L. and Konopka, M. (2021) "*In vivo* quantification of polyhydroxybutyrate (PHB) in the alphaproteobacterial methanotroph, *Methylocystis* sp. Rockwell" in Applied Microbiology and Biotechnology. https://doi.org/10.1007/s00253-021-11732-x. As co-primary authors, Ravindra Gudneppanavar and I were responsible for experimental design, data collection, analysis, conceptualization, and manuscript writing. Kyle Whiddon was working on the project prior to Ravindra Gudneppanavar; he collected some of the data. Dr. Michael Konopka, Dr. Dominic Sauvageau and Dr. Lisa Stein were supervisors that helped with data analysis, conceptualization, and editing the manuscript.

Chapter 4 will be submitted for publication as Lazic, M., Sugden, S., Sharma, H.K., Sauvageau, D., and Stein, L. "The combined effect of methane and methanol on growth and

PHB production in the alphaproteobacterial methanotroph *Methylocystis* sp. Rockwell". As primary author, I was responsible for experimental design, data collection and analysis, as well as manuscript writing. Hem Kanta Sharma, a PhD candidate at the University of Alberta, helped with data collection and analysis, and his previous findings served as a basis for hypothesis design. Scott Sugden helped with writing and statistical analysis. Dr. Dominic Sauvageau and Dr. Lisa Stein helped with conceptualization and manuscript editing.

Chapter 6 will be submitted for publication as Lazic, M., Stein, L., and Sauvageau, D. "*In vitro* detection of PHB using a recombinant fluorescent protein". As primary author, I was responsible for experimental design, data collection and analysis, as well as manuscript writing. Dr. Dominic Sauvageau and Dr. Lisa Stein helped with experimental analysis, conceptualization, and manuscript editing.

Appendix 1 is given as an excel sheet with supplemental data for Chapter 2.

Appendix 2 is published as Sugden, S., Lazic, M, Sauvageau, D., and Stein, L. (2021) "Transcriptomic and Metabolomic Responses to Carbon and Nitrogen Sources in *Methylomicrobium album* BG8" in Applied and Environmental Microbiology 87: e00385-21. https://doi.org/10 .1128/AEM.00385-21. Scott Sugden wrote the manuscript and analyzed transcriptomic data, and I analyzed metabolomic data and contributed to the writing of the manuscript. Phillip Sun and Melissa Harrison collected biomass, performed sample collection for transcriptomic and metabolomic analysis. Dr. Lisa Stein and Dr Dominic Sauvageau helped with conceptualization, data analysis and manuscript writing.

Appendix 3 is a table with the list of primers used in gene designs for Chapter 6.

*This thesis is dedicated to my closest family, my son Luka Dragan Lazic, my beloved husband Nikola Lazic, and my kitties Koza and Saki.*

*Thank you for being part of my life….*

**Acknowledgements**

At the beginning of this thesis section, I would like to express my enormous gratitude to two people who are “responsible” for bringing this to the completion - Dr. Lisa Stein and Dr. Dominic Sauvageau. I came to this research group after 18 months of waiting and fighting against the system and for the justice. Dr. Stein gave me a hand, and she was among rare people who believed in me, many others who knew me better did not. Lisa, honest, supportive, and encouraging, advised me to fight for the truth and to believe in myself and in the justice, and thanks to her advice I moved forward, won, and come here. There was a feeling in me, something that motivated me move on, since I knew that this research ill be a crown of my success. Coming here was not easy, and first few months were even harder, but having both helped me to stay strong and to become better scientist, and better person. There were moments when I felt alone here, and somehow, person who can always bring hope back is Dr. Dominic Sauvageau. Thank you, Lisa, and Dominic, for being the best supervisors in this world! It is my honor to be part of your research group. Next, I would like to mention two special people who made my scientific life possible, Scott Sugden and Hem Kanta Sharma. Scott was a big support during writing, and I learned most of writing and some thinking strategies from him. Hem was (and still is) my closest friend in the laboratory, and he and I established many experiments together, went through failed and celebrated successful experiments. I am grateful to all members of Stein and Sauvageau research group, especially to Sujani Gomes, Brittany Sauter and Mariah Hermary who supported me mostly during my pregnancy.

In terms of my family and friends, I really had hard time deciding who thank first, and to whom to express my greatest gratitude. My first BSc thesis as dedicated fully to my mother Ljiljana Serafimovic. Her support was there at the time and is there now, and she will always be my best person. My two-master thesis in Serbia I dedicated to my husband, Nikola

Lazic, and I will forever be grateful to him for being with me in good and bad, in sickness in heath, being rich and being poor. He is love of my life, and I love him tremendously. Our baby buy, Luka Dragan Lazic has been born during the work on this thesis and he is the light of my life, and my reason to get up every morning. My third master thesis was dedicated to Father Dragan Vojinovic, I want to believe that he watches me from heaven, and he believes in me. My mother-in-law, Vesna Lazic – without her chapters 4 and 6 would not be completed, she stayed here with us and helped me raising Luka and taking care of me, she is a second mother for me, and I will always be grateful. My sister-in-la Mirjana Lazic and my auntie Marina Aleksic, two strong women who make me feel good each time when I hear them. Many people helped and many people deserve to be in my acknowledgement. My best friends Richik Nilay Mukherjee, Tatijana Jovanov Kseniya Polyakova, Family Jevtic (Ana, Predrag, Emilija, and Luka), my old friends Vera Troselj and Adam Suluburic and my new friend Maida Djapo, they all motivated me at some point to move on and to reach this point. However, I feel like I never gave enough acknowledgement to the person who succeed to bring this to the end and never gave up – myself. At the end, I would like to say that I am very proud of myself and for the first time in 36 years of my life I feel like I may say this. I was working hard, I was fighting and grew strong, stronger every day. I believe in science, I believe in justice, I believe that the world needs more scientists, more people persistent like me, more people who will not give up and ho always walk toward the goal with head up, straight forward knowing why something is done. Only like that, we can hope that we are leaving healthy planet to the future generations. As already mentioned later, we don't have planet B!

**Table of contents**

## List of Tables

## List of Figures

## List of abbreviations

2-PG: 2 phospho glycerate

2.3-BDO: 2.3 butanediol

3-PG: 3 phospho glycerate

6PGDH: 6 phospho gluconolactone dehydrogenase

Ab': primary antibody

Ab'': secondary antibody

AMO: ammonia monooxygenase

Amp: ampicillin

AMS: ammonium mineral salts

ANAMMOX: anaerobic ammonia-oxidizing

ANME: anaerobic methane oxidation

ANOVA: analysis of variance

AOB: ammonia oxidizing bacteria

AR: area ratio

Asp: aspartate

ATP: adenosine triphosphate

BCAA: branch chain amino acids

BS: Bifidobacterium shunt

CAT: catalytical domain

CBB: Calvin-Benson-Basham pathway

DHAP: dihydroxy acetone phosphate

DL-FalDH: dye linked formaldehyde dehydrogenase

DNA: deoxy ribonucleic acid

DW: dry weight

EB: elution buffer

EDD: Entner-Doudoroff pathway

EMP: Embden-Meyerhof-Parnas pathway

EPS: exopolysaccharide

ESI: ion mode electrospray ionization

ETC: electron transport chain

FA: fatty acids

FAD+: flavine adenine dinucleotide (oxidized)

FADH2: flavine adenine dinucleotide (reduced)

Fae: formaldehyde activating enzyme

FalDH: formaldehyde dehydrogenase

FBPA: Fructose Bis Phosphate Aldolase

Fdh: formate dehydrogenase

FDP: fructose 1,6-bisphosphate

FM: fluorescent microscopy

FMP: Fructose-Monophosphate

GAP: glyceraldehyde 3-phosphate

GC-FID: gas chromatography with flame ionizing detector

GC-TCD: gas chromatography with thermal conductivity detector

GC: gas chromatography

GEM: genome scale metabolic model

GHG: greenhouse gas

Glu: glutamate

GMP: glucose 6-phosphate

GPI: glucose 6 phosphate isomerase

MMO: methane monooxygenase

MOB: methane oxidizing bacteria

MOB: methane oxidizing bacteria

MtdB: methylene-H4MPT dehydrogenase

MTK: malate thiokinase

NAD+: nicotinamide dinucleotide (oxidized)

NADH: nicotinamide dinucleotide (reduced)

NADP+: nicotinamide dinucleotide phosphate (oxidized)

NADPH: nicotinamide dinucleotide phosphate (reduced)

NBA: Nile Blue A

NMR: nuclear magnetic resonance

NMS: nitrate mineral salts

NoN: no nitrogen

NR: Nile red

OAA: oxaloacetate

OD540 : optical density at 540 nm wave length

ORF: open reading frame

PCA: principal component analysis

PCR: polymerase chain reaction

PEP: phosphoenol pyruvate

PHA: polyhydroxyalkanoates

PHB: polyhydroxybutyrate

PHBV: polyhydroxybutyrate-co-valerate

PLA: polylactic acid

pMMO: particulate methane monooxygenase

PP: pentose phosphate

PQQ: pyrroloquinoline quinone

RiMP: ribose-5-phosphate

ROIArea: region of interest

ROS: reactive oxygen species

RP/UPLC-MS/MS: reverse-phase ultrahigh-performance liquid chromatography-tandem mass spectroscopy

RuMP: ribulose-monophosphate

SBD: substrate binding domain

SCP: single cell protein

SDS-PAGE: sodium dodecyl sulfate–polyacrylamide gel electrophoresis

SFG: S-formylglutathione

sfGFP: super folded green fluorescent protein

SGAT: serine-glyoxylate aminotransferase

SHMT: serine hydroxymethyltransferase

sMMO: soluble methane monooxygenase

SMP: septulose-7-phosphate

sPLS-DA: sparse partial least squares discriminant analysis

SRB: sulphate reducing bacteria

TCA: tricarboxylic acid cycle

TEA: terminal electron acceptor

TEM: transmission electronic microscopy

THF: tetrahydrofolate

WB: western blot

XuMP: xylulose-5-phosphate

# Chapter 1

## Introduction: Rationale and Context

### 1.1 PHB production by the alphaproteobacterial methanotroph *Methylocystis* sp. Rockwell

A doubling in atmospheric methane concentrations occurred from the glacial to interglacial periods, ranging from 360 -700 ppb. About 5,000 years ago, the increase in atmospheric methane was linked to emission from the southern tropics (Lan et al., 2021). However, the highest observed peak in atmospheric methane was detected more recently, starting from the industrial revolution in the 18$^{th}$ century when atmospheric methane levels increased by approximately 150%. The most significant peak was observed after 2006 at ~1879 ±0.6 ppb. About 50% of recent global methane emissions are caused by human activities, mainly due to a growing population and industrial development in Europe, North America, and China (Kirschke et al., 2013). Regardless of the reasons behind these increasing methane emissions, all records are showing that methane has a significant impact on climate change (Lan et al., 2021)

Atmospheric methane absorbs infrared radiation at a wavelength of 7.6 μm. This event affects the radiation balance in the atmosphere and increases global temperature, and leads to the climate changes that we have been witnessing over the past few decades. Most methane in the atmosphere and soils is removed via abiotic oxidation driven by hydroxyl radicals (OH•) (Nazaries et al., 2013). Additional abiotic sinks include reactions with chlorine and atomic oxygen radicals in the stratosphere and the marine boundary layer (Nazaries et al., 2013). In addition to the highly important abiotic sinks, it is impossible to omit the only biotic methane sink: methane oxidizing microbes. Even though some data report microbial contributions to atmospheric methane mitigation as “negligible” (Colin Murrell & Jetten, 2009; Nazaries et al., 2013) – accounting for around 5 -7% of the total methane sink –, over

90% of the methane produced by soil archaea is oxidized by methanotrophic microbes before it reaches the atmosphere (Colin Murrell & Jetten, 2009). Although understanding methane sources and sinks is complex, it is crucial for the development of efficient strategies to attenuate harmful methane emissions that damage the environment and human health (Colin Murrell & Jetten, 2009).

Another recent environmental problem caused by human activities is the increased level of plastic pollution. This pressing issue encourages the development of environmentally friendly biodegradable alternatives with reduced use of toxic chemicals. One such alternative is the group of biopolymers known as polyhydroxyalkanoates (PHAs), among which polyhydroxybutyrate (PHB) is the most widely studied (Zaldívar Carrillo et al., 2018). Thanks to its beneficial properties – such as biodegradability, biocompatibility, and thermoplasticity, PHB represents a promising alternative to produce environmentally friendly biodegradable plastic. Biodegradability of the material refers to "the ability of material to be decomposed by the action of biological agents (bacteria or fungi), with or without oxygen while getting assimilated into the natural environment". Biodegradable material does not cause ecological harm during decomposing process (https://youmatter.world/en/definition/biodegradable-plastic/). Biocompatible materials refer to those that are compatible with living tissue and does not produce any toxic or immunological response after body fluids exposure (https://www.spine-health.com/glossary/biocompatibility). Thermoplasticity of material refers to the temperature stability, and is defined as "the ability of softening or fusing when heated and of hardening again when cooled" (https://www.merriam-webster.com/dictionary/thermoplastic).

Current industrial production of PHB mainly involves sugars as a feedstock, which is not only expensive, but is also mired in the food vs fuel debate. From that perspective, a specialized group of aerobic methane-oxidizing bacteria,alphaproteobacterial methanotrophs,

have been investigated as a means for PHB production from methane and/or methanol (Chidambarampadmavathy et al., 2015). These bacteria contain enzymatic machinery that enables the metabolic conversion of single-carbon substrates to the bioplastic precursor PHB (Pieja et al., 2017). The use of low value industrialby-products as starting material for PHB production reduces the cost of the entire process while contributing to the reduction of GHG emissions. One of the most famous low-cost carbon sources is carbon dioxide. Carbon Dioxide is another GHG highly emitted as industrial byproduct, and the idea of capturing it for industrial bioconversion has been explored in various aerobic and anaerobic organisms. Cyanobacteria were one of the most interesting targets, as they have been established as the efficient platform for biodiesel production (Nozzi et al., 2013). However, the attempts to screen PHB-producing cyanobacteria did not give promising results. The % of PHB identified in these organisms ranged from 0.15 – 6.44 % only, while the addition of expensive, food vs fuel debate trigger, glucose was required to improve PHB content to 26.37% (Ansari and Fatma, 2016). In addition to carbon dioxide only, there have been attempts to optimize PHB production from synthetic gas (syngas) which is the $H_2$, $CO_2$, and CO mixture (Jin et al., 2020). The process of syngas conversion cam be completed by microorganisms that can oxidize $H_2$ and fic $CO_2$ and CO while producing acetyl-CoA, which is the molecular base for PHB synthesis. In these organisms, acetyl-CoA is immediately converted to the acetate to gain ATP (Cestellos-Blanco et al., 2021). Even though the production of PHB from syngas can be relatively high (12.6 mg/L per hour in continuous culture), the production yield could not be maintained, as these cells were depleting PHB to acquire carbon and energy (Cestellos-Blanco et al., 2021). The production of PHB from carbon fixing acetogenes usually require genetic modifications of the strain (Jin et al., 2020), which might result in disrupted redox balance and affect biomass production. Regardless of successful improvement, the amount of PHB reached approximately 22–27 mg/L (de Souza Pinto Lemgruber et al, 2019), which is not enough to justify commercialization. In addition,

hydrogen oxidation is required to support cellular growth, which generates the problem of potential reactor explosion during fermentation process. It is true that lowering hydrogen amount reduces the risk of explosion and improves PHB content up to 70% dw/L (Miyahara et al. (2020), but the process bear risks which can be avoided if other feedstock is used to support both, PHB and biomass production. In addition, carbon dioxide fixation is energetically expensive metabolic route, and the production of biomass might not follow production of PHB. However, carbon dioxide should still be considered as a feedstock, especially in methanotroph-cyanobacterial co-culturing, where simultaneous use of both GHG can be achieved (Hill et al., 2017).

The production of PHB from methane and methanol has been successful in past few decades. Companies such as Mango Materials and New Light are actively engaged in commercial PHB production from methane, and they are constantly seeking for production improvement. Regardless of being britt and stiff, PHB still remains optimal polymer for bioplastic productions. The reason behind that is the ability to improve its quality with alternative purification methods (Olivera et al., 2009; McAdam et al., 2020).

The production of PHB by alphaproteobacterial methanotrophs is typically accomplished by providing an excess of carbon, followed by a starvation signal that triggers PHB synthesis (Pieja, Rostkowski, et al., 2011). Even though all alphaproteobacterial methanotrophs utilize the same metabolic pathways for PHB production, there is substantial variability in terms of preferable carbon and nitrogen source that enhances PHB synthesis in different species (Rostkowski et al., 2013; Zaldívar Carrillo et al., 2018; T. Zhang et al., 2017). In addition, PHB yield, and quality is affected by pH, temperature, other macronutrients (phosphorus, sulfur, potassium, magnesium sodium), and trace metals (copper, iron, zinc, manganese, and cobalt) (Strong et al., 2015). Despite the importance of methane-based PHB production, the physiological effects of media formulation and diversity among PHB-producing strains has not been widely investigated. Studies have resolved the

impact of carbon source on metabolic distribution (Kalyuzhnaya et al., 2013) and shifting towards preferred metabolites (Fu et al., 2019; O. K. Lee et al., 2016; Sugden et al., 2021). However, these studies were performed on gammaproteobacterial methanotrophs, while PHB-producing methanotrophs remained largely unexplored. A recent study revealed the diverse growth requirements of three different alphaproteobacterial methanotrophs where the common features were low growth followed by high formate excretion when methanol was used as the sole carbon source (Tays et al., 2018). Despite valuable information on the effect of the carbon source on bacterial physiology, its impact on PHB production remains relatively unexplored.

Regardless of their ability to utilize ammonia or nitrate mineral salts (AMS or NMS), most studies on methanotrophic metabolism have been performed with nitrate as the nitrogen source (Fu et al., 2019; Matsen et al., 2013; Yang et al., 2013). The discovery that ammonia can serve as a better nitrogen source than nitrate in some organisms has led to comparisons of physiology and growth between the two sources of nitrogen (Nyerges et al., 2010; Nyerges & Stein, 2009). In addition, PHB-producing methanotrophs can utilize atmospheric nitrogen due to the presence of nitrogen fixing enzymatic machinery (Dam et al., 2014; Stein et al., 2011). Even though there was substantial evidence of differences in preferable nitrogen source for growth among isolates (Campbell et al., 2011; Nyerges et al., 2010; Stein et al., 2011; Tays et al., 2018), the effect of nitrogen source on PHB production was not investigated among all alphaproteobacterial methanotrophs. The only common feature was the need for starvation or stress signal to initiate PHB synthesis (Zaldívar Carrillo et al., 2018; T. Zhang et al., 2017; Y. Zhang et al., 2008). Among all known alphaproteobacterial methanotrophs, most of them has been investigated as potential platform for PHB synthesis. The well-known model organism *Methylosinus trichosporium* OB3b has been studied by various researchers (Zhang et al., 2017; Zaldivar-Carrilo et al., 2018) and gave promising results achieving around 52%

without (Zaldivar-Carrilo et al., 2018) and 51% of PHB dw/L with existing oxygen limitation (Zhang et al. 2017). Another organism Methylocystis hirsuta accumulates over 40% dw/L (Bordel et al., 2019). However, even though *M. trichosporium* OB3b produces significant amounts of PHB followed by biomass increase after optimization (Zaldivar-Carrilo et al., 2018), our comparative analysis showed that under identical growth conditions where stress signal was not applied (methane-nitrate growing conditions), the model organism used in this study *Methylocystis* sp. Rockwell produced detectable PHB amounts, while *M. trichosporium* OB3b did not (Lazic et al., 2021). These findings suggest that Methylocystis sp. Rockwell should be explored for further PHB production, especially due to the fact that this organism thrives well on ammonia as the source of nitrogen, which leaves possibility to use ammonia-containing wastewater as a simple growing medium. Nevertheless, there are a few unexplored alphaproteobacterial methanotrophs (such as *Methylocystis* sp. WRRC1) that remain to be investigated and screened for PHB production in future.

1.2. PHB detection and quantification in alphaproteobacterial methanotroph *Methylocystis* sp. Rockwell

Interest in the production of PHB has intensified as plastic waste continues to accumulate and interfere with ecosystems and wildlife (https://www.unep.org/news-and-stories/story/world-leaders-set-sights-plastic-pollution). Because PHB is non-toxic and biodegradable, and has properties that resemble traditional plastic materials, much effort has been invested to reduce the cost of microbial production by identifying cheaper carbon sources (Oehmen et al., 2005) and/or by modifying existing PHB-producing strains (McAdam et al., 2020). In addition, efforts have been made to improve polymer recovery, detection and quantification (Godbole, 2016). The success of any type of production (including PHB) requires an efficient, rapid, and simple method for product analysis. It is critical to know the exact amount of synthetized and recovered material, especially when the

focus is to compare between different production conditions. There are numerous available methods for PHB detection and quantification, and they include microscopy-based staining reactions, spectrophotometric methods, High Performance Liquid Chromatography (HPLC), Gas Chromatography (GC), and NMR Spectroscopy. Each of these methodologies has advantages and disadvantages, but in terms of precision and accuracy, the method based on depolymerization and esterification of PHB followed by indirect detection of methylated monomer with GC-flame ionization detector (FID) has been reported as the most successful (Godbole, 2016.; Oehmen et al., 2005; Zaldívar Carrillo et al., 2018). However, this approach not only involves the use of harmful solvents (such as chloroform and sulfuric acid) but is also time consuming. Thus, the present study aimed to develop novel, environmentally friendly and cheaper approaches for PHB detection and quantification.

The first approach was based on staining with Nile Blue A (NBA), a fluorescent dye, followed by microscopy (Lazic et al., 2022). The spectral properties of NBA enables selective detection of PHB among other lipid-based cellular components, making it easily visible under a fluorescent microscope. In addition, this methodology enabled single-cell analysis and evaluation of PHB granules.

The second approach was based on the ability of a PHB-degrading enzyme, PHB depolymerase (PhaZ), to interact tightly with its PHB substrate (Martínez-Tobón et al., 2020a). PhaZs are hydrolytic enzymes that contain catalytic (CAT) and substrate-binding domains (SBD) linked by a fibronectin-like domain (Clark et al., 2019; Costa et al., 2014). A framework for the production and purification of PhaZ-recombinant fusion proteins (Martínez-Tobón et al., 2020b) was adapted to design and recover a synthetic module for PHB detection. The design involved the replacement of the CAT domain by fluorescent reporter Superfolded Green Fluorescent Protein (sf GFP), resulting in a novel synthetic fusion sfGFP-SBD enzyme capable of binding to PHB and emitting a strong fluorescent signal. The

idea of using fusion proteins as reporters of expression levels is widely explored in multiple areas of science, but has not been investigated for the detection and quantification of PHB. This new approach enables detection of PHB in specific organisms and screening for novel PHB-producing species in the environment.

1.3. Scope and summary of the thesis

This study integrates the scientific and industrial potential of methanotrophs. *Methylocystis* sp. Rockwell belongs to the phylum Proteobacteria and the class Alphaproteobacteria. With the continuous increases in methane emission and plastic waste generation, organisms that can solve both issues like *Methylocystis* sp. Rockwell represent an important area of investigation.

The initial goals of this work were to (i) understand the metabolic regulation of biochemical pathways in *Methylocystis* sp. Rockwell, and (ii) to improve its production of PHB. This was achieved through complex omics-based analysis that can serve as a guide for the optimization of nutrient combinations to support the highest possible bacterial biomass, followed by the highest possible PHB production. The secondary goals of this work aimed to develop novel, environmentally friendly methods for in vivo (iii) and/or in vitro (iv) PHB detection that serve as efficient alternatives to the current costly and toxic approaches.

Chapter 2 summarizes previous work in methanotroph physiology and biochemistry, with specific focus on the effects of carbon and nitrogen sources on growth and PHB production. Because of scientific and industrial integration in this work, Chapter 2 emphasizes the most important value-added compounds that can be made from methane via methanotrophs. In addition, Chapter 2 covers the most significant methodologies used to detect and quantify PHB, with advantages and disadvantages for each of them. Chapter 2 also describes the main characteristics of PHB, as it is the focus of interest in this thesis.

Chapter 3 reports detailed metabolomic profiles of the model organism, *Methylocystis*

sp. Rockwell, grown on four different nutrient conditions (methane-ammonium, methane-nitrate, methanol-ammonium, and methanol-nitrate). A version of this chapter was published in FEMS Microbiology Letters (Lazic et al., 2021).

Chapter 4 focuses on the effect that methanol has on PHB production, along with simultaneous growth and biomass production.

Chapter 5 describes the development of an *in vivo* fluorescence detection system for PHB. A version of this chapter was published in Applied Microbiology and Biotechnology (Lazic et al., 2022).

Chapter 6 describes the development of a novel synthetic PHB binding protein for *in vitro* detection of PHB.

Chapter 7 offers a closing perspective and future directions for the research.

## 1.4. Significance of this study

The increasing amount of methane in the atmosphere and the accumulation of plastics in the environment are two major global concerns. Methanotrophs can be used to mitigate both issues through their consumption of methane and its conversion to PHB. Thus, it is highly beneficial to understand the metabolic pathways that regulate production of biodegradable polymers from methane in these organisms. Having this accurate metabolic "roadmap" will help determine the most efficient pathway for biopolymer synthesis. The results reported in this thesis will serve as a guideline for future processes and/or genetic modifications to improve methanotrophic bacterial strains for useful purposes.

# Chapter 2

# Literature Review

## 2.1. The global budget and significance of methane

Methane ($CH_4$) is the main component of natural gas and considered to be the second most prevalent greenhouse gas after carbon dioxide ($CO_2$) (Nazaries et al., 2013). It has been estimated that methane has a Global Warming Potential (GWP-100) 28 times greater than carbon dioxide on a molecule-to-molecule basis (Saunois et al., 2020). In the lower parts of the atmosphere (troposphere) methane contributes to the production of ozone ($O_3$), which has a negative influence on the environment. It also is oxidized by hydroxy radical present in the atmosphere to form formaldehyde and carbon monoxide; the latter is further oxidized to create carbon dioxide. At the same time, nitrogen dioxide is split by sunlight into nitric oxide and an oxygen atom, and the oxygen atom combines with molecular oxygen to create ozone (Sanderson, 2007). In general, it has been established that rapid photochemical oxidation of carbon monoxide and hydrocarbons in the presence of nitrogen oxides contributes to increased levels of ozone in the troposphere (Fiore et al., 2002). On the other hand, in upper parts of the atmosphere, methane emissions contribute to the destruction of the ozone layer, mostly through decomposition mediated by hydroxy and chlorine radicals (M. Li et al., 2018)
.

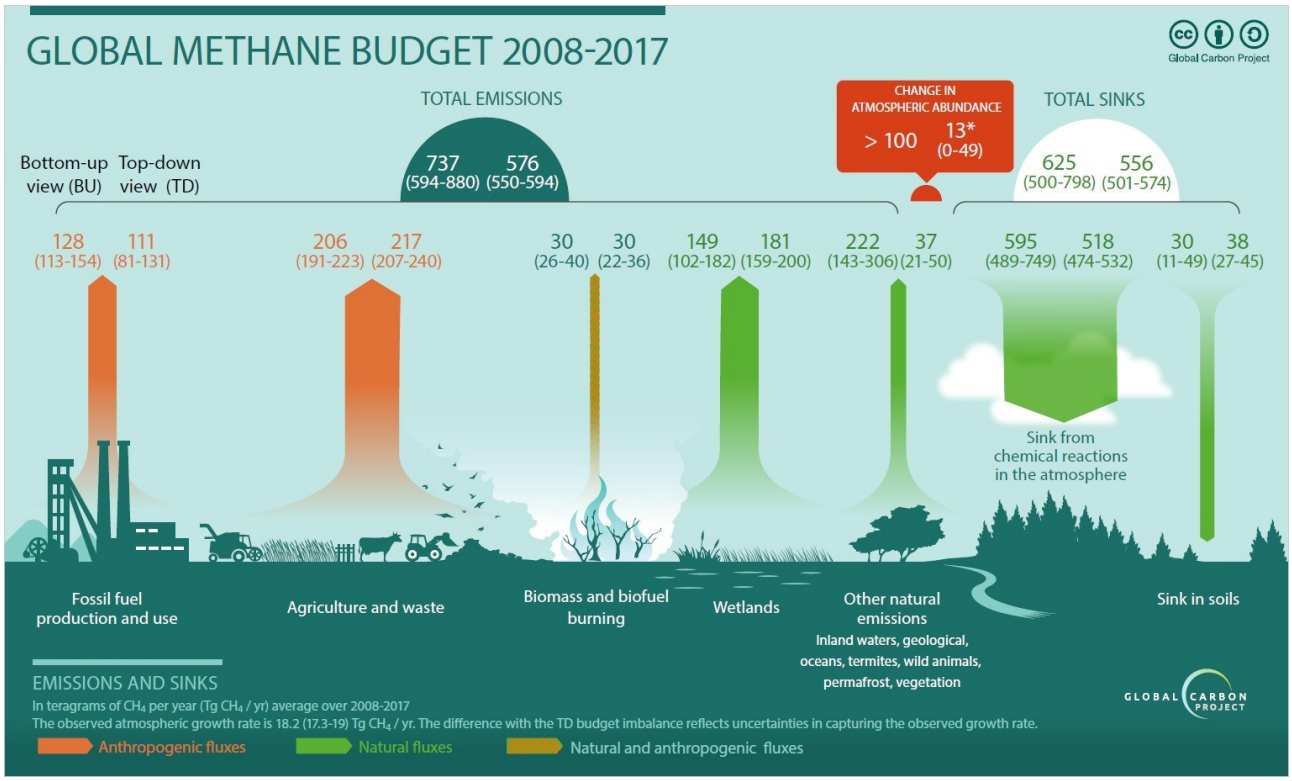


Figure 2.1. Global Methane Budget for the period 2008-2017. The main sources of methane emissions are human activities, including agriculture, waste generation and the use of fossil fuels. Significant contributions also originate from wetlands and other anaerobic environments where methanogenic archaea produce methane. Not shown in this figure, methanotrophic bacteria oxidize methane to carbon dioxide. This figure is adapted from (Saunois et al.,2017).

According to data obtained from studies on ice cores and firn, the first significant increase in methane emission in Earth's history was during glacial to interglacial periods, with an increase from 360 ppb to approximately 700 ppb (Lan et al., 2021). Even though this change may have been triggered by variations in the main ecological and geological parameters of the Earth (land, water, structure of the atmosphere), the initial increase in methane emission most likely was due to feedback loops in the carbon cycle (Lan et al., 2021). Another period of high methane emission was observed 5,000 years ago and was linked to natural emissions from the southern tropics. Nevertheless, these records are generating enough evidence to connect methane with episodes of global warming and obvious climate change.

In general, the main causes of increased methane emission (from 720 to 1879 ±0.6 ppb) from the pre-industrial period to present day are human activities. The production and use of fossil fuels, along with intensified agriculture and waste generation, account for about 50% of total methane emissions (Fig. 2.1). Inland waters, oceans, permafrost, and vegetation contributes to approximately 20% of total methane emissions, while the contributions from biomass and biofuel burning are negligible (around 7%) (Fig. 2.1). Even though abiotic reactions are responsible for the majority of atmospheric methane oxidation (abiotic sink), most methane generated in anaerobic environments is oxidized by bacteria and archaea known as methanotrophs. In oxygen-depleted environments, small amounts of hydrogen and organic compounds are produced by microbial fermentation. Methanogenic archaea consume dihydrogen while reducing carbon dioxide, which results in methane production (methanogenesis) (Topp et al., 1997.). Methanotrophs inhabit surface layers of the soil where they can access methane and oxidize it to carbon dioxide, thereby generating energy required for metabolic processes. The oxidation of methane to carbon dioxide completes the carbon cycle (Topp et al., 1997). In other words, methanotrophs represent the only biological sink for

methane and thus play a crucial role in regulating the global carbon cycle. Without these microorganisms, mitigation of methane emissions would not be possible (Colin Murrell & Jetten, 2009).

## 2.2. Methane-oxidizing microorganisms

The biotic oxidation of methane is performed by highly diverse methane-oxidizing microorganisms from the bacterial and archaeal domains of life. These organisms oxidize methane in fully oxic, hypoxic and anoxic environments. In anoxic environments, methanotrophs couple methane oxidation to the reduction of alternative electron acceptors such as sulfate, nitrate, nitrite, iron, or manganese (Ettwig et al., 2009, 2010; Haroon et al., 2013; Milucka et al., 2012). Certain methane-oxidizing bacteria can scavenge oxygen at low concentrations and thrive under hypoxia by oxidizing methane while reducing nitrate (Kits et al., 2015; Stein, 2019), or fermenting formaldehyde via central carbon pathways (Kalyuzhnaya et al., 2013). The aerobic oxidation of methane is performed by methanotrophs (a.k.a. Methane-Oxidizing Bacteria, a.k.a. MOB) largely belonging to the Proteobacteria phylum, where they are divided into two main groups, Gammaproteobacteria and Alphaproteobacteria (Trotsenko & Murrell, 2008). Both groups are significant from a biotechnological perspective due to their highly diverse metabolic machinery that enables them to produce various value-added compounds (Strong et al., 2015, 2016).

While methanotrophic archaea are considered anaerobic (they do not require oxygen as terminal acceptor), bacteria that oxidize methane are strict aerobes with highly diverse methane metabolism (Stein, 2019; Trotsenko & Murrell, 2008). Following oxygen requirements, archaeal and bacterial methanotrophs evolved with different enzymes used for methane oxidation. Aerobic methane oxidation relies on the methane monooxygenase

enzyme (MMO) (Ettwig et al., 2009) while the main enzyme in anaerobic methane oxidation is methyl-coenzyme M reductase (MCR) (Evans et al., 2019).

### 2.2.1. Anaerobic Methane-Oxidizing microorganisms

In the early 1970s, Martens and Berner provided an initial explanation regarding methane consumption in the anaerobic marine environment (Martens and Berner, 1977.). These authors proposed the ability of sulfate-reducing bacteria (SRB) to co-metabolize methane, which would explain its significant decrease in anoxic Long Island Sound sediments (Martens and Berner, 1977). The reaction of methane oxidation paired with sulfate reduction is energetically plausible, but pure cultures of SRB were not able to perform the process. Moreover, all known methane oxidizers known at the time were obligate aerobes. A few years later, Reeburgh reported anaerobic methane oxidation in the sulfate-reducing zone in anoxic marine sediments (Reeburgh, 1980). At the same time Zehnder and Brock identified nine methanogenic strains that were capable of simultaneous methane production and anaerobic consumption. They proposed the model of methane oxidation by methanogenic archaea when paired with $H_2$-consuming SRB (Zehnder and Brock, 1979). In addition to Zehnder and Brocks findings, anaerobic methane oxidation has been reported after the addition of sulfate, acetate in combination with methane and acetate to the Lake Mendota surface sediments (Panganiban et al., 1979). At the same time, Kosiur and Warford analyzed methane oxidation rate in Santa Barbara Basin sediments in vitro and concluded that the oxidation of methane indeed occurs under anaerobic conditions describing so called "quasi-in-situ" measurements of anaerobic methane oxidation (Kosiur and Warford, 1979). Later reports confirmed the link between anaerobic methane oxidation and sulfate reduction (“sulfate-stimulated methane oxidation”) (Hoehler et al., 1994; McGlynn, 2017). The process, termed “reverse methanogenesis” (Hallam et al., 2004), involves a consortium of methanogenic archaea and SRB. Reversely operating

methanogenic archaea oxidize methane to carbon dioxide, sharing the energy yield with sulfate-reducing bacteria (SRB). SRB perform sulfate respiration ($SO_4^{2-}$ reduction) which results in hydrogen-sulfide ($H_2S$) production (Boetius et al., 2000; Hinrichs et al., 1999; Hoehler et al., 1994). However, the most recent findings exclude the syntrophically linked sulfate-reducing partner (Milucka et al., 2012). According to these findings, methane oxidation can involve only one organism (ANaerobic Methane oxidizing Euryarchaeota or ANME), which allows in-cell energy conservation (Milucka et al., 2012).

In addition to sulfate, nitrate (NO3−), nitrite (NO2−), manganese (Mn4+) and Iron (Fe3+), can serve as electron acceptors to support methane oxidation. The most significant process for methane consumption is certainly sulfate-dependent, however, anaerobic methane oxidation via iron reduction occurs in some marine and freshwater environments that are described as sulfate nitrate depleted (Yang et al., 2021). The absence of sulfides in deep water facilitated the accumulation of $Fe^{2+}$ at high concentrations (Crowe et al., 2008), while experimental results by Beal et al. reported the involvement of ferrihydrite in anaerobic methane oxidation process in the absence of sulfates (Beal et al., 2009). Nevertheless, it is confirmed that anaerobic methane oxidation can be coupled with ferric iron ($Fe^{3+}$) reduction resulting in the production of $CO_2$ and ferrous iron ($Fe^{2+}$) in stoichiometric amounts (Ettwig et al., 2009, 2010).

Haroon et al. confirmed that ANME species Candidatus *Methanoperedens nitroreducens* was able to couple methane oxidation with nitrate ($NO_3$-) reduction (nitrate respiration) which results in nitrite ($NO_2$-) generation. The nitrite was further consumed by syntrophically linked anaerobic ammonium-oxidizing bacteria (ANAMMOX) (Haroon et al., 2013). The link between anaerobic and aerobic methane oxidation can also be accomplished syntrophically with *Methanoperedens* and the bacterium Candidatus *Methylomirabilis oxyfera* (NC10 phylum). Bacteria in the NC10 phylum oxidize methane andreduce nitrite to NO, which is then dismutated intracellularly to produce $N_2$ and $O_2$. Methane oxidation then

commences under anoxic conditions using intracellularly produced $O_2$ (Ettwiget al., 2010; He et al., 2015).

2.2.2. Facultative methanotrophs

According to comprehensive reviews on methanotrophy published in the beginning of 2000s, (Trotsenko & Murrell, 2008; Op den Camp et al., 2009; Semrau et al., 2010), methanotrophs isolated in 50s and 60s in the past century are known by the ability to utilize only methane or methanol for growth (Dworkin & Foster, 1956; Brown et al., 1964; Foster & Davis, 1966). However, in 1970, Whittenbury reported various methanotrophic strains that exhibited enhanced growth with malate, acetate, and succinate in combination with methane (Whittenbury et a., 1970). These findings were indication that facultative methanotrophy exists and there are methanotrophic isolates that can thrive on multicarbon compounds as a sole growth substrate (Semrau et al., 2011). A few years after Patt et al. isolated facultative methanotrophs from freshwater lake sediments and described their ability to use organic acids and sugars as growth substrate (Patt et al., 1974). In early 2000s, novel acidophilic methanotrophs have been identified and named *Methylocella palustris* (Dedysh et al., 2000), *Methylocella silvestris* and *Methylocella tundrae* (Dunfield et al., 2003; Dedysh et al., 2004). These organisms were able to utilize methane or methanol, but surprisingly, they did not express p MMO and were not able to utilize sugars as the growth substrate. The absence of sugar utilization in addition to C1 substrates categorized *Methylocella* species as obligate methanotrophs (Semrau et al., 2011). However, later findings confirmed that *Methylocella* sp. can utilize acetate, pyruvate, succinate, malate, and ethanol (Dedysh et al., 2005) in addition to methane and methanol, which is the indicator of facultative methanotrophy. Up to date, it has been reported that *Methylocella sylvestris* can thrive on methylamine, pyruvate, succinate, malate, and ethanol (Semrau et al., 2011). Furthermore, the growth yield, carbon conversion efficiency and growth rate on acetate vs methane in *Methylocella sylvestris* were higher, suggesting that acetate may be the preferred growth substrate (Semrau et al., 2011).

*Methylocella palustris* exhibits the same pattern, while *Methylocella tundrae* growth can be achieved with formate in addition to the reported organic acids (Semrau et al., 2011). Among acidophilic methanotrophs, the isolate *Methylocapsa aurea* had the ability to utilize acetate, but neither of tested sugar substrates (glucose, fructose, maltose) could be used as a sole growth substrate (Dunfield et al., 2010).

### 2.2.3. Aerobic Methane-Oxidizing Bacteria

Aerobic methanotrophs are a subset of the larger physiological group of organisms known as methylotrophs (Bezirhan and Ozsoy, 2015). Methylotrophs can oxidize a variety of single-carbon (C1) compounds including methane, methanol, halomethanes, methylated amines and sulfur-containing methylated compounds (Trotsenko & Murrell, 2008). The best-studied C1-oxidizers are bacteria that utilize methane and/or methanol as the sole carbon and energy source. The most studied aerobic methanotrophs are classified as Gammaproteobacteria and Alphaproteobacteria (Trotsenko & Murrell, 2008). For both groups, methane is oxidized to methanol, methanol to formaldehyde, and formaldehyde is further converted to carbon dioxide via a formate intermediate (Fig. 2.2). The branching point between gamma- and alphaproteobacterial methanotrophs is the assimilation of formaldehyde. While gammaproteobacterial methanotrophs assimilate it through the ribulose monophosphate (RuMP) pathway (Fig. 2.2), alphaproteobacterial methanotrophs perform formaldehyde assimilation via the serine cycle (Fig. 2.2).

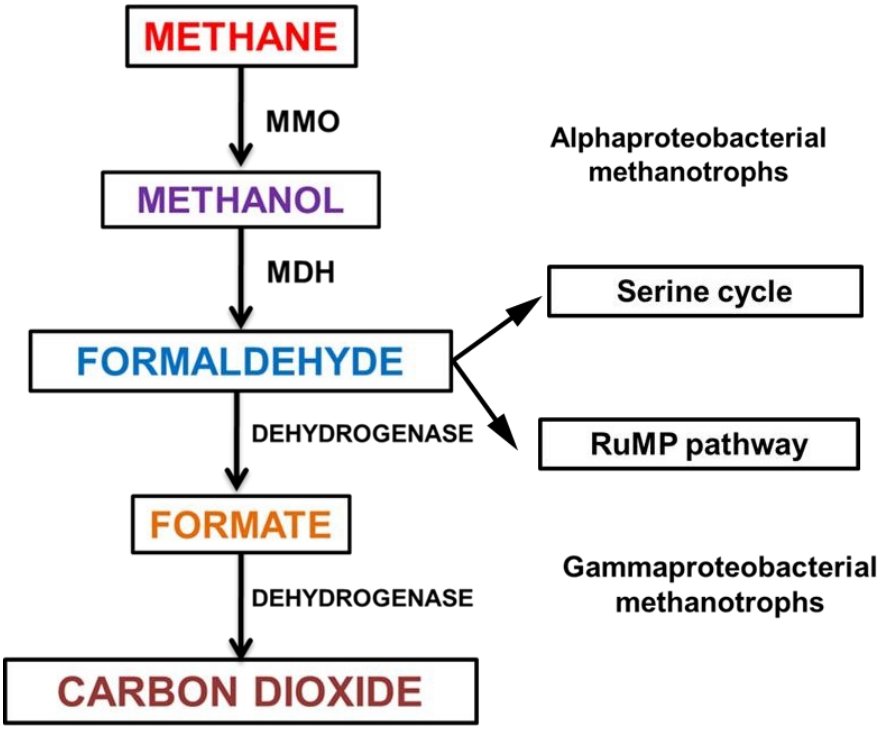


Figure 2.2. Schematic representation of initial steps in methane metabolism in gammaproteobacterial and alphaproteobacterial methanotrophs. The branching point is formaldehyde assimilation through the RuMP (gammaproteobacterial methanotrophs) and serine (alphaproteobacterial methanotrophs) pathways.

Older literature describes Type X methanotrophs, like *Methylococcus capsulatus* Bath, that contain enzymes of both the RuMP and serine cycles (Murrell and Jetten, 2009). However, the most recent classification recognizes Type X as gammaproteobacterial methanotrophs that assimilate formaldehyde via the RuMP cycle (Trotsenko & Murrell, 2008). More recently discovered methanotrophs denoted as extremophilic species belong to the Verrucomicrobia phylum. The optimal growth conditions for these extremophiles are pH 2.0 and temperatures between 30-65ºC. Verrucomicrobia were also identified in areas of Russia and Italy (Conrad, 2009; Islam et al., 2008; Khadem et al., 2012). For these organisms, methane represents only the energy source, while carbon assimilation is performed through the Calvin-Benson-Basham (CBB) cycle (Khadem et al., 2012). All aerobic methanotrophs contribute to methane removal from the environment, which makes them extremely important participants in the global carbon cycle. They inhabit various environments, such as freshwater and marine communities, ground and wastewater, sewage sludge, landfill cover soils and extreme environments such as hot springs, Antarctic lakes, and volcanic mud pots (Colin Murrell & Jetten, 2009).

### 2.3. Central carbon metabolism of aerobic methane-oxidizing bacteria

The ability of MOB to thrive in diverse environmental conditions has been linked to a variety of different enzymatic systems present in these organisms (Colin Murrell & Jetten, 2009; Trotsenko & Murrell, 2008). Methane oxidation enzymes are connected to central metabolic pathways and regulatory networks that control metabolism and nutritional responses in different habitats (Trotsenko & Murrell, 2008). The complex metabolic network in methanotrophs provides high capacities for degradation of environmental pollutants that are considered hazardous to human and animal health (Semrau, 2011; Pieja et al., 2017).

### 2.3.1. Methane oxidation to methanol

The initial step in methane oxidation is performed by the enzyme known as methane monooxygenase (MMO) (Fig. 2.2). This is generally well-characterized enzyme that is capable of oxidizing C-H to C-OH groups with the expense of molecular oxygen ($O_2$). One oxygen atom is incorporated into methanol ($CH_3OH$), while the other one is reduced to $H_2O$ (Fig. 2.3) (Jeremy D. Semrau, 2010; DiSpirito et al., 2004; Trotsenko & Murrell, 2008).

MMO exists in two forms, soluble (s MMO) present in cytoplasm, and particulate (p MMO) embedded in intracellular membranes (Semrau et al., 2010). The expression of these two forms is highly dependent on the organism type, but also on nutrient concentration (methane, nitrate, copper, or biomass density). Almost all known methanotrophs express p MMO (Drummond et al., 1989), while only certain genera express both versions. The exception is genera *Methylocella* (Bordel et al., 2020) and *Methyloferula* (Vorobev et al., 2011) that contain only soluble version of MMO. Methanotrophs that express both biochemical forms of MMO are subjected to the differential regulation vi copper concentration (Dalton et al., 1984; Semrau et al., 2010). Methanotrophs that express pMMO have higher biomass yield than organisms that only express sMMO. The significant difference in growth rate has been related to the reduction of energetic requirements and higher substrate affinity of pMMO compared to sMMO (Trotsenko & Murrell, 2008).

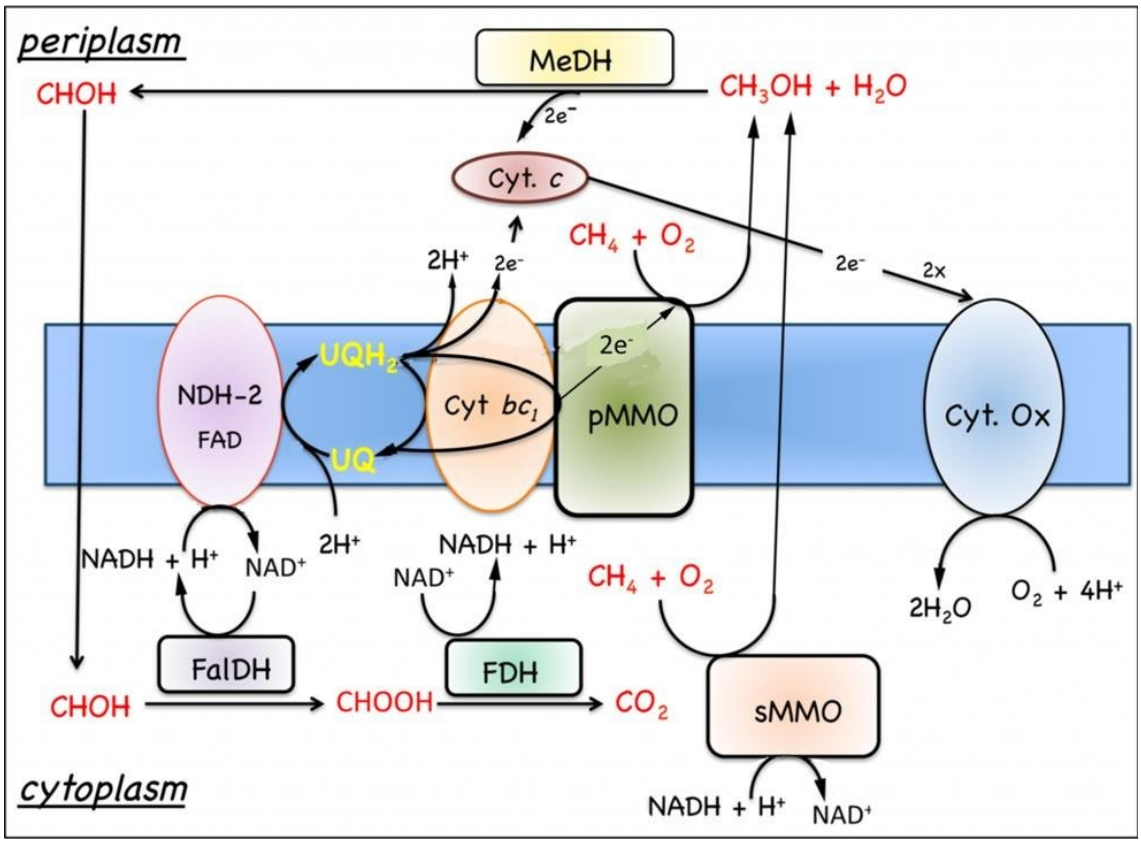


Figure 2.3. The model of methane oxidation via two forms of methane mono-oxygenase (MMO): particulate MMO (pMMO), embedded in the membrane, and soluble MMO (sMMO), a free-floating form. The oxidation model presented in this figure is from *Methylococcus capsulatus* Bath. The enzymes are sMMO, pMMO, methanol dehydrogenase (MeDH), formaldehyde dehydrogenase (FalDH), and formate dehydrogenase (FDH). Respiratory components are cytochromes bc1 and c (cyt bc1 and cyt c). The terminal oxidase is completing the final step in the Electron Transport Chain (ETC) by reducing oxygen ($O_2$) to water (H2O). This Figure is reproduced with permission from (DiSpirito et al., 2004).

The soluble MMO (s MMO) is cytoplasmic enzyme initially described in 1985$^{th}$ in *M. capsulatus* Bath (Green and Dalton, 1985), followed by the alphaproteobacterial members *M. trichosporium* OB3b (Fox et al., 1989) and *Methylocystis* sp. (Nakajima et al., 1992). The s MMO is encoded by the mmoXYBZDC operon is (Erguder et al., 2009) and controlled with a σ54-dependent promoter located upstream of the *mmo* gene cluster. The σ54 transcription regulation (Iguchi et al., 2010) has been linked to nitrogen limitation, which indicates a connection between methane and nitrogen metabolism in methanotrophs (Iguchi et al., 2010). The s MMO contains three components: hydroxylase, reductase and regulatory protein (Colby et al., 1977; Colby & Dalton, 1978; Woodland & Dalton, 1984; Fox et al., 1989; Pilkington & Dalton, 1990; Wallar and Lipscomb, 1996, 2001; Semrau et al., 2010). Hydroxylase component adopts trimeric structure containing α (54 kDa), β (42 kDa) and γ (22 kDa) subunits organized as (αβγ)2 (Semrau et al., 2010). Reductase component contains one subunit molecular mass 38-40 kDa which contains FeS clusters and FAD cofactor (Fox et al., 1989). Component B is the smaller part of s MMO also known as a colorless protein that does not contain cofactors (Lipscomb, 1994). The active site (methane catalysis) is in hydroxylase component and is characterized by the specific "oxygen bridged diiron cluster" (Fox et al., 1988, 1989; Rosenzweig et al., 1993; Elango et al., 1997; Semrau et al., 2010). Unlike p MMO (described later) that can oxidize only smaller hydrocarbons, s MMO has broader substrate specificity and oxidizes various substrates, such as alkanes, alkenes, aliphatic, aromatic, and halogenated hydrocarbons (Wendland et al., 2010; Chidambarampadmavathy et al., 2015). The sequence of sMMO is highly conserved among methanotrophs, especially the gene encoding the hydroxylase component. This gene is often used as a DNA probe to detect the presence of methane-oxidizers in different environments (Chidambarampadmavathy et al., 2015).

Membrane-bound particulate MMO (pMMO) is encoded by the *pmo*CAB operon; methanotrophs generally contain multiple copies of this operon with significant sequence divergence (Colin Murrell & Jetten, 2009). The pMMO enzyme resembles a trimeric structure (αβγ)3 composed of the PmoB (α) (~45 kDa), PmoA (β) (~26 kDa), and PmoC (γ) (~23 kDa) subunits. Regardless of described crystal structure, the full description of physiological nature that involves the number and function of metal centers as well as the nature of electron donor for p MMO was not defined during many years. Regardless of different hypothesis, everyone agrees that p MMO expression relies on copper ions (Semrau et al., 2013). Both versions of MMO are tightly regulated by transition metals, iron for s MMO and copper for p MMO. At extremely high copper levels (> 50 μM) the expression of p MMO is inhibited due to the strong metal interaction with the reductant (Balasubramanian et al., 2010; Nguyen et al., 1994; Yu et al., 2003; Chidambarampadmavathy et al., 2015). The result of this interaction is hydrogen peroxide which reversibly inhibits p MMO (Chidambarampadmavathy et al., 2015). However, the differential expression of p MMO vs s MMO is linked to the copper- biomass ratio. At high copper-biomass ratio the enzyme that performs methane oxidation is p MMO, but the addition of iron can stimulate the expression of soluble version (s MMO). In general, at high copper/biomass the p MMO is expressed, while at lower copper/biomass ratio, the dominant enzyme is s MMO. At high copper concentration s MMO is losing its activity because of copper binding to the FeS clusters in reductase component of s MMO, preventing the electron flow from FAD cofactors (Jahng et al., 1996). The loss of s MMO activity is followed by the expression of p MMO, which is copper-regulated MMO form. The copper regulation is described as “copper switch” (Semrau et al., 2013; Chidambarampadmavathy et al., 2015). The theory behind the copper switch states that s MMO will be expressed only at low copper/biomass ratio, while as the ratio increase, the expressed MMO form will be particulate (p MMO) (Semrau et al., 2013). The central regulator of this mechanism is chalkophore methanobactin (Mb) described in

detail elsewhere (Kim et al., 2004; Choi et al., 2010; Semrau et al., 2013). This is siderophore-like molecule that is known as the molecule that increases the availability of copper, and thus can control the expression of copper-regulated s MMO/p MMO switch (Knapp et al., 2007). Methanobactin is characterized as small polypeptide that contains up to six imidazole, oxazolone or pyrazinedione rings along with enethiol groups that are capable of copper binding (Choi et al., 2006; Bandow et al., 2012; El Ghazouani et al., 2012; Semrau et al., 2013). Methanobactin is genetically encoded polypeptide, as it was confirmed in M. trichosporium OB3b (Stein et al., 2010). The Mb precursor in the same organism is MbnA encoded by gene mbnA and is absolutely required for the expression of Mb (Semrau et al., 2013). Along with methanobactin, another polypeptide MmoD is actively involved in copper switch mechanism. As proposed in recent model, at low copper/biomass ratio, MmoD increases the expression of s MMO and Mb proteins while repressing the expression of p MMO. Thus, when the availability of copper is decreased, Mb will be highly synthetized to support copper uptake. If the ratio copper/biomass is high (high copper availability), Mb will interact with copper, which will cause the decrease in mmo gene expression and reduced level of s MMO. This activity will substantially lead to the reduced activity of mbn gene for methanobactin, and eventually reduce methanobactin production at higher copper levels. At high copper levels he MmoD regulator will bind to metal forming MmoD-Cu. In this way, MmoD will not be able to decrease *pmmo* or increase *mmo* operon expression (Chidambarampadmavathy et al., 2015; Semrau et al., 2013).

As previously mentioned, the p MMO resembles trimeric structure containing three subunits PmoB (α), PmoA (β), and PmoC (γ). Each subunit is transmembrane, where PmoB contains large periplasmic domain (Lieberman et al., 2005; Ro SY et al., 2018; Ross et al., 2019). The crystal structure of p MMO defines three copper-binding sites: $Cu^{+}$, $Cu_B$ and $Cu_C$. The first Cu+ is ligated by two histidines (bis-His), and the lack of conservation among organisms indicates that this cannot be catalytical site (Balasubramanian et al., 2007). In $Cu_B$,

copper is also coordinated with two histidines, but one of controversy was that this site is dicopper ($Cu^{2+}$). However, dicopper site was not identified in all species, and it remained unclear whether in monocopper species the copper was lost during purification, or the site was truly monocopper (Ross et al., 2019). One more copper binding site is identified in PmoC also coordinated with two histidines with the addition of one aspartate (Sirajuddin et al., 2014). The recent publication by Ross et al (2019) finally identified two monocopper binding sites in PmoB where the active site of methane catalysis is. However, the exact nature of catalytical site was not clear as well as PmoB location. The proposed catalytically active copper sites were $Cu_B$ and $Cu_C$ (in PmoB and PmoC, respectively). After the discovery that $Cu_B$ mutant can still perform methane oxidation, the $Cu_B$ as the active site was excluded (Ross et al., 2019). On the other hand, $Cu_C$ mutation resulted in complete activity loss in *Mycobacterium* NBB4 (Liew et al., 2014), suggesting that this might be the catalytical site. However, the difficulties in engineering of p MMO out of its natural membrane – embedded environment makes it characterization difficult. In addition, the p MMO strictly requires specific membrane compartment to be properly active, which disables the possibility to engineer methane oxidation in non-methanotrophic organisms. Instead, scientists are mainly focused on the next step in methane metabolism (methanol oxidation to formaldehyde), as methanol is acceptable C1 carbon source as well.

### 2.3.2. Methanol oxidation to formaldehyde

The conversion of methanol to formaldehyde is catalyzed by the enzyme methanol dehydrogenase (MDH) (Trotsenko & Murrell, 2008). There are two different forms of this enzyme in methanotrophs: the calcium-dependent MxaFI type, and the lanthanide-containing XoxF type (Chu & Lidstrom, 2016).

MxaFI type MDH is encoded by the *mxa*FI operon (Chistoserdova, 2015). This

operon is composed of genes that encode the large (*mxa*F) and small (*mxa*I) subunits of MDH, the cytochrome *c* electron acceptor (*mxa*G) and proteins for calcium insertion (*mxa*ACKL). Expression of *mxa*FI is controlled by the MxcQE and MxbDM two-component system, as well as by an orphan response regulator, MxaB (Chistoserdova, 2015). The $Ca^{2+}$-dependent MDH (MxaFI type) contains two distinct subunits, α and β, and resembles a tetrameric α2β2 structure. The α subunit is a peptide ~66 kDa in size that contains a pyrroloquinoline quinone (PQQ) molecule and a $Ca^{2+}$ ion. The β-subunit is very small (~8.5 kDa) and folds around the α-component (Anthony, 2004; Chistoserdova, 2015).

XoxF type MDH is encoded by *xox*F genes, and expression is regulated by rare-earth elements (lanthanides) like lanthanum or cerium (Chu & Lidstrom, 2016). Lanthanide-dependent MDH has been isolated from various methanotrophic species during growth in lanthanide-supplemented media (Hibi et al., 2011; Nakagawa et al., 2012; Pol et al., 2014). PQQ-linked Xox enzymes containing lanthanides indicate the existence of alternative metals that contribute to MDH activation and regulation. Since lanthanides are recognized as stronger Lewis acids than calcium, the electrophilic strength of the PQQ molecule is significantly greater than in MxaFI type MDH, which leads to increased efficiency of electron removal from methanol (Chu & Lidstrom, 2016)

### 2.3.3. Formaldehyde oxidation to formate

Formaldehyde ($CH_2O$) is a key intermediate in the oxidation of methane to carbon dioxide by methanotrophic bacteria (Murrell & Jetten, 2009; Trotsenko & Murrell, 2008). The formaldehyde formed from methanol oxidation can be assimilated into cellular carbon via the serine or RuMP pathways (Fig. 2.3) (Pieja et al., 2017). The alternative fate of formaldehyde is its oxidation to formate via formaldehyde dehydrogenase (FalDH) (Trotsenko & Murrell, 2008). Formaldehyde-oxidizing enzymes are divided into two groups: group 1 includes $NAD(P)^+$-linked aldehyde dehydrogenases that may or may not require

reduced glutathione or other co-factors, and group 2 includes dye (cytochrome)-linked dehydrogenases (DL-FalDH). The activity of group 2 dehydrogenases is measured by the reduction of dyes like 2,6-dichlorophenol (Attwood et al., 1992). In methanotrophs, DL-FalDH are less studied than the $NAD^+$-linked enzymes. The DL-FalDH enzyme isolated from *Methylosinus trichosporium* OB3b is described as "a broad-substrate-range aldehyde (C1 to C10) dehydrogenase with a subunit molecular mass of 22,000 Da" (Zahn et al., 2001).

One of the best-characterized formaldehyde oxidation pathways is the tetrahydromethanopterin ($H_4$MPT)-linked $CH_2O$ oxidation (Fig. 2.3) (Trotsenko & Murrell, 2008). The whole process is performed through 4 steps: the formaldehyde activating enzyme (Fae) condenses $CH_2O$ with $H_4$MPT and forms methylene-$H_4$MPT, methylene-$H_4$MPT is oxidized by $NADP^+$ dependent methylene-$H_4$MPT dehydrogenase (MtdB), methenyl-$H_4$MPT is converted to formyl-$H_4$MPT via Methenyl-$H_4$MPT cyclohydrolase (Mch) and formyl-transferase-hydrolase converts formyl-$H_4$MPT to formate (Martens and Berner, 1977.; Trotsenko & Murrell, 2008).

### 2.3.4. Formate oxidation to carbon dioxide

The last step of aerobic methane oxidation in methanotrophs is the oxidation of formate ($CH_2O_2$) to $CO_2$. This reaction is catalyzed by a $NAD^+$-dependent formate dehydrogenase (Fdh) located in the cytoplasm (Trotsenko & Murrell, 2008). While some methanotrophs favor the cyclic pathway of methane oxidation that assumes formaldehyde assimilation through the RuMP or serine cycle, other methanotrophs utilize a linear type of methane oxidation that results in $CO_2$production at the end of the process (Pieja et al., 2017) . The final oxidation of formate is an important step because it generates NADH, an important metabolic reductant (Martens and Berner, 1977.; Tays, 2019).

## 2.4. Carbon assimilation in methanotrophs

Methane-derived formaldehyde is assimilated to form intermediates of the central metabolic routes that are subsequently used for biosynthesis of cell material. Methanotrophs are characterized by large metabolic diversity, and they employ a wide variety of carbon assimilation pathways (RuMP pathway, serine cycle, Embden-Meyerhof-Parnas (EMP) pathway, Entner-Doudoroff (EDD) pathway, Bifidobacterium shunt (BS), the Ethylmalonyl-CoA pathway, Calvin-Benson-Basham (CBB) cycle, Reductive acetyl-CoA (Wood-Ljungdahl) pathway and the Reductive TCA cycle (Kalyuzhnaya & Xing, 2018)).

### 2.4.1. Ribulose-Monophosphate pathway (RuMP) for formaldehyde assimilation

The RuMP pathway was first described in the late 1960s. This pathway for formaldehyde assimilation is characteristic of gammaproteobacterial methanotrophs (Trotsenko & Murrell, 2008)). Initially, it was believed that two enzymes from the RuMP cycle are unique for C1-oxidizing organisms (Yasueda et al., 1999). Later investigations have shown that both enzymes also exist in heterotrophic species where they play a role in formaldehyde detoxification (Mitsui et al., 2003).

The RuMP cycle consists of three main parts: fixation, cleavage, and rearrangement (Fig. 2.4). Each of these steps contains metabolic reactions that are catalyzed by specific enzymatic systems (Trotsenko & Murrell, 2008):

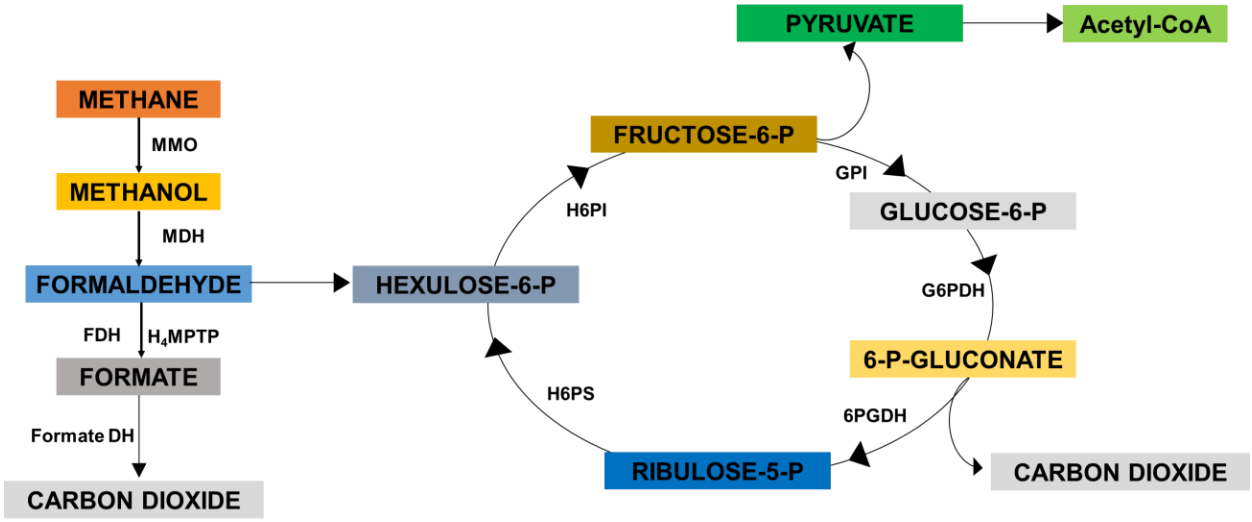


Figure 2.4. Simplified metabolic pathway of Ribulose Monophosphate (RuMP) cycle in gammaproteobacterial methanotrophs. Formaldehyde is generated from methanol via methanol dehydrogenase (MDH). Formaldehyde is then either oxidized to formate via formaldehyde dehydrogenase (FDH) or assimilated spontaneously to create methylene tetrahydropteryn ($H_4$MPTP). Formate generated after formaldehyde oxidation via FDH is oxidized to carbon dioxide via formate dehydrogenase. D-arabino-3-hexulose-6-phosphate (hexulose-6-P) is built in the reaction of formaldehyde with ribulose-5-phosphate (catalyzed by 3-hexulosephosphate synthase (H6PS). The unstable product is rapidly isomerized to fructose-6-P via hexulose-6-phosphate isomerase (H6PI). The enzyme glucose-6-phosphate isomerase (GPI) converts fructose to glucose-6-phosphate, and glucose-6-phosphate dehydrogenase creates 6-phospho gluconate. 6-phosphogluconate dehydrogenase (6PGDH) regenerates ribulose-5-phosphate with the release of carbon dioxide, and hexulose-6-phosphate synthetase (H6PS) condenses formaldehyde with regenerated ribulose-5-phosphate.

2.4.2. Serine pathway for formaldehyde assimilation

Assimilation of formaldehyde via the serine cycle (Fig. 2.5) is the strategy employed by alphaproteobacterial methanotrophs (Trotsenko & Murrell, 2008). This pathway is also the precursor pathway to produce PHB.

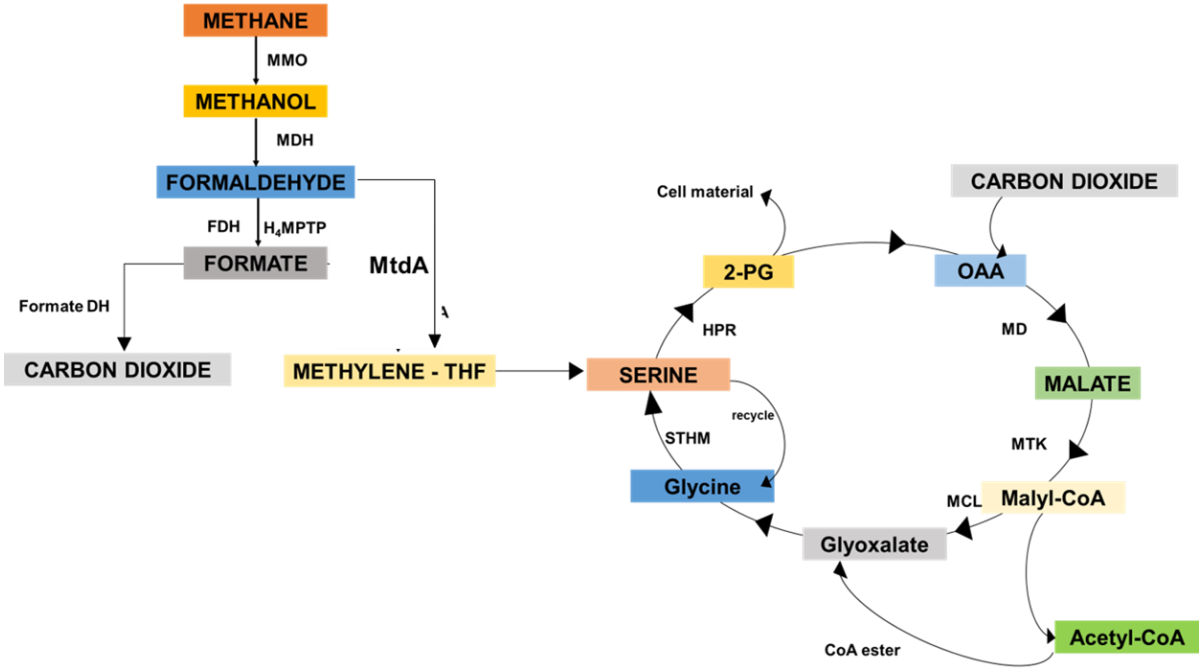


Figure 2.5. Simplified serine cycle in methanotrophic bacteria. Formaldehyde is generated via methanol dehydrogenase (MDH), and formaldehyde can either be oxidized to formate via formaldehyde dehydrogenase (FDH) or be assimilated spontaneously to create methylene tetrahydropteryn ($H_4$MPTP). Formate generated after formaldehyde oxidation via FDH is oxidized to carbon dioxide via formate dehydrogenase. Formaldehyde is condensing with tetrahydrofolate (THF) to create N5,N10-methylene THF; next is condensation with glycine to create serine (catalyzed by serine hydroxytransmethylase (SHTM). The enzyme serine-glyoxylate aminotransferase (SGAT) transfers amino group to the glyoxalate forming glycine and hydroxypyruvate (catalyzed by hydroxypyruvate reductase (HPR)). After phosphorylation of hydroxypyruvate by ATP glycerate kinase 2-phosphoglycerate is created

(2-PG). 2-PG is isomerized to phosphoenol pyruvate (PEP) and carboxylated to oxaloacetate (OAA). OAA is converted to malate via malate dehydrogenase (MD). Malate is converted to malyl-CoA via malate thiokinase (MTK). Malyl-CoA is split to glyoxalate and acetyl-CoA via malyl-CoA lyase (MCL). Acetyl-CoA is the main product of serine cycle.

### 2.4.3. Other carbon assimilation pathways in methanotrophs

Methanotrophs that belong to Verrucomicrobia (such as *Methylacidiphilum fumariolicum* SolV) contain enzymes from the Calvin-Benson-Basham (CBB) cycle, which indicates their ability to fix carbon dioxide (Khadem et al., 2012). In gammaproteobacterial methanotrophs, 5-15% of cellular biomass originates from carbon dioxide assimilation and alphaproteobacterial methanotrophs assimilate carbon dioxide to up to 50% of their biomass (Strong et al., 2015, 2016). One of the most important biochemical pathways for C1 assimilation is the Ethyl-Malonyl-CoA (EMC) cycle (Matsen et al., 2013; Yang et al., 2013). In the initial steps of the serine cycle, serine-hydroxymethyltransferase (SHMT) utilizes glycine to form serine via metabolic condensation with methylene-THF (Khadem et al., 2012). While serine is transaminated to hydroxypyruvate, the regeneration of glycine is done via transaminase using glyoxalate (Trotsenko & Murrell, 2008). The EMC pathway yields glyoxylate that will further be used for regeneration of glycine enabling the continuous operation of the serine cycle. Moreover, glyoxalate can be used for malate generation via malate synthase, which will replenish TCA cycle metabolites required for further cellular biosynthesis (O. K. Lee et al., 2016).

## 2.5. The role of carbon source in methanotrophic metabolism

The common feature among all methanotrophs is their ability to thrive on methane or methanol (C1 compounds). However, there is substantial differences between gammaproteobacterial and alphaproteobacterial methanotrophs in terms of preferable carbon source. While many gammaproteobacterial organisms grow equally well on both carbon sources (Fu et al., 2019): alphaproteobacterial methanotrophs generally show strong preference for methane (Lazic et al., 2021; Sugden et al., 2021). Since methanol-based biotechnology is a rapidly evolving field for bioproduction (Fu et al., 2019), and since methanol is a readily available substrate not burdened by mass transfer issues, having a single strain that can thrive on both carbon sources is highly beneficial.

From a physiological point of view, growth on methane and methanol is expected to be similar, as there is only one enzyme, MMO, upstream of methanol metabolism. In the case of methane, pMMO (or sMMO) uses molecular oxygen, where one O atom is used to create methanol, and the other is incorporated into water. The electrons that drive this oxidation originate from different sources for gamma- and alphaproteobacterial methanotrophs. Electrons that drive methane oxidation in gammaproteobacterial methanotrophs originate from methanol dehydrogenase (MDH). This mechanism is called “direct coupling.” Briefly, the reduction of an oxidized electron donor (which occurs simultaneously with consumption of molecular oxygen) is coupled to the oxidation of methanol to formaldehyde via MDH. Another methane-to-methanol oxidation mechanism, known as “uphill electron transfer”, is also present in gammaproteobacterial methanotrophs. In this mode of action, electrons that drive methane oxidation originate from cytochrome *c* and complex III in the electron transport chain. On the other hand, the electron donor for methane oxidation in alphaproteobacterial methanotrophs has not been resolved yet (Kalyuzhnaya et al., 2015). The biomass yield that these organisms generate while growing on methane is significantly

lower than in gammaproteobacterial methanotrophs, which was attributed to the relatively expensive route for formaldehyde assimilation via the serine cycle. However, recent progress in Genome Scale Metabolic Models (GEM) revealed another reason for lower biomass yield in alphaproteobacterial methanotrophs (Bordel et al., 2019) associated with a different electron donor for methane oxidation. Instead of direct coupling or uphill electron transfer, alphaproteobacterial methanotrophs employ a mechanism called the "redox arm". In this system, the ubiquinone supplies electrons that originate from complex I (NADH dehydrogenase) to the pMMO (Bordel et al., 2019). This hypothesis was recently confirmed when the catechol-driven inhibition of complex I prevented methane oxidation in *Methylocystis hirsuta* (Bordel et al., 2019) .

When growing on methanol as the carbon source, no methane oxidation takes place, thus the energetic balance is significantly altered (Fu et al., 2019). Since methanol oxidation to formaldehyde generates electrons that would be used to support methane oxidation in the direct coupling mechanism (Bordel et al., 2019), in the absence of methane these electrons enter the electron transport chain, which is followed by oxygen consumption, proton pumping, and ATP synthesis through oxidative phosphorylation. The consequence of the electron re-distribution is a lower level of NADH dehydrogenase flux and less ATP generated through oxidative phosphorylation (Fu et al., 2019), which can explain the slower growth of alphaproteobacterial methanotrophs on methanol.

However, gammaproteobacterial methanotrophs do not exhibit growth reduction on methanol, which is explained by a more efficient formaldehyde detoxification strategy (Sugden et al., 2021). Despite its toxicity, formaldehyde is a significant cellular metabolite. In general, it is generated by methylotrophs and methanotrophs during the oxidation of short-chain hydrocarbons and its further metabolic fate is specific for each group of organisms.

Among methanotrophs, the Gammaproteobacteria *Methylomicrobium album* BG8 is one that thrives exceptionally well on methanol due to glutathione (GSH)-dependent formaldehyde detoxification (Chen et al., 2016). Briefly, this organism performs a nucleophilic addition of GSH to formaldehyde to form S-hydroxymethylglutathione (HMGS). This reaction can be spontaneous, but in *M. album* BG8 it is likely catalyzed by a formaldehyde-activating enzyme (Sugden et al., 2021). Next, the HMGS is oxidized to S-formylglutathione (SFG) via zinc-containing $NAD^+$-dependent alcohol dehydrogenase. In the final step, formate is produced, where GSH is regenerated and able to participate in further detoxification processes (Chen et al., 2016). Carbon source dependent metabolic changes are notable in gammaproteobacterial methanotrophs, not only at the level of formaldehyde detoxification, but also in formaldehyde assimilation (Nguyen et al., 2020; Sugden et al., 2021). Unlike *Methylomicrobium alcaliphilum* 20Z, *M. album* BG8 performs the EDD variant of the RuMP cycle for formaldehyde assimilation when growing on methanol (Kalyuzhnaya et al., 2013; Sugden et al., 2021), whereas *Methylomicrobium buryatense* 5GB1 directs formaldehyde toward the EDD pathway (Fu et al., 2019). However, the pentose phosphate (PP) variant of the RuMP cycle has been identified only in *M. album* BG8 thus far (Sugden et al., 2021). Unlike many gammaproteobacterial methanotrophs, little is known about alphaproteobacterial methanotrophs and their metabolic response to methanol except that they grow poorly or not at all, and that growth on methanol leads to stress-related (starvation) metabolic pathways (Tays et al., 2018).

## 2.6. The role of nitrogen source in methanotrophic metabolism

Methanotrophic bacteria are an important link between the global carbon and nitrogen cycles, and factors that influence their metabolism must be assessed and evaluated (Strong et al., 2015, 2016). Findings that reported the negative influence of nitrogen fertilizers on methane consumption (Duc Nguyen et al., 2021) directed methanotrophic researchers toward evaluation and determination of nitrogen influence on methane metabolism (Bodelier & Laanbroek, 2004). The kinetics of methane oxidation in soil is divided into high affinity and low-affinity oxidation (Bender & Conrad, 1992). Low-affinity methane oxidation occurs in wetlands and other methane-producing soils. Methanotrophic communities in these soils contain MMO enzymes with Km values for methane in the μM range (Bender & Conrad, 1992; Bodelier & Laanbroek, 2004). High-affinity methane oxidation is observed in forest soils with low methane flux that originates from atmospheric diffusion. Thus, methanotrophs that inhabit forest ecosystems developed MMO with lower Km values (Bender & Conrad, 1992; Bodelier & Laanbroek, 2004).

Methane consumption was evaluated in upland and wetland soils, and it was a general conclusion that ammonium inhibits methane uptake (Bodelier & Laanbroek, 2004). One of the potential explanations of this phenomenon is the high similarity between MMO and ammonia monooxygenase (AMO) (Norton et al., 2002). Ammonia-oxidizing bacteria (AOB) are physiologically close to aerobic methanotrophs. Both groups can oxidize a similar substrate range, including ammonia and methane (Bedard & Knowles, 1989.; Schnell & King, 1996). The difference in the kinetics of oxidation is related to the different Km values of MMO and AMO for their substrates (Nyerges & Stein, 2009). The activity of both AMO and pMMO is stabilized by copper, which is part of their active sites (Ensign et al., 1993). The ability of some methanotrophs to produce hydroxylamine ($NH_2OH$) by ammonia oxidation reveals the possibility that inhibition of methane uptake could occurs due to

hydroxylamine toxicity (Chandran et al., 2011). On the other hand, some methanotrophic strains express an enzymatic system for hydroxylamine detoxification (hydroxylamine dehydrogenase enzymes or HAO) and, for them, growth reduction mainly originates from competitive inhibition of MMO by ammonia (Campbell et al., 2011). Even though methane and ammonia oxidation processes are physiologically similar (Klotz & Stein, 2008), one substantial difference is related to the ability of these organisms to utilize electrons from hydroxylamine oxidation. Where AOB possess the hydroxylamine ubiquinone redox module (c552 and c554) that delivers electrons from hydroxylamine oxidation to the ubiquinone pool enabling further ETC operation and energy generation, methanotrophs lack these two cytochromes; thus, they cannot use ammonia as an energy source (Klotz & Stein, 2008).

Nitrate ($NO_3$-) also affects the metabolism of methane by some methanotrophs (Klotz & Stein, 2008). For example, *Methylocystis* sp. strain Rockwell is extremely sensitive to nitrate/nitrite toxicity, while strains that express nitrite and nitric oxide reductase enzymes can detoxify nitrite (Klotz & Stein, 2008). Nitrate-related growth inhibition might occur in strains that can produce nitrous oxide ($N_2O$) as well (Klotz & Stein, 2008). However, other groups of methanotrophs can utilize nitrate as a terminal electron acceptor and survive under hypoxic conditions (Kits et al., 2015). A recent study showed that *Methylomonas denitrificans* FJG1 is not only capable of respiring nitrate and coupling this activity to ATP generation, but the terminal product of this activity is nitrous oxide ($N_2O$) (Kits et al., 2015). Moreover, $N_2O$ can trigger the Reactive Oxygen Stress (ROS) response (Zhao et al., 2007) , thus growth will be further decreased relative to oxygen respiration (Kits et al., 2015). However, $N_2O$ production does not necessarily mean growth inhibition. In *M. denitrificans* FJG1, the denitrification pathway that occurs under hypoxia provides cellular energy (Kits et al., 2015). In fact, the existence of alternative electron acceptors is beneficial in natural ecosystems (Klotz & Stein, 2008). However, for industry, nitrate might be seen as an

inhibitory factor that affects yield and production of particular methanotrophic strains at large scale, making it a "cost-driver" of production (Tays et al., 2018).

In general, methanotrophs can use nitrate or ammonia as a nitrogen source (Stein, 2018), but the preference varies among strains (Tays et al., 2018; Zaldívar Carrillo et al., 2018) and optimization must be accomplished on a strain-to-strain basis. This is not surprising, as earlier studies showed the distinct effect of nitrogen source on methane metabolism in natural environments (Chandran et al., 2011; Klotz & Stein, 2008). In addition, one of the first comparative studies from 1994 (*M. album* BG8 vs *M. trichosporium* OB3b) revealed distinct response to different nitrogen forms in organisms. According to these findings, gammaproteobacterial methanotroph (*M. album* BG8) was more sensitive to nitrite than alphaproteobacterial organism (*M. trichosporium* OB3b). However, the inhibition of methane oxidation by nitrite was abolished at higher methane concentrations, while the increased level of ammonium was followed by reduced methane oxidation (King and Schnell, 1994). These findings showed differential sensitivity to different nitrogen sources among methanotrophs, but also showed that ammonium inhibition originates from cometabolism by MMO, while nitrite inhibition is indirect (King and Schnell, 1994). Nevertheless, it has been clear that the nitrogen response is variable, and the detailed physiological and metabolic studies are required before field or laboratory experiments that involve methanotrophs are performed. At the same time, another study a compared the growth of the same two organisms and showed that both, *M trichosporium* OB3b and *M. album* BG8 can thrive on a combination of methane and methanol, but *M. trichosporium* OB3b had better growth under nitrogen limitation (Graham et al., 1993). Later, it was confirmed that *M. trichosporium* OB3b encodes the ability to fix atmospheric nitrogen ($N_2$) (Stein, 2010). Another study compared the strains *Methylocystis* sp. Rockwell and *M. album* BG8. While nitrate significantly inhibited growth of the former, *M. album*

BG8 had increased growth withnitrate. The situation was the opposite with ammonia as the nitrogen source (Nyerges et al., 2010). High ammonia tolerance was also identified in another species, *Methylocystis* sp. strain SC2 (Dam et al., 2014).

The effect of nitrogen source is highly dependent on the type of carbon source (methane or methanol) provided to the strain. Nitrate did not inhibit the growth of methanotrophs while they were growing on methane; however, when growing on methanol, nitrate had a stronger inhibitory effect than ammonia (Tays et al., 2018). Overall, results from various studies under laboratory conditions clearly indicate that nutrient combination and concentration must be analyzed and optimized on an individual, strain-by strain level (Chandran et al., 2011; Dam et al., 2014; Tays et al., 2018). Even though metabolic pathways for most methanotrophs are well understood, there is no available universal tool that can predict the optimal conditions for high biomass yield. Furthermore, the type and level of metabolites change depending on available nutrient sources (Tays et al., 2018), hence, it would be beneficial to develop an algorithm-based model for simulating a variety of growth conditions to better predict the optimal nutrient combinations that will result in the highest biomass and product yield.

## 2.7. The production of value-added products by methanotrophs

The metabolism of aerobic methanotrophic bacteria has been studied in detail for decades (Trotsenko & Murrell, 2008) with numerous reports about specific and diverse enzymatic networks enabling methanotrophs to thrive under many environmental conditions (Murrell & Jetten, 2009; Kalyuzhnaya & Xing, 2018; O. K. Lee et al., 2016; Trotsenko & Murrell, 2008). Interest in methanotrophic metabolism has expanded in the last few decades when the potential to transform methane into valuable bioproducts was discovered (Pieja et al., 2017). The abundance and low price of natural gas contributed to the increased interest in methane metabolism in the scientific as well as the industrial communities (Strong et al., 2015, 2016). The best studied products from methane include methanol, polyhydroxyalkanoates, and single cell protein (Strong et al., 2015, 2016). However, there are other value-added chemicals (such as biofuels) that can be generated by methanotrophs (Pieja et al., 2017; Strong et al., 2015, 2016). The expansion of metabolic/genetic engineering manipulations in various species can result in improved production of target bioproducts (Lee et al., 2016; Pieja et al., 2017; Strong et al., 2015, 2016) .

### 2.7.1. Single cell protein

The production of single cell protein (SCP) began in the 1950s due to a shortage of protein for animal nutrition, which is disconnected from human protein sources (Lee et al., 2016; Strong et al., 2015, 2016). Even though the production of low-cost soy protein had a negative influence on methane-derived SCP (Gao et al., 2012), SCP is still considered to be the most successful, commercially produced methane-derived product (Lee et al., 2016; Strong et al., 2015). The pioneers in commercial production of methanotrophic SCP was a company based in Denmark in the 1980s (UniBio A/S) (Strong et al., 2015). The term "single–cell protein" was introduced in the food industry as a "protein-rich nutrient that serves as a dietary supplement for livestock and humans" (Ritala et al., 2017). This methane-derived protein source has been used widely for nutrition of pigs, broiler chickens, mink, fox, Atlantic salmon, rainbow trout, and Atlantic halibut (Strong et al., 2015). One of the most famous SCP foods is marmite, the spread manufactured by Unilever (Ritala et al., 2017). Marmite is a result of *Saccharomyces cerevisiae* digestion of starch. Vegemite is a similar product made in Australia (Kerr & Schulz, 2016). Another fungi-based SCP is called Quorn. Quorn is produced by *Fusarium venenatum* using oxygen, nitrogen, glucose, and minerals (Ritala et al., 2017). The disadvantage of sugar-based production of SCP is high cost and interference with food supplies (Ritala et al., 2017; Strong et al., 2015, 2016). In comparison, methane is a highly abundant and cheap industrial waste (Strong et al., 2015, 2016). One of the potential problems with microbial SCP production is their high DNA/RNA content that can trigger an immune response in consumers (Strong et al., 2015). This was revealed in toxicology studies on UniBio A/S products that resulted in increased immune response and significant bladder and gut damage in rats. Thus, SCP was approved only as food for animals with a short lifespan (NCSF, 2006). The other problem is contamination, the most common issue in microbiology research and commercial production (Strong et al., 2015). SCP-

producing *Methylococcus capsulatus* Bath cultures were repeatedly contaminated by three different bacterial genera (*Aneurinibacillus, Brevibacillus*, and *Ralstonia*) (Bothe et al., 2002). However, none of these contaminants were toxic and their presence was even beneficial since they stabilized the culture by consuming other metabolic products that could cause growth inhibition (Bothe et al., 2002; Strong et al., 2015).

### 2.7.2. Lipids

Methanotrophic cells contains complex internal membrane systems (ICM) that hold and stabilize pMMO enzymes (Bowman et al., 1991). The ICM arrangement varies among alpha- and gammaproteobacterial methanotrophs. While membranes in alphaproteobacterial methanotrophs resemble the structure of stacked discs, ICM organization in gammaproteobacterial methanotrophs follows the contour of the outer membrane (Trotsenko & Murrell, 2008). The membrane lipids (phospholipids) in methanotrophs are categorized as phosphatidylglycerol and phosphatidylethanolamine (Strong et al., 2016). In gammaproteobacterial and alphaproteobacterial methanotrophs the most prevalent fatty acids are C16:1 and C18:1, respectively (Bowman et al., 1991; Fang et al., 2000; Fei et al., 2014) Methanotrophs accumulate up to 20% lipids in their biomass; hence, they have high potential for use in biofuel production (Conrado & Gonzalez, 2014). The slight improvement in methanotrophic lipid content (20% to 35%) would justify their use in biofuel production as an alternative for petroleum-derived fuels. Microbial production of lipid-based biofuels has been researched extensively in the last few decades (Strong et al., 2015, 2016). Yeast and microalgae accumulate lipids (Eshinimaev et al., 2002) up to 20% of dry mass; hence, these organisms have been exploited as biofuel producers for years (Strong et al., 2016). Microbial lipids are synthesized in a short life cycle, and unlike plants, microbes are not as dependent on location, season or climate, which opens possibilities for easier scale-up production. However, the cost of carbon source and the food vs fuel debate often prevent efficient

commercialization of microbial lipids in the biofuel industry (Q. Li et al., 2008). The accumulation of lipids in methanotrophic cells occurs in the presence of sufficient carbon and nutrient deficiency. Under these stress-related conditions the cell synthesizes lipids and stores them as a source of energy and reductant (Fei et al., 2014). Currently, there is a patent (US20150353971) for lipid-containing methanotrophic/methylotrophic biomass conversion into oil that is further refined to generate fuel (Strong et al., 2015, 2016). However, the difficulties in the process of transformation and extraction of phospholipids slows down their commercial production. On the other hand, non-structural lipids are more promising as a platform for biofuels. The University of Washington has developed a project funded by ARPA-E that is focused on genetic modifications of methanotrophs to increase synthesis of non-structural lipids that are easier to extract and transform into biofuel (Strong et al., 2015). Microbially-derived lipids can be applied to the human health industry as well. Lipids are commercially produced as food supplements that decrease the ratio of LDL/HDL cholesterol and increase the level of immunoprotectant docosahexaenoic acid in the plasma (Müller et al., 2004).

### 2.7.3. Ectoine

Ectoine is cyclic imino acid that helps bacteria survive in salty conditions. The primary function of ectoine in bacteria is molecular stabilization of enzymes, nucleic acids, and DNA-protein complexes (Strong et al., 2015, 2016). This molecule is often used in the cosmetic industry to produce moisturizer (Mustakhimov et al., 2010). The commercial strain for ectoine production is *Halomonas elongata* DSM 2581T (Schwibbert et al., 2011). Among methanotrophs, commercial production of ectoine has been performed by *Methylomicrobium alcaliphilum* 20Z (Mustakhimov et al., 2010). In this organism, three key enzymes participate in ectoine synthesis: diaminobutyric acid aminotransferase, diaminobutyric acid

acetyltransferase, and ectoine synthase. The complete metabolic system is regulated by a "MarR-like" transcription regulator (Mustakhimov et al., 2010).

### 2.7.4. Bioproducts from genetically engineered methanotrophs

The concept of genetic engineering in methanotrophs was established in the last century when *Methylosinus* sp. strain 6 was modified using a Tn5-transposon system (Toukdariant & Lidstromt, 1984). Over the past few decades, the large biotechnological potential of methanotrophs has been heavily exploited (Strong et al., 2015, 2016) and the idea of commercial production of a value-added product using cheap single-carbon feedstock brought up the approach that assumes application of metabolic engineering in methanotrophic species (Kalyuzhnaya et al., 2015). Even though genetic tools are available for some strains, few products are successfully produced by engineered methanotrophs. The most famous products obtained from engineered methanotrophs are isoprene (Strong et al., 2015), 2,3-butanediols (Duc Nguyen et al., 2021), farnesene (Strong et al., 2016) and lactate (Henard et al., 2016). Among these three compounds, farnesene is probably the most important for global needs. This molecule is a precursor for diesel, lubricants, rubber, plastic, and it is commonly used in the cosmetic industry (Strong et al., 2015, 2016). Another successfully produced class of compound are carotenoids – yellow-to-orange terpenoids that play a role in oxidative damage prevention (Heider et al., 2014). Carotenoids are commonly used in the food, medical and cosmetic industries (Strong et al., 2016). In terms of carotenoids, methylotrophs are considered more successful than methanotrophs, as methanol is another abundant, low cost and unlike methane, soluble carbon source. The genes for carotenoids biosynthesis have been identified in facultative methylotroph *Methylobacterium extorquens* AM1 that is known to produce pink carotenoid (Peel and Quayle, 1961; Downs and Harrison, 1974). Th detailed genomic characterization along with genetic tools' development was done in 2003 (Van Dien et al., 2003). Currently, there is an established production of carotenoids

by *Methylomonas* sp. strain 6 that was initiated with the expression of the canthaxanthin (carotenoid) gene in combination with enzymatic systems for its conversion to astaxanthin in this organism (Ye et al., 2007).

Methanotrophs are commonly used as a platform to produce recombinant proteins andenzymes, such as MMO and β-glucuronidase (Strong et al., 2015). Theoretically, species thatnaturally produce surface layers (such as *Methylococcus, Methylothermus*, and *Methylomicrobium*) are potential candidates for genetic engineering and commercial production of exogenous therapeutic or IgG proteins (Khmelenina et al., 2015).

### 2.7.5. Polymers

Polymers are substances whose molecular structure contains more than one same/similar units, bonded together via specific chemical bonds (Liu et al., 2020). Broadly, biopolymers can be categorized as externally and internally stored molecules, and each of these two groups has a different role in metabolism. In addition, both types of polymers can be significant from an industrial perspective and can be produced from methane and methanol by methanotrophs.

### 2.7.6. External biopolymers

The most famous external biopolymers are extracellular polysaccharides (EPS). Due to their colloid and adhesive properties, EPS are often used in the food industry, as well as in pharmaceutical, textile, and oil industries. The current industrial production of EPS relies on algae and plants (Koffas et al., 2003). However, the controversy of food vs fuels motivated researchers to seek for alternative, “nonedible raw material” that can be used for EPS production (Malashenko et al., 2001; Strong et al., 2015). Methane satisfied these criteria for alternative feedstock. In addition, methanotrophs contain genetic machinery that enables them to synthetize EPS (Dedysh et al., 2002; Malashenko et al., 2001; Strong et al., 2015).

Methane-based EPS production was performed in chemostats via gammaproteobacterial methanotrophs, and production ranged from 0.03-0.43 g/L. Moreover, the achieved viscosity was comparable to the viscosity of EPS synthesized by other known producers (2.2 to 4.0 $mm^2/s$) (Malashenko et al., 2001; Strong et al., 2015). However, one possible complication with methanotrophic EPS production is the negative influence of accumulated polysaccharide on further gas uptake (Dedysh et al., 2002), which might delay growth and EPS production from methane.

### 2.7.7. Internal biopolymers

Another class of biopolymers are internally produced metabolites that serve as storage molecules. The accumulation of internal biopolymers occurs in response to nutrient limitation in the presence of sufficient carbon (Strong et al., 2015). The most significant internal biopolymers are polyhydroxyalkanoates (PHA) (such as polyhydroxybutyrate (PHB) and polyhydroxybutyrate covalerate (PHBV)) (Chidambarampadmavathy et al., 2015). PHAs have multiple beneficial properties such as biodegradability, biocompatibility, and thermoplasticity, which make them a potential alternative to conventional, petroleum-derived plastics (Strong et al., 2016). Plastic materials are used worldwide and have numerous applications and enormous significance in all types of industrial activities (Chidambarampadmavathy et al., 2015). However, oil derived (conventional) plastics are only 5-7% recyclable, and consequences to the environment are enormous (https://greenhome.co.za/the-pros-and-cons-of-bioplastics/). At least 50% or more of plastic waste is disposed into landfills. The strategy of disposal eventually leads to accumulation of material, and lack of oxygen prevents the efficient breakdown of disposed waste https://www.unep.org/news-and-stories/story/world-leaders-set-sights-plastic-pollution. More harm to the environment is done when plastic waste is littered (around 45%). Plastic waste is washed into oceans, rivers and streams where it is degraded into smaller pieces and

commonly introduced into the food chain (Bezirhan Arikan & Duygu Ozsoy, 2015). A study from 2010 revealed 580,000 pieces of plastic are present per square kilometer in the ocean, which is extremely harmful to all lifeforms in and around these ecosystems (World Leaders Set Sights on Plastic Pollution, 2018). Plastic degradation releases toxic chemicals, which is an additional threat to wildlife, humans, and the environment (Chidambarampadmavathy et al., 2015). Because of these many environmental issues, researchers have focused on exploring environmentally friendly materials such as biodegradable plastic. Biopolymers such as PHB and PHBV are stored as granules intracellularly in microorganisms where they serve as a source of energy and/or reducing power during starvation conditions (Mitra et al., 2022).

2.8. PHB pathway

The metabolic pathway for PHB production (Fig. 2.6) involves three enzymes encoded by the *pha*CAB operon. The enzyme PhaA catalyzes condensation of two acetyl-CoA molecules to form acetoacetyl-CoA. In the next step, the enzyme PhaB reduces acetoacetyl-CoA to the (R)-3-hydroxybutyryl-CoA monomer. In the final step, PHB synthase (PhaC) catalyzes formation of stable polymer (Fig. 2.6) (Pieja, Rostkowski, et al., 2011).

The catabolism of PHB involves two types of degrading enzymes known as PHA depolymerases (PhaZ). Intracellular depolymerases (iPhaZ) perform active hydrolysis of PHB accumulated asPHB granules in the cell. This degradation is often linked to energy extraction during starvation (Jendrossek & Handrick, 2002; Sudesh & Abe, 2010; Volova et al., 2006). iPhaZs can only recognize and degrade native, amorphous forms of PHB (except for iPhaZ from *Bacillus megaterium* which can degrade external layers of native PHB granules (H. J. Chen etal., 2009; Sznajder & Jendrossek, 2011). The degradation of native PHB granules usually involves an activator protein, which is replaced with trypsin or alkaline treatment during *in vitro* experiments (Merrick &

Doudoroff, 1964). In some cases, PHB granules can be self- hydrolyzed (Uchino et al., 2007). The complete intracellular PHB degradation involves oxidation of 3-hydroxybutyrate monomers to acetoacetate via NADPH-dependent 3- hydroxybutyrate dehydrogenase, followed by the esterification of acetoacetyl-CoA via 3-ketoacid-CoA transferase (CoA is derived from succinyl-CoA or acetoacetyl-CoA synthases) (Martinez-Tobón, 2019.; Miller & Seebach, 1993).

Another type of PHB degrading enzymes is extracellular depolymerase (ePhaZ). These enzymes are used by non-PHB producing organisms that can utilize PHB as the sole carbon source. Extracellular PhaZs usually do not resemble the structure of intracellular enzymes, and they recognize crystalline and semi-crystalline forms of PHB.

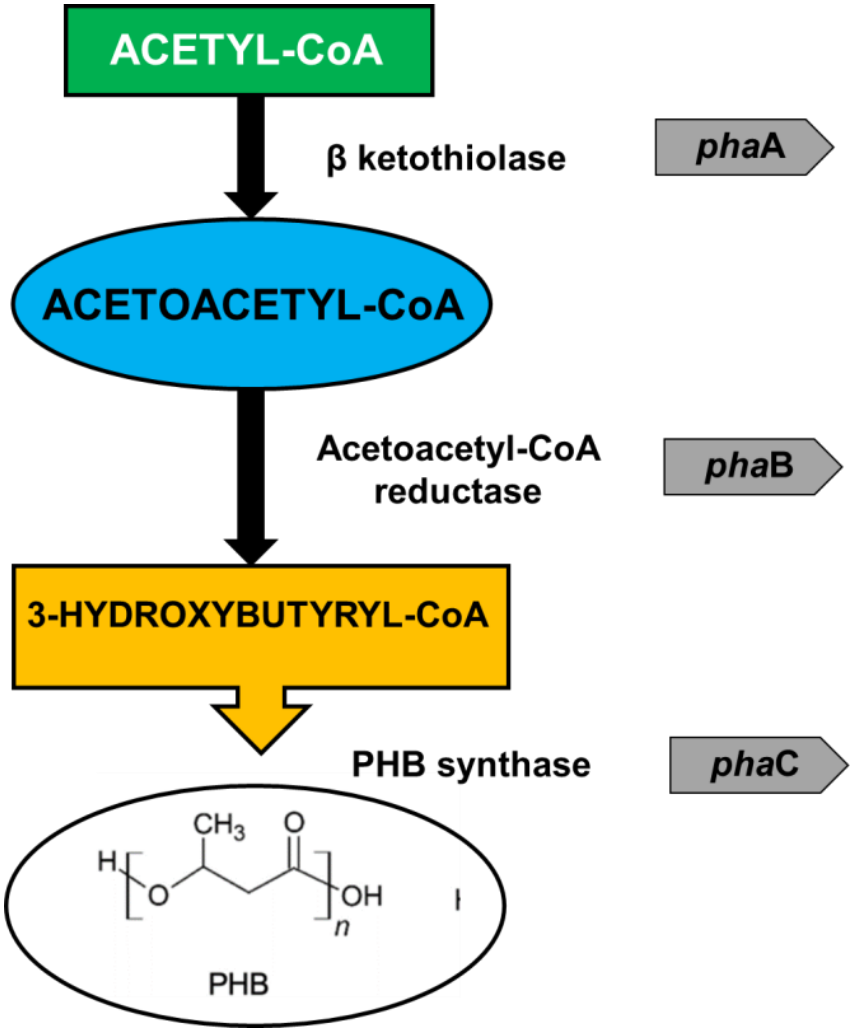


Figure 2.6. Biosynthetic pathway for polyhydroxybutyrate (PHB) synthesis in methanotrophs. Two acetyl-CoA molecules are condensed via β ketothiolase encoded by gene *phaA*. The acetoacetyl-CoA created in previous reaction is reduced to 3-hydroxybutyryl-CoA via acetoacetyl-CoA reductase (encoded by gene *phaB*). In the final step, the enzyme PHB synthase encoded by gene *phaC* creates PHB.

### 2.8.1. Microbial PHB production

The production of PHB has been documented in alphaproteobacterial, but not gammaproteobacterial, methanotrophs through the serine cycle for formaldehyde assimilation. The yield of PHB is highly affected by pH, temperature, trace elements, macronutrients and the type and amount of available carbon source (Mitra et al., 2022; Strong et al., 2016). Currently, there are three routes for PHB production: bacterial fermentation, genetically modified plants, and cell-free systems using enzymatic catalysts (Tobón-Martinez, 2019). Microbial PHB production has been commercialized using glucose, cane starch, palm oil, cassava waste, wheat bran and molasses as carbon sources (feedstock) (Isabel- Tobón, 2019). However, the cost of feedstock is significantly slowing down the industrialization of bioplastic from these carbon sources (Strong et al., 2015, 2016). The price of PHB is strongly influenced by the type of organism and feedstock used for its production. For example, in 2015, PHB synthetized by *Cupriavidus necator* cost $16/kg (Chidambarampadmavathy et al., 2015), which was four times greater than the production by recombinant *E. coli* in 2000 ($4/kg) (Suk Ahn et al., 2000).

Considering the high cost and difficulties of commercialization, there has been increased interest in discovering microbial producers that can utilize cheap carbon sources for production of biopolymers such as PHB or PHBV. Methanotrophs fit perfectly in this model (Strong et al., 2015, 2016). However, when compared to the famous PHB producer *Alcaligenes eutrophus*, methanotrophs did not show promising results. The PHB produced by *Methylobacterium* had a lower molecular weight and the extraction was difficult compared to *Alcaligenes*-produced PHB (Mitra et al., 2022). Regardless of existing disadvantages and difficulties, cheapness and availability of feedstock keep methanotrophs as the primary choice for bioplastic commercialization (Khosravi-Darani et al., 2013) and several companies are now successfully making PHB using methanotrophs with methane as feedstock. The

methanotrophic species *M. trichosporium* OB3b has been used as a PHB-producing platform using a combination of methane, methanol, and citric acid as the carbon source (Y. Zhang et al., 2008). This experiment resulted in production of high-quality PHB (Mw $1.5\times10^6$ Da), which comprised around 40% of total cell mass (Strong et al., 2015; Zhang et al., 2008). *Methylocystis* sp. was also a successful producer of high-quality PHB (Mw $2.5\times10^6$ Da), with 51% biopolymer cell content from a two-stage nonsterile process under phosphorous deficiency (Helm et al., 2008). Another example of improved PHB production involved genetically modified *Methylosinus* sp. that overexpressed the enzyme pMMO that was able to accumulate 50% PHB cell content over 120 h with biomass yield up to 18 g/l (Shah et al., 1996). *Methylosinus* sp. has been proven as an excellent PHB producer in potassium-limiting conditions, generating a polymer of Mw $3.1\times10^6$ MDa (Helm et al., 2008). The increased PHB production (57% of total cell mass) was observed in two-phase partitioning bioreactors using *Methylobacterium organophilum* with 10% v/v of silicone oil and 1% methane as the carbon source (Zúñiga et al., 2011).

In addition to PHB production, the co-polymer of PHB and PHBV, PHB-co-HV, has an even higher potential for commercial production. However, researchers must continue to identify potential industrial strains that can synthesize larger amounts of PHB and bring its production to large scale (Khosravi-Darani et al., 2013). Currently, companies like Mango Materials Inc. and Newlight Technologies Inc. have successfully used methane to produce bioplastics at scale. The potential to use metabolic engineering approaches to successfully increase production of value-added compounds, including PHB in methanotrophs, has a strong potential (Pham et al., 2022). Since the reconstruction of C1 pathways in heterotrophic bacteria did not give desired results (very low biomass yield on methane or methanol in *E. coli*), researchers efficiently engineered gammaproteobacterial methanotrophs to utilize sugars (specifically xylose) as co-substrate for growth (Duc Nguyen et al., 2021). Xylose as a

co-substrate in *M. alcaliphilum* 20Z cultures resulted in increased production of certain metabolites, among which are 2,3-butanediol (2,3-BDO), acetoin and 3-hydroxybutyric acid (Duc Nguyen et al., 2021). The introduction of enzymatic machinery that can convert 3-hydroxybutyric acid to 3-hydroxybutyryl-CoA (the monomer for PHB production) can be additional approach to enhance PHB synthesis in engineered methanotrophs. However, gammaproteobacterial methanotrophs cannot produce PHB naturally and the addition of PHB synthesis genes might result in redox disbalance which can negatively affect the growth. Alternatively, gammaproteobacterial methanotrophs have tendency to accumulate glycogen or polyphosphate as storage polymers, and the accumulation of PHB might require additional gene knockouts which can negatively affect remaining cellular processes.

Overall, the microbial methane based PHB production has been studied in detail (Table 2.1) and there are many possibilities and potential for further improvement for bioplastic production.

Table 2.1. Alphaproteobacterial methanotrophic strains tested for PHB production in batch and bioreactor cultures.

| Organism | Growing conditions | Stress trigger | % PHB | Reference* |
|---|---|---|---|---|
| *Methylocystis* sp. GB 25 DSM 7674 | Bioreactor | Nitrogen depletion | 51.3 | (Wendlandt *et al.*, 2001) |
| *Methylocystis* sp. GB 25 DSM 7674 | Bioreactor | Phosphorus depletion | 46.3 | (Wendlandt *et al.*, 2001) |
| *Methylocystis* sp. GB 25 DSM 7674 | Bioreactor | Magnesium depletion | 28.3 | (Wendlandt *et al.*, 2001) |
| *Methylocystis* sp. GB 25 DSM 7674 | Bioreactor | Sulphur depletion | 32.6 | (Helm *et al.*, 2008) |
| *Methylocystis* sp. GB 25 DSM 7674 | Bioreactor | Potassium depletion | 33.6 | (Helm *et al.*, 2008) |
| *Methylocystis* sp. GB 25 DSM 7674 | Bioreactor | Iron depletion | 10.4 | (Helm *et al.*, 2008) |
| *Methylocystis parvus* OBBP | Bioreactor | Nitrogen depletion | 6 | (Pfluger *et al.*, 2011) |
| *Methylosinus trichosporium* OB3b | Bioreactor | Nitrogen depletion | 10 | (Pfluger *et al.*, 2011) |
| Mixed consortium | Bioreactor (copper and iron addition) | Nitrogen depletion | 2.1-4.7 | (Chidambarampadmavathy *et al.*, 2015) |
| *Methylocystis parvus* OBBP | Batch | Nitrogen depletion | 30.5 – 50.3 | (Pieja *et al.*, 2011) |
| *Methylocystis parvus* OBBP | Batch | Nitrogen depletion | 36.5 | (Pieja *et al.*, 2011) |
| *Methylosinus trichosporium* OB3b | Batch | Nitrogen depletion | 38 | (Pieja *et al.*, 2011) |
| *Methylosinus trichosporium* OB3b | Batch (no $O_2$ limitation) | Methanol | 48.7 | (Zaldívar-Carrillo *et al.*, 2018) |
| *Methylosinus trichosporium* OB3b | Batch (ammonium) | Nitrogen depletion | 45.2 | (Zhang *et al.*, 2017) |
| *Methylosinus trichosporium* OB3b | Batch (nitrate) | Nitrogen depletion | 51 | (Zhang *et al.*, 2017) |
| *Methylocystis* sp. Rockwell | Batch (ammonium) | Methanol | 24.8 | This study |
| *Methylocystis* sp. Rockwell | Batch (nitrate) | Methanol | 16.9 | This study |
| *Methylocystis* sp. Rockwell | Batch (ammonium or nitrate) | N/A | 7.36 – 9.39 | This study |

### 2.8.2. PHB properties

PHB is an optically active polymer with approximate native density of 1.18 g/cm$^3$. Crystallization increases its density up to 1.26 g/cm$^3$. The melting temperature varies from 165-180℃, depending on crystallization. PHB monomers of biological origin are always in (R) configuration, and in polymeric form; they can build the structure up to several million Da (Doi, 1995.; Mansour et al., 1999.; Sudesh & Abe, 2010; Volova et al., 2006). The most important property of PHB is its biodegradability (Sudesh & Abe, 2010). The PHB monomer R- 3- hydroxybutyrate has been detected in humans at very low concentrations (0.03-0.1 mg/ml in blood), and its lethal dose is recorded at >5,000 mg/kg (Holmes 1988.; Pawan & Semple, 1983.; Sudesh & Abe, 2010). PHB cannot absorb UV light due to the lack of aromatic compounds and double bonds. These properties make it more resistant to the UV light than polystyrene, which makes it great material that can be use in medical implant manufacturing (Holmes 1988.; Tobón-Martinez, 2019). Thermodynamically, PHB is very stable without many changes to its mechanical properties (Tobón-Martinez, 2019). The only disadvantage of PHB is its low elongation at break, which makes it stiff and brittle (Sudesh & Abe, 2010; Volova et al., 2006).

### 2.8.3. Methods for detection and quantification of PHB

Because of their importance, there have been continuous efforts invested in the methods for detection, evaluation, and quantification of PHAs in microorganisms. Currently, the most common approaches for PHB detection and quantification in microorganisms include staining reactions, spectrophotometric analysis, flow cytometry, gas and liquid chromatography (HPLC and GC-FID) and NMR spectroscopy (Godbole et al., 2016). More detailed molecular characterizations are often completed through molecular weight determination by gel permeation chromatography (GPC) followed by thermal analysis of

extracted polymer (Godbole, 2016). Staining reactions involve the use of PHB-binding dyes, such as Sudan Black, Nile Red or Nile Blue A (Godbole, 2016). Sudan Black-based staining is one of the earliest methodologies used for screening of large numbers of isolates on plates via phase- contrast microscopy (Godbole, 2016). However, Sudan Black has specificity towards all lipidcomponents in the cell (lipids, triglycerides, lipoproteins), which cannot be distinguished clearly from PHB granules. In addition, some Sudan Black dyes are known as carcinogenic chemicals (Pan et al., 2012). Another well-known PHB-binding dye is Nile Red. This molecule belongs to the benzophenoxazine dyes and is known for its intense colors and extremely lipophilic nature. Nile Red is a non-charged molecule that emits intense fluorescence in non-polar media. In water, Nile Red is poorly soluble and does not emit any fluorescence. However, due to its high chromophore adaptability in various solvents, Nile Red chromophore has a broad solvato-chromic range. This dye was extensively used for screening of PHB-producing isolates in water-treatment plants and environmental sample isolates (Godbole, 2016; Kung et al., 2007; Oshiki et al., 2008). It can also be detected via flow cytometry, which was exploited for high-throughput screening of optimal conditions for PHB production in *Methylocystis parvus* OBBP in a microbioreactor system (Sundstrom & Criddle, 2015). Unlike Nile Red, another benzophenoxazine dye, Nile Blue A, is cationic andhas a higher level of solubility in water compared to the Nile Red. Compared to Nile Red, Nile Blue A has a redshifted-absorbance spectra, which makes it more suitable for biological imaging (Martinez & Henary, 2016).

In terms of spectroscopy, there are three approaches commonly used for PHB detection. The UV-based approach assumes conversion of PHB to crotonic acid via heating and acidification. Crotonic acid has an absorption maximum at 235 nm, which is used to determine PHB level in the sample indirectly (Godbole, 2016). The infrared spectroscopy approach is based on carbonyl group absorption in 1728 $cm^{-1}$ in the infrared spectrum.

Microbial cells are first dried, PHB is extracted via chloroform and absorbance that originates from the carbonyl group is measured using classical spectrophotometry (Godbole, 2016). The third spectroscopy-based approach is through nuclear magnetic resonance (NMR) technology. NMR analysis requires dissolving PHB in deuteriated chloroform, followed by recording of NMR high resolution spectra (Caballerot et al., 1994).

A more accurate methodology used in PHB detection is chromatography. High Performance Liquid Chromatography (HPLC) involves digestion and acidification of PHB granules at high temperature in the presence of highly concentrated sulfuric acid. Like UV-spectroscopy, this approach assumes production of crotonic acid, which absorbs light at wavelength of 210 nm. It is then quantified via HPLC (Karr et al., 1983). The most common approach used for PHB detection and quantification is Gas Chromatography (GC). This methodology assumes direct hydrolysis of the PHB polymer under acidic (or alkaline) conditions at high temperature, followed by esterification and production of the monomeric methyl-3-hydroxybutyrate. The use of flame ionization detection (FID) significantly improves sensitivity, and this approach has become one of the most accurate and precise methodologies commonly used for PHB detection and quantification.

Regardless of its accuracy and precision, the GC-FID conventional approach is laborious and time consuming. Experimental preparation time increases with an increased number of samples for analysis, and the complete procedure involves harmful solvents and chemicals. Thus, there have been extensive efforts to develop novel, less harmful and less time-consuming approaches that will be equally precise as GC-FID. PHB-binding dyes are promising tools for this purpose. To generate precise PHB quantification with Nile Red staining additional equipment is required; flow cytometry showed solid success in those terms (Alves et al., 2017; M. Li & Wilkins, 2020). Moreover, Nile Red is not highly PHB specific, and it is not possible to distinguish between PHB granules and the rest of cellular

lipid components. Thus, Nile Blue A (NBA) is another PHB dye with specific spectral properties that enables selective imaging of PHB granules (Martinez & Henary, 2016).

# Chapter 3

## Metabolome profiles of the alphaproteobacterial methanotroph *Methylocystis* sp. Rockwell in response to carbon and nitrogen source

*A version of this mansuscript has been published as: Lazic, M., Sugden, S., Sauvageau, D., Stein, L.Y. Metabolome profiles of the alphaproteobacterial methanotroph Methylocystis sp. Rockwell in response to carbon and nitrogen source. 2021. FEMS Microbiol. Lett. 368, 2021, fnaa219. doi: 10.1093/femsle/fnaa219*

### 3.1 Abstract

Methanotrophs use methane as a sole carbon source and thus play a critical role in its global consumption. Intensified interest in methanotrophs for their low-cost production of value-added products and large-scale industrialization has led to investigations of strain-to-strain variation in parameters for growth optimization and metabolic regulation. In this study, *Methylocystis* sp. Rockwell was grown with methane or methanol as a carbon source and ammonium or nitrate as a nitrogen source. The intracellular metabolomes and production of polyhydroxybutyrate, a bioplastic precursor, were compared among treatments to determine how the different combinations of carbon and nitrogen sources affected metabolite production. The methane–ammonium condition resulted in the highest growth, followed by the methane–nitrate, methanol–nitrate and methanol–ammonium conditions. Overall, the methane–ammonium and methane–nitrate conditions directed metabolism toward energy-conserving pathways, while methanol–ammonium and methanol–nitrate directed the metabolic response toward starvation pathways. Polyhydroxybutyrate was produced at greater abundances in methanol-grown cells, independent of the nitrogen source. Together, the results revealed how *Methylocystis* sp. Rockwell altered its metabolism with different

combinations of carbon and nitrogen source, with implications for production of industrially relevant metabolites.

## 3.2. Introduction

Methane is a potent greenhouse gas that contributes to nearly one-third of the current global warming effect (IPCC, 2013). Biotic control of methane is partially done through the action of aerobic methane-oxidizing bacteria (MOB), or methanotrophs, belonging to the phyla Proteobacteria and Verrucomicrobia (Semrau et al., 2010). Despite their physiological diversity, all aerobic methanotrophs share the ability to oxidize methane as their sole carbon source to conserve energy and generate reducing equivalents that drive biochemical processes in the cell (Trotsenko & Murrell, 2008). Two groups of proteobacterial methanotrophs, Gammaproteobacteria and Alphaproteobacteria, perform methane oxidation to methanol via methane monooxygenase (MMO) and methanol oxidation to formaldehyde via (PQQ)-dependent methanol dehydrogenase (MDH). The branching point distinguishing gamma- from alpha-proteobacterial methanotrophs is formaldehyde assimilation, wherein gammaproteobacterial methanotrophs assimilate formaldehyde via the ribulose monophosphate (RuMP) cycle and alphaproteobacterial methanotrophs use the serine cycle (Trotsenko & Murrell, 2008).

The primary products of the first part of the serine cycle are glyoxalate and acetyl-CoA. While glyoxalate serves as the substrate for transamination and glycine regeneration, acetyl- CoA has various fates in alphaproteobacterial methanotrophs (Trotsenko & Murrell, 2008). Acetyl-CoA can be either oxidized to glyoxalate, enabling continuous serine cycle operation, or it can feed into the synthesis of polyhydroxybutyrate (PHB). Alternatively, the PHB cycle intermediate (R)-3-hydroxybutyryl- CoA can be converted to crotonyl-CoA, which feeds into the ethyl-malonyl-CoA (EMC) cycle (Matsen et al., 2013; Yang et al.,

2013). Acetyl-CoA from the serine cycle participates in fatty acid and phospholipid biosynthesis as well as in the tricarboxylic acid (TCA) cycle, enabling production of essential amino acids (Trotsenko & Murrell, 2008; Vorobev et al., 2014). Many proteobacterial methanotrophs have also been shown to grow on methanol as their sole carbon source (Tays et al., 2018). However, despite the decreased energetic demands for the use of methanol, its toxicity can sometimes result in lower biomass yields (Tays et al., 2018). Specifically, while some gammaproteobacterial methanotrophs can overcome methanol toxicity and grow to high yields (Akberdin et al., 2018; Gilman et al., 2017; Tays et al., 2018), alphaproteobacterial methanotrophs, such as *Methylocystis* sp. Rockwell, *Methylosinus trichosporium* OB3b and *Methylocystis* sp. WRRC1, exhibit poor growth and low yields when using methanol as their sole carbon source (Tays et al., 2018).

Aside from carbon source, studies investigating the effect of nitrogen source for growing alphaproteobacterial methanotrophs have shown broad strain-to-strain variation in their preference for ammonium versus nitrate (Klotz & Stein, 2008; Matsen et al., 2013; Nyerges et al., 2010; Nyerges & Stein, 2009), and no single nitrogen source can support optimal growth of all strains (Dam et al., 2014; Tays et al., 2018; Zaldívar Carrillo et al., 2018). For example, *Methylocystis* sp. Rockwell prefers ammonium, whereas *Methylosinus trichosporium* OB3b grows more robustly on nitrate (Tays et al., 2018; Zaldívar Carrillo et al., 2018). On the other hand, *Methylocystis* sp. SC2 has a more diverse nitrogen metabolism, resulting in efficient growth by fixing atmospheric nitrogen as its sole nitrogen source (Dam et al., 2014). Due to this variability in nitrogen preference, establishing optimal media conditions for growth and metabolite production by alphaproteobacterial methanotrophs requires strain-by-strain investigation.

The availability and low cost of methane as a feedstock has generated interest in using methanotrophic bacteria for industrial purposes (Cantera et al., 2019; Strong et al., 2016). The

successful industrialization of alphaproteobacterial methanotrophs requires a deep understanding of how carbon and other nutrients, like nitrogen, affect metabolism. This understanding is essential for optimizing growth rates, biomass yield, and the yield and recovery of industrially valuable metabolites. The most recent studies on alphaproteobacterial methanotrophs included multi-omics approaches that facilitated the efficient reconstruction of biochemical networks in response to different nutrient combinations (Matsen et al., 2013; Vorobev et al., 2014; Yang et al., 2013). While genomic and transcriptomic data can be mined to identify metabolic pathways, metabolomics allows for rapid comparison of hundreds of potentially valuable metabolites across different growth conditions, facilitating an easy (and potentially cost-effective) optimization of metabolite production. In the present study, we compared the metabolomic profiles of the alphaproteobacterial methanotroph *Methylocystis* sp. Rockwell growing on four combinations of carbon and nitrogen sources, with the goal of identifying carbon–nitrogen combinations that lead to the production of valuable metabolites. *Methylocystis* sp. Rockwell has the potential to become an important industrial strain, especially for the production of the bioplastic precursor molecule PHB (Stein et al., 2011). Metabolomic analysis of *Methylocystis* sp. Rockwell with different carbon–nitrogen combinations provide valuable information for designing and optimizing conditions for maximizing its growth along with production of a number of valuable metabolites.

## 3.3. Materials and methods

### 3.3.1. Growth and maintenance of *Methylocystis* sp. Rockwell

Cultures of *Methylocystis* sp. Rockwell (ATCC49242) were grown in Wheaton media bottles (250 ml) closed with butyl-rubber septa caps and filled with 100 mL of ammonium- (AMS) or nitrate mineral salts (NMS) medium buffered to pH 6.8 with 1.5 mL of phosphate buffer, as previously reported (Tays et al., 2018). Each replicate was inoculated with 1 mL (1% v/v) of previously grown cultures that had been passaged at least once under identical conditions. For cultures grown with methane, 2.5 mmol methane was injected through a 0.22-μm filter-fitted syringe, following the prior removal of gas headspace to maintain pressure at 1.05 atm. For cultures grown with methanol, the initial pressure was 1 atm and 1 mmol of pure high-performance liquid chromatography (HPLC)-grade methanol was added, as this corresponded to the maximum concentration at which *Methylocystis* sp. Rockwell is still able to grow, although at significantly lower rates and yields relative to methane (Fig.3.1) (Tays et al., 2018). All cultures were incubated at 30◦C with shaking at 150 rpm. Growth data has been averaged across two separate experiments to generate a growth curve containing six replicates (n = 6) for time points 0–96 h and 168 h, four replicates (n = 4) for time points 120 and 144 h, and one replicate (n = 1) for 192 and 218 h. Growth was monitored using optical density measurements at a wavelength of 540nm ($OD_{540}$) in a 48-well microplate (Multiskan Spectrum, Thermo Scientific). Culture purity was assured by visual examination using phase-contrast microscopy and by plating on TSA/nutrient agar plates, where a lack of growth confirmed a lack of contamination. Cell dry weight was measured by extracting 35 mL of culture and centrifuging at 10 000 × g at 4◦C for 10 min (Sorvall RC 6 Plus, SS-34 rotor; Thermo Scientific). The supernatant was discarded, and the pellet was resuspended in 10 mL of deionized water and transferred to a tarred weigh dish. The dish was placed in an oven at 60◦C for drying overnight followed by weighing. Cell dry weight is reported in mg/L.

### 3.3.2. Metabolite extraction

Biomass (100 μg) in late exponential phase was retrieved from cultures for metabolite analysis using cultures grown independently from those used to generate the growth curve shown in Fig. 6. For methane–ammonium and methane–nitrate cultures, biomass was retrieved at 44 and 72 h, respectively. For methanol–ammonium and methanol–nitrate cultures, biomass was retrieved at 168 h. Frozen cell pellets were sent to Metabolon (New York, NY) for global metabolite profiling using their HD4 platform. Samples were prepared using the automated MicroLab STAR R ® system (Hamilton Company) and analyzed both by reverse-phase ultrahigh-performance liquid chromatography-tandem mass spectroscopy (RP/UPLC-MS/MS; Waters Corp.) using positive and negative-ion mode electrospray ionization (ESI) and by hydrophilic interaction (HILIC) UPLC-MS/MS using negative-ion mode ESI. For internal consistency, a constant amount of sample pellet (100 μg) was processed per volume of extraction solvent. Procedures were performed according to Metabolon standard protocols ((https://www.metabolon.com/).

### 3.3.3. PHB quantification

PHB was quantified as previously described (Zaldívar Carrillo et al., 2018) . Briefly, PHB was extracted from 10 mL of culture (n = 3 for each condition) harvested at the same times as above for metabolite extraction (Fig. 3.1) and then hydrolyzed and esterified with methanol to produce methyl hydroxybutyrate following modified protocols (Oehmen et al., 2005; Zaldívar Carrillo et al., 2018). Methyl hydroxybutyrate was analyzed via a gas chromatograph (7890A, Agilent Technologies) equipped with an autosampler (G4513A, Agilent Technologies) and fitted with a 30 m × 250 μm DB- 5ms column (Agilent Technologies). The injector temperature was 250°C and the oven temperature was held at 80°C for 1min, raised to 120°C at a rate of 10°C/min, and then to 270°C at 30°C/min, before

being held at that temperature for 3min. Samples were injected at a split ratio of 1:10. A flame ionization detector at 300°C was used. Helium was used as the carrier gas at a flowrate of 1.5 mL/min. The peak of methyl hydroxybutyrate was resolved at 2.8 min; an internal standard of methyl benzoate was resolved at 5.4 min. The concentration of methyl hydroxybutyrate was established based on a calibration curve using a prepared standard. The percentage of PHB per dry cell weight was calculated as previously described (Zaldívar Carrillo et al., 2018).

### 3.3.4. Statistical analysis

Raw peak areas were scaled to the median value for each metabolite; missing values were imputed as one-half the lowest detected abundance of that metabolite. Principal component analysis (PCA; R package vegan (Oksanen O, 2016) and sparse partial least squares discriminant analysis (sPLS-DA; R package mixOmics (Oksanen O, 2016) were performed to assess overall differences in metabolite profiles among treatments and identify metabolites driving these differences. PCA clustering effects were tested using a permutational analysis of variance (PERMANOVA) with 1000 permutations. The optimal number of sPLSDA components and variables per component were determined by finding the minimum misclassification rate using 100 iterations of 3-fold cross validations with increasing numbers of components (up to 5) and metabolites (between 5 and 100). In addition, individual metabolites that were significantly differentially abundant among treatments were identified using an ANOVA followed by Tukey's honestly significant differences post hoc test with the Benjamini–Hochberg correction for multiple comparisons. Metabolites with corrected $P \leq 0.05$ were considered significant. To further analyze the metabolite profiles of *Methylocystis* sp. Rockwell, we categorized metabolites based on the fold changes in median-scaled metabolite abundances between treatments. Fold-changes were categorized into five classes based on their magnitude. In addition, we used linear regression

models with both carbon and nitrogen source as predictors to evaluate how metabolite abundances were affected by changes in one nutrient source (carbon or nitrogen) while controlling for the other. For each nutrient source comparison (carbon or nitrogen), we calculated 'controlled' fold-changes for each metabolite as (β0+ βn)/β0, where β0 was the model intercept and βn was the coefficient for the given nutrient.

## 3.4. Results

### 3.4.1. General metabolite profiles of *Methylocystis* sp. Rockwell grown in four carbon–nitrogen combinations

Metabolomic analysis of *Methylocystis* sp. Rockwell cultures grown in four different combinations of carbon and nitrogen sources yielded 355 metabolites of known identity belonging to eight metabolic superpathways (Fig. 3.2; Table 3.1). All four treatments resulted in significantly different metabolite profiles (PERMANOVA df = 3, R2 = 0.75, P < 0.001) that were consistent among treatment replicates (Fig. 3.3). The carbon source was the main driver of metabolomic differences, with a pronounced general decrease in metabolite yield in cultures grown with methanol. This methanol-induced effect was more prominent when ammonium was the nitrogen source (Fig. 3.2). In sPLS-DA, treatment groups were separated along three components based on 17 metabolites (Fig. 3.4). The methanol–ammonium treatment group separated along the first component (Fig.3.3) and was distinguished by increased abundances of N-acetylserine, thioproline and 2-methylserine (Fig. 3.4). The second sPLS-DA component separated the methanol– nitrate treatment group based on an increased abundance of seven amino acids and nucleotide derivatives (Fig. 3.4). The two methane treatments separated along the third component based primarily on the abundance of

methylsuccinate in the methane–ammonium treatment and N-acetylleucine and Acetylisoleucine in the methane–nitrate treatment (Fig. 3.4).

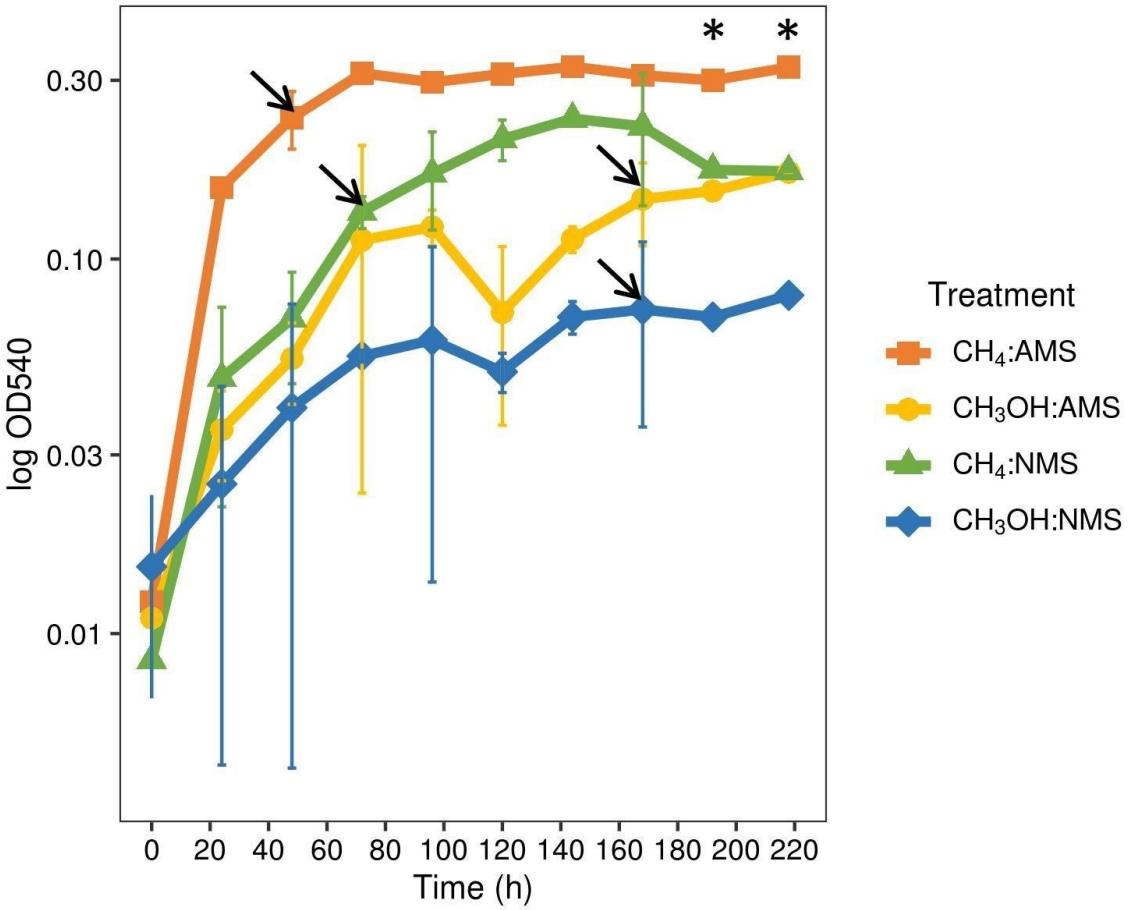


Figure 3.1. Log scale of $OD_{540}$ over time from 100-ml cultures of methanotrophic bacteria provided with 10 mM ammonium or nitrate and 2.5 mmol methane or 1 mmol methanol Growth curve containing six replicates (n=6) for time points 0 – 96 h and 168 h, four replicates (n=4) for time points 120 h and 144 h, and one replicate (n=1) for 192 h and 218 h. Asterisk (*) indicates one replicate only for time points 192 h and 218 h. Growth data has been averaged across two separate experiments. Growth rates calculated across exponential growth phase for each condition are methane-ammonium = 0.015 $h^{-1}$, methanol-ammonium = 0.0098 $h^{-1}$, methane-nitrate = 0.021 $h^{-1}$ and methanol-nitrate = 0.0074 $h^{-1}$. Arrows indicate harvesting time for each condition.

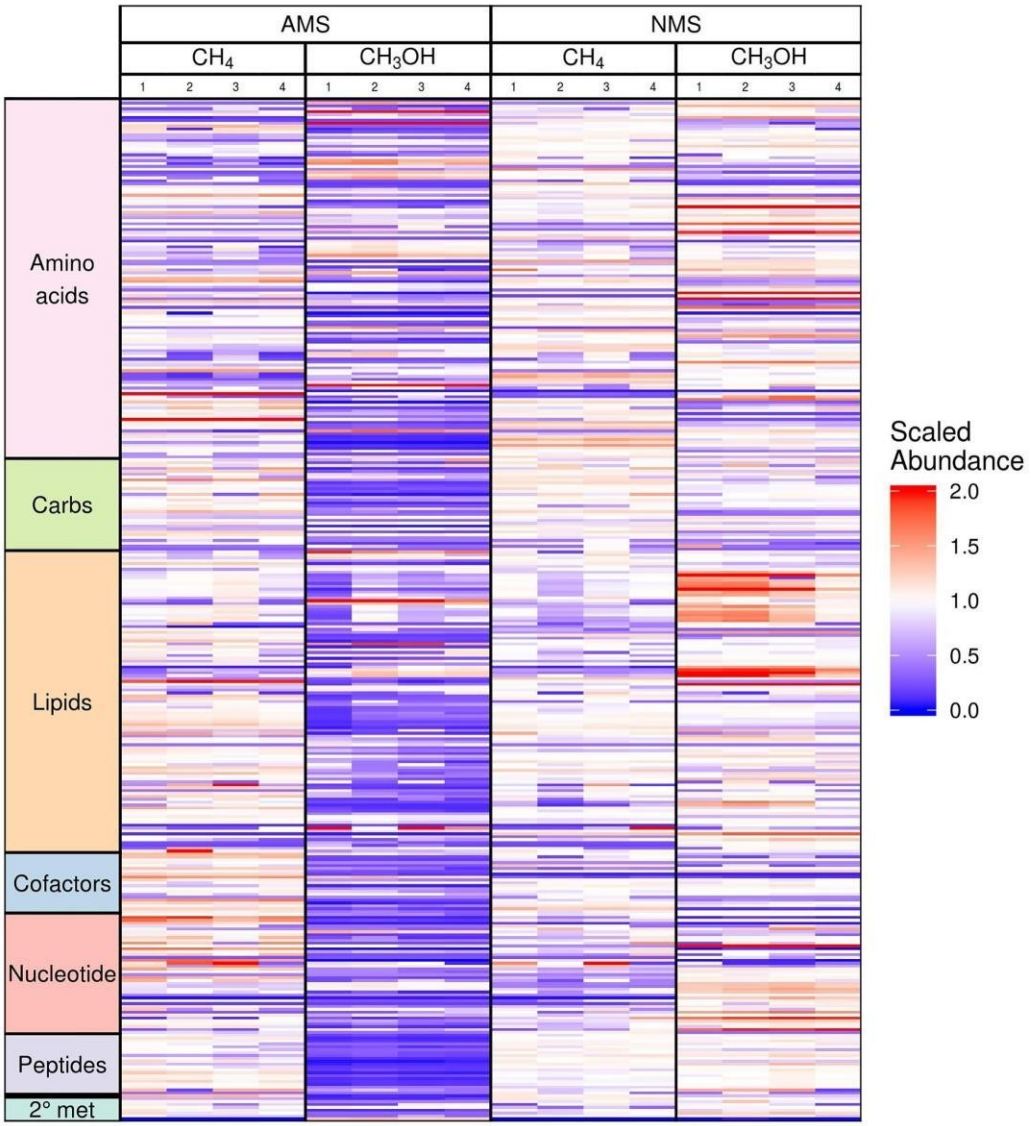


Figure 3.2 Overview of general metabolite abundances in Methylocystis sp. Rockwell. Scaled median metabolite abundances are shown for each sample (n = 4) and separated by treatment group. Metabolites are grouped by their associated metabolic superpathway. One superpathway, 'xenobiotics', consisted of only two metabolites and therefore is not labeled in this figure.

Table 3.1. Metabolites categorized by fold-change between treatments based on median-scaled abundances; [a] Mean" metabolite abundances for cultures grown in methanol were divided by the corresponding mean metabolite abundances for cultures grown in methane to determine the fold change. [b]Mean metabolite abundances for cultures grown with nitrate were divided by the corresponding mean metabolite abundances for cultures grown with ammonium to determine the fold change.

| | **Methanol/Methane[a]** | | | **Nitrate/Ammonium[b]** | | |
|---|---|---|---|---|---|---|
| **Fold change** | No. metabolites | No. metabolites | Shared metabolites | No. metabolites | No. metabolites | Shared metabolites |
| | Ammonium | Nitrate | | Methane | Methanol | |
| **>4.00** | 21 | 25 | 35 | 9 | 104 | 22 |
| **2.00-4.00** | 19 | 46 | 38 | 27 | 82 | 16 |
| **0.50-2.00** | 146 | 237 | 173 | 285 | 144 | 236 |
| **0.25-0.50** | 67 | 35 | 80 | 26 | 14 | 61 |
| **<0.25** | 102 | 12 | 29 | 8 | 11 | 20 |

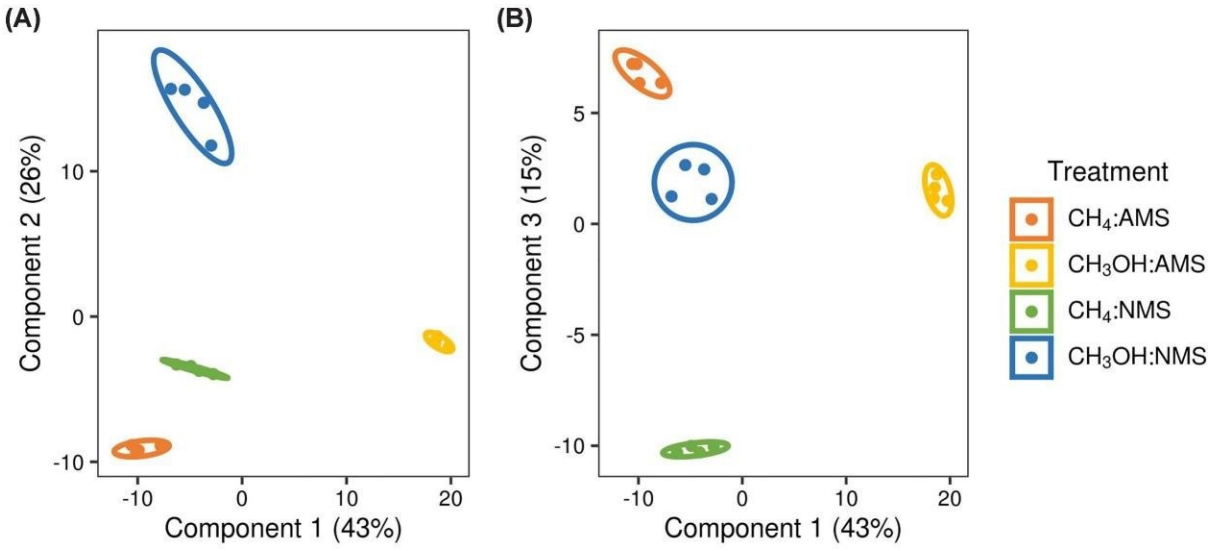


Fig. 3.3. sPLS-DA performed on log-transformed median-scaled metabolite abundances. Ellipses represent 95% confidence intervals.

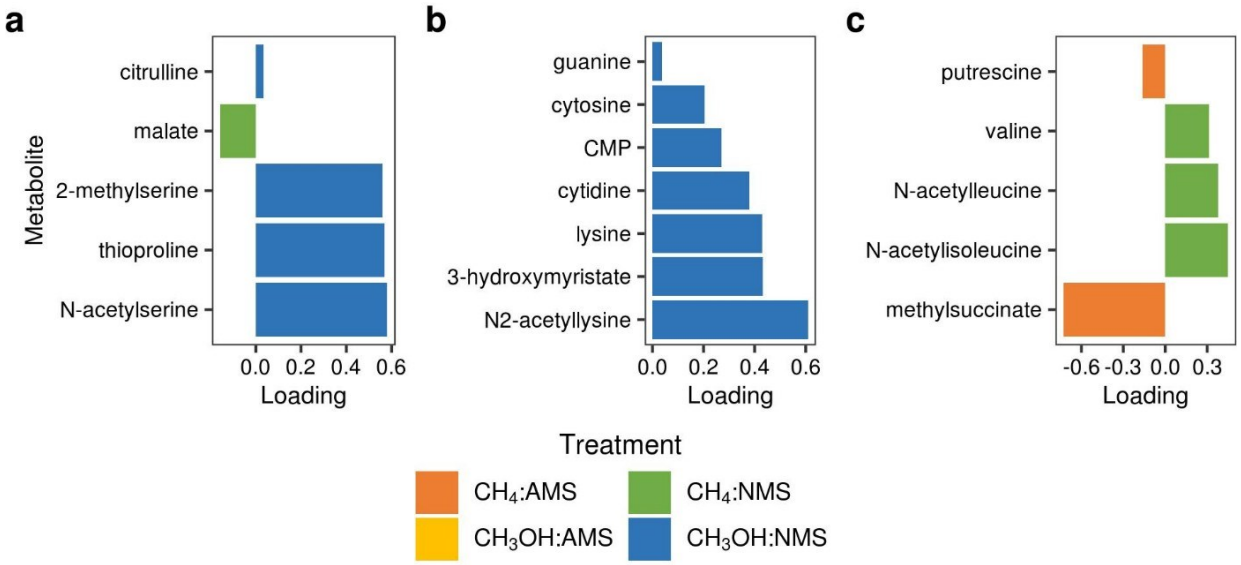


Figure 3.4. Metabolites that drive differences among different treatment groups in Methylocystis sp. strain Rockwell (based on the sparse partial least squares discriminant analysis [sPLS-DA].

3.4.2 Metabolic effect of carbon and nitrogen source in *Methylocystis* sp. strain Rockwell

To further analyze the effects of carbon and nitrogen source combinations, we categorized the detected metabolites into five categories based on the fold change between mean values of scaled imputed data for each metabolite (Table 3.1). For the carbon source effect, fold changes were calculated by dividing mean metabolite abundances in methanol by the corresponding abundance in methane, in ammonium and nitrate. For the nitrogen source effect, fold changes were similarly calculated by dividing abundances in nitrate by abundances in ammonium, in methane and methanol. Categorizing metabolites by their fold changes revealed that the carbon source effect was accentuated with ammonium, whereas nitrogen source effect was more prominent in methanol (Table 3.1).

Table 3.2 Mean values of the median-scaled abundance of selected metabolites under the four carbon–nitrogen combinations. Primary metabolism refers to biosynthetic and energy-conserving (ATP-generating) pathways whereas starvation metabolism refers to a stress response. Asterisks indicate specific metabolites that are produced at significantly higher abundances in the specified condition (the list of all detected metabolites is provided at the end of the document as the excel file Appendix 1).

| **Biochemical pathway** | | **Metabolites** | **Conditions** | | | |
|---|---|---|---|---|---|---|
| | | | methane-ammonium | methanol-ammonium | methane-nitrate | methanol-nitrate |
| **Primary metabolism** | Glycolysis | 3-PG | 1.49* | 0.08 | 1.54* | 0.95 |
| | | PEP | 1.59* | 0.13 | 1.56* | 1.15 |
| | | Pyruvate | 2.02 | 0.29 | 1.35 | 0.74 |
| | | Glycerate | 0.99 | 0.09 | 1.20 | 0.94 |
| | TCA cycle | Succinate | 1.09 | 0.15 | 1.72 | 0.86 |
| | | Fumarate | 1.06 | 0.24 | 1.19 | 0.94 |
| | | Malate | 1.03 | 0.22 | 1.16 | 0.99 |
| | Asp/Glu metabolism | Aspartate | 1.54 | 0.18 | 1.12 | 0.86 |
| | | Glutamate | 2.51 | 0.42 | 1.57 | 0.56 |
| **Starvation metabolism** | Ser/Thr/Gly metabolism | Serine | 0.33 | 2.78 | 0.45 | 1.54 |
| | | Glycine | 0.88 | 0.16 | 1.17 | 1.37 |
| | | Threonine | 0.97* | 0.67 | 1.12* | 1.15* |
| | BCAA metabolism | Leucine | 0.73 | 0.94 | 1.04 | 1.45 |
| | | BHBA | 1.69 | 0.42 | 0.53 | 3.01 |
| | | Valine | 0.57 | 0.80 | 1.81 | 1.09 |
| | | 3-met-2-oxovalerate | 0.42 | 1.70 | 0.84 | 1.12 |
| | | Ethylmalonate | 4.81 | 0.19 | 1.13 | 0.48 |
| | | Isoleucine | 0.81 | 1.17 | 1.81 | 0.95 |
| | PHB cycle | PHB | 0.50 | 1.70* | 0.64 | 1.16* |

### 3.4.3 Effect of carbon–nitrogen combinations on production of industrially relevant metabolites

When grown on methane, *Methylocystis* sp. Rockwell directed its metabolism toward primary energy-conserving (ATP generating) pathways (glycolysis, TCA cycle, and Asp/Glu metabolism), independent of the nitrogen source (Table 3.2 and Fig. 3.5). On the other hand, growth on methanol directed the metabolic response toward starvation and stress-related pathways (ser/thr/gly metabolism, branched chain amino acid [BCAA] metabolism and the PHB cycle), again independent of nitrogen source (Table 3.2 and Fig. 3.5). However, the effect of nitrogen source was observed in the relative production of several specific metabolites (Table 3.2 and Fig. 3.5). Since PHB could not be detected through the general metabolomics protocols used in the Metabolon platform, we analyzed it independently to evaluate the effects of the different carbon and nitrogen source combinations on production of PHB. *Methylocystis* sp. Rockwell produced the highest dry weight PHB percentage when grown in methanol (ANOVA F, df, P); the effect of nitrogen source was not significant (Fig. 3.6).

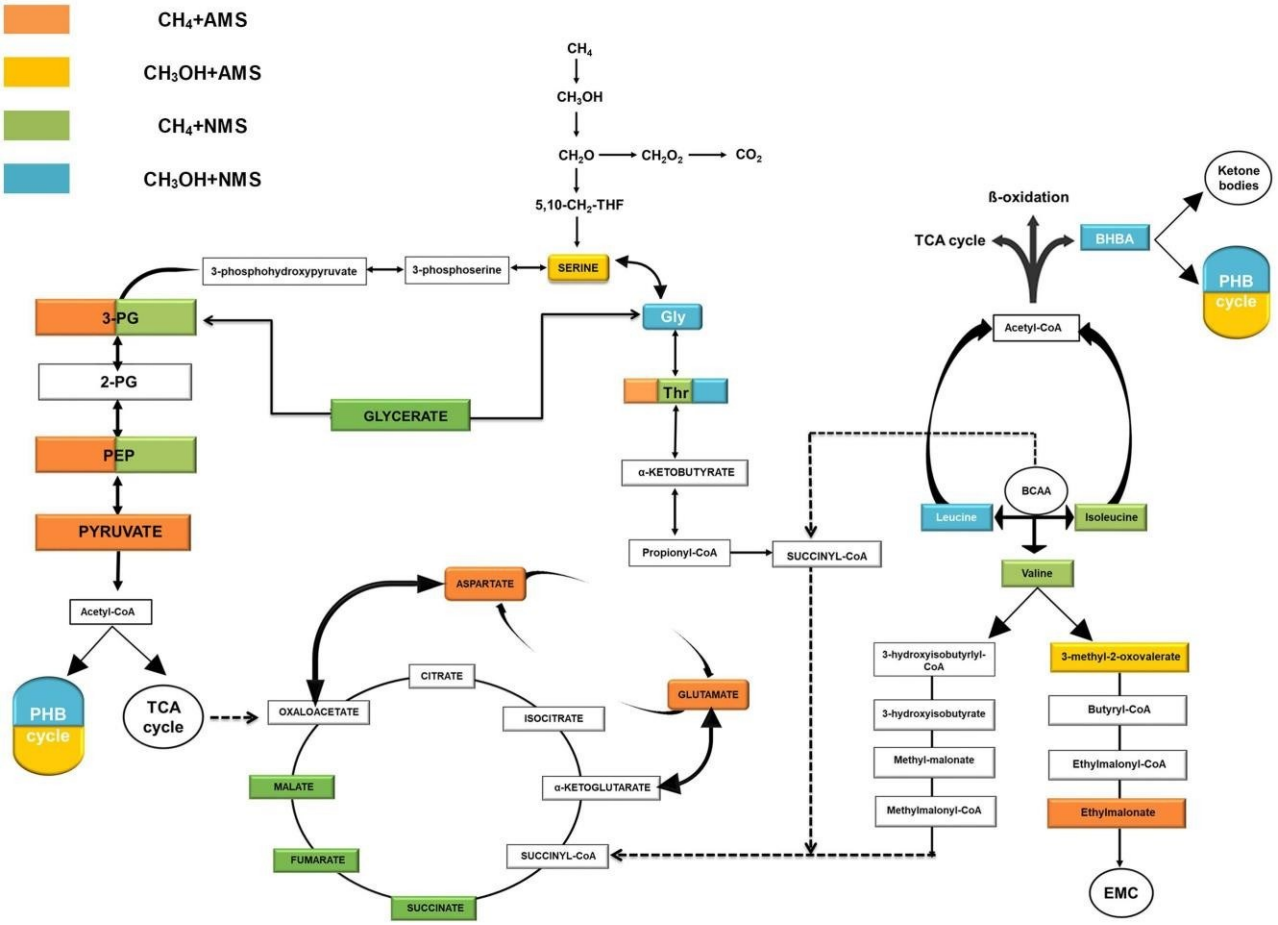


Figure 3.5. Metabolites in main pathways of Methylocystis sp. strain Rockwell affected by growth on various combinations of methane or methanol and ammonium or nitrate. Orange = methane–ammonium, yellow = methanol–ammonium, green = methane–nitrate, blue = methanol–nitrate. The color of specific metabolites corresponds to the carbon–nitrogen combination in which its presence was most abundant (e.g. PHB production was the highest in methanol–ammonium and methanol–nitrate).

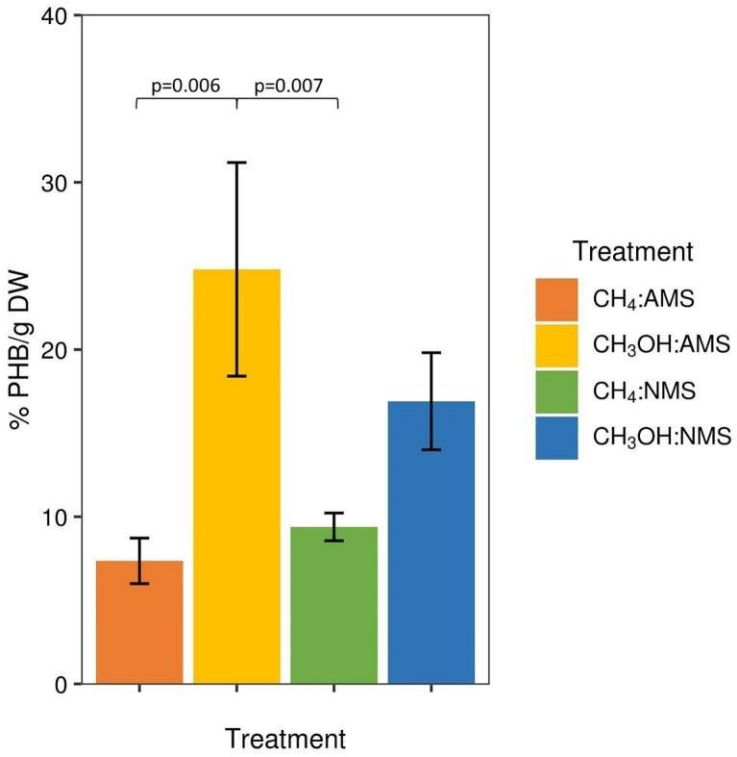


Figure 3.6. PHB production in the four carbon–nitrogen growth combinations, expressed as a percentage of total dry weight (DW). Error bars represent standard deviation (n = 4). P-values showing significant differences between conditions were calculated using analysis of variance (ANOVA).

## 3.5. Discussion

The goal of this study was to evaluate the effect of four different combinations of carbon and nitrogen sources on the intracellular metabolite profiles of the alphaproteobacterial methanotroph *Methylocystis* sp. Rockwell, and to identify culture conditions favorable for production of industrially relevant metabolites. Overall, the carbon source had a stronger effect on global metabolomic differences (Fig. 3.2.) and metabolic pathway distribution, whereas the nitrogen source had a stronger effect on the production of specific metabolites (Table 3.2 and Fig. 3.5). The fact that clustering analysis could clearly discriminate among all four growth conditions indicates that both carbon and nitrogen sources had significant effects on differentiating the metabolite pools (Fig. 3.4). Growth analysis (Fig. 3.1) confirmed previous findings that methane is the preferred carbon source and ammonium is the preferred nitrogen source for optimal growth of *Methylocystis* sp. Rockwell (Tays et al., 2018). The poor growth on methanol is reflected thorough the increased pools of metabolites related to stress responses.

Previous studies have shown that methanotroph strains differ in their preferred nitrogen source (Dam et al., 2014; Klotz & Stein, 2008; Nyerges et al., 2010; Nyerges & Stein, 2009; Tays et al., 2018; Zaldívar Carrillo et al., 2018). In this study, we observed alterations in the abundance of specific metabolites in response to the nitrogen source. In robustly-growing methane–ammonium cultures, the lack of serine, 3-phosphoglycerate (3-PG) and 2-phosphoglycerate (2-PG) accumulation was indicative of efficient carbon assimilation via the serine cycle, which is characteristic of alphaproteobacterial methanotrophs (Trotsenko & Murrell, 2008). On the other hand, the increased abundance of metabolites in the phosphoenol pyruvate (PEP)-pyruvate reaction node and the lack of oxaloacetate and malate accumulation in cultures growing with ammonium indicated rapid PEP carboxylation to oxaloacetate, which feeds into aspartate/glutamate metabolism. Another

branch of oxaloacetate bioconversion is its reduction to malate, which feeds into the EMC cycle (Matsen et al., 2013; Yang et al., 2013). The increased pool of ethylmalonate, an intermediate of the EMC cycle, under methane–ammonium growth conditions—also observed with other alphaproteobacterial methanotrophs in previous studies (Matsen et al., 2013; Vorobev et al., 2014; Yang et al., 2013) confirms the integration of the serine and EMC cycles for carbon assimilation in these organisms. In cultures grown with nitrate, serine accumulation was not observed, suggesting sub-optimal growth relative to that with ammonium. However, unlike cultures grown with ammonium, cultures grown with nitrate

accumulated metabolites in the glycerate-3-PG reaction node where PEP and pyruvate are rapidly assimilated through the TCA cycle, as indicated by the abundance of malate, fumarate, and succinate. The accumulation of the BCAAs valine and isoleucine in the methane–nitrate growth condition suggested the possibility of increased BCAA biosynthesis, which, again, could be considered a sub-optimal growth response (Kaiser & Heinrichs, 2018).

Interestingly, regardless of poor growth, the accumulation of the industrially relevant metabolite PHB increased during growth on methanol, likely because PHB is a secondary metabolite related to starvation conditions. The accumulation of serine in cultures grown on methanol–ammonium was a further indication that the cells were directing serine-derived acetyl-CoA towards PHB instead of towards the TCA and EMC cycle, or aspartate/glutamate metabolism, signifying starvation rather than growth (Pieja, Rostkowski, et al., 2011; Pieja, Sundstrom, et al., 2011; Zaldívar Carrillo et al., 2018). On the other hand, the lack of serine and glyoxalate accumulation combined with the abundance of glycine and threonine in methanol–nitrate cultures suggest a potential metabolic branch of the serine cycle feeding glycine and threonine into BCAA metabolism, resulting in leucine accumulation. The accumulation of BHBA in cultures grown on methanol was another indicator of stress-associated conditions. However, in the methanol–nitrate cultures, the BHBA precursor pool was split between ketone bodies and the PHB cycle, which might be the reason for observing slightly less PHB in the methanol-nitrate versus the methanol–ammonium conditions (Fig. 3.6). Without any attempt at optimization, *Methylocystis* sp. Rockwell performed intermediate levels of PHB synthesis that were comparable to those reported for other alphaproteobacterial methanotrophs undergoing some levels of optimization (Fig. 3.6 and Table 3.2). Thus, this organism could be considered a potential novel industrial platform for bioplastic production, with methanol as the stress inducer leading to PHB accumulation. Unlike other alphaproteobacterial methanotrophs (Zaldívar Carrillo et al., 2018), in the

absence of stress (methane– ammonium and methane–nitrate), *Methylocystis* sp. Rockwell still produced PHB (Fig. 3.6). In addition, *Methylocystis* sp. Rockwell prefers ammonium as the nitrogen source (Fig. 3.1). This is an important feature for production of bioplastic precursors using ammonium-rich wastewater as a growth medium.

An important challenge for the industrial production of PHB and other industrially useful metabolites by *Methylocystis* sp. Rockwell is that it grows most robustly under methane-ammonium conditions, whereas the production of industrially useful metabolites such as PHB requires the induction of stress, which can be achieved by growth on methanol. Also, different alphaproteobacterial methanotrophs experience stress under different nutrient combinations: PHB synthesis in *M. trichosporium* OB3b was optimal with a combination of methane (30%) and methanol (70%) (Zaldívar Carrillo et al., 2018), whereas our results with *Methylocystis* sp. Rockwell showed maximum PHB biosynthesis with methanol as the carbon source and ammonium as the nitrogen source. That said, we did not test a mixture of methane/methanol, and it remains possible that PHB synthesis is *Methylocystis* sp. Rockwell maybe further increased by combination of the two carbon sources. The effect of carbon–nitrogen source combination on PHB biosynthesis justifies a two-stage fed-batch strategy, thereby separating biomass from PHB production (Wang et al., 2012) . On the other hand, another primary metabolite of industrial significance, succinic acid (Potera, 2005), could be adequately produced under methane–nitrate growth conditions if biomass production could be further optimized. In order to use metabolomic data for the industrialization of *Methylocystis* sp. Rockwell, the detailed evaluation of specific nutrient combinations and the associated production of metabolites must be accompanied by an optimized feeding strategy to ensure both sufficient biomass and robust product yields. This work revealed how combinations of carbon–nitrogen source are important considerations towards optimized metabolite production by methanotrophic bacteria.

# Chapter 4

# The combined effect of methane and methanol on growth and PHB production in the alphaproteobacterial methanotroph *Methylocystis* sp. Rockwell

## 4.1 Abstract

Methane is a highly potent greenhouse gas mostly released through anthropogenic activities. Methane represents a low-cost and sustainable feedstock used for biological production of value-added compounds by bacteria known as methanotrophs. In addition to methane, these organisms can utilize methanol, another cheap carbon source that is a common industrial byproduct. Alphaproteobacteria methanotrophs can utilize both methane and methanol to produce the biopolymer polyhydroxybutyrate. The goal of this study was to examine the effect of methanol on polyhydroxybutyrate production in *Methylocystis* sp. Rockwell and to identify the optimal methane:methanol ratio that will improve PHB without reducing biomass production. Three methane:methanol ratios (4, 2.5., and 0.5) and three nitrogen source (ammonium or nitrate) concentrations (10 mM, 1 mM, and 0.1 mM) were combined to generate 18 growing conditions (9 per carbon source). The production of polyhydroxybutyrate and biomass were analyzed at the end of growth. Overall, the methane:methanol ratio that promoted polyhydroxybutyrate synthesis without reducing biomass were 4 and 2.5 and the optimal nitrogen concentration was 1 mM for both ammonium and nitrate. The physiological mechanism behind the beneficial effect of combining methane and methanol as carbon source remains to be discovered. One possibility is that methanol has a dual role as carbon source at lower concentrations and as a stringent response trigger at higher concentrations. Nevertheless, the beneficial effect of methanol and optimal nitrogen concentration for PHB production was confirmed, providing a basis for future physiological analysis and conditions for process scale-up.

## 4.2. Introduction

With over 300 million tons of plastic waste produced every year and plastic production expected to double by 2050, there is an urgent need to find biodegradable polymers that can replace the toxic materials currently used to produce conventional plastics (Ritchie & Roser, 2018.; Verma et al., 2016). One of the most promising groups of biodegradable polymers is polyhydroxyalkanoates (PHAs), of which polyhydroxybutyrate (PHB) is the most widely studied (Pieja et al., 2017; Pieja, Rostkowski, et al., 2011; Pieja, Sundstrom, et al., 2011). PHB is a short-chain length methyl-ester synthetized by bacteria as a storage biopolymer under nutrient limitation and conditions of carbon excess (Pieja et al., 2017; Rostkowski et al., 2013; Zaldívar Carrillo et al., 2018; T. Zhang et al., 2017). Due to its biocompatibility and similarity to conventional plastics (McAdam et al., 2020), PHB is viewed as efficient substitute biodegradable plastic. Industrial production of PHB from microbes currently mostly relies on sugar-based feedstocks (Govil et al., 2020; Sirohi et al., 2020), which are expensive and often require the removal of agricultural products from the food supply chain. Thus, there is an increased interest in alternative feedstocks such as methane and methanol. These compounds are common industrial byproducts and are significantly less expensive than sugar-based feedstocks for industrial production of PHB (Lazic et al., 2021; Tays et al., 2018; Zaldívar Carrillo et al., 2018). In addition, using waste methane to produce PHB represents an efficient strategy for reducing GHG emissions.

Biological methane- and methanol-based PHB production requires the use of alphaproteobacterial methanotrophs (Cal et al., 2016; Pieja et al., 2017; Pieja, Sundstrom, et al., 2011). These organisms utilize methane and methanol as carbon and energy sources (Trotsenko & Murrell, 2008). Alphaproteobacterial methanotrophs grow poorly with methanol as the sole source of carbon even though methanol is readily available in media and methanotrophs can oxidize it to formaldehyde (Tays et al., 2018). However, our recent study

on *Methylocystis* sp. Rockwell identified methanol as the stress trigger that directs metabolism toward increased PHB production and demonstrated an inverse correlation between biomass and PHB yield (Lazic et al., 2021). The beneficial influence of methanol on PHB production has been demonstrated previously (Lazic et al., 2021; Zaldívar Carrillo et al., 2018; Zhang et al., 2008). Zhang et al. confirmed that the addition of methanol in a non-sterile process improved PHB production from 12-40% cell dw/l (Y. Zhang et al., 2008). Furthermore, it was shown in *Methylosinus trichosporium* OB3b that the combination of 30% methane and 70% methanol was optimal for increased PHB production without compromising biomass production (Zaldívar Carrillo et al., 2018) .

In general, alphaproteobacterial methanotrophs can utilize nitrate or ammonia mineral salts (NMS or AMS) for growth. However, most studies so far used only nitrate as the source of nitrogen. The reason is due to competitive inhibition of methane monooxygenase (MMO) by ammonia, followed by release of the toxic intermediate hydroxylamine from the oxidation of ammonia by MMO (Nyerges et al., 2010; Nyerges & Stein, 2009). Unlike many other alphaproteobacterial methanotrophs, *Methylocystis* sp. Rockwell shows high nitrate sensitivity but thrives when cultivated with ammonia (Nyerges et al., 2010; Nyerges & Stein, 2009; Tays et al., 2018) .

Despite sharing identical central metabolic pathways for carbon and nitrogen assimilation, alphaproteobacterial methanotrophs display substantial strain-to-strain variation in terms of the optimal carbon-nitrogen combination that supports growth and PHB production. For example, both *M. trichosporium* OB3b and *Methylocystis parvus* OBBP prefer methane over methanol for growth (Tays et al., 2018), but for PHB production, *M. trichosporium* OB3b prefers nitrate (Zaldívar Carrillo et al., 2018) whereas *M. parvus* OBBP prefers ammonium (Zhang et al., 2017). Despite these differences, both organisms require

nitrogen limitation to initiate PHB production (Zaldívar Carrillo et al., 2018; Zhang et al., 2017).

Unlike many other alphaproteobacterial methanotrophs, *Methylocystis* sp. Rockwell produces detectable amounts of PHB without nitrogen limitation (Lazic et al., 2021, 2022). However, the highest PHB production in this species was achieved under nitrogen starvation where the only source of nitrogen was N-fixation (Lazic et al., 2022). Even though *Methylocystis* sp. Rockwell produces PHB in the absence of nitrogen stress (Lazic et al., 2021), the amount was very low and biomass production was poor, necessitating further optimization to design efficient bioreactor strategies for scaling-up production. Since the lack of nitrogen might cause significantly reduced growth, the determination of the N:C ratio that is high enough to support biomass but low enough to trigger PHB synthesis is required. Identifying an optimal N:C ratio would help avoid a two-stage production process and reduce production costs (Zaldívar Carrillo et al., 2018).

The optimization of biomass and PHB production in alphaproteobacterial methanotrophs has already been attempted for *M. trichosporium* OB3b via statistical regression analysis and Response Surface Methodology (RSM) (Zaldívar Carrillo et al., 2018). The efficiency of this approach has been confirmed in heterotrophic organisms where PHB production was successfully increased at small- and large-scale in *Rhodococcus pyridinivorans* BSRT1-1 (Trakunjae et al., 2021). It also helped define the effect and significance of multiple variables (carbon source, nitrogen source and N:C ratio) toward the response of interest. In addition, the combination of statistical tools enabled the determination of the combination of nutrients that resulted in the highest yields of biomass and PHB. In this study, a similar approach is investigated for *Methylocystis* sp. Rockwell to establish optimal conditions and determine the range of favorable conditions between species.

## 4.3. Materials and Methods

### 4.3.1. Growth and maintenance of *Methylocystis* sp. Rockwell

Cultures of *Methylocystis* sp. Rockwell (ATCC 49242) were maintained as previously described (Lazic et al., 2021; Tays et al., 2018). Briefly, bacteria were maintained in 1-L Kimble Bottles closed with butyl-rubber septa caps, filled with 100 mL ammonium (AMS) or nitrate mineral salts (NMS) buffered to pH 6.8 with 1 mL phosphate buffer with 5 mmol (120 ml) methane. Fresh inoculum was prepared from maintained stocks in Wheaton media bottles (250 mL) closed with butyl-rubber septa caps, filled with 100 mL AMS or NMS media, buffered to pH 6.8 with 1 mL of phosphate buffer. Each replicate was inoculated with 1 mL of 3- to 5-day old growing culture (1% v/v). The corresponding amount of methane was injected through a 0.22-μm filter syringe, following the prior removal of gas headspace to maintain pressure at 1.1 atm (Table 4.1).

Table 4.1 Experimental conditions and combinations for full factorial design with two predictors, methane:methanol ratio (4, 2.5, and 0.5) and nitrogen concentration (10 mM, 1 mM, and 0.1 mM AMS or NMS). The amount of carbon was kept at 6 mmol. N:C ratio was calculated in 100 mL of nutrient media.

| **Experiment Name/Number** | **%$CH_4$** | **%$CH_3OH$** | **Nitrogen (mM) (AMS or NMS)** | **$CH_4/CH_3OH$ ratio** | **N/C ratio** |
|---|---|---|---|---|---|
| **1** | 33 | 67 | 1 | 0.5 | 0.017 |
| **2** | 80 | 20 | 1 | 4 | 0.017 |
| **3** | 72 | 28 | 10 | 2.5 | 0.17 |
| **4** | 72 | 28 | 1 | 2.5 | 0.017 |
| **5** | 80 | 20 | 0.1 | 4 | 0.0017 |
| **6** | 72 | 28 | 0.1 | 2.5 | 0.0017 |
| **7** | 80 | 20 | 10 | 4 | 0.17 |
| **8** | 33 | 67 | 10 | 0.5 | 0.17 |
| **9** | 33 | 67 | 0.1 | 0.5 | 0.0017 |
| **$CH_4$_10** | 100 | 0 | 10 | N/A | 0.17 |
| **$CH_4$_1** | 100 | 0 | 1 | N/A | 0.017 |
| **$CH_4$_0.1** | 100 | 0 | 0.1 | N/A | 0.0017 |
| **$CH_3OH$_10** | 0 | 100 | 10 | N/A | 0.17 |
| **$CH_3OH$_1** | 0 | 100 | 1 | N/A | 0.017 |
| **$CH_3OH$_0.1** | 0 | 100 | 0.1 | N/A | 0.0017 |

Pure high performance liquid chromatography (HPLC)-grade methanol was added to each replicate to the desired concentration (ranging from 0 to 60 mM; Table 4.1). All growth experiments were done in 1-L bottles in triplicates to avoid oxygen limitation during growth (n=3). Cultures were incubated at 30℃ with shaking at 150 rpm. Growth data was averaged across triplicates to generate a growth curve (Fig. 4.1). Growth was monitored using optical density measurements at a wavelength of 540 nm ($OD_{540}$) in a 48-well microplate (Multiskan Spectrum, Thermo Scientific). Culture purity was assured by plating on TSA/nutrient agar plates, where a lack of growth confirmed a lack of contamination. Cell dry weight was measured by extracting 15 mL of culture and centrifuging at 5,000 × g at 4℃ for 20 min. The supernatant was discarded, and the pellet was resuspended in 5 mL of deionized water and transferred to a tarred weigh dish. The dish was placed in an oven at 30℃ for 48 h for drying, followed by weighing. Cell dry weight is reported in mg/L.

### 4.3.2. Analysis of headspace gases

The amount of methane and oxygen in the culture headspace was measured as previously described via a Gas Chromatograph with TCD detector (GC-TCD, Shimadzu) fitted with a molecular sieve 5A and Hayesep Q column (Alltech) (Tays et al., 2018). Briefly, 250-mL gas-tight syringe (SGE Analytical Science; 100 mL/injection) was used to extract and inject headspace samples. Injection and detection temperatures were 120℃ with oven temperature 90℃, current set to 90 mA (column 1), using helium carrier gas (Ultra High Purity, Praxair) at 200 kPa. Gas concentrations were calculated using standard curves of known amounts of the respective pure gases (Praxair).

### 4.3.3. PHB quantification

PHB was quantified as previously described (Lazic et al., 2021; Zaldívar Carrillo et al., 2018). Briefly, 10 mL of bacterial cultures was spun at 5,000 × g at 20℃, supernatant was discarded, and the pellet was fully resuspended in 2 mL of chloroform, 1 mL of methanol, followed by the addition of 1 mL of methanol acidified with sulfuric acid to produce methyl-hydroxybutyrate. Methyl hydroxybutyrate was analyzed via a gas chromatograph (7890A, Agilent Technologies) equipped with an autosampler (G4513A, Agilent Technologies) and fitted with a 30 m × 250 μm DB-5ms column (Agilent Technologies). The injector temperature was 250 ℃ and the oven temperature was held at 80℃for 1 min, raised to 120 ℃ at a rate of 10 ℃/min, and then to 270 ℃ at 30℃/min, before being held at that temperature for 3 min. Samples were injected at a split ratio of 1:10. A flame ionization detector (FID) at 300 ℃ was used. Helium was used as the carrier gas at a flowrate of 1.5 mL/min. The peak of methyl hydroxybutyrate was resolved at 2.8 min; an internal standard of methyl benzoate was resolved at 5.4 min. The concentration of methyl hydroxybutyrate was established based on a calibration curve using a prepared standard. The percentage of PHB per dry cell weight was calculated as previously described (Lazic et al., 2021; Zaldívar Carrillo et al., 2018).

### 4.3.4. Statistical analysis

Statistical comparisons between treatments were performed using two-tailed t-test. Significance was determined for $P < 0.05$. Results from these analyses can be found in Appendix 2 at the end of the document.

## 4.4. Results

### 4.4.1 Effect of methanol addition on growth and biomass production

Control cultures grown with methane or methanol as the sole carbon source in 10 mM or 0.1 mM AMS media showed no significant difference in growth or biomass; but reduced growth and biomass was observed for methanol- versus methane-grown cultures with 1 mM AMS (Table 4.2; Figs. 4.1 and 4.2 panels A, B, C). The only experiment showing a significant increase in growth (Fig. 4.1) and final biomass (Fig. 4.2) relative to the methane-only control was with a methane:methanol ratio of 0.5 in 0.1 mM AMS (Experiment 9; Fig. 4.1 and 4.2 panel C). All other methane:methanol ratios and AMS concentrations resulted in similar or decreased growth relative to the methane-only control.

Growth and biomass were significantly reduced in control cultures with NMS concentrations of 10 mM and 1 mM when methanol was the sole carbon source compared to methane-grown cultures (Table 4.3; Figs. 4.1 and 4.2 panels D, E, F). Methanol addition only significantly improved growth and biomass production at a methane:methanol ratio of 4 with 1 mM NMS (Figs. 4.1 and 4.2, panel E). All other methane:methanol ratios and NMS concentrations resulted in similar or decreased growth relative to the methane-only control.

### 4.4.2. Effect of methanol addition on oxygen and methane consumption

For AMS-growing cultures, the addition of methanol significantly affected oxygen consumption only at low methane:methanol ratio 0.5 for 1 and 0.1 mM nitrogen) (Table 4.2, Appendix 2). Unlike for AMS, in NMS-growing cultures at 10mM nitrogen, the addition of methanol significantly affected oxygen consumption and the difference between controls (methane only vs methanol only) was significant (lower oxygen consumption with methanol). For 0.1 mM nitrogen, the addition of methanol significantly affected oxygen consumption at low methane:methanol ratio of 0.5 (Table 4.3, Appendix 2).

The methane consumption in AMS-growing cultures was significantly affected with methanol addition only at 1 mM nitrogen (Table 4.2, Appendix 2). In NMS-growing cultures, the addition of methanol significantly affected methane consumption only at 10 mM nitrogen with methane:methanol ratios of 4 and 0.5 (Table 4.3, Appendix 2).

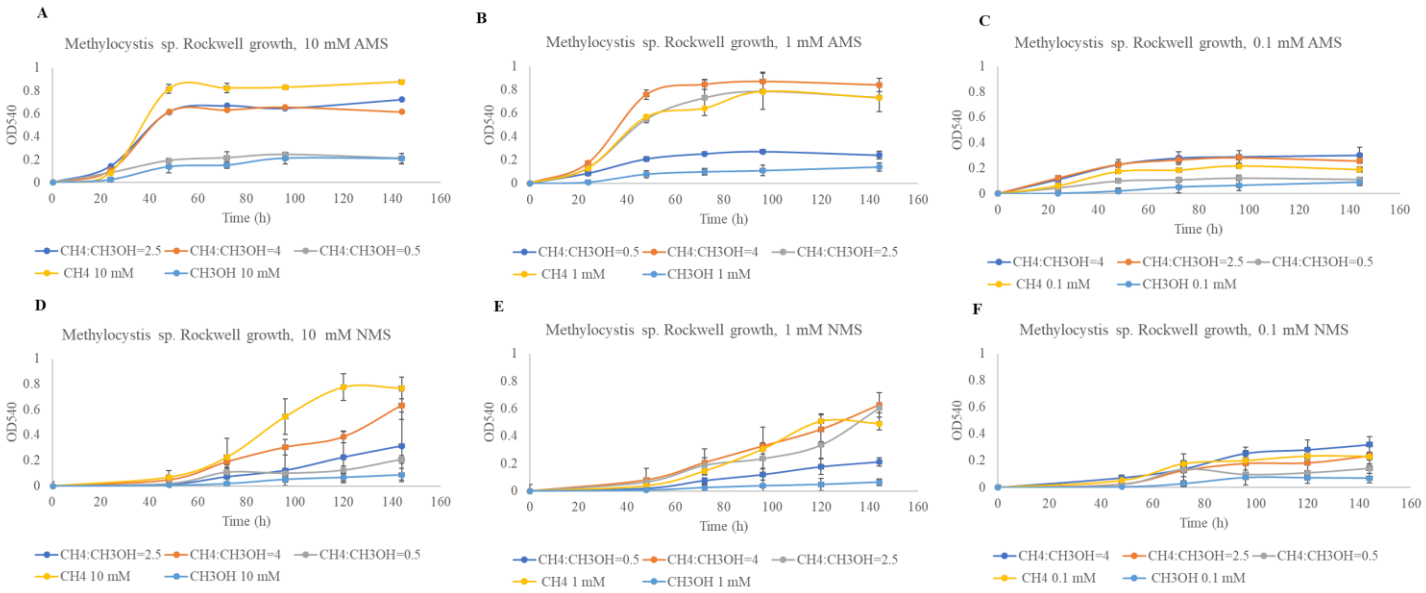


Figure 4.1. Growth of *Methylocystis* sp. Rockwell cultures measured over six days for AMS (panels A, B, C) and NMS (panels D, E, F). Three nitrogen concentrations were combined with three ratios methane:methanol ratios creating nine growing conditions (full factorial design) per nitrogen source. Cultures were grown in 100 mL media in 1000 mL bottle to prevent oxygen limitation (n=3). Error bars represent standard deviation.

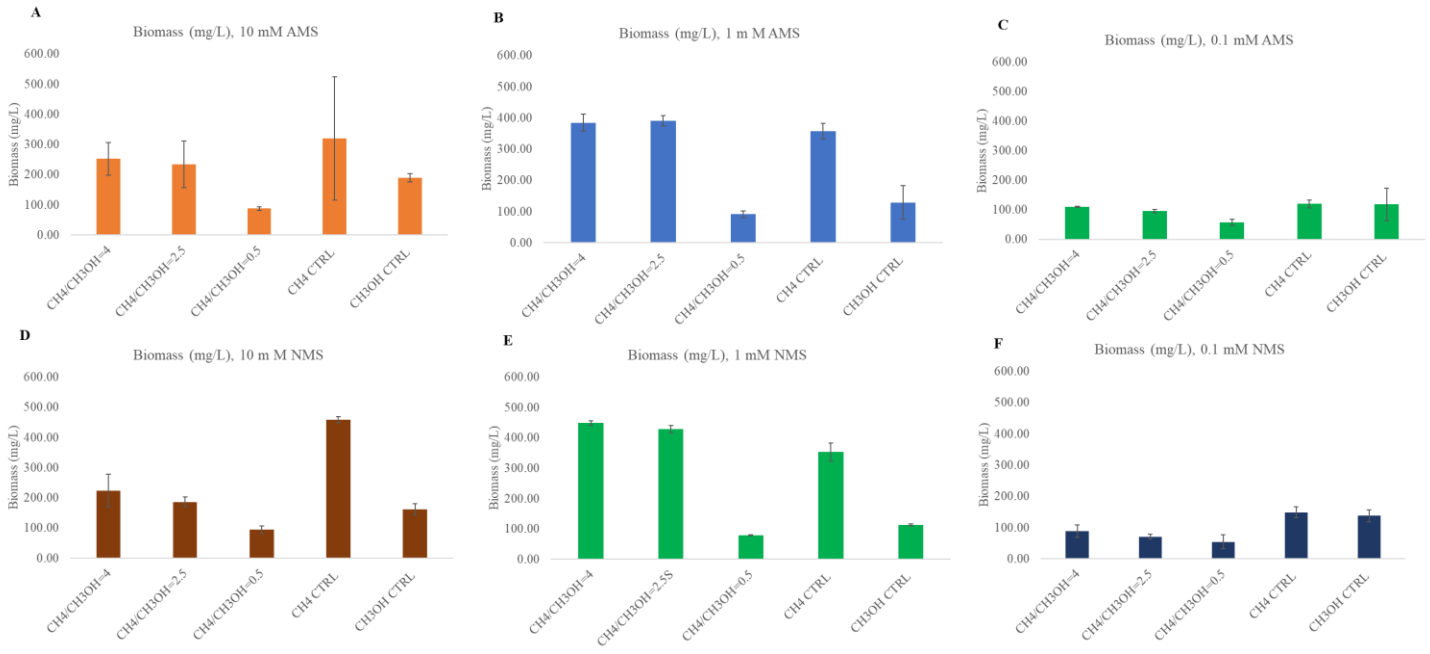


Figure 4.2. Biomass cell dry weight (mg/L) of *Methylocystis* sp. Rockwell cultures measured at day six. Three nitrogen concentrations were combined with three methane:methanol ratios creating nine growing conditions (full factorial design) per nitrogen source. Error bars represent standard deviations (n=3)

Table 4.2. Experimental results from full factorial design with two predictors and controls with 6 mmol carbon source(s) on AMS. Details of experimental conditions are presented in Table 4.1.

| Experiment Name/Number | Biomass (mg/L) | PHB (mg/L) | % PHB (dw) | $O_2$ consumed (mmol) | $CH_4$ consumed (mmol) | $O_2/CH_4$ ratio |
|---|---|---|---|---|---|---|
| 1 | 91.43±10.30 | 23.44±8.03 | 26.45±5.16 | 0.11±0.03 | 0.04±0.00 | 2.63±0.65 |
| 2 | 384.44±27.76 | 271.53±14.25 | 70.70±1.45 | 0.89±0.06 | 0.58±0.05 | 1.52±0.03 |
| 3 | 234.29±76.77 | 37.34±0.59 | 16.89±5.79 | 0.63±0.05 | 0.33±0.02 | 1.92±0.03 |
| 4 | 391.11±16.78 | 268.03±17.05 | 68.74±7.36 | 0.70±0.12 | 0.35±0.10 | 2.03±0.28 |
| 5 | 109.52±1.65 | 62.88±18.55 | 57.52±17.51 | 0.17±0.05 | 0.04±0.03 | 5.80±3.45 |
| 6 | 95.71±6.06 | 60.41±8.79 | 58.78±4.56 | 0.16±0.03 | 0.03±0.01 | 6.91±2.27 |
| 7 | 252.38±54.69 | 35.71±0.90 | 15.35±5.19 | 0.63±0.11 | 0.37±0.07 | 1.67±0.01 |
| 8 | 87.62±5.95 | 37.53±4.05 | 42.76±2.10 | 0.20±0.01 | 0.01±0.01 | 20.71±11.78 |
| 9 | 57.14±9.90 | 29.10±6.16 | 48.86±3.18 | 0.24±0.03 | 0.03±0.01 | 9.37±4.56 |
| CH4_10 | 320.00±204.29 | 23.95±0.28 | 5.39±0.50 | 1.020±0.21 | 0.94±0.17 | 1.08±0.03 |
| CH4_1 | 357.78±25.24 | 163.15±22.70 | 45.96±8.75 | 0.951±0.05 | 0.9±0.08 | 1.12±0.05 |
| CH4_0.1 | 120.00±13.33 | 37.65±8.11 | 31.23±4.00 | 0.104±0.04 | 0.1±0.03 | 1.04±0.07 |
| CH3OH_10 | 190.00±14.14 | 37.85±0.18 | 19.97±1.39 | 0.104±0.06 | N/A | N/A |
| CH3OH_1 | 128.89±53.47 | 41.52±4.19 | 36.49±15.46 | 0.136±0 | N/A | N/A |
| CH3OH_0.1 | 117.78±55.51 | 4.55±0.57 | 4.45±2.11 | 0.084±0 | N/A | N/A |

Table 4.3. Experimental results full factorial design with two predictors and controls with 6 mmol of carbon source(s) on NMS. Details of experimental conditions are presented in Table 4.1.

| Experiment Name/Number | Biomass (mg/L) | PHB (mg/L) | % PHB (dw) | $O_2$ consumed (mmol) | $CH_4$ consumed (mmol) | $O_2/CH_4$ ratio |
|---|---|---|---|---|---|---|
| 1 | 79.05±10.03 | 14.88±1.88 | 18.84±1.14 | 0.12±0.02 | 0.06±0.05 | 3.55±2.57 |
| 2 | 448.89±34.21 | 200.80±7.53 | 44.89±3.57 | 0.69±0.27 | 0.62±0.33 | 1.220.29 |
| 3 | 185.71±16.16 | 41.04±2.03 | 22.23±3.03 | 0.43±0.02 | 0.26±0.06 | 1.72±0.34 |
| 4 | 428.89±64.75 | 210.28±11.91 | 49.70±7.44 | 0.68±0.11 | 0.38±0.09 | 1.83±0.28 |
| 5 | 88.57±19.79 | 66.48±6.79 | 76.70±11.06 | 0.15±0.24 | 0.10±0.10 | 3.37±0.63 |
| 6 | 70.48±7.19 | 45.74±11.09 | 66.40±23.25 | 0.27±0.04 | 0.38±0.23 | 0.91±0.65 |
| 7 | 223.81±54.54 | 39.30±3.18 | 18.22±4.52 | 0.76±0.44 | 0.53±0.26 | 1.44±0.29 |
| 8 | 94.29±13.09 | 20.88±2.23 | 22.28±2.29 | 0.05±0.04 | 0.00±0.00 | 1.27±0.16 |
| 9 | 54.29±22.31 | 20.97±1.10 | 45.04±23.44 | 0.00±0.00 | 0.00±0.00 | 0.00±0.00 |
| CH4_10 | 457.78±10.18 | 18.57±1.76 | 4.06±0.46 | 1.49±0.12 | 1.47±0.07 | 1.02±0.09 |
| CH4_1 | 353.33±23.09 | 142.48±29.86 | 40.77±10.64 | 1.10±0.16 | 0.99±0.09 | 0.97±0.06 |
| CH4_0.1 | 148.89±16.78 | 60.87±12.13 | 41.41±10.16 | 0.10±0.01 | 0.17±0.06 | 0.64±0.31 |
| CH3OH_10 | 162.22±18.86 | 22.81±2.46 | 19.09±0.95 | 0.08±0.01 | N/A | N/A |
| CH3OH_1 | 113.33±29.06 | 14.69±2.79 | 13.98±6.32 | 0.23±0.00 | N/A | N/A |
| CH3OH_0.1 | 137.78±19.25 | 25.10±2.18 | 18.42±2.73 | 0.12±0.09 | N/A | N/A |

4.4.3. The effect of methanol on PHB production

Control experiments showed significantly higher PHB production for cultures grown with methane versus methanol as the sole carbon source; this held for both AMS and NMS at 1 mM and 0.1 mM nitrogen concentrations (Fig. 4.4; Tables 4.3 and 4.4). At 10 mM, the nitrogen concentration was too high to show appreciable PHB production under any condition. In some instances, low levels of improved PHB production were observed with methanol addition at 10 mM AMS or NMS, but overall production remained low. The strongest improvement was observed with 1 mM AMS or NMS and a methane:methanol ratio of 4 or 2.5 (Fig. 4.4, Tables 4.2 and 4.2). Although the % PHB per unit dry weight (dw) was high in experiments with 0.1 mM nitrogen, the biomass was quite low, and did not represent a desirable condition. However, the average percentage of PHB per unit biomass for cells grown with a methane:methanol ratio of 4 and 2.5 was 70% for 1 mM AMS and 48% for 1 mM NMS with high biomass (Table 4.1). To compare, cells grown with methane alone had 46% PHB per unit dw for 1 mM AMS and 41% PHB per unit dw for 1 mM NMS (Table 4.2 and 4.3).

In summary, the addition of methanol in the range of 20-28% (Experiments 2 and 4; methane:methanol ratios = 4 and 2.5) improved PHB production in AMS and NMS without compromising biomass production (Fig. 4.4).

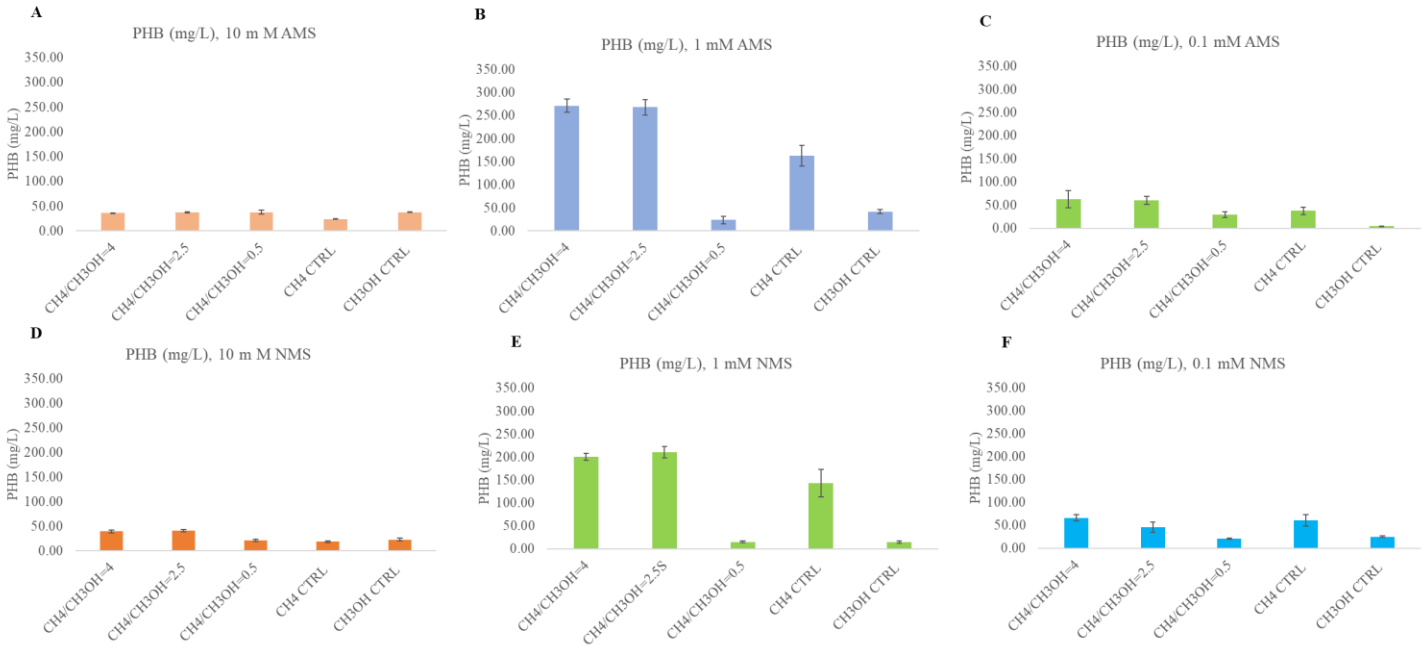


Figure 4.3. The PHB amount (mg/L) was measured in *Methylocystis* sp. Rockwell culture at day six. Error bars represent standard deviations (n=3).

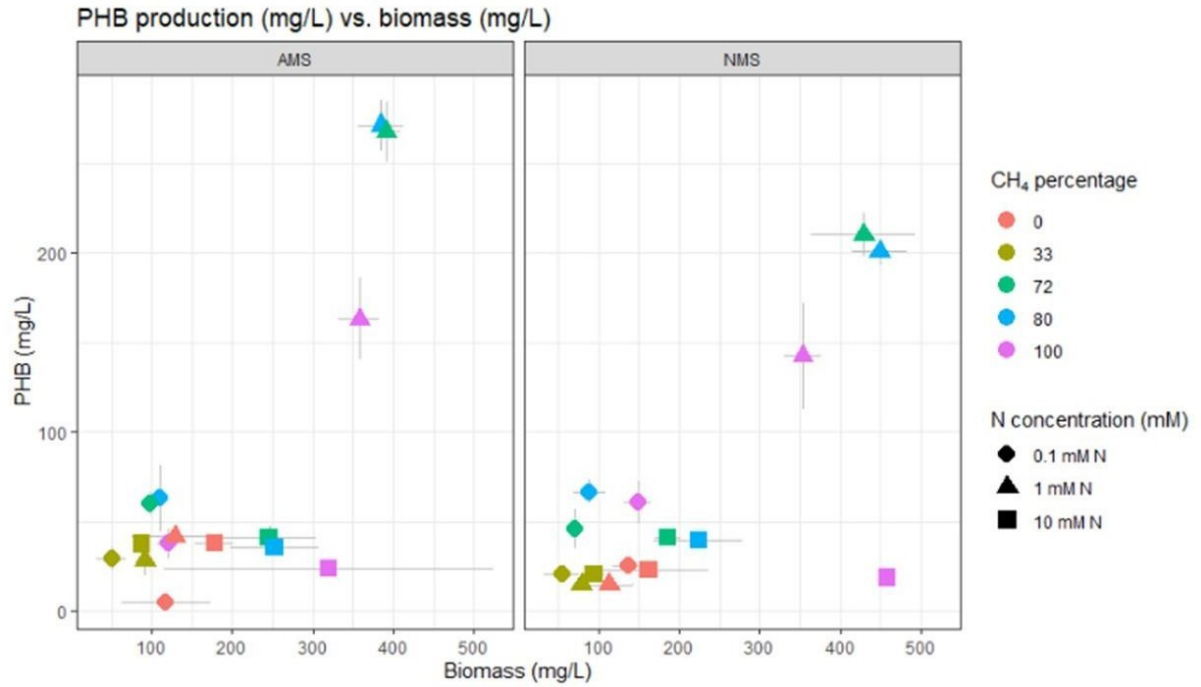


Figure 4.4. Biomass and PHB production in *Methylocystis* sp. Rockwell cultures across all nine experimental treatments for two nitrogen sources – AMS (left panel) and NMS (right panel) (Table 4.1). Treatments that maximize both PHB production and biomass are towardsthe top right of the graphs.

## 4.5. Discussion

The goal of this study was to evaluate the potential beneficial effect of methanol addition on biomass and PHB production *Methylocystis* sp. Rockwell cultures relative to cells grown in methane only in. We also aimed to assess the effects of N-source (AMS or NMS) on these cultures. Our previous study revealed that methanol acts as a stress-related metabolic trigger directing bacterial metabolism toward PHB production (Lazic et al., 2021). However, to justify industrial scale-up, it is required to ensure high bacterial biomass production in addition to PHB. Since methanol triggers a stress response, metabolic biosynthetic pathways are reduced, leading to the decreased growth and biomass production when grown solely with methanol (Lazic et al., 2021). Thus, regardless of a high % PHB level, low biomass production prevents further scale-up processes with methanol as a sole source of carbon. Since methanol is an inexpensive waste-derived carbon source (Fei et al., 2015; Strong et al., 2015; Tays et al., 2018), and unlike methane it is readily available to cells, a methanotroph that can consume both carbon sources and produce value-added compounds (such as PHB) is highly significant and beneficial.

Overall, the addition of methanol reduced production of biomass and growth at a methane:methanol ratio of 0.5, while methane:methanol ratios of 4 and 2.5 were not detrimental to growth (Figs .4.1, 4.2, and Tables 4.2 and 4.3). The oxygen consumption was significantly affected with methanol addition in AMS and NMS at low nitrogen (0.1 m M) and low methane/methanol ratio (0.5). At high nitrogen concentration (10 m M), oxygen consumption was affected only in NMS. The difference in oxygen consumption between methane and methanol control was significant only in NMS-growing cultures with 10 mM nitrogen (Tables 4.2 and 4.3, Appendix 2). The methane consumption was reduced only at 1 mM AMS and at 10 mM NMS, methane:methanol ratios 4 and 0.5 (tables 4.2 and 4.3, Appendix 2).

Both the amount (mg/L) and % PHB per unit dw were vastly improved with methane:methanol ratios of 4 and 2.5 with 1 mM AMS or NMS (Figs. 4.3 and 4.4, Tables 4.2 and 4.3) indicating that these are the appropriate amounts of methanol and nitrogen to test in bioreactors for scale-up of PHB production by *Methylocystis* sp. Rockwell. Moreover, the N:C ratio of these optimal conditions was 0.017, which is similar to the ratio of 0.016 found for PHB production by *M. trichosporium* OB3b (Zaldivar Carrillo et al., 2018).

The beneficial effect of methanol on PHB accumulation in alphaproteobacterial methanotrophs had been shown for *M. trichosporium* OB3b (Zaldivar Carrillo et al., 2018) and *M. trichosporium* IMV3011 (Zhang et al., 2008). In the case of *M. trichosporium* OB3b, a higher methane:methanol ratio tended to promote PHB production in AMS whereas a lower methane:methanol ratio promoted PHB production in NMS (Zaldivar-Carrilo et al., 2018). On the other hand, *Methylocystis* sp. Rockwell did not show a nitrogen source dependence forPHB production, but the N:C ratio was an important parameter. Furthermore, improvement ofPHB production did not require nitrogen starvation; in fact, low nitrogen levels of 0.1 mM did not improve production. These results clearly indicate the importance of establishing the optimal N:C ratio that promotes PHB synthesis without negatively affecting growth and biomass production for alphaproteobacterial methanotrophs. Similarly to *M. trichosporium* OB3b, *Methylocystis* sp. Rockwell benefited from a methane/methanol combination to boost PHB synthesis without compromising biomass production. The positive synergistic effect of these two C1 substrates was also observed in *M. trichosporium* IMV3011 (Zhang et al., 2008). In addition, two substrates can affect quality of the polymer produced as shown in the methylotrophic bacterium, *Mehylobacter exotermus* (MW of PHB was reduced from $1.7\times10^6$ Da to $0.6\times10^6$ Da) (Anderson et al., 1992). Despite this effect, alterations in PHB structures have not yet been observed in alphaproteobacterial methanotrophs with methane/methanol mixtures and could be an excellent area for future investigation.

The exact effect that methanol has on cellular physiology is not fully understood. It is known that gammaproteobacterial methanotrophs can tolerate high levels of methanol due to their efficient GSH-dependent detoxification of formaldehyde (Sugden et al., 2021) and energetically more efficient RuMP cycle for formaldehyde assimilation (Kalyuzhnaya et al., 2013; Ngyan et al., 2020). On the other hand, the serine cycle used by alphaproteobacterial methanotrophs is less efficient and energetically more expensive (Bordel et al., 2019; Trotsenko and Murrell, 2008). Alphaproteobacterial methanotrophs also lack GSH-dependent formaldehyde detoxification. For these reasons, they do not grow robustly on methanol as the sole carbon source (Tays et al., 2018; Lazic et al., 2021). However, the presence of small amounts of methanol (high methane:methanol ratio) in *Methylocystis* sp. Rockwell cultures did not negatively affect biomass and improved PHB production (Fig. 4.4). Thus, it is possible that the fate of methanol varies depending on its concentration. When present as the sole carbon source, methanol should be assimilated into biomass. When methanol is added along with methane where methane is the dominant carbon source, it could act as a stringent response regulator. A recent study by Benett et al. (2020) found that an engineered methylotrophic *E. coli* was unable to grow on methanol due to its inability to synthetize essential amino acids. Thus, they improved the stringent response through enhanced activation of ppGpp, DksA and RpoS (ϱs), which enabled efficient protein biosynthesis and improved methanol utilization (Bennett, 2020). However, these authors did not test the effect of different amounts of methanol on stringent response activation, but instead focused on genetic modification. It might be possible that methanol at low levels acts as a stringent response trigger in *Methylocystis* sp. Rockwell, which promotes protein biosynthesis through activation of alternative sigma factors. However, this stringent response can be considered "fake", as cultures are not also exposed to a nutrient stress. In this scenario, protein biosynthesis is diverted, and cells can direct metabolic pools toward PHB synthesis while stillgrowing. In favor of this hypothesis, TCA cycle inhibition tends to improve PHB

production (Zhang et al., 2008). The TCA cycle is a major source of amino acid precursors, so if a stringent response were to trigger de novo amino acid biosynthesis, then the consumption of TCA cycle metabolites would increase. This might result in acetyl-CoA re-direction toward PHB rather than towards the TCA cycle. In terms of stringent response connections to the PHB biosynthesis it is worth of mentioning studies on cyanobacteria that showed relation between ppGpp (main stringent response indicator) and PHB production (Juengert et al., 2017). In famous PHB producer, *R. eutropha* H16, deletion of spoT genes reduced PHB synthesis (Juengert et al., 2017), which indicates potential connections between stringent response and PHB synthesis. In addition to the stringent response, PHB synthesis has been linked to the redox balance maintenance (NADH/NAD+), and it has been shown that PHB serves as the electron sink and maintain NADH/NAD+ ration in the cell (Hauf et al., 2013). It is possible that with methanol, the organism is pumping electrons toward PHB to balance the excess of reductants that are generated and not used for methane oxidation be MMO. However, the amount of formaldehyde produced must be balanced as well to prevent toxicity, which is not possible with methanol as the sole carbon source. The unresolved question remains whether the methanol promotes PHB synthesis in combination with methane (ratio methane:methanol), or the effect of methanol is strictly linked to the methanol concentration that would be low enough to prevent overproduction of formaldehyde and high enough to support stringent response and ensure synthesis of electron sink to maintain the balance of reduction equivalents.

In conclusion, this study confirms that the combination of methane and methanol at elevated ratios of the former benefit PHB production at an N:C of 0.017. The exact physiological mechanism remains to be elucidated and will require additional experimentation, including $^{13}C$ metabolic tracing of consumed carbon, analysis of stringent response components at different time points, and proteomic analysis. Additional omics data

can be incorporated into a Genome Scale Metabolic Model (GEM) to enable *in silico* metabolic simulation to better track biochemical and metabolic fluxes in this microbe.

Chapter 5

# In vivo quantification of polyhydroxybutyrate (PHB) in the alphaproteobacterial methanotroph, *Methylocystis* sp. Rockwell

*A version of this mansuscript has been published: Lazic, M., Gudneppanavar, R., Whiddon, K., Stein, L.Y., Sauvageau, D., Konopka, M. 2022. In vivo quantification of polyhydroxybutryate (PHB) in alphaproteobacterial methanotrophs. Appl. Microbiol. Biotechnol. 106(2):811-819 doi:10.1007/s00253-021-11732-x*

## 5.1 Abstract

Methane is a common industrial by-product that can be used as feedstock for production of the biopolymer polyhydroxybutyrate (PHB) by alphaproteobacterial methanotrophs. *In vivo* assessment of PHB production would shed light on the biosynthesis process and guide design of improved production strategies, but it is currently difficult to perform efficiently. In this study, the alphaproteobacterial methanotroph *Methylocystis* sp. Rockwell was grown on methane with three different nitrogen sources (ammonium, nitrate, and atmospheric nitrogen), and biomass samples were harvested at defined time points during lag, exponential, and stationary growth phases. PHB cell content was analyzed at these sampling points via a standard gas chromatography-flame ionization detector method, which requires hydrolysis of PHB and esterification of the resulting monomer under acidic conditions, and a novel, rapid, cost-effective approach based on fixation and staining of bacterial cells via Nile Blue A fluorescent dye enabling differential staining of cell membranes and intracellular PHB granules for single-cell analysis through fluorescence microscopy. Overall, the two PHB quantification approaches were in agreement at all stages of growth and in all three growing conditions tested. The PHB cell content was greatest with

atmospheric nitrogen as a nitrogen source, followed by ammonium and nitrate. Under atmospheric nitrogen and ammonium conditions, PHB cell content decreased with growth progression, while under nitrate conditions PHB cell content remained unchanged in all growth phases. In addition to presenting a rapid, efficient method enabling in vivo quantification of PHB production, the present study highlights the impact of nitrogen source on PHB production by *Methylocystis* sp. Rockwell.

## 5.2. Introduction

Polyhydroxybutyrate (PHB) is a biopolymer that accumulates in microorganisms as a result of nutrient limitation and availability of excess carbon (Pieja, Rostkowski, et al., 2011; Pieja, Sundstrom, et al., 2011; Strong et al., 2016). Due to its biodegradability and physical properties, PHB shows potential as an alternative to petroleum-derived polymers (Strong et al., 2016). While most microbial production of PHB relies on using sugars as feedstocks (Harding et al., 2007), the relatively high cost and food vs. fuel controversy have motivated researchers to investigate greener and more economical feedstock alternatives. Agricultural waste has been recognized as one of the least expensive feedstock options for PHB production. Two recent studies reported PHB production *by Bacillus drentensis* strains BP17 and *Zobellellae tiwanensis* strain DD5 while growing on pineapple or banana peels (Penkhrue et al., 2020). However, agricultural wastes are heterogeneous and complex, and some components can interfere with efficient bioconversion. Thus, there is continuous interest in seeking alternative feedstocks, such as methane ($CH_4$), that are inexpensive, structurally simple, abundant, and that do not impede on food sources. Methane is an abundant and potent greenhouse gas (GHG) that is estimated to contribute approximately 40% of the current radiative forcing attributed to anthropogenic greenhouse gas emissions (IPCC, 2013). Methane is also a sole carbon and energy source for aerobic methane-oxidizing bacteria, or

methanotrophs (Trotsenko & Murrell, 2008). The most widely studied methanotrophs belong to the Proteobacteria phylum within the classes of Alphaproteobacteria and Gammaproteobacteria. Alphaproteobacterial methanotrophs assimilate formaldehyde via the serine pathway, and, under nutrient limitation, carbon is gated from the serine to the PHB biosynthesis pathway (Pieja, Sundstrom, et al., 2011). Despite their identical carbon metabolism pathways, optimal PHB production by alphaproteobacterial methanotrophs varies from strain to strain in terms of their preferred carbon and nitrogen sources (Zaldívar Carrillo et al., 2018). For example, previous studies showed that addition of methanol to culture media can improve PHB production in *Methylosinus trichosporium* IMV3011 and *Methylosinus trichosporium* OB3b (Zaldívar Carrillo et al., 2018; Zhang et al., 2008). In terms of nitrogen source, *Methylosinus trichosporium* OB3b produced more PHB upon nutrient deprivation when cultivated with nitrate, while *Methylocystis parvus* OBBP produced PHB optimally when grown with ammonium (Rostkowski et al., 2013; Zhang et al., 2017). The common factor in these studies is the presence of a stress signal, i.e., the presence of methanol or nitrogen depletion, that triggered PHB biosynthesis. Since stress can often result in lower biomass yield, the industrialization of alphaproteobacterial methanotrophs requires evaluation of specific nutrient combinations that favor the production of both biomass and PHB.

The detection and quantification of PHB with a rapid, simple, reliable, and cost-efficient method are essential tools in the development of strategies for improved cellular production and efficient bioprocessing. The standard method for PHB quantification involves derivatization (i.e., depolymerization under acidic conditions and esterification with methanol) followed by gas chromatography (GC-flame ionization detector: GC-FID). While this method has high sensitivity, accuracy, and reproducibility, it is extremely time consuming and requires the use of hazardous chemicals at high temperature. In addition, the

method is destructive and does not enable in vivo assessment of PHB. Thus, there is increased interest in seeking alternative methods to derivatization/ GC-FID-based PHB detection and quantification. Previously, flow cytometry and transmission electronic microscopy (TEM) have been successfully used to visualize and quantify PHB (Li & Wilkins, 2020; Tian et al., 2005); however, the expenses and facilities required for these techniques may preclude their widespread adoption.

The present work presents a fluorescence microscopy-based method that relies on a stable lipophilic fluorescent dye that targets intracellular PHB granules. Some commonly used dyes for PHB assessment include Nile Red and Sudan Black (Kung et al., 2007), but here we used the cationic oxazinic compound, Nile Blue A (NBA) (Martinez & Henary, 2016). The spectral properties of NBA are dependent on the pH and polarity of its solvent. In addition to staining lipids, NBA was also shown to target intracellular granules of PHB in *Azotobacter chrococcum* and *Bacillus megaterium* KM cells and was non-specific toward glycogen and polyphosphate (Ostle & Holt, 1982). Moreover, the broad spectral properties of NBA make it possible to visualize cell membranes and PHB granules at different excitation wavelengths (Martinez & Henary, 2016).

In this study, we demonstrate specific staining of intracellular PHB granules and cell membranes of the methanotroph *Methylocystis* sp. strain Rockwell by NBA. We applied this single-cell, in vivo fluorescence microscopy method to quantify PHB cell content during cultivation of *Methylocystis* sp. strain Rockwell growing on methane and three different nitrogen sources. We further validated the microscopy method by comparing our results to the derivatization/ GC-FID method for PHB quantification on the same cell samples. This single-cell fluorescence microscopy method for PHB quantification avoids the use of hazardous solvents and time-consuming manipulations and will be valuable in rapidly assessing PHB bioproduction by methanotrophic bacteria in an industrial context.

## 5.3. Materials and methods

### 5.3.1. Bacterial strains and cultivation

*Methylocystis* sp. Rockwell (ATCC 49242) and *Methylosinus trichosporium* OB3b (NCIMB 11131) strains were cultivated in sterile 250-mL sealed serum bottles containing 100 mL ammonium mineral salts (AMS) medium (10 mM $NH_4Cl$), nitrate mineral salts (NMS) medium (10 mM $KNO_3$), or no nitrogen mineral salts medium (NoN). Each medium formulation contained per L: 1 g $MgSO_4 \cdot 7H_2O$, 0.2 g $CaCl_2 \cdot 2H_2O$, 1 µM $CuSO_4 \cdot 5H_2O$, 3.8% w/v FeEDTA solution, 0.1% w/v $NaMo \cdot 4H_2O$, Whittenbury trace elements solution, and phosphate buffer at pH 7.0 (Whittenbury & Wilkinson, 1970). Cultures were grown in the presence of 3:2 air: methane mixture in the headspace. Methane gas was injected using a sterile 0.2-µm size filter after extracting the same amount of air from the headspace. Cultures were incubated at 30 °C and 200 rpm in an orbital shaker (MaxQ6000, Thermo Scientific). Bacterial cultures were grown under the same conditions for both methods for PHB detection and harvested in lag, log, and stationary phase. Samples were analyzed via GC/FID derivatization and fluorescent microscopy.

### 5.3.2. Sample preparation for fluorescence microscopy

Cell samples were collected in lag phase ($OD_{540}$ ~ 0.100), exponential phase ($OD_{540}$ ~ 0.200), and stationary phase ($OD_{540}$ ~ 0.300) as determined by spectrophotometry at a wavelength of 540 nm (Implen, Nanophotometer P330). Cells were centrifuged at 10,000 × g for 5 min and re-suspended into 1% phosphate buffered saline solution (PBS, pH 6.9–7.0). Cells were fixed immediately using 4% paraformaldehyde solution (Sigma-Aldrich). Prior to imaging, fixed cells were stained with Nile Blue A (Sigma Aldrich), which was dissolved at a concentration of 0.05% (w/v) ethanol and added to samples to a final concentration of 10 µL/mL (14.13 µM). Staining was performed for 30 min at 30 °C in an orbital shaker at 200 rpm.

5.3.3. Quantification of PHB in single cells using fluorescence microscopy

Nile Blue A-stained cells were imaged using a Nikon A1 inverted confocal microscope. Imaging was done on 0.01% polylysine (Sigma Aldrich) -coated cover slips and glass slides with the 100 × Plan Apo λ (NA 1.45) oil objective. Excitation was performed with multiple wavelengths using solid-state lasers, and emission was selected by band pass filters. Specifically, excitation at 561 nm was filtered for emission in the 575–625 nm range, while 647-nm excitation was filtered for the 650–720 nm range. Laser intensity was maintained at 1% with HV gain below the pixel oversaturation limit. Emission signals were captured using GaAsP (for $\lambda_{ex}$ = 561 nm) and photomultiplier tube (for $\lambda_{ex}$ = 647 nm) detectors with the pinhole radius at 0.3 μm. All the imaging was performed at room temperature immediately after staining. Images were analyzed using the NIS-Elements AR Analysis 4.20.00 software (Nikon). The volume of each individual cell and internal PHB granules were calculated based on the region of interest (ROI) with fluorescence intensity above the threshold value. Cell surface area and PHB granules area were obtained from the ROI using standard settings for image analysis. Based on the two-dimensional (2D) region of interest, percent PHB per cell was calculated as:

$$\%\ PHBa\ (ROI_{Area}) = \frac{\sum_{i=1}^{n} A_i}{A_c} \qquad \text{Eq. (5.1)}$$

where Ai is the area of individual granules within a cell and Ac is the total area of a cell. Parameters obtained from the 2D analysis such as cell radius and length were converted to three-dimensional (3D) volume-based percent PHB per cell:

$$\%\ PHBv\ (ROI_{Area}) = \frac{\sum_{i=1}^{n} V_i}{V_c} \qquad \text{Eq. (5.2)}$$

where Vi is the volume of individual granules within a cell and Vc is the total volume of a cell. Further, volume percent was converted to mass percentage (% PHBm) using PHB density factor of 1.099 (corresponding to the ratio of densities between PHB (1.22 g/mL) and bacterial cells (1.11 g/mL)). Plots show that notches contain a 95% confidence interval around the median (+ / − 1.5 × interquartile). Upper and lower whiskers display 75$^{th}$ and 25$^{th}$percentile. Notches with similar shapes (ranges) and median overlaps indicate similar variance and populations, respectively.

5.3.4. Quantification of PHB by derivatization/GC-FID

The quantification of PHB in each of the cultures was validated by derivatization/GC-FID as described previously (Zaldívar Carrillo et al., 2018). Briefly, 10 mL of culture was centrifuged at 5000 × g for 30 min. The supernatant was discarded, and the pellet was re-suspended in 2 mL chloroform, 1 mL methanol, and 1 mL of benzoic acid solution (40 mg/l) dissolved in methanol and acidified with 3% concentrated sulfuric acid. The sample was digested for 5 h in a capped glass vial in a boiling water bath in order to depolymerize the PHB polymer to its monomer and esterify it with methanol. After cooling, 1 mL deionized water was added, and the sample was vortexed for 20 s before standing overnight for phase separation. The organic phase was analyzed for monomer, using a gas chromatograph (7890A, Agilent Technologies) equipped with an autosampler (G4513A, Agilent Technologies) and fitted with a 30 m × 250 μm DB-5ms column (Agilent Technologies). The percentage of PHB per dry cell weight was calculated as previously described (Zaldívar Carrillo et al., 2018). The amount of PHB in the sample was calculated using the area ratio (AR) of the methyl- 3-hydroxybutyrate peak to the internal standard peak and a calibration curve relating AR to the analyte concentration.

5.3.5. Cell dry weight measurements

Cell dry weight was measured by extracting 35 mL of culture and centrifuging at 10,000 × g and 4 °C for 10 min (Sorvall RC 6 Plus, SS-34 rotor; Thermo Scientific). The

supernatant was discarded, and the pellet was re-suspended in 10 mL deionized water and transferred to a pre-weighed weigh dish. The dish was placed in an oven at 60 °C for drying to constant weight. The cell dry weight per volume was then calculated based on the difference in mass. All measurements were performed in triplicates (n = 3).

## 5.4. Results

### 5.4.1. Single-cell staining and microscopic visualization of PHB granules

We visualized and compared the abundance of intracellular PHB granules in cells of *Methylocystis* sp. Rockwell when cultivated with methane and ammonium (AMS), nitrate (NMS), or atmospheric nitrogen (nitrogen starvation; NoN) as the N-source. To determine the effects of distinct growth phases on PHB accumulation, cells were sampled in lag, exponential, and stationary phases of growth. Collected cells were fixed and stained using Nile Blue A perchlorate (NBA) and visualized via fluorescence microscopy. Distinct multi-emission properties of NBA enabled differential visualization of cell membrane ($\lambda_{ex}$ = 647 nm) and PHB granules ($\lambda_{ex}$ = 561 nm) (Fig. 5.1). Significant photobleaching was not observed (laser intensity: 1%), and 2D slices of images minimized possible photobleaching. The use of high magnification objectives (100 × 1.45 NA) facilitated analysis of individual PHB granules on a cell-to-cell basis, no matter the variation in granule size. As a negative control for the staining protocol, we performed the same procedure with the alphaproteobacterial methanotroph *Methylosinus trichosporium* OB3b under conditions that do not lead to the production of PHB granules.

No fluorescence emission was detected under the excitation condition expected for PHB granules; the only fluorescence signal was indicative of labeling of the cell membrane by NBA (Fig. 5.2). The absence of PHB was also confirmed using derivatization/GC-FID analysis.

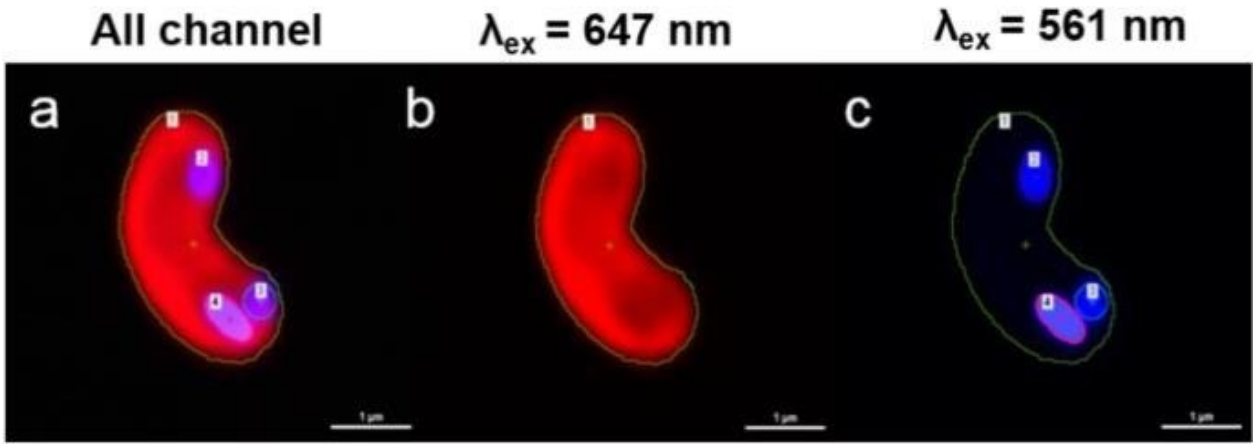


Figure 5.1. Fluorescence images of Nile Blue A (0.05% in ethanol) -stained *Methylocystis* sp. Rockwell. "All channel" represents merging of $\lambda_{ex}$ = 647 nm and $\lambda_{ex}$ = 561 nm, whereas "far red fluorescence" ($\lambda_{ex}$ = 647 nm) represents the membrane and "near red fluorescence" ($\lambda_{ex}$ = 561 nm) represents the PHB granules. Individual PHB granules are internalized spherically and dispersed in the cell. Nile Blue A-stained regions above the threshold for fluorescence intensity were marked as region of interest (ROI). (a) Stacked fluorescent image channels of membrane and granules with marked ROIs. ROIs corresponding to the membrane or area of the cell (b) and PHB granules (c). The % PHBv per cell was calculated by dividing volume of granules by the volume of the cell. Scale bar = 1 μm.

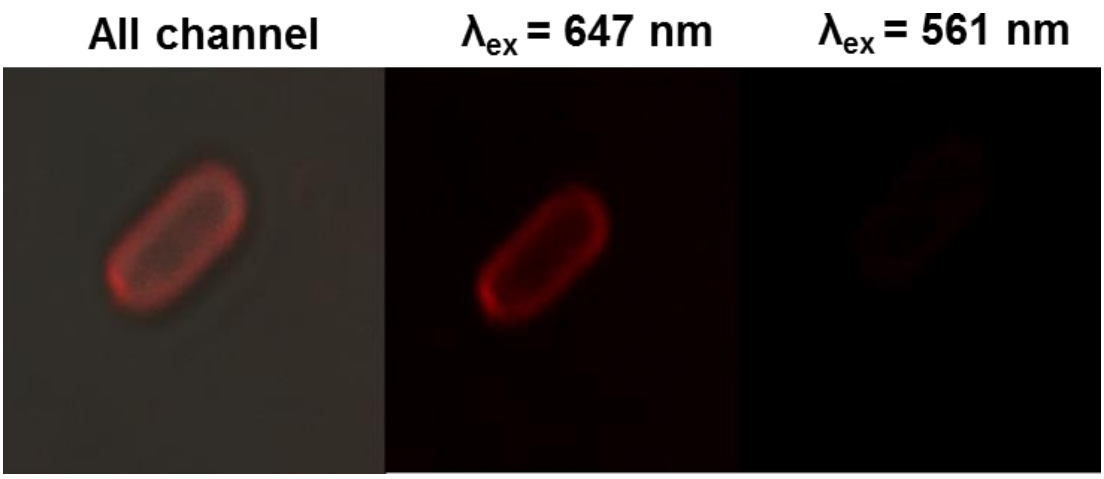


Figure 5.2. Fluorescence imaging of Nile Blue A (0.05% in ethanol) -stained *Methylosinus trichosporium* OB3b cells. "All channel" represents merging of $\lambda_{ex}$ = 647 nm and $\lambda_{ex}$ = 561 nm whereas "far red fluorescence" ($\lambda_{ex}$ = 647 nm) represents the membrane and "near red fluorescence" ($\lambda_{ex}$ = 561 nm) represents the PHB granules. As shown, PHB was not observed in Methylosinus trichosporium OB3b. Scale bar = 1μm.

5.4.2. Quantification of PHB granules

2D single-cell images (n = 300 per sample) with distinct fluorescence channels for cell membrane and PHB were assessed to calculate the area and volume of both the cell and intracellular PHB granules. Images taken using confocal microscopy used an adjusted pinhole to ensure that captured images included the intracellular contents with sections of PHB granules in the x–y plane while minimizing out-of-focus fluorescence (Fig. 5.1). 2D images showing cells and PHB granules were converted to volumes as follows: radius and length of each cell were determined from the cell membrane image ($\lambda_{ex}$ = 647 nm), and the cell volume was estimated to be a cylinder capped with two hemispheres. The fluorescent PHB granules were considered as individual equivalent spheres, each displaying distinguished and separate boundaries. The equivalent diameter of each granule was extracted from the PHB image ($\lambda_{ex}$ = 561 nm) and used to determine the equivalent radius and volume of individual PHB granules in each cell (Fig. 5.3). Three measurements of PHB per cell were reported: PHB content on an area basis (% $PHB_a$), volumetric basis (% $PHB_v$) and mass basis (% $PHB_m$). The % $PHB_a$ was assessed using 2D imaging to obtain the ratio of the area occupied by intracellular PHB granules over the area of the corresponding cell (Fig. 5.4). Volumetric PHB per cell (% $PHB_v$) was calculated by taking the ratio of the sum of the intracellular PHB granule volumes over the volume of the corresponding cell. This volumetric PHB cell content was converted to mass PHB content (% $PHB_m$) using the density of PHB (~ 1.22 g/mL) and bacterial cells (~ 1.11 g/mL) (Figs. 5.6b, 5.7b, and 5.8b). The resulting % $PHB_m$ obtained from microscopy could then be compared to % $PHB_m$ obtained using the derivatization/GC-FID quantification methodology (Figs. 5.6c, 5.7c, and 5.8c). This comparison between methodologies is summarized across the three nitrogen conditions during growth of the bacteria on methane (i.e., AMS, NMS, or NoN) in Fig. 24. The $R^2$ value for agreement

between the two methods was 0.94783. Single-cell analysis also enabled us to report the average number of PHB granules per cell for each growth condition (Fig. 5.5).

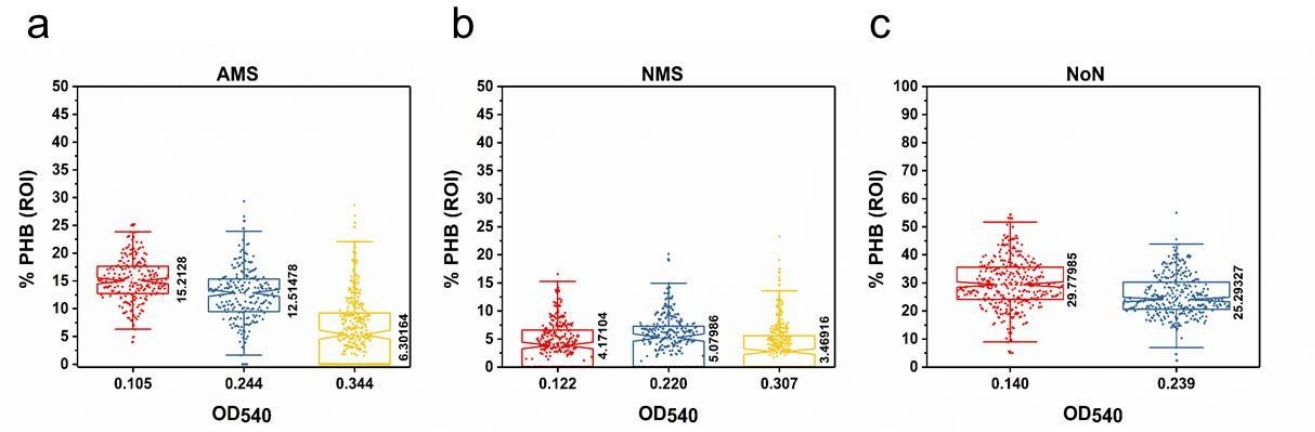


Figure 5.3. Quantification of PHB in *Methylocystis* sp. Rockwell using fluorescence imaging. % $PHB_a$ quantification per cell was based on the fluorescent 2D region of the interest area by calculating the percent ratio of fluorescence area of PHB granules within the cell membrane. Notched plots show % $PHB_a$ distribution in lag phase, exponential phase and stationary phase based on fluorescence images of *Methylocystis* sp. Rockwell grown in (**a)** ammonium mineral salts (AMS), (**b)** nitrate mineral salts (NMS) and (**c)** no nitrogen mineral salts (nitrogen starvation, NoN). Each dot represents a single cell % $PHB_a$ in lag, exponential and stationary phases. Plots contain 300 cells from triplicate cultures. Under these conditions the %$PHB_a$ decreased gradually towards stationary phase from lag phase. However, the trend remained unchanged in NMS grown cells. (c plot y axis range is 0 to 100 whereas a and c plots y axis range is 0 to 50).

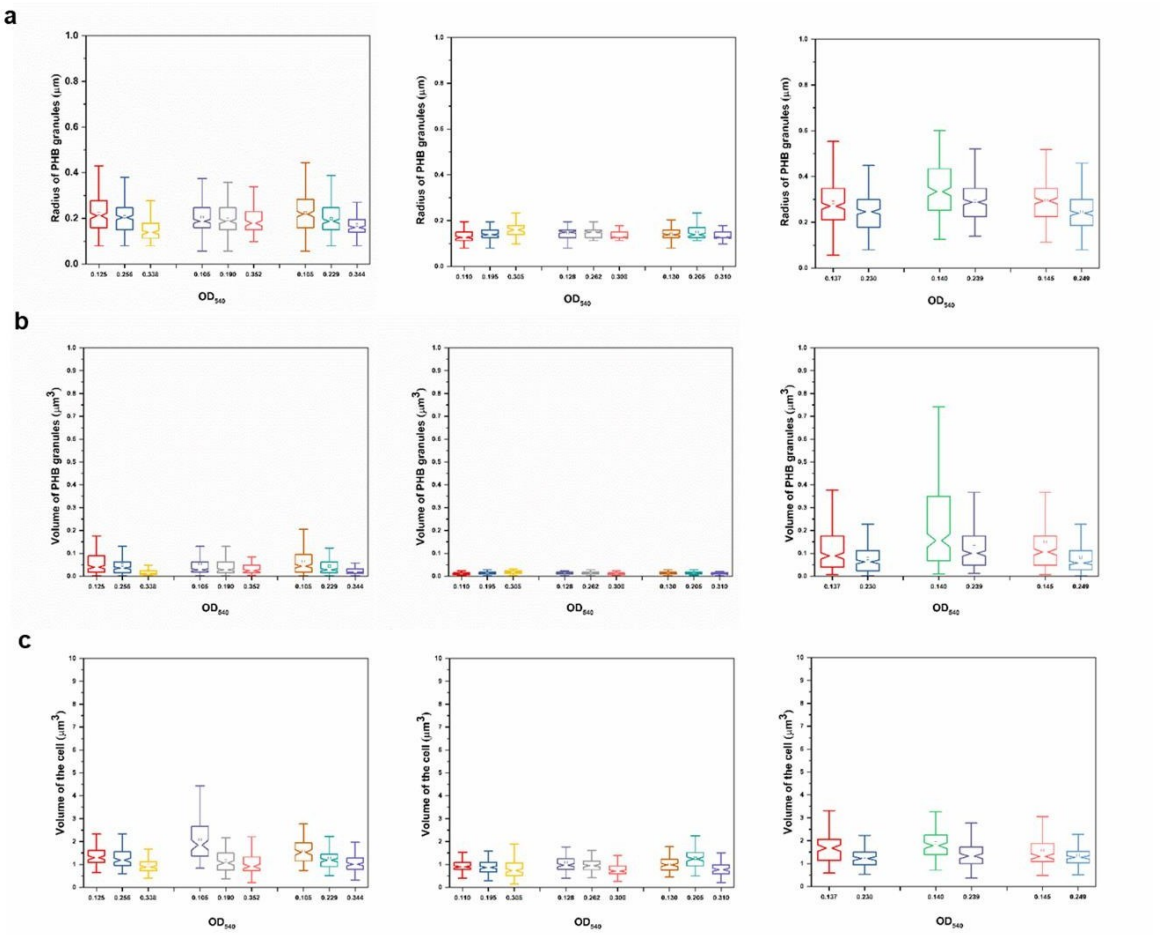


Figure 5.4. Plots represent (a) Radius, (b) Volume of individual PHB granules and (c) Volume of *Methylocystis* sp. Rockwell cells grown in AMS, NMS and Nitrogen starvation media (NoN) in lag phase ($OD_{540}$~0.100), exponential phase ($OD_{540}$~0.200) and stationary phase ($OD_{540}$~0.300). Radius, volume of PHB granules, and volume of cells decreased from the lag to stationary phase in AMS and NoN conditions. However, they remained constant in NMS. Each notched plot sampled 100 cells for each of triplicate samples (n=300).

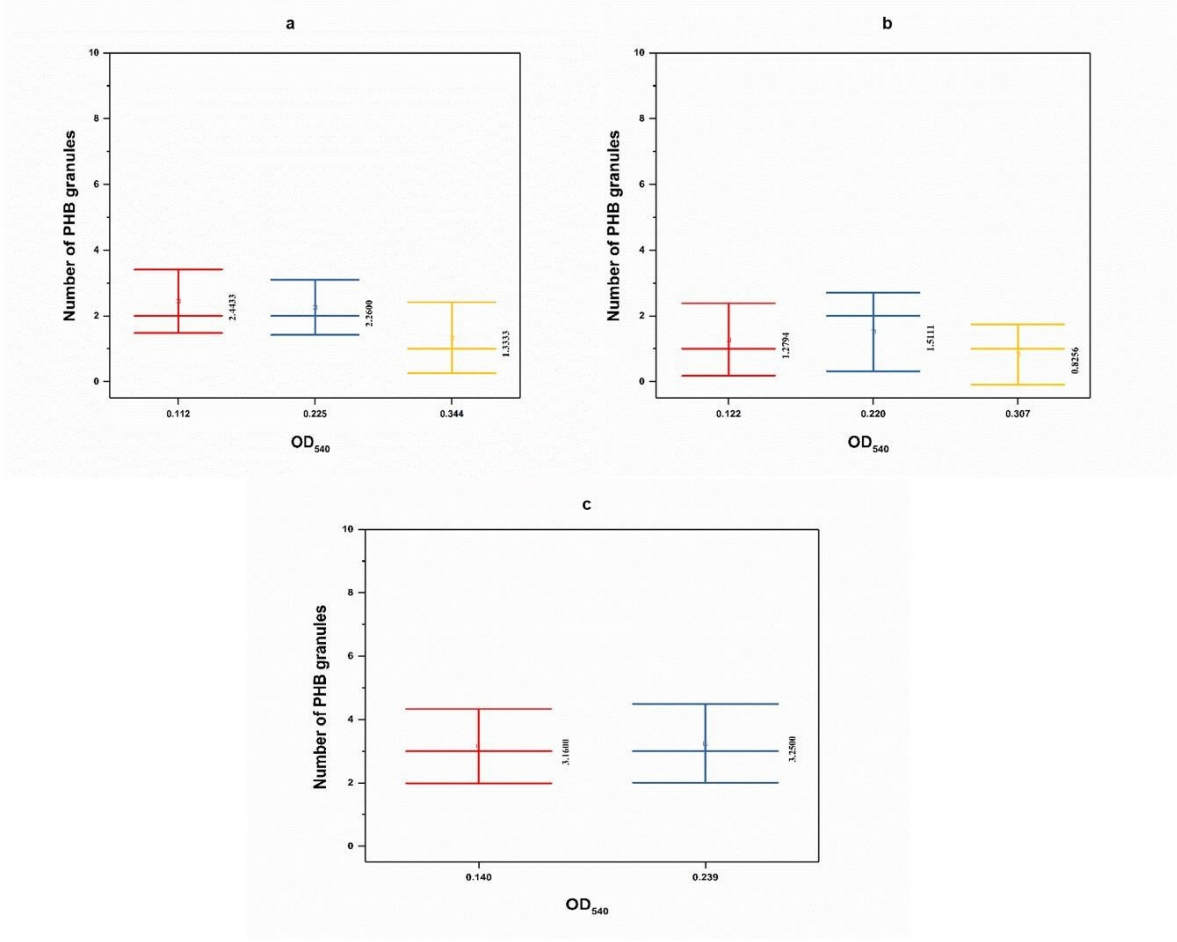


Figure 5.5. Total number of PHB granules per *Methylocystis* sp. Rockwell cell (n = 100 per sample in triplicate; n =300 per $OD_{540}$) grown in (a) AMS, (b) NMS and (c) Nitrogen starvation (NoN) media. In all three conditions, the number of PHB granules remained constant during lag and exponential phases and decreased in stationary phase. No granules were detected in stationary phase in NoN medium; thus, this data point was not plotted.

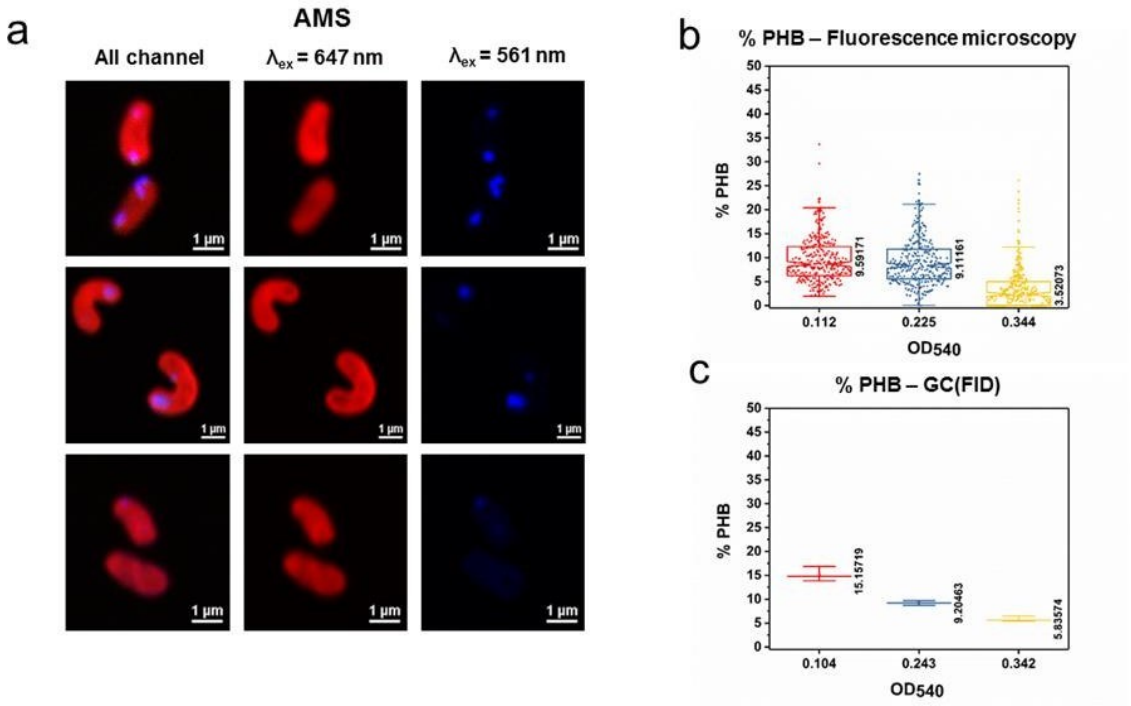


Figure 5.6. Single-cell quantification of PHB using fluorescence imaging and verified using derivatization/GC-FID. (a) Fluorescence images of *Methylocystis* sp. Rockwell grown in AMS and methane and stained with Nile Blue A. "All channel" represents merging of $\lambda_{ex}$ = 647 nm and $\lambda_{ex}$ = 561 nm, whereas $\lambda_{ex}$ = 647 nm image represents membrane staining and λex = 561 nm represents PHB granule staining (false blue color). Images imply PHB granule variation in lag (top row), exponential (middle row), and stationary (last row) phases. Notched plots of % $PHB_m$ distribution at lag phase ($OD_{540}$ = 0.112 and 0.104), exponential phase ($OD_{540}$ = 0.225 and 0.243), and stationary phase ($OD_{540}$ = 0.344 and 0.342) based on fluorescence images (b) and GCFID data (c), respectively.

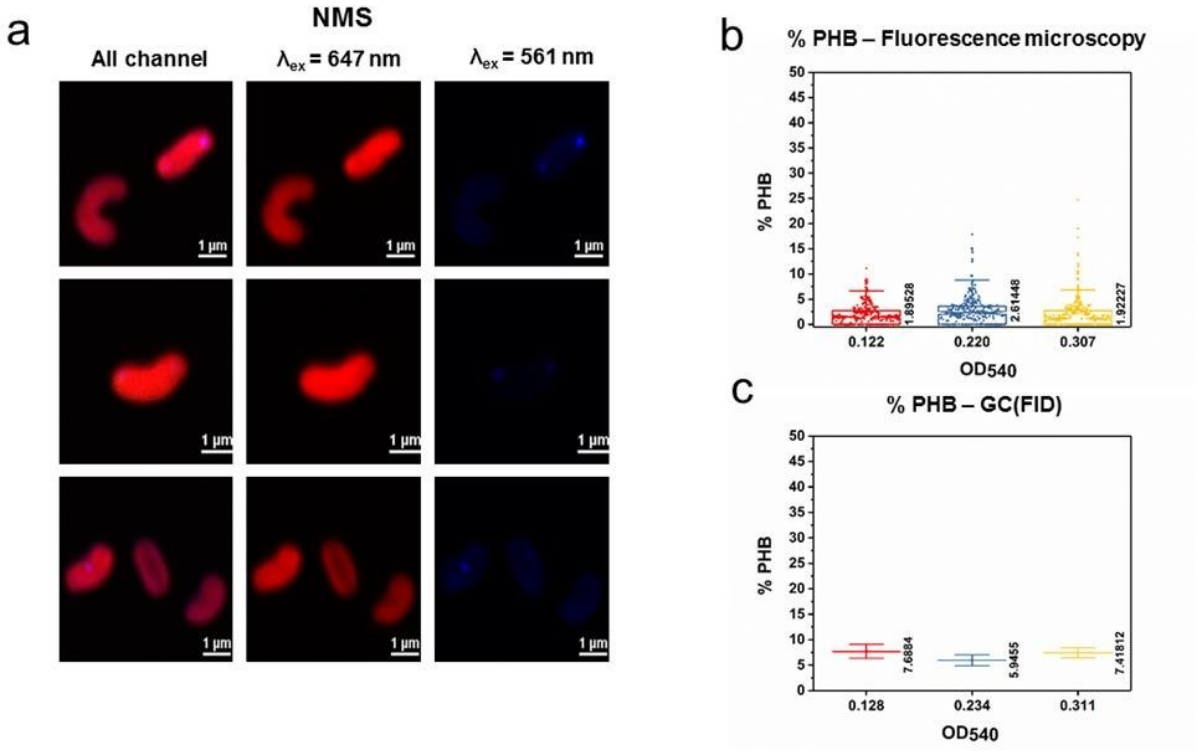


Figure 5.7. Single-cell quantification of PHB using fluorescence imaging. (a) Fluorescence images of *Methylocystis* sp. Rockwell grown in NMS and methane and stained with Nile Blue A. "All channel" represents merging of $\lambda_{ex}$ = 647 nm and $\lambda_{ex}$ = 561 nm, whereas $\lambda_{ex}$ = 647 nm image represents membrane staining and $\lambda_{ex}$ = 561 nm represents PHB granule staining (false blue color). Images imply PHB granule variation in lag (top row), exponential (middle row), and stationary (last row) phases. Scale bar = 1 µm. Notched plots of % $PHB_m$ distribution at lag phase ($OD_{540}$ = 0.122 and 0.128), exponential phase ($OD_{540}$ = 0.220 and 0.234), and stationary phase ($OD_{540}$ = 0.307 and 0.311) based on fluorescence images (b) and GCFID data (c), respectively.

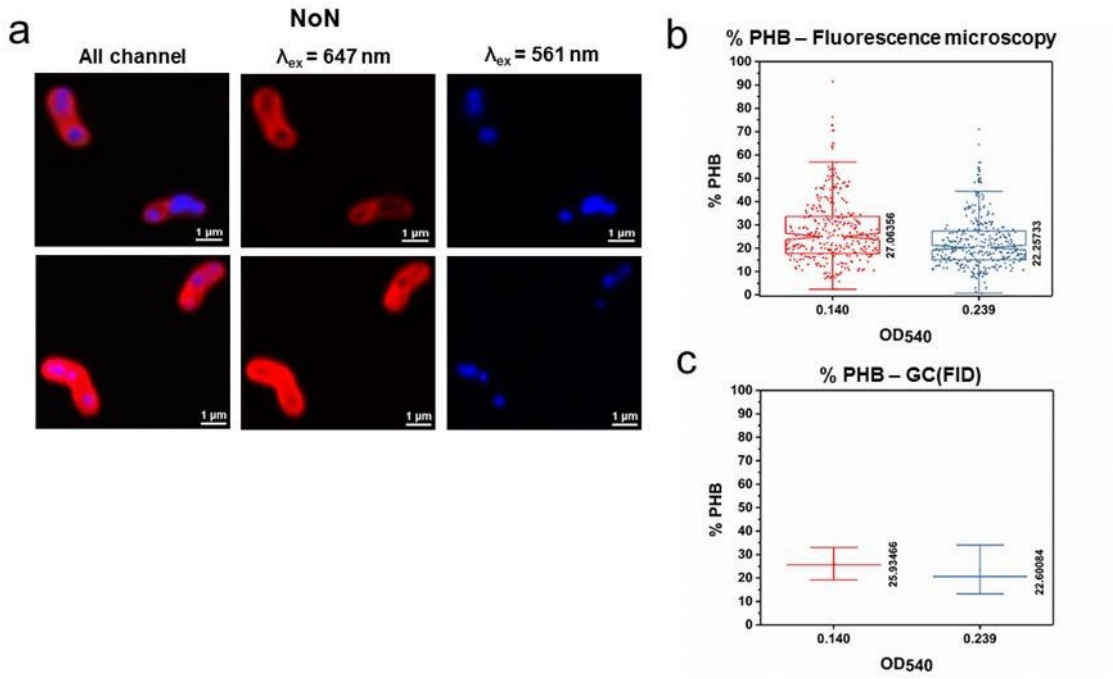


Figure 5.8. Single-cell quantification of PHB using fluorescence imaging. (a) Fluorescence images of *Methylocystis* sp. strain Rockwell grown without nitrogen source (NoN) in the presence of methane and stained with Nile Blue A. "All channel" represents merging of $\lambda_{ex}$ = 647 nm and $\lambda_{ex}$ = 561 nm, whereas $\lambda_{ex}$ = 647 nm image represents membrane staining and $\lambda_{ex}$ = 561 nm represents PHB granule staining (false blue color). Images imply PHB granule variation in lag (top row), exponential (middle row), and stationary (last row) phases. Scale bar = 1 µm. Notched plots of % $PHB_m$ distribution at lag phase ($OD_{540}$ = 0.122 and 0.128), exponential phase ($OD_{540}$ = 0.220 and 0.234), and stationary phase ($OD_{540}$ = 0.307 and 0.311) based on fluorescence images (b) and GC-FID data (c), respectively.

5.4.3. Effects of growth phase and nitrogen source on PHB production in *Methylocystis* sp. Rockwell

To analyze the effects of growth phase and nitrogen source on PHB accumulation in *Methylocystis* sp. Rockwell, we characterized the % $PHB_m$ for cells grown in AMS, NMS, and NoN media in lag, exponential, and stationary phases. When growing on AMS, the % $PHB_m$ assessed by both methods was highest in the lag phase (9.6% for microscopy and 15.2% for derivatization/GC-FID) and decreased in the exponential (9.11% for microscopy and 9.20% for derivatization/GC-FID) and stationary (3.52% for microscopy and 5.84% for derivatization/GC-FID) phases (Fig. 5.6b, c). When growing on NMS, both methodologies confirmed that the % $PHB_m$ was lower for *Methylocystis* sp. Rockwell compared to growth in AMS and remained constant regardless of growth phase (ca. 2.1% for microscopy and 7.0% for derivatization/ GC-FID) (Fig. 5.7b, c). For growth with only atmospheric nitrogen (NoN), both methodologies showed the highest % $PHB_m$ in lag phase (27.1% for microscopy and 25.9% for derivatization/GC-FID) and decreased during exponential growth (22.3% for microscopy and 22.6% for derivatization/ GC-FID) (Fig. 5.8b, c). No PHB granules were detected in NoN cultures at stationary phase. Furthermore, the total number of PHB granules per cell was consistently higher in lag and exponential phases than in stationary phase for all three nitrogen conditions (Fig. 5.9).

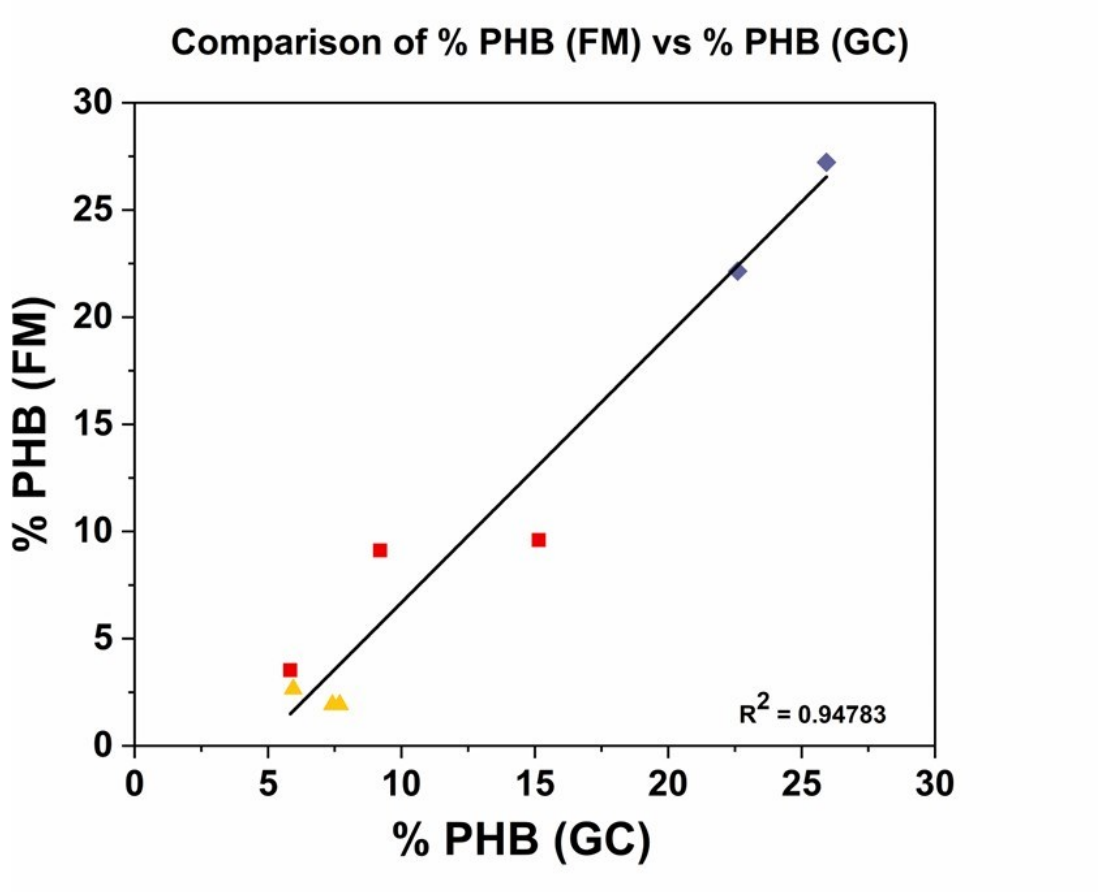


Figure 5.9. Comparison of % $PHB_m$ obtained between the fluorescence microscopy (FM) and derivatization/GC-FID (GC) techniques. Red dots represent % $PHB_m$ of cells grown in AMS, yellow dots represent % $PHB_m$ of cells grown in NMS, and violet dots represents % $PHB_m$ of cells grown under nitrogen starvation conditions (NoN). Linear regression fit (y = mx + c) follows the correlation among % $PHB_m$ characterized for the two techniques under the three nitrogen conditions.

## 5.5. Discussion

The main goal of this study was to establish a novel single cell approach for in vivo PHB detection and quantification. To test this approach, we evaluated the effect of nitrogen source on PHB production in the alphaproteobacterial methanotroph *Methylocystis* sp. Rockwell. Prior to development of our fluorescence microscopy method, the most accurate direct visualization tool for PHB detection and quantification was unbiased stereology, which involved analysis of 2D TEM images followed by calculation of average cell volume and total surface area occupied by PHB granules (Tian et al., 2005) . A similar principle was applied in the present study in which Nile Blue A dye was used to individually discriminate between cell membrane and PHB granules (Fig. 5.1) to assess PHB cell content on a per area, per volume, and per mass basis. Overall, the % $PHB_m$ quantified using the fluorescent microscopy approach (Figs. 5.6b, 5.7b, and 5.8b) correlated well with the results obtained through standard derivatization/GC-FID methodology (Figs. 5.6c, 5.7c, and 5.8c). The agreement between the two methods across all the experiments was high, with R2 = 0.94783 in a linear regression model (Fig. 5.9). Both methods validated that the highest amount of PHB produced by *Methylocystis* sp. Rockwell was obtained under nitrogen starvation (NoN, Fig. 23b, c) followed by ammonium as N-source (AMS, Fig. 5.6b, c) and then nitrate as N-source (NMS, Fig. 5.7b, c). The effect of nitrogen source on PHB production in methanotrophs is consistent with results observed in previous studies (Rostkowski et al., 2013; Zaldívar Carrillo et al., 2018; T. Zhang et al., 2017). These studies showed that PHB was produced to greater levels under nitrogen deprivation, although the preferred nitrogen source varied from stain to strain. The present study confirmed PHB production was greatest under nitrogen starvation in *Methylocystis* sp. Rockwell, where more PHB was present during lag and exponential phases than in the stationary phase of growth. This result indicates that PHB accumulation occurred during cell growth rather than solely as a stationary phase

response, as seen in other methanotrophic bacteria (Pieja, Rostkowski, et al., 2011) . However, unlike *Methylocystis parvus* OBBP, *Methylocystis* sp. Rockwell biomass increases followed PHB decrease, indicating that PHB might be used as carbon source, in addition to the reduction equivalent source (Pieja, Rostkowski, et al., 2011; Pieja, Sundstrom, et al., 2011) . Moreover, the results confirm that ammonium is the preferred N-source for growth of *Methylocystis* sp. Rockwell over nitrate or atmospheric nitrogen (Lazic et al., 2021; Tays et al., 2018) , as the final $OD_{540}$ of the cultures was highest for the methane-ammonium condition (Figs. 5.6, 5.7 and 5.8). Based on our results, *Methylocystis* sp. Rockwell is an ideal bacterium for industrial production of PHB using methane and ammonium-rich wastewater as feedstock as this combination would be advantageous for both biomass and PHB production. To overcome the relatively low PHB, optimization strategy involves the separation of biomass growth from PHB production using a two-stage fed-batch bioreactor (Wang et al., 2012). In Phase 1, high biomass yield and moderate PHB production can be achieved through exponential growth without restricting ammonium, and then in Phase 2, PHB synthesis can be enhanced by limiting the ammonium or providing another stress factor, like methanol. In conclusion, the present study demonstrates a novel, non-toxic fluorescence microscopy method for the rapid and accurate quantification of PHB granules in single cells. This method can facilitate the optimization and industrialization of PHB production by methanotrophic bacteria.

# Chapter 6

## *In vitro* detection of PHB using a recombinant substrate-binding fluorescent fusion protein

### 6.1 Abstract

The increased level of plastic pollution has stimulated interest in discovering biodegradable alternatives that possess similar properties to conventional plastic materials. In addition, the medical field progress requires identification of material that has balanced biodegradability and stability for design of medical implants that would be safe for human and animal use. Polyhydroxybutyrate (PHB) is a biodegradable polymer that meets many of these requirements. This molecule is produced in microbial cells as a storage polymer during nutrient starvation. There have been the extensive efforts to optimize microbial PHB production from cheap carbon sources. The production is usually followed by optimization of purification and polymer recovery, which can significantly affect its quality and purity. Both characteristics are important to evaluate biodegradability of material. This work presents preliminary data on novel synthetic purity detector created via genetic engineering and synthetic biology approach. A fusion protein combining the PHB depolymerase (PhaZ) Substrate Binding Domain (SBD) from *Comamonas testosteroni* was fused to sf GFP and placed downstream of an arabinose-inducible pBAD or a PlacT7 promoter to generate the ARA sfGFP-SBD and T7 sfGFP-SBD expression cassettes. The ability to bind PHB was tested *in vitro* with pure preparations of polymers. In addition, the effect of concentration and incubation time was evaluated for proteins from both expression systems. High expression under PlacT7 promoter caused a saturation effect over long incubation periods and a high level of fluorescence, which was reflected by a poor correlation (low $R^2$) with the standard GC-FID approach for PHB quantification. The expression of the fusion protein under the pBAD promoter did not show a saturation effect, and the correlation was stronger (higher $R^2$

values) than with the PlacT7 promotor. The fusion protein produced could thus be used as a specific marker for PHB, as it differentiates it from PHBV in commercial preparations, thus, it can be used a quality control marker to asses biodegradability.

## 6.2. Introduction

Everyday usage of plastic materials causes tremendous plastic waste accumulation in soils, rivers, and especially in oceans. Regardless of their harmful impact, plastic materials are cheap, durable, and easy to process, which makes them one of the most used materials in everyday society. Recent analysis from 2017 estimated that the global plastic production reached 8,300,000 metric tons, while around 6,300,000 tons ended up as waste. Unfortunately, only a small portion of this waste (around 9%) is recycled, while the vast majority is disposed in landfill (79%) or incinerated (12%) (Tobón-Martinez, 2019). In addition, chemical recycling is costly, mechanical recycling is labor intensive, and thermal destruction has a negative environmental impact (Jendrossek & Handrick, 2002). The reason behind extensive plastic waste accumulation is the non-biodegradable and non-renewable nature of most polymers used for production of traditional plastics. The most used polymers are polyethylene, polypropylene, polystyrene, nylon, and polyurethane. These synthetic polymers originate from petrochemical resources, and there is no available machinery in nature that can efficiently degrade them (Tobón-Martinez, 2019). A recent study revealed the ability of the bacterium *Ideonella sakaiensis* to degrade synthetic polymers (Shosuke Yoshida, 2016). However, widespread use of these bacteria is yet to be developed and commercialized.

A promising alternative to synthetic petroleum-derived polymers are the biodegradable polylactides (PLAs) and polyhydroxyalkanoates (PHAs) (Jendrossek & Handrick, 2002). PLA is synthetized through esterification of lactic acid produced via fermentation, and its degradation involves the activity of proteinase K, serine proteases, lipases, cutinase-like enzymes, and specific PLA depolymerases (Karamanlioglu et al., 2017; Tokiwa & Calabia, 2006). PLA biodegradation occurs under specific temperature and moisture conditions (Tobón-Martinez, 2019), which slows down the process and increases

the total cost of their removal. PHAs are a group of biodegradable biopolyesters, of which polyhydroxybutyrate (PHB) is the most widely studied. Since its thermoplasticity and thermostability are in the same range as synthetic polymers, PHB represents one of the most promising alternatives for biodegradable plastic materials. PHB is biologically produced in various microbes as a hydrophobic carbon storage polymer that can be depolymerized and used as a source of reducing power during starvation conditions in some organisms (Pieja, Sundstrom, et al., 2011). Most PHB production relies on glucose as a carbon source (Zaldívar Carrillo et al., 2018). However, production is costly and sugar feedstock invokes the food vs fuel debate. Thus, efforts have been made to identify cheaper and more suitable carbon sources (fruits peels, lignocellulose, methane, methanol etc.) along with microbes that can use them. Identifying optimal biological PHB production conditions and scale-up would accelerate the reduction in the use of traditional petroleum-derived polymers and decrease the level of plastic waste accumulation in the environment.

The process of PHB degradation can be explained as depolymerization of long PHB ester chains which results in the formation of oligomers and monomers. In addition to the thermal and chemical hydrolysis, biodegradation of PHB involves enzymes known as PHB depolymerases (PhaZs) (Martínez-Tobón et al., 2020). These enzymes perform intracellular (iPhaZ) and extracellular (ePhaZ) PHB degradation, with the difference residing in the structure of PHB that they recognize. While iPhaZs recognize amorphous, non-crystalline PHB structures (Handrick et al., 2004), ePhaZs interact and degrade semi-crystalline PHB – binding on crystalline regions and hydrolyzing chains in the amorphous region –, which makes them more suitable for commercial production and process development.

In terms of PHB degrading enzymes, PhaZs, a recent study reported the successful expression and purification of recombinant PhaZ (rPhaZ) from various organisms (Martinez-Tobon et al., 2020). These enzymes expressed different levels of activities confirmed through

a simple plate-based PHB degradation assay (Martínez-Tobón et al., 2020). The variation in activities suggests that further genetic manipulations and combinations are possible to generate novel recombinant enzymes with improved PHB degrading, or binding function.

Understanding the mechanism behind PHB synthesis and degradation is crucial for efficient process development. Like any other value-added compound, the process of PHB production/degradation needs to include precise and accurate approaches to quantify the presence and the state of the molecule. Regardless of the high production cost, PHA (among which PHB is the best studied) are still broadly used for biomedical applications such as drug delivery systems (Pouton et al., 1988, Williams et al., 2005; Valappil et al., 2006), stents (Unverdorben et al., 2002, Valappil et al., 2006) or wound management (Löbler et al., 2003, Valappil et al., 2006). In fact, these biopolymers are known as "the leading class of biomaterials under investigation for the development of tissue-engineering scaffolds" (). Because one of the primary targets for large scale production of PHB would be its implantation in vivo systems, the purity of the polymers must be carefully considered, as well as their biodegradability. Since composition of biopolymers (PHA) varies (PHB combined with PHBV or PHV), it is reasonable to expect that the physical and chemical properties of material will be significantly different, which can affect their degradation rate in biological tissues. For example, the polymer PHB (P3HB) is very stiff and rigid, thus it can be easily broken (Valappil et al., 2006). However, the polymer version P4HB is highly elastic, and its addition to the P3HB mixture can significantly improve material elasticity (Valappil et al., 2006). One of the issues that might occur is the level of biodegradability of modified material. For example, if we consider the degradation and disposal route for the material and create recombinant enzymatic system do degrade PHB-based material, it is critical to know the level of PHB present in material so we can optimize degradation protocol. From medical implant perspective, there have been investigation on biodegradation of PHB (version P3HB), but also on co-polymers, as it has been confirmed that the addition of various

copolymers can improve elasticity and avoid high brittleness of crystalline P(3HB), which is disadvantage for any biomedical material. According to these studies, the addition of copolymers did not affect level of biodegradability in tissue, but it cased mild immune response during implantation. The immunogenic reaction was followed by migration of lymphocytes and eosinophils lasting 6 months, while the immune response with PHB without copolymer was relative acute immunological reactions (Qu et al., 2006, Valappil et al., 2006). Nevertheless, before in vivo implantation, the assessment of purity is required. Since PHB (and other biopolymers) extraction methods involve solvent extraction and application of highly toxic chemicals, there are many efforts to employ environmentally friendly extraction approaches (Valappil et al., 2006, Lazic et al. 2021). Even though these methodologies might offer the advantage for the environment, the purity of the polymer and later the level of crystallinity has significant influence on the material that will be offered potentially for biomedical purposes or being disposed to the degradation facility. Thus, the nature and the purity of polymers or polymers mixture has to be carefully assessed.

Following the principle of PHB specific binding applied in the most recent study (Lazic et al., 2022), this worked aimed to develop a novel synthetic PHB specific module that can be used to assess the purity of purified crystalline biopolymer PHB. The principle of this approachis summarized in Fig. 6.1. The catalytic domain of PhaZ has been replaced with sfGFP fluorescent protein, while leaving the Substrate Binding Domain (SBD) intact. The specificity of SBD enables this domain to bind to PHB exclusively, while emitting sfGFP-derived fluorescence.

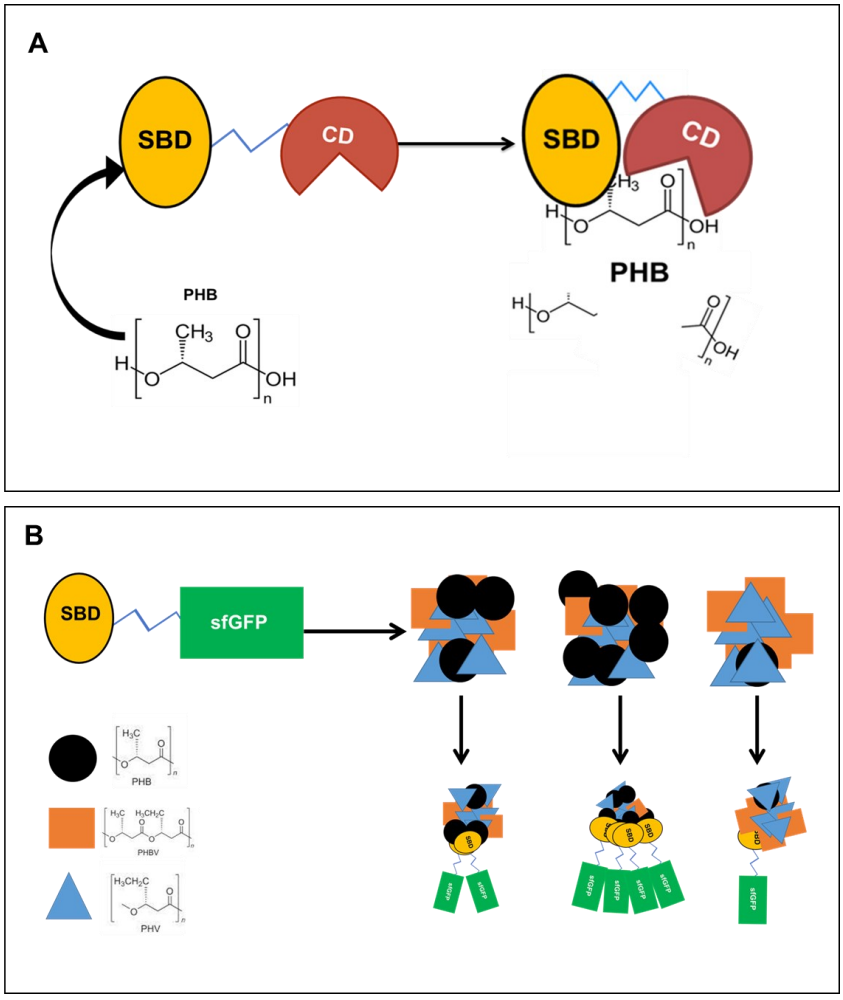


Figure 6.1. Schematic representations. (A) The concept of enzyme substrate interaction in bacterial cell: PhaZ enzyme is composed of a substrate binding domain (SBD) and a catalytical domain (CD); upon SBD binding to PHB, CD cleaves an ester bond of aPHB molecule. (B) Synthetic enzymatic module (sfGFP-SBD) for PHB purity evaluation consisting of a PhaZ for which CD was replaced with the fluorescent protein sfGFP. The SBD domain will bind specifically to the surface area of crystalline PHB molecule. The level of fluorescence will increase as the number of granules (amount of PHB increases). The level of fluorescence will vary depending on the level of PHB in copolymer mixture and on the purity level.

## 6.3. Materials and Methods

### 6.3.1. Bacterial strains and growth conditions

The bacterial strain used for isolation of the PhaZ Substrate Binding Domain (SBD) was *Comamonas testosteroni*. The full gene sequence was previously cloned in *E. coli* DH5-α strain on pET-22b (+) vector (Novagen) (amp) (Martínez-Tobón et al., 2020b). Super Folded Green Fluorescent Protein (sfGFP) was stored in *E. coli* DH5β strain on pQSDPgap plasmid (kan). The vectors used in cloning pBAD and pET-22b (+) were stored in *E. coli* DH5α. Cultures were grown in LB media with appropriate antibiotic concentrations for selection (100 μM ampicillin and 50 μM kanamycin). Cell growth was monitored by measuring optical density at a wavelength of 600 nm ($OD_{600}$) using UV-Vis spectrophotometer (Biochrom, Ultrospec 50). After 18 h of growth at 37 ℃, all plasmids were extracted using ZymoPURE Plasmid Miniprep. Constructs with either arabinose inducible (ARA) and T7 promotors were introduced in *E. coli* Rosetta-gami B(DE3) strain. The growth of cultures was performed in LB medium containing ampicillin (100 μM) and an appropriate inducer.

### 6.3.2. Genetic engineering of synthetic modules

The gene segment coding for SBD and the linker from PhaZ and the gene coding for sfGFP were amplified by polymerase chain reaction (PCR). PCR conditions and primer sequences are listed in Appendix 3. A 6-His sequence was introduced in both Reverse primers to enable later protein purification. Both inserts were extracted via Zymoclean Gel DNA Recovery Kit. For the construct ARA sfGFP-SBD: plasmid vector pBAD for restriction digestion was extracted via ZymoPURE Plasmid Midiprep and cut with restriction enzymes XhoI and HindIII at 37 ℃, overnight. For the construct T7 sfGFP-SBD: plasmid vector pET-22b (+) for restriction digestion was extracted via ZymoPURE Plasmid Midiprep and cut with restriction enzymes NcoI-HF and HindIII-HF, at 37 ℃, overnight. Both constructs were cloned via Gibson Assembly (Gibson et al., 2009) into DH5α *E. coli* previously rendered

chemically competent. The correct sequence was confirmed by colony PCR and sequencing. For protein expression, constructs were introduced into the *E. coli* Rosetta-gami B(DE3) strain previously rendered chemically competent.

6.3.3. Protein expression and extraction

5 mL of transformed *E. coli* Rosetta-gami B(DE3) at $OD_{600}$ of 0.5 was added to 1 L LB with antibiotics. Cultures were grown at 30°C for approximately 7 h, until $OD_{600}$ reached 0.6 – 0.8. 1 mM IPTG and 2% arabinose were added, and the cultures were incubated overnight at 8°C to induce expression. Cultures were then centrifuged at 5,000 × g and 4 °C for 20 min, and the pellets were placed at −20 °C. Protein extraction was performed on thawed pellets using 5 mL of B-PER II mixture with Halt™ Protease Inhibitor Cocktail, EDTA-Free (100×) (ThermoFisher Scientific) to obtain Soluble Fraction containing ARA and T7 sfGFP-SBD. Purification was performed at 4 °C using His GraviTrap columns (GE Healthcare). Equilibration was done with 10 mL of B-PER II before extracted soluble fractions were applied to the column, followed by a wash with 10 mL of binding buffer (50 mM sodium phosphate, 500 mM NaCl, pH 7.4). All three solutions contained 20 mM imidazole. sfGFP-SBD were eluted with 3 – 5 mL of elution buffer (20 mM sodium phosphate, 500 mM NaCl, pH 7.4 with 500 mM). Purified proteins were verified through SDS-PAGE and quantified using a Bradford Protein Assay (microassay procedure, Bio-Rad) using bovine serum albumin as the standard. Additional Western Blot confirmation was performed using 6X -His Tag Monoclonal Antibody along with Goat anti-Mouse IgG (H+L) Cross-Adsorbed Secondary Antibody, HRP.

6.3.4. PHB detection assay

Different amounts of blank PHB powder (Sigma Aldrich) 0.0060 ±0.0005 g, 0.0146 ±0.0010 g, and 0.0263 ±0.0012 g were placed in wells of a fluorescence assay plate (Thermo Scientific™ Nunc™ MicroWell™ 96-Well, Nunclon Delta-Treated, Flat-Bottom Microplate) and centrifuged briefly (30 sec, 1,000 rpm, [centrifuge model and supplier]). sfGFP-SBD fusion proteins were diluted to fluorescence levels of 250, 500, and 1000 RFU. 0.25 mL of protein solution was added to sample wells. As negative control, an equal amount of elution buffer used in protein purification (see previous section) was added to some PHB-containing wells. The plate was incubated at room temperature for 15 min or overnight, washed with EB, and the level of fluorescence was measured at 485/528 (excitation/emission) nm wavelength. PHB binding specificity was confirmed by performing the same methodology with ground PHBV and PLA.

6.3.5. GC-FID analysis

The standard GC-FID PHB detection and quantification methodology was applied to confirm the accuracy of the protein-based detection methodology. The principle of this approach involves depolymerization of polymer under acidic conditions and esterification with methanol. 0.24 g PHB was dissolved in 18 mL chloroform (corresponding to 2 mL chloroform to dissolve 0.0263 g). For each PHB amount three replicates were prepared (2 mL of PHB solution, 1 mL of PHB solution with 1 mL of chloroform, and 0.5 mL of PHB solution with 1.5 mL of chloroform). Next, 1 mL methanol and 1 mL of benzoic acid solution (40 mg/L) were dissolved in methanol and acidified with 3% concentrated sulfuric acid. The sample was digested for 5 h in a capped glass vial in a boiling water bath to depolymerize the PHB polymer to its monomer and esterify it with methanol. After cooling, 1 mL deionized water was added, and the sample was vortexed for 20 s before standing overnight for phase separation. The organic phase was analyzed for methyl 3-hydroxybutyrate, (Lazic et al.,

2022; Zaldívar Carrillo et al., 2018) using a gas chromatograph (7890A, Agilent Technologies) equipped with an autosampler (G4513A, Agilent Technologies) and fitted with a 30 m × 250 μm DB-5ms column (Agilent Technologies) as previously described (Lazic et al., 2022; Zaldívar Carrillo et al., 2018). Ratios between methyl 3-hydroxybutyrate methyl-benzoate were calculated and measured against levels of fluorescence for each construct, under each condition.

## 6.4. Results

### 6.4.1. Expression and purification of sfGFP-SBD

*E. coli* Rosetta-gami B(DE3) was chosen as the expression strain for the engineered PhaZ-derivative sfGFP-SBD. The theoretical isoelectric point (pI) and molecular weight (MW) of this fusion protein were calculated via ExPASY Bioinformatic Resource Portal (SIB) and estimated to be: pI 6.27, MW=42955 Da. The instability index was predicted to be 25.75, which classifies the protein as stable, with an estimated half-life >10 h in *E. coli*. This protein was determined as highly hydrophobic with an aliphatic index of 69.16 and a grand average of hydropathicity of -0.449 (https://web.expasy.org/cgi-bin/protparam/protparam). Since sfGFP-SBD is derived from PhaZ, and PhaZs are classified as "insoluble" (solubility score 0.503) (Martínez-Tobón et al., 2020), one potential problems with purification is insolubility. The novel protein sfGFP-SBD has a solubility of 0.35 (proteins with values higher than 0.45 are predicted to have higher solubility than stable *E. coli* proteins, whereas proteins with lower values are less soluble) (https://web.expasy.org/cgi-bin/protparam/protparam). To overcome this problem, induction was done at low temperature (8-10 ℃). Both plasmid vectors without the gene of interest (GOI) were expressed in *E. coli* Rosetta-gami B(DE3). Purification was performed, and protein extracts were analyzed via SDS-PAGE. However, since both plasmid vectors already contained the 6xHis tag, this signal

was detected via Western Blot and was thus not a sufficient negative control. For the negative control, the complete purification protocol was performed from a non-transformed expression strain, and the absence of signal on SDS-PAGE and Western blot is shown in Fig. 6.2, panels A and B. The presence of proteins for each dilution was confirmed via SDS-PAGE (Fig. 6.2, panels A and C). Western blot was also performed for each protein dilution (Fig. 6.2 C and D). The signal that corresponds to the expected size (42 kDa) was observed for all dilutions for both ARA and T7 sfGFP-SBD. Absence of Western blot signal was noted for ARA sfGFP-SBD (Fig.6.2 C and D) regardless of protein concentration (Fig. 6.2 D), and very low or non-specific signal for non-diluted proteins (Fig. 6.2 B).

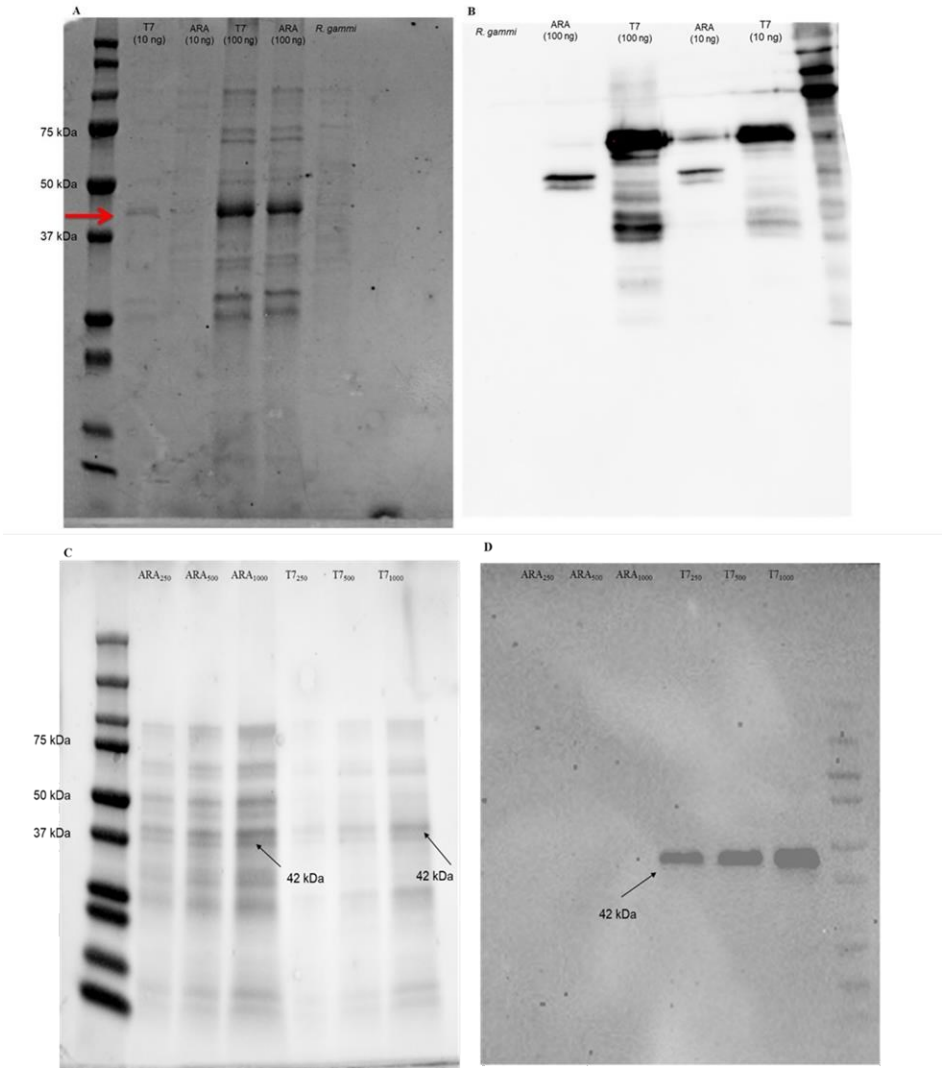


Figure 6.2. SDS-PAGE (A and C) and Western Blot (B and D) for ARA sfGFP-SBD and T7sfGFP-SBD. Panels A and B represent undiluted proteins after purification was performed. The concentration was determined via standard Bradford Assay as previously described () and concentrations were relatively close in this preparation (5 ng/µL). Proteins were loaded in indicated amounts (10 ng (2 µL) and 100 ng (20 µL)). Negative control was the cellular extract from E. coli Rosetta gammi (10 µL of extract loaded). Panels C and D represent working dilutions of proteins based on fluorescence (ARA250, ARA500, ARA1000, and T7250, T7500, and T71000) used in experiments. 10 µl of sample was loaded for both SDS-PAGE andWestern blot. The concentration of proteins was not specifically measured for each RFU, as the purpose of this analysis was qualitative representation of data. Instead, RFU was measured for each version of protein and proper dilutions were loaded on the SDS-PAGE and WB.

6.4.2. The effect of sfGFP-SBD concentration on PHB-specific fluorescence emission

To evaluate the effect of protein concentration on PHB-binding and efficiency, proteins from both expression systems were diluted to achieve set levels of initial fluorescence at 485/528 nm (250F, 500F, and 1000F). The assay was performed with ARA sfGFP-$SBD_{250}$ and resulted in fluorescence correlating with the amount of PHB (g) in the assay plate for both short (Fig. 6.3A) and long incubations (Fig. 6.3B).

The assay performed with T7 sfGFP-$SBD_{250}$ showed a similar trend for short incubation times (Fig. 6.3A). However, during long incubation times with T7 sfGFP-$SBD_{250,}$ a saturation effect was observed (Fig.6.3 B).

The assay performed with ARA sfGFP-$SBD_{500}$ resulted in an increased level of fluorescence corresponding to increased amounts of PHB (g) over short and long incubation times (Fig. 6.4). The assay performed with T7 sfGFP-$SBD_{500}$ resulted in an accurate trend for a short incubation time (Fig. 6.4A). However, the absence of a linear trend was observed over a long incubation time (Fig. 6.4B).

The assay performed with ARA sfGFP-$SBD_{1000}$ resulted in an increased level of fluorescence similarly as the previous two concentrations (Fig. 6.5). When the assay was performed with T7 sfGFP-$SBD_{1000}$, a linear increasing trend over a short incubation time could be observed (Fig. 6.5A). However, the obvious saturation effect was observed over the long incubation period (Fig. 6.5B). The absence of fluorescence signal in samples containing PHBV and PLA was indicative of highly specific PHB binding (Fig.6.6, panels A and B).

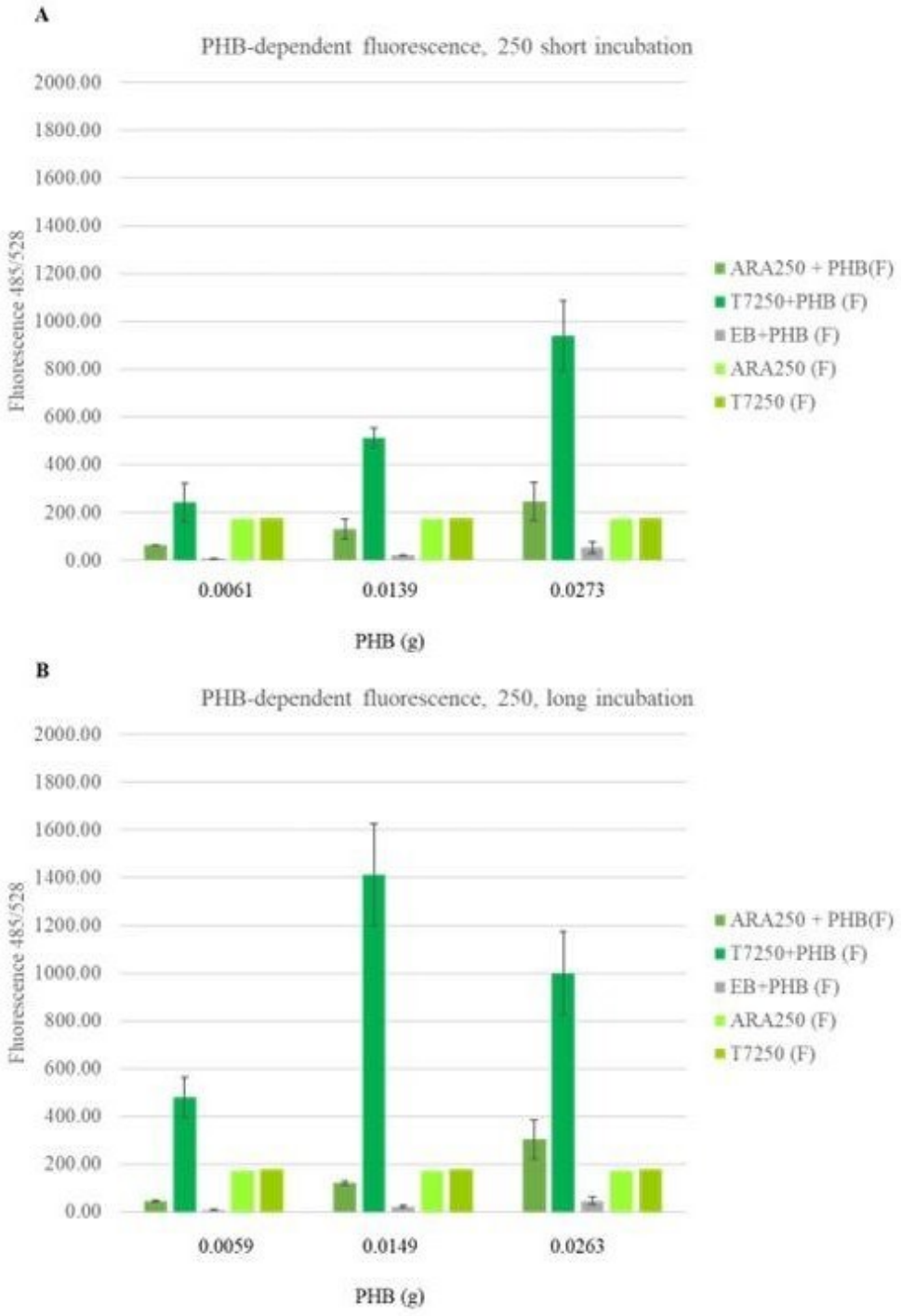


Figure 6.3. The PHB-bound sfGFP-SBD emitted fluorescence for protein dilutions at 250 RFU ($ARA_{250}$ and $T75_{250}$) during short (A) and long (B) incubation. Each well was treated with 0.25 mL of protein in elution buffer (EB). Negative control was performed with an equal

amount of EB without PHB. Positive control consisted of proteins alone in 0.25 mL of EB. The absence of fluorescence signal in negative control confirms sfGFP-SBD does not bind to the well material and that unbound proteins are removed by the methods. The presence of a fluorescence signal in the positive control confirms correct protein folding and activity.

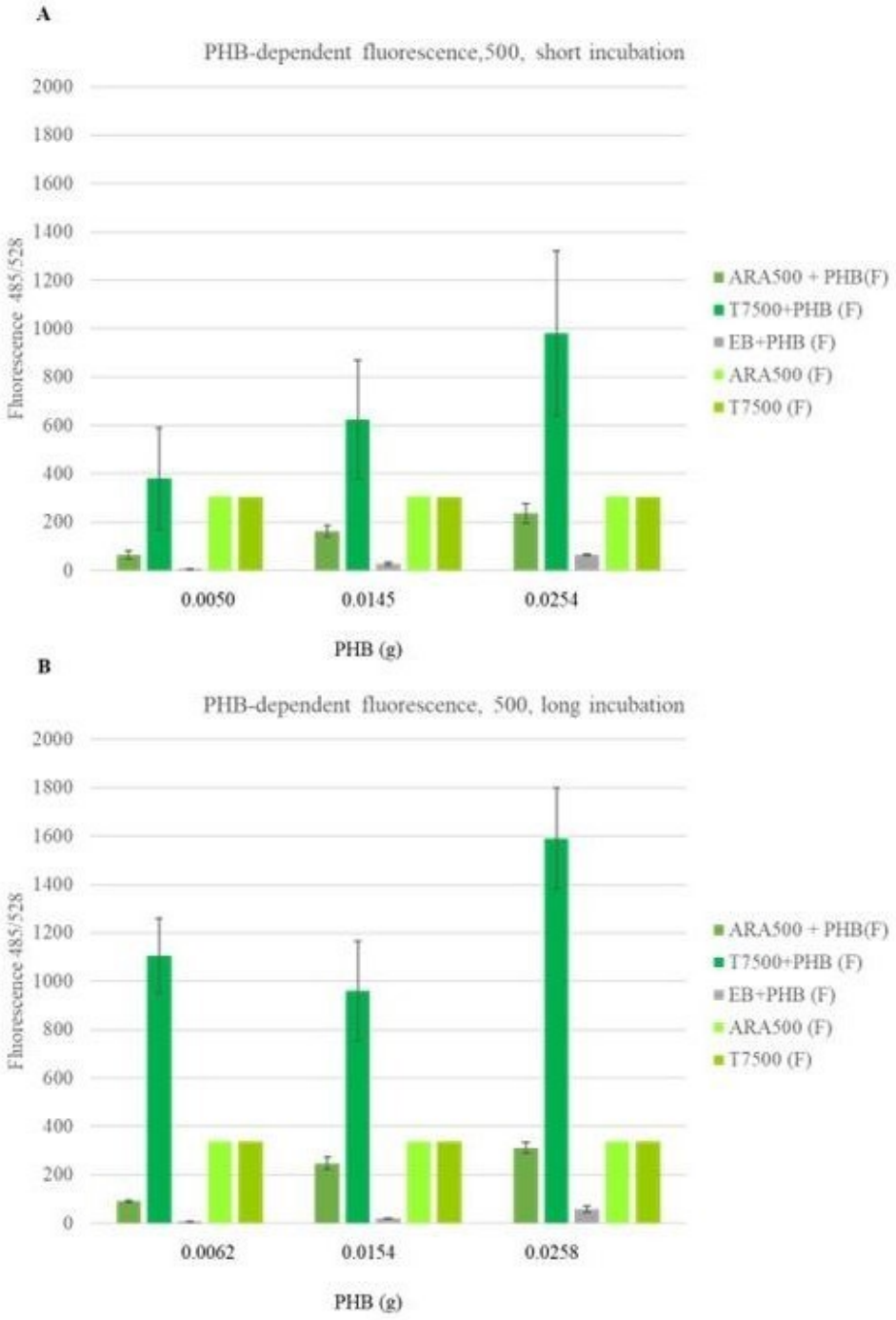


Figure 6.4. The PHB-bound sfGFP-SBD emitted fluorescence for protein dilution 500 RFU ($ARA_{500}$ and $T7_{500}$) during short (A) and long (B) incubation. Approximately same amount of PHB (g) was measured for each protein in each condition and the average was calculated. Each well was treated with 0.25 ml of protein in elution buffer (EB). The negative control

was performed with the equal amount of EB. The positive control are proteins only (0.25 ml of each without PHB in the well). The absence of fluorescence signal in the negative control confirms the existing PHB-dependent protein binding activity. The presence of fluorescence signal in the control confirms correct protein folding and activity.

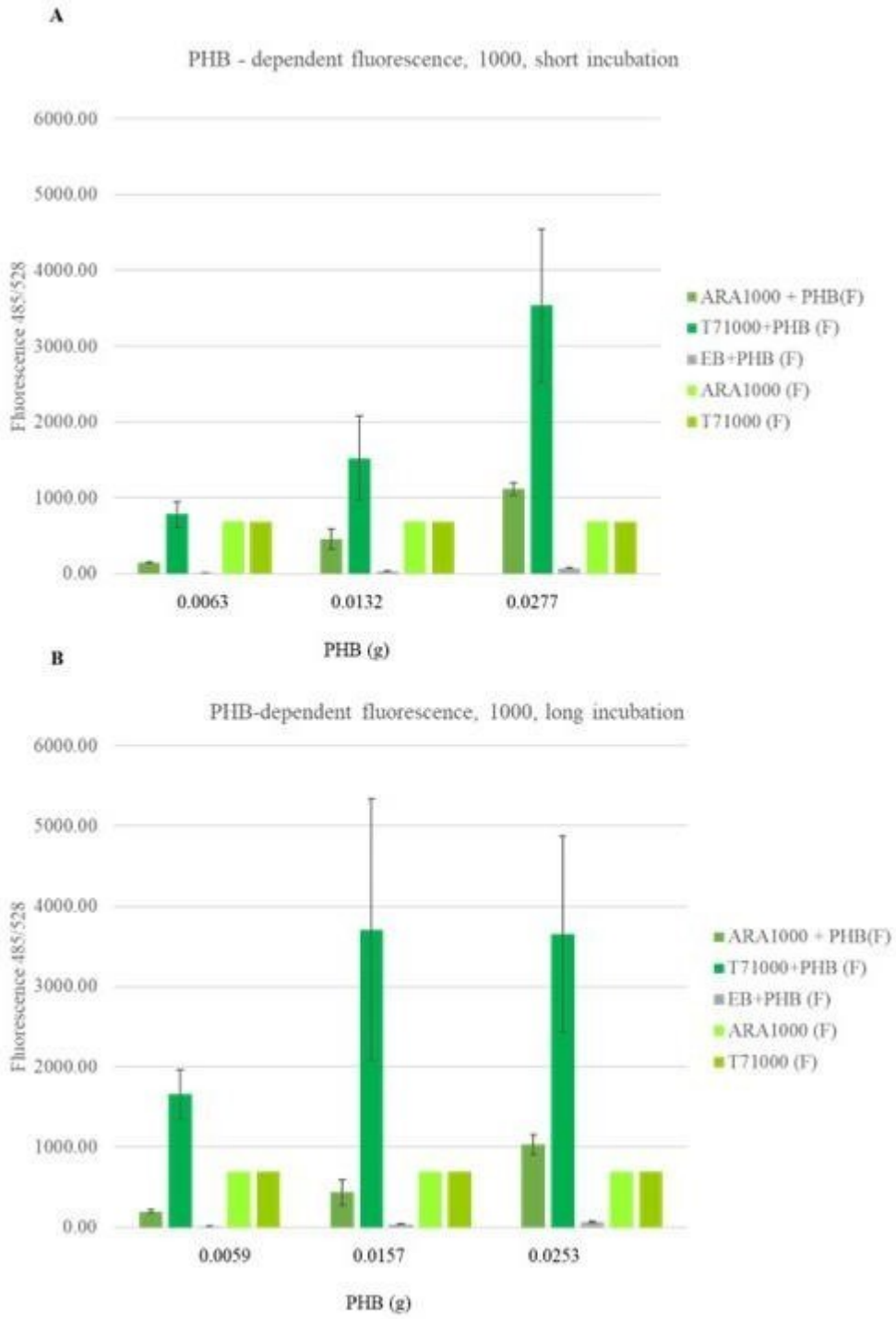


Figure 6.5. The PHB-bound sfGFP-SBD emitted fluorescence for protein dilution 1000 RFU($ARA_{1000}$ and $T7_{1000}$) during short (A) and long (B) incubation. Approximately the same amount of PHB (g) was measured for each protein in each condition and the average was calculated. Each well was treated with 0.25 ml of proteins in elution buffer (EB). Negative control was performed with an equal amount of EB. Positive control are proteins only (0.25

ml of each without PHB in the well). The absence of fluorescence signal in the negative control confirms the existing PHB-depending protein binding. The presence of fluorescence signal in the control confirms correct protein folding and activity.

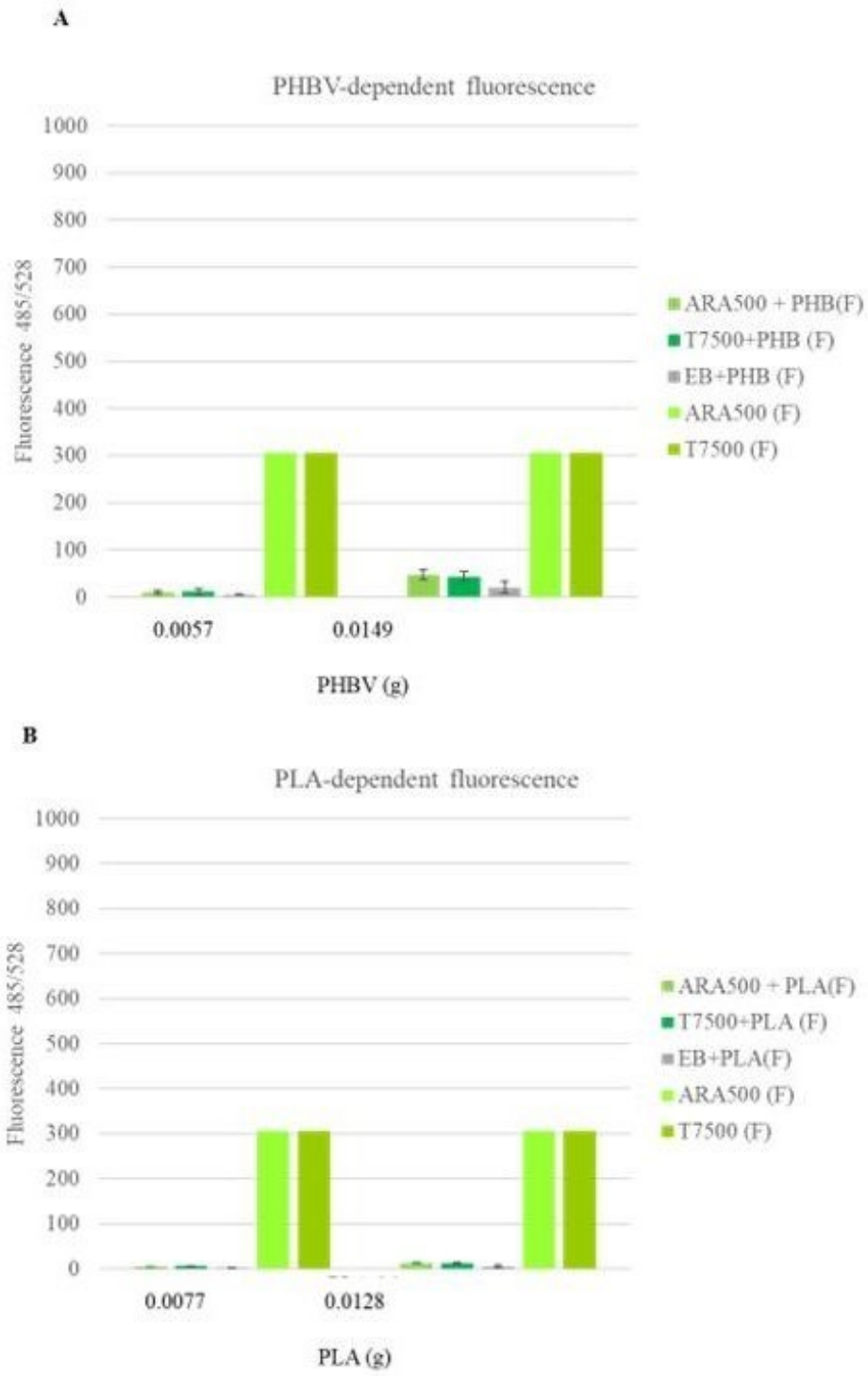


Figure 6.6. PHBV- and PLA-bound sfGFP-SBD binding. ARA and T7 sfGFP-SBD were used at 500 F ($ARA_{500}$ and $T7_{500}$). The experiment was performed as 15 minutes “short incubation." Each well was treated with 0.25 ml of sfGFP-SBD fusion proteins in elution buffer (EB). Negative control was performed with an equal amount of EB. Positive control are proteins only (0.25 ml of each without polymers in the well). The absence of fluorescence

signal in the negative control and in PHBV and PLA-containing wells confirms the existing PHB-dependent protein binding. The presence of fluorescence signal in the control confirms correct protein folding and activity.

### 6.4.3. The effect of incubation time on PHB-specific fluorescence emission

The fluorescent signal emitted after ARA sfGFP-SBD binding to PHB remained unchanged and stable after prolonged incubation periods at a protein concentration corresponding to 250 F (Fig. 6.3). Stable patterns of fluorescence emission regardless of incubation time were observed for concentrations of 500 F (Fig. 6.4) and 1000 F (Fig. 6.5).

Unlike for ARA sfGFP-SBD, the fluorescence signal emitted after T7 sfGFP-SBD binding to PHB was highly affected by incubation time and the saturation effect. An absence of correlation was generally observed across the conditions tested (Fig. 6.3, 6.4, 6.6). At a protein concentration of 250 F, a slight increase in the fluorescence signal was observed after a prolonged incubation period, but the saturation affect was obvious (Fig. 6.3). As the concentration of protein increased, the effect of the long incubation period was more prominent (Fig. 6.5).

### 6.4.4. The effect of expression promotor (ARA vs T7) on PHB-specific fluorescence emission

For all three protein concentrations tested (250 F, 500 F, and 1000 F), the fluorescence signal emitted after ARA sfGFP-SBD binding to PHB was lower than the signal emitted after T7 sfGFP-SBD binding, regardless of the incubation time (Fig. 6.3 to 6.5). For the 250 F short incubation time, the signal was 3.9-fold lower for ARA sfGFP-$SBD_{250}$ than for T7 sfGFP-$SBD_{250}$ (Fig. 6.3A); for 250 F long incubation time, the signal was 10-fold lower before the saturation effect appeared (Fig. 6.3B). For 500 F short incubation time, the signal was 4.6-fold lower for ARA sfGFP-$SBD_{500}$ than for T7 sfGFP-$SBD_{500}$ (Fig. 6.4A); for 500 F long incubation time, the signal was  -fold lower, but the absence of a linear trend was observed (Fig. 6.4B). For 1000 F short incubation time, the signal was 3.9-fold lower for ARA sfGFP-$SBD_{1000}$ than for T7 sfGFP-$SBD_{1000}$ (Fig. 6.5A); for 1000 F long incubation time, the signal was 8-fold lower before the saturation effect appeared (Fig. 6.5B).

### 6.4.5. Comparison of PHB measurements from sfGFP-SBD and GC-FID

To determine the quantity of PHB detected by the sfGFP-SBD approach, equal amounts of PHB were assessed with this method and the depolymerization/derivatization GC-FID method. The results were introduced into a linear regression model to evaluate "the goodness of fit" between the two methods. The $R^2$ values were calculated, and results are shown in Table 6.1, Fig. 6.7, 6.8, and 6.9. For ARA sfGFP-SBD, the $R^2$ was relatively high (>0.7), except for $ARA_{250}$ where the $R^2$ was 0.647. For T7 sfGFP-SBD, the $R^2$ values were lower than for ARA sfGFP-SBD at all concentrations and incubation times, with the highest $R^2$ at 0.818 and 0.7247 during the short incubation time (Table 6.1, Fig. 6.7, 6.8, 6.9).

Table 6.1. Fit of linear regression between GC-FID and protein fluorescence measurements for short incubation time (15 min, room temperature).

| Protein name | Incubation time | $R^2$ |
|---|---|---|
| $ARA_{250}$ | short | 0.647 |
| $ARA_{250}$ | long | 0.9573 |
| $T7_{250}$ | short | 0.818 |
| $T7_{250}$ | long | 0.0814 |
| $ARA_{500}$ | short | 0.7705 |
| $ARA_{500}$ | long | 0.7401 |
| $T7_{500}$ | short | 0.4025 |
| $T7_{500}$ | long | 0.5577 |
| $ARA_{1000}$ | short | 0.9099 |
| $ARA_{1000}$ | long | 0.9748 |
| $T7_{1000}$ | short | 0.7247 |
| $T7_{1000}$ | long | 0.1104 |

The average values were calculated for all experiments and $R^2$ were re-calculated for all experimental conditions (Table 6.2, Fig. 6.10, 6.11 and 6.12). In general, $R^2$ were higher than in individual replicate analysis (Table 6.1 vs Table 6.2, and Fig 6.7, 6.8, 6.9 vs Fig. 6.10, 6.11, 6.12). However, even after calculating the average between replicates, extremely low $R^2$ was observed for T7 sfGFP-SBD, especially after long incubation period (Table 6.2, Fig. 6.10, 6.11 and 6.12 panels B and D).

Table 6.2. Fit of linear regression between GC-FID and protein fluorescence measurements for all experiments together.

| Protein name | Incubation time | $R^2$ |
|---|---|---|
| $ARA_{250}$ | short | 0.9992 |
| $ARA_{250}$ | long | 0.9964 |
| $T7_{250}$ | short | 0.9977 |
| $T7_{250}$ | long | 0.1609 |
| $ARA_{500}$ | short | 0.9419 |
| $ARA_{500}$ | long | 0.8414 |
| $T7_{500}$ | short | 0.9955 |
| $T7_{500}$ | long | 0.7098 |
| $ARA_{1000}$ | short | 0.9988 |
| $ARA_{1000}$ | long | 0.9953 |
| $T7_{1000}$ | short | 0.9928 |
| $T7_{1000}$ | long | 0.5662 |

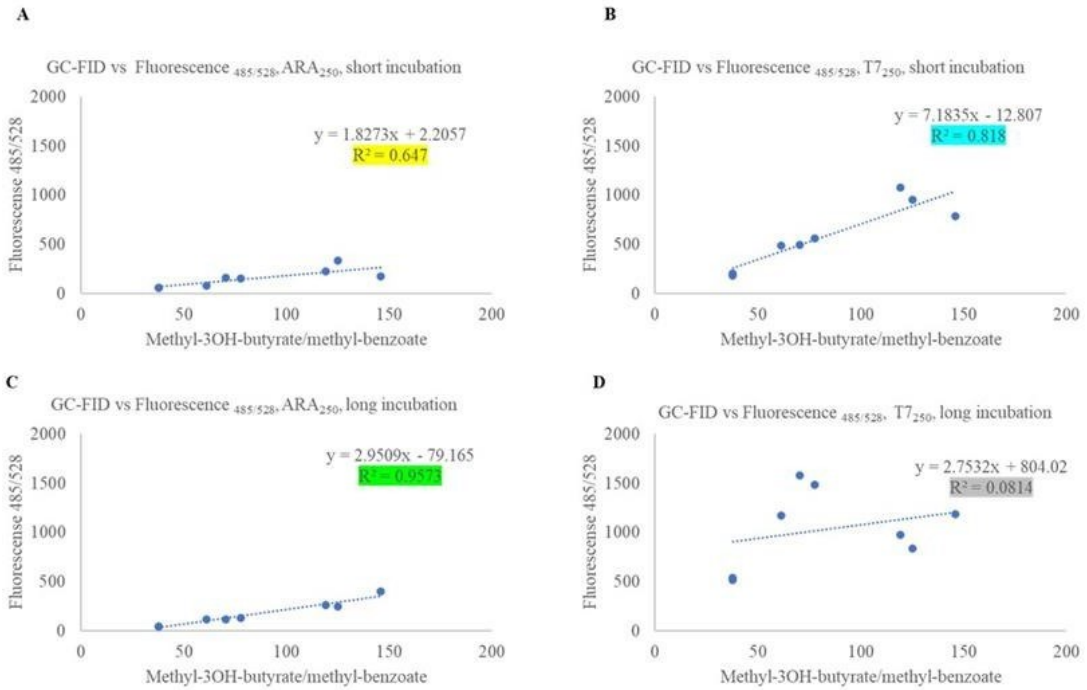


Figure 6.7. Comparison between fluorescent signal emitted from $ARA_{250}$ and $T7_{250}$ sfGFP-SBD and detection by GC-FID for the approximately the same amounts of PHB. Linear regression fit y=mx+c follows correlation between the two techniques. $R^2$ values are color coded for each condition (e.g. protein, short/long incubation).

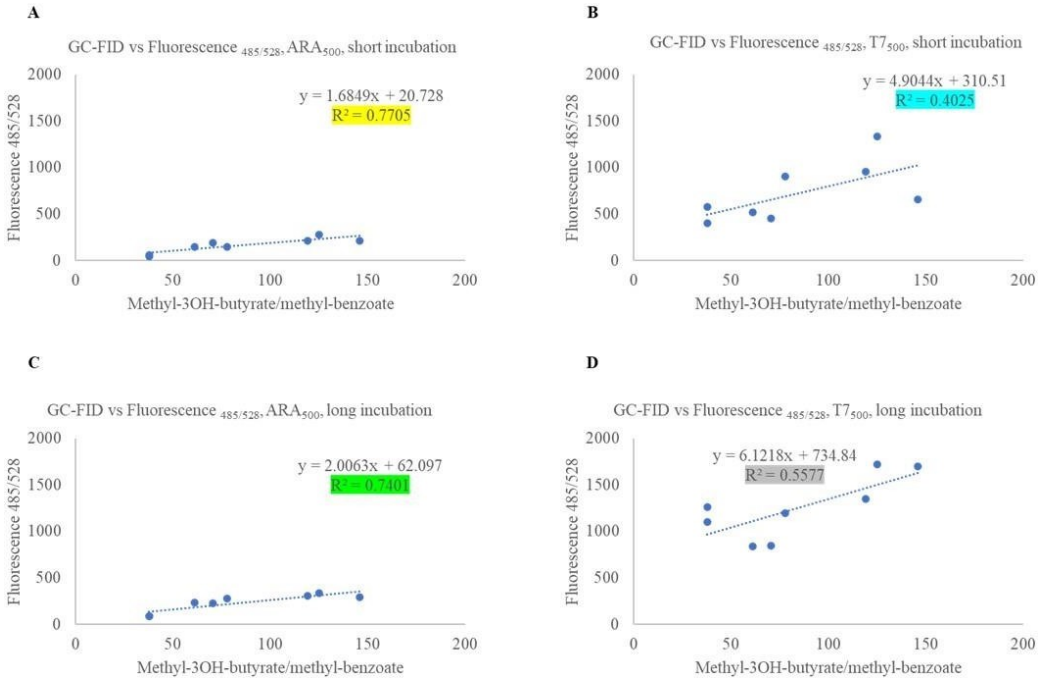


Figure 6.8. Comparison between fluorescent signal emitted from $ARA_{500}$ and $T7_{500}$ sfGFP-SBD and detection by GC-FID for the approximately the same amounts of PHB. Linear regression fit y=mx+c follows correlation between the two techniques. $R^2$ values are color coded for each condition (e.g. protein, short/long incubation).

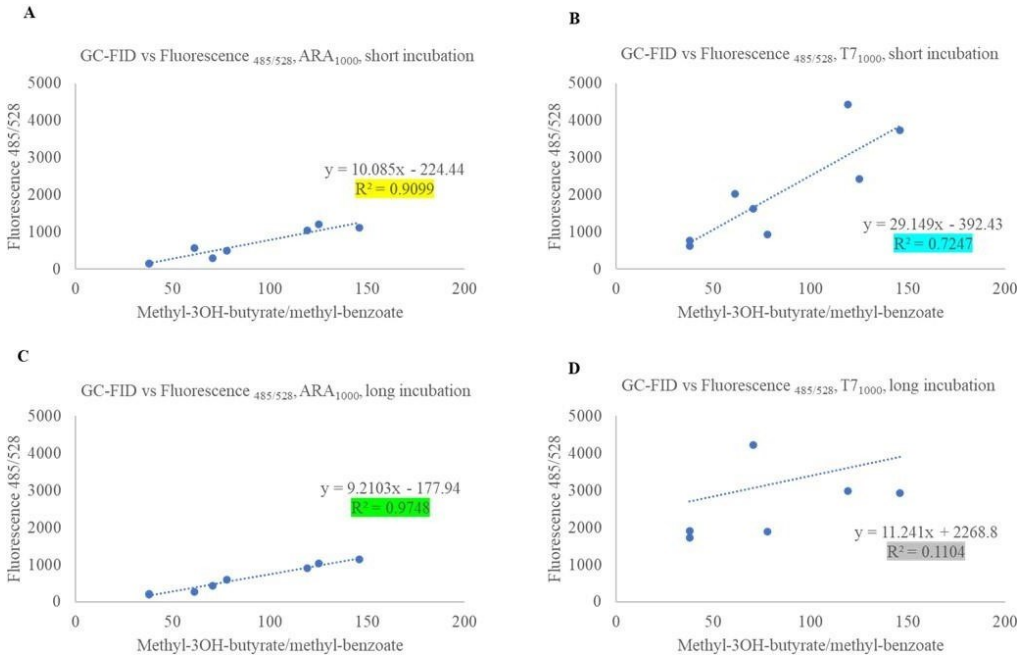


Figure 6.9. Comparison between fluorescent signal emitted from $ARA_{1000}$ and $T7_{1000}$ sfGFP-SBD and detection by GC-FID for the approximately the same amounts of PHB. Linear regression fit y=mx+c follows correlation between the two techniques. $R^2$ values are color coded for each condition (e.g. protein, short/long incubation).

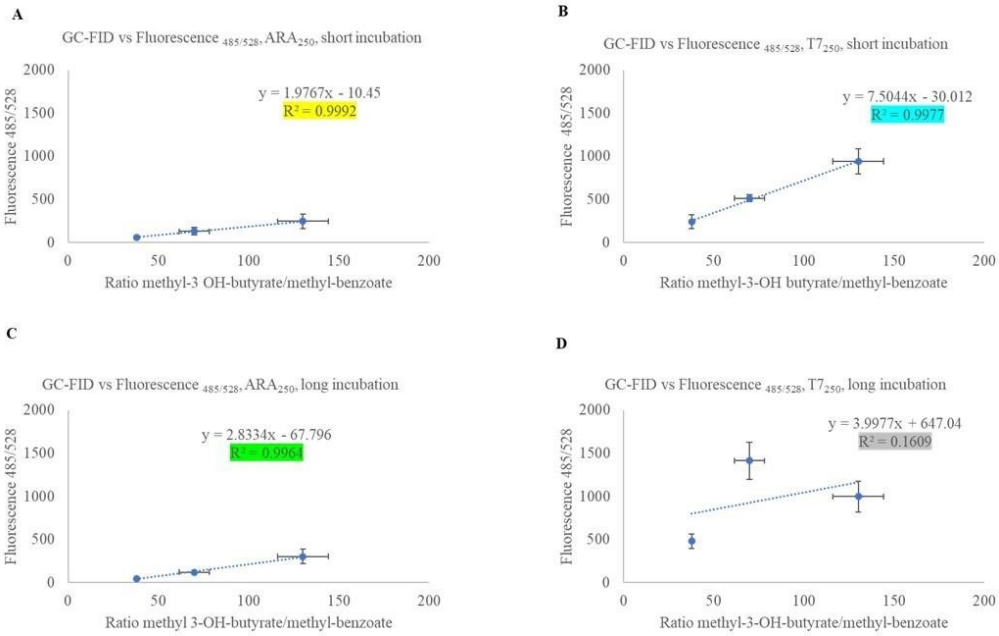


Figure 6.10. Comparison between fluorescent signal emitted from $ARA_{250}$ and $T7_{250}$ sfGFP-SBD and detection by GC-FID for the approximately the same amounts of PHB. Linear regression fit y=mx+c follows correlation between the two techniques. $R^2$ values are color coded for each condition (e.g. protein, short/long incubation).

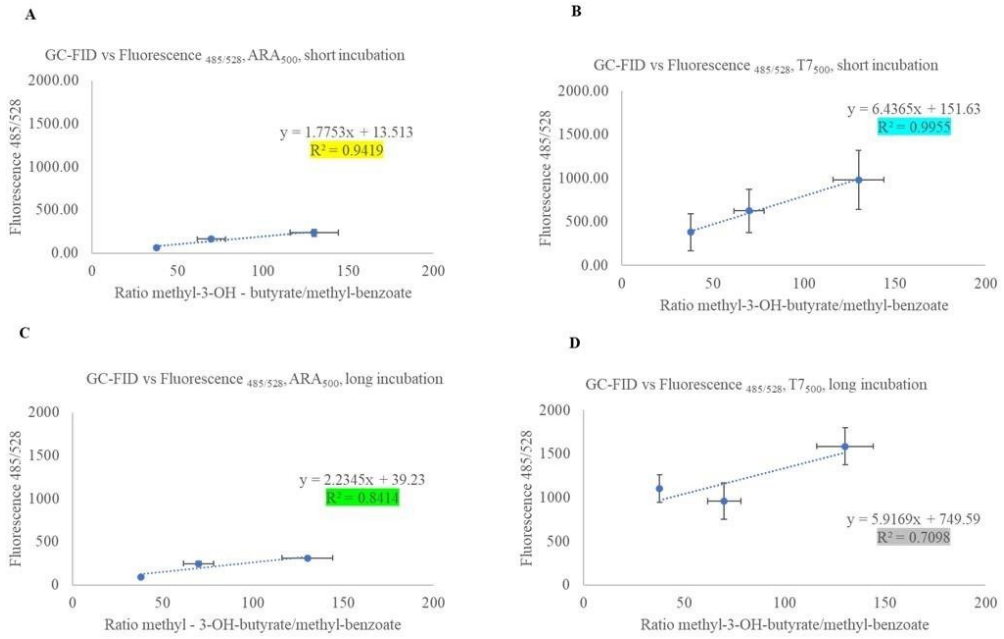


Figure 6.11. Comparison between fluorescent signal emitted from $ARA_{500}$ and $T7_{500}$ sfGFP-SBD and detection by GC-FID for the approximately the same amounts of PHB. Linear regression fit y=mx+c follows correlation between the two techniques. $R^2$ values are color coded for each condition (e.g. protein, short/long incubation)

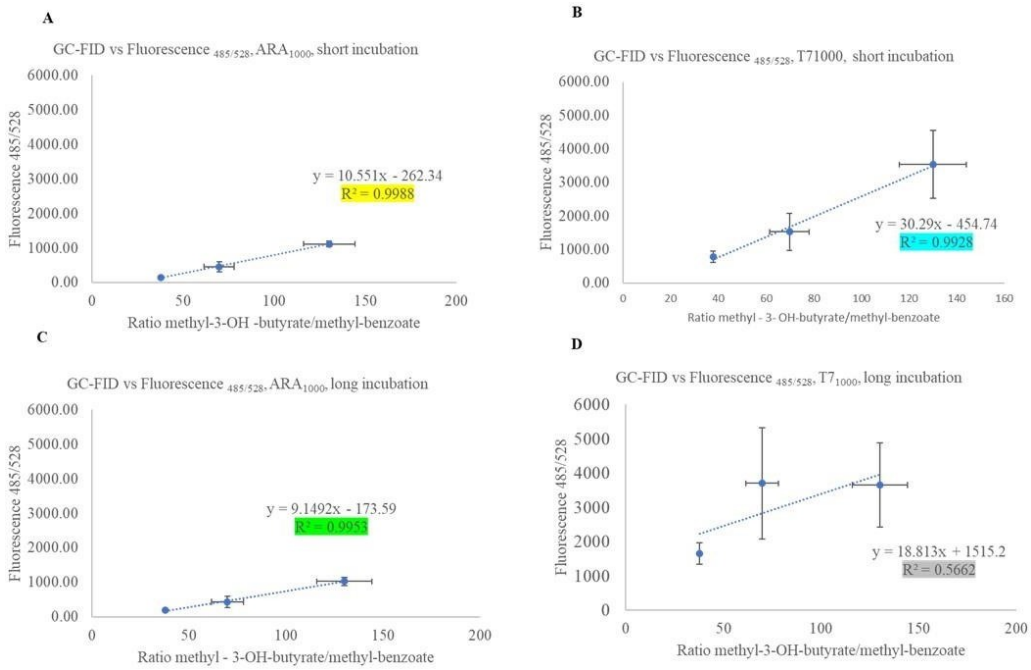


Figure 6.12. Comparison between fluorescent signal emitted from $ARA_{1000}$ and $T7_{1000}$ sfGFP-SBD and detection by GC-FID for the approximately the same amounts of PHB. Linear regression fit y=mx+c follows correlation between the two techniques. $R^2$ values are color coded for each condition (e.g. protein, short/long incubation).

## 6.5. Discussion

The goal of this study was to develop a sensitive and specific PHB sensor for *in situ* detection that can be expressed and purified using an established expression system. The PHB-binding fusion protein sfGFP-SBD was designed and produced using two expression systems: ARA sfGFP-SBD and T7 sfGFP-SBD (Fig. 6.1). Their ability to bind semi-crystalline PHB was tested. In addition, we established the correlation of this method with PHB quantification by the standard PHB-detection GC-FID method. Proteins from both expression systems showed effective PHB binding. however, fluorescence from PHB-bound ARA sfGFP-SBD correlated strongly with GC-FID results regardless of protein concentration or incubation time. On the other hand, T7 sfGFP-SBD generally showed poor correlation with GC-FID results (Fig. 6.7, 6.8, 6.9, 6.10, 6.11, and 6.12), despite emitting fluorescence (Fig. 6.3, 6.4, and 6.5).

For the expression of recombinant fusion proteins, the *E. coli*-based recombinant protein production system was selected. Previous studies confirmed that this system has been successful for production of recombinant PhaZs (Takaku et al., 2006; Takeda et al., 2000; Wang et al., 2012; Martinez-Tobon et al., 2018, 2020). Since the SBD portion of both fusion proteins is derived from PhaZs, it is reasonable to expect that the same system will be equally successful. In addition, *E. coli* is the most popular and desirable system for recombinant protein expression as it has an extremely fast growth rate, molecular tools have been fully developed and optimized, and it can achieve high cell density using inexpensive media formulations (Bhatwa et al., 2021). Specifically, the *E. coli* expression strain Rosetta-gami Bl21 (DE3) was chosen due to its ability to express genes cloned under a strong PlacT7 promotor (T7 sfGFP-SBD), and it contains the plasmid pRARE that enables expression of rare codons that might be present in the SBD of PhaZ. For expression of genes cloned under the arabinose inducible promotor, such as the AraC dimer, they are usually present on the

plasmid pBAD, and any expression system can be used. However, the plasmid used to express genes under the PlacT7 promotor, pET 22b (+) was previously used to express recombinant PhaZs, and it was shown that this plasmid is optimal. The plasmid pET 22b (+) contains pelB N-terminal signal sequence for periplasmic localization. If the protein contains disulfide bonds (S-S), periplasmic localization is required for disulfide bond formation (Ma er al., 2011).

One of the problems that often appears during production of recombinant proteins is insolubility and tendency to form inclusion bodies (IB) (Lozano-Terol et al., 2021). The formation of IBs is driven either by physicochemical protein structure or by the expression rate (Bhatwa et al., 2021; Dyson et al., 2004; Goh et al., 2004). Since, in many cases of recombinant protein production, overexpression is required, IB formation is a common problem. In rPhaZ (the source of SBD for ARA sfGFP-SBD and T7 sfGFP-SBD) a large portion of the protein was detected in the insoluble fraction (IF), suggesting that inclusion bodies may have formed (Martinez-Tobon et al., 2018). In fact, induction temperature was an important parameter. To avoid IB/IF issues, induction should be done at low temperature (e.g. 15 ℃ as in (Martinez-Tobon et al., 2018) or 8-10 ℃ as described here). Alternatively, induction can be done at 4 ℃ over a period of 48 h to avoid misfolding. The lack of cellular machinery for post-translational modification might be a reason for protein misfolding and the reason for IB formation (Walsh et al., 2010; Bhatwa t al., 2021). Thus, careful considerations should be made in the selection of the expression system.

In addition to the choice of expression system, the choice of promoter when designing recombinant proteins is important. PlacT7 is considered a strong promoter, while the other choice in this study, the ARA inducible promoter, is a medium strength promoter (Lozano-Terol et al., 2021). These two promoters have different types of regulation: LacI-negative for PlacT7, and arabinose-positive for pBAD promoter (https://blog.addgene.org/plasmids-101-

inducible-promoters). Due to its strength, expression under PlacT7 was higher than under the pBAD promoter resulting in higher fluorescence from the cell lysate after expression (Fig. 6.3, 6.4, and 6.5). A similar effect was observed in a study by Lozano-Terol et al. (2021). In the case of IPTG (PlacT7 inducer), yellow fluorescence expression was achieved at 0.1 mM, while for the pBAD promoter, the concentration of the inducer, arabinose, had to be 2 mM. Both promoters are driving gene expression as "all-or-none" when induction occurs with the natural inducer (lactose for PlacT7 and arabinose for pBAD). However, IPTG used as the inducer is a lactose analog and it is not metabolized. Thus, homogenous expression can be achieved at lower concentrations. Lowering IPTG for expression of T7 sfGFP-SBD might be one alternative to avoid the saturation effect and IB formation. In the case of the arabinose inducible promoter, there is no available non-metabolized analog, thus it is not possible to avoid this phenomenon (Afroz et al., 2014).

Detection and quantification are important steps required for each study that involves recombinant proteins, regardless of its purpose. In this study SDS-PAGE and Western blot were used to detect proteins (Fig. 6.2). Regardless of $Ni^{2+}$-NTA resins that should bind only 6xHis-tagged proteins, the presence of non-specific products was observed in SDS-PAGE (Fig. 6.2, panels A and C). To avoid this issue, a change in purification protocol must be implemented. One of the main considerations in protein purification is the choice of buffer. Although the general content of buffers follows a similar pattern in terms of content, the choice between Tris, HEPES, MOPS or phosphate-based solutions will depend on the experimental applications, financial resources, and protein structure. For enzymes, maintaining protein structure for further application is often required, thus the choice of extraction buffer is usually HEPES, as it does not contain primary amines that can affect overall protein structure. Thus, even though HEPES is costly compared to the other buffers (Tris or Phosphate-based), benefits for future applications must be considered. The extraction

buffer for rPhaZs was optimized in a previous study (Martinez-Tobon et al., 2018). However, results from this study show that the change of buffer system to HEPES and/or additional washing steps with higher imidazole concentration might be required to achieve better purity. Another issue that occurred during protein detection was the absence of visible fragments that corresponded to the 42 kDa size (Fig. 6.2, panels B and D). The reason behind this can be impurity of extracted proteins or the protein structure itself. In both cases, the 6xHis tag is not exposed for detection with primary antibody, which results in an inability to visualize protein on Western blot (Debeljak et al., 2006).

Regardless of the concentration of the proteins (250, 500, and 1000F), they each interacted with PHB and emitted fluorescence even once bound to PHB (Fig. 6.3, 6.4, and 6.5). The level of fluorescence corresponded to the concentration level, with the highest fluorescence emitted with 1000F for proteins from both expression systems (Fig. 6.5). A likely saturation effect was observed after long incubation at high concentrations (500 and 100F) for T7 sfGFP-SBD. The potential reason for this could be that extremely high expression was achieved with the PlacT7 promoter. Since sfGFP-SBD is derived from rPhaZs that are considered highly insoluble with a high level of hydrophobic amino acids (Martinez-Tobón et al., 2018), it is possible that a portion of proteins remains embedded in hydrophobic “pockets” without exposure to the hydrophilic environment. Thus, the initial fluorescence is equal for both proteins (250, 500, and 1000 RFU); however, during incubation the “hidden” portion is released and interacts with PHB, which results in the difference in fluorescence emission. Potentially released proteins are interacting with each other giving the effect of saturation and the plateau in fluorescence emission (saturation effect).

Overall, the expression approach for ARA sfGFP-SBD and T7 sfGFP-SBD was established, while the purification and detection approaches need additional improvements. Alternatively, expression can be done in T7 Express lysY/Iq, which enables cloning and expression of toxic genes through“tight control of expression by laclq and of T7 RNA Polymerase by lysozyme." (Martinez- Tobón et al., 2018). The engineered sfGFP-SBD can also be used to assess the purity of PHB samples. PHB is often associated with its co-polymer PHBV. Both proteins designed in this study werePHB specific and did not bind PHBV or PLA (Fig. 6.6).

Even though PHB is often defined as brittle, stiff, its usage in biomedical productions is undeniable. The addition of copolymers does not cause significant change in the immune response in patients, but the quality of material is improved. Thus, PHB is often packed with other copolymers such as PHBV, or PHV (Valappil et al., 2006). For this mixture, knowing its level of purity is important to establish biodegradation protocol. There have been intensive efforts to design recombinant PHB degrading enzymes (Martinez- Tobón et al., 2018), and depending on the material content (PHB, PHV and PHBV percentage), additional degradation protocols must be evaluated. To establish that approach, the need to identify PHV and PHBV specific degrading enzymes, and after confirming PHB recognition proof of concept in this study, the same principle can be applied and design recombinant PHBV and PHV degrading enzymes. In the next step, the specific purity detection synthetic modules can be created to evaluate level of copolymers in the mixture, by simple replacing SBD for PHB with SBD for PHBV or PHV. In this way, the appropriate disposal procedures can be established to ensure the efficient and safe removal of biomedical materials .

Since the SBD is derived from PhaZ that binds crystalline PHB (extracellular PhaZ) (Sudesh et al., 2010), it is reasonable to expect that this enzyme might not be able to interact with intracellular amorphous PHB. However, the expression approach is optimized, and the replacement of SBD can be achieved by using an intracellular PhaZ that recognizes amorphous structures (Sznajder and Jendrossek, 2011).

In terms of significance, the need to develop novel, accurate, but environmentally friendly PHB-detection methods in undeniable. The use of toxic solvents, costly materials and labor-intensive preparation can affect the motivation and interest for extensive PHB-related research. On the other hand, the level of plastic pollution is rapidly increasing, and there is strong need to improve production of sustainable materials. Among many available methods (Godbole., 2016), the only methodology that involves specific PHB binding are NR (Li and Wilkins, 2020), NBA (Lazic et al., 2021), and Sudan-black (Godbole, 2016) -based approaches. However, NR and Sudan black dyes can bind other cellular lipid components, which might affect the accuracy of results. Having a specific sensor that can bind only PHB inside or outside the cell is highly beneficial and has potential to be used as an accurate, precise, and environmentally friendly PHB-detection system.

# Chapter 7

## Closing remarks

We are living at a point in history when facing the reality of climate change is paramount to our survival. The Earth is heating up, and it is inevitable that in a few decades we might face internal protein denaturation as temperatures regularly exceed 50°C. Nevertheless, the global population is still growing, and industry continues to rapidly develop. The emission of greenhouse gases from landfills, industrial facilities and agricultural fields is not stopping, and in fact, GHG emissions continue to increase year-to-year. There have been efforts to implement hybrid and electric vehicles, but the technology is expensive, and the majority of the population cannot afford these luxuries. Some efforts have been made to reduce usage of plastic bags in grocery stores. However, the economic situation does not allow everyone to give up plastic materials and less expensive gas-fueled cars.

Methanotrophs are microbes that have the potential to solve many environmental issues. We must not forget that these organisms are soldiers in the first line of defense against methane emissions. They inhabit upper parts of soils, preventing release of initial methane emissions originating from anaerobic methanogens. Without methanotrophs, this planet would have become uninhabitable a long time ago. On one hand, they can be observed as natural methane consumers and the only biological methane sink. On the other hand, they are considered as microbial biofactories, as they are often used to produce a plethora of value-added compounds. Methanotrophs that grow fast (gammaproteobacterial methanotrophs) have the potential to be used for production of biofuels, since they are extremely lipid rich. Another group, alphaproteobacterial methanotrophs can be useful biological platforms for production of bioplastic precursors (biopolymers). Since the increased amount of methane in the atmosphere and the accumulation of non-recyclable plastics are two major environmental

issues that contribute to the climate change, it is reasonable to conclude that alphaproteobacterial methanotrophs have the potential to help mitigate both issues. Thus, it is highly beneficial to understand the metabolic pathways that regulate production of biodegradable polymers from methane in these organisms. Having this accurate metabolic road map will help in determining the most efficient pathway for biopolymer synthesis.

The molecular tools for manipulation in methanotrophs have been recently reviewed (Pfam et al., 2022). Significant progress has been made in developing molecular systems and optimizing genetic engineering of methanotrophs. However, multiple drawbacks prevent faster progress. The metabolic map of entire cellular pathways will help in understanding the flux of carbon and nitrogen and determine appropriate target genes for knock-out or overexpression. It is critically important to understand the fate of reducing equivalents and metabolic precursors used for specific bioproduction. Instead of labor intensive and time-consuming experiments, metabolic mapping along with computer simulations (Genome Scale Metabolic Model-GEM) will be important tools that will facilitate not only engineering, but also in optimizing feeding strategies.

In this study, genetic engineering was not applied in methanotrophs, rather attempts were made to identify optimal nutrient conditions that will promote production of biopolymer (PHB) without affecting biomass production. This work was dedicated to solving the effect of carbon and nitrogen source on cellular physiology, and my hope is that data generated in this thesis will be of use in future GEM construction for the model organism *Methylocystis* sp. Rockwell. Methanol has been established as a PHB production trigger; it is clear that the combination of methane/methanol has potential to improve PHB synthesis in many alphaproteobacterial methanotrophs. The optimal nitrogen concentration and N:C value was also established, and it is ten times lower than the standard concentration that has been used to grow methanotrophs for decades. Next steps in the field include further investigations of

optimal methane:methanol ratios and testing growth in continuous bioreactors. In addition, proteomic analysis should be done to complete the metabolic map, implement data in a GEM, and determine the physiological basis for how methanol affects PHB production. Overall, the long-term goal for generations to come (including myself), we will have a sustainable system that operates on single-carbon substrates (Fig. 7.1).

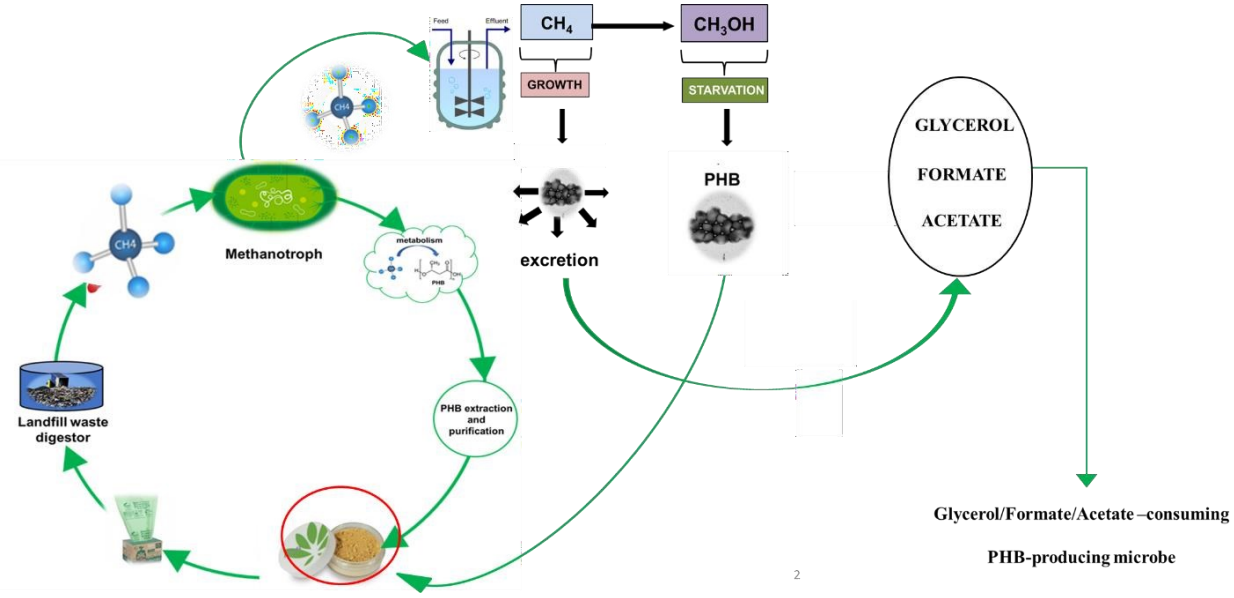


Figure 7.1. Methanotrophs as a sustainable platform for production of PHB. The methane-emitting landfill digestor is linked to the bioreactor. The bioreactor contains alphaproteobacterial methanotrophs and engineered heterotrophs. In the first scenario, methanotrophs are growing on methane and excrete metabolic products (glycerol, formate, acetate). They are co-cultured with engineered heterotrophs, modified to use excreted compounds and create PHB. Remaining methanotrophic biomass can be used for production of SCP, other products, or growth media. In the second scenario, methanotrophs would grow only on methane until they reach enough biomass, after which they are "stressed" with methanol to stimulate PHB production.

In addition to optimization, each production must have an efficient approach to detect and quantify the target molecule of interest. In this work, novel methodologies were developed - Single Cell Approach for precise and environmentally friendly in vivo, direct PHB detection, and in vitro methodology for PHB purity evaluation. The accuracy and precision of in vivo methodology was confirmed, and it the hope exists that this will become a common approach in most of the research facilities worldwide. One potential drawback must be noticed, and refers to the ability to detect PHB amount >30%. The methodology was applied in oxygen – limiting conditions (Lazic et al., 2022, Chapter 5), where M. sp. Rockwell produces ~28% in methane-N2 (NoN) conditions. In Chapter 4 where oxygen was not limiting, it was clear that this organism can produce up to 70% dw/L PHB. Thus, the dye saturation might occur. Nevertheless, it remains to be tested whether this approach can be efficient with organisms that produce PHB in higher amounts (>30% dw/L). In terms of in vitro PHB detection, this approach represents preliminary study showing (i) the possibility to create polymer purity detection system and (ii) the ability to improve production and purification of recombinant proteins involved in biopolymer detection.

To aim high and achieve long-term goals, small steps must be made. Each of these steps might be too small for direct implementation, but for the future of this planet, these steps are important. It might not be obvious at the moment, but in a few years, maybe decades or even centuries, my hope is that the work generated here can be implemented in preventing this world from melting. We need to ensure that we leave this planet in an appropriate condition for generations to come, as well as for us. Remember, there is no Planet B!

References

Akberdin, I. R., Thompson, M., Hamilton, R., Desai, N., Alexander, D., Henard, C. A., Guarnieri, M. T., & Kalyuzhnaya, M. G. (2018). Methane utilization in Methylomicrobium alcaliphilum 20ZR: A systems approach. Scientific Reports, 8(1). https://doi.org/10.1038/s41598-018-20574-z

Alves, L. P. S., Almeida, A. T., Cruz, L. M., Pedrosa, F. O., de Souza, E. M., Chubatsu, L. S., Müller-Santos, M., & Valdameri, G. (2017). A simple and efficient method for poly-3-hydroxybutyrate quantification in diazotrophic bacteria within 5 minutes using flow cytometry. Brazilian Journal of Medical and Biological Research, 50(1). https://doi.org/10.1590/1414-431X20165492

Ansari, A. and Fatma, T. (2016). Cyanobacterial Polyhydroxybutyrate (PHB): Screening, Optimization and Characterization. PLOS ONE | doi: 10.1371/journal.pone.0158168.

Anthony, C. (2004). The quinoprotein dehydrogenases for methanol and glucose. In Archives of Biochemistry and Biophysics (Vol. 428, Issue 1, pp. 2–9). https://doi.org/10.1016/j.abb.2004.03.038

Attwood, M. M., Arfman, N., Weusthuis, R. A., & Dijkhuizen, L. (1992). Purification and characterization of an NAD § formaldehyde dehydrogenase from the facultative RuMP cycle methylotroph Arthrobacter P1 Abbreviation: RuMP-Ribulose monophosphate. In Antonie van Leeuwenhoek (Vol. 62). Kluwer Academic Publishers.

Balasubramanian, R. and Rosenzweig, A.C. (2007). Structural and mechanistic insights into methane oxidation by particulate methane monooxygenase. Acc. Chem. Res 40, 573–580.

Balasubramanian, R., Smith, S. M., Rawat, S., Yatsunyk, L. A. et al. (2010). Oxidation of methane by a biological dicopper center. Nature, 465, 115–119.

Bandow, N.L., Gallagher, W.H., Behling, L., Choi, D.W., Semrau, J.D., Hartsel, S.C., et al. (2011). Isolation of methanobactin from the spent media of methane oxidizing bacteria. Methods Enzymol 495B, 259–269.

Basch, K. M. H. (1999). Mechanism of the Methane f Methanol Conversion Reaction. J. Am. Chem. Soc., Vol. 121,, 7249-7256.

Beal, E.J. House, C.H., Orphan, V.J. (2009). Manganese- and iron-dependent marine methane oxidation. Science, 325, 184–187.

Bedard-;-And, C., & Knowles, R. (n.d.). Physiology, Biochemistry, and Specific Inhibitors of CH4, NH4+, and CO Oxidation by Methanotrophs and Nitrifiers.

Bennett, R.K. & A. A.-H. (2020). Triggering the stringent response enhances syn 1 thetic methanol utilization in Escherichia. Metabolic Engineering 61, 1-10.

Bender, M., & Conrad, R. (1992). Kinetics of CH4 oxidation in oxic soils exposed to ambient air or high CH4 mixing ratios. FEMS Microbiology Ecology, 10(4), 261–269. https://doi.org/10.1111/j.1574-6941.1992.tb01663.x

Bodelier, P. L. E., & Laanbroek, H. J. (2004). Nitrogen as a regulatory factor of methane oxidation in soils and sediments. In FEMS Microbiology Ecology (Vol. 47, Issue 3, pp. 265–277). Elsevier. https://doi.org/10.1016/S0168-6496(03)00304-0

Boetius, A., Ravenschlag, K., Schubert, C. J., Rickert2, D., Widdel, F., Gieseke, A., Amann, R., Jùrgensen, B. B., Witte, U., & Pfannkuche2, O. (2000). A marine microbial consortium apparently mediating anaerobic oxidation of methane. In NATURE (Vol. 407). www.nature.com

Bonthrone, K. M., Clauss, J., Horowitz, D. M., Hunter, B. K., & Sanders, J. K. M. (1992). The biological and physical chemistry of polyhydroxyalkanoates as seen by NMR spectroscopy. FEMS Microbiology Letters, 103(2–4), 269–277.

https://doi.org/10.1111/j.1574-6968.1992.tb05848.x

Bordel, S., Rodríguez, Y., Hakobyan, A., Rodríguez, E., Lebrero, R., & Muñoz, R. (2019). Genome scale metabolic modeling reveals the metabolic potential of three Type II methanotrophs of the genus Methylocystis. Metabolic Engineering, 54, 191–199. https://doi.org/10.1016/j.ymben.2019.04.001

Bothe, H., Møller Jensen, K., Mergel, A., Larsen, J., Jørgensen, C., Bothe, H., & Jørgensen, L. (2002). Heterotrophic bacteria growing in association with Methylococcus capsulatus (Bath) in a single cell protein production process. Applied Microbiology and Biotechnology, 59(1), 33–39. https://doi.org/10.1007/s00253-002-0964-1

Bowman, J. P., Skerratt, J. H., Nichols, P. D., & Sly, L. I. (1991). Phospholipid fatty acid and lipopolysaccharide fatty acid signature lipids in methane-utilizing bacteria. FEMS Microbiology Letters, 85(1), 15–22. https://doi.org/10.1111/j.1574-6968.1991.tb04693.x

Brown, L.R., Strawinski, R.J. and McCleskey, C.S. (1964). The isolation and characterization of Methanomonas methanooxidans. Canadian Journal of Microbiology 10, 791–799.

Caballerot, K. P., Karel, S. F., & Register, R. A. (n.d.). Biosynthesis and characterization of hyd roxybutyrate-hyd roxyca p roate copolymers.

Cal, A. J., Sikkema, W. D., Ponce, M. I., Franqui-Villanueva, D., Riiff, T. J., Orts, W. J., Pieja, A. J., & Lee, C. C. (2016). Methanotrophic production of polyhydroxybutyrate-co-hydroxyvalerate with high hydroxyvalerate content. International Journal of Biological Macromolecules, 87, 302–307. https://doi.org/10.1016/j.ijbiomac.2016.02.056

Campbell, M. A., Nyerges, G., Kozlowski, J. A., Poret-Peterson, A. T., Stein, L. Y., & Klotz,

M. G. (2011). Model of the molecular basis for hydroxylamine oxidation and nitrous oxide production in methanotrophic bacteria. FEMS Microbiology Letters, 322(1), 82–89. https://doi.org/10.1111/j.1574-6968.2011.02340.x

Cantera, S., Bordel, S., Lebrero, R., Gancedo, J., García-Encina, P. A., & Muñoz, R. (2019). Bio-conversion of methane into high profit margin compounds: an innovative, environmentally friendly and cost-effective platform for methane abatement. In World Journal of Microbiology and Biotechnology (Vol. 35, Issue 1). Springer Netherlands. https://doi.org/10.1007/s11274-018-2587-4

Cestellos-Blanco, S., Friedline, S., Sander, K.B., Abel, A.J., Kim, J.M., Clark, D.S., Arkin, A.P. and Yang, P. (2021). Production of PHB From CO2-Derived Acetate With Minimal Processing Assessed for Space Biomanufacturing. Frontiers in Microbiology 12. 700010. doi: 10.3389/fmicb.2021.700010.

Chandran, K., Stein, L. Y., Klotz, M. G., & van Loosdrecht, M. C. M. (2011). Nitrous oxide production by lithotrophic ammonia-oxidizing bacteria and implications for engineered nitrogen-removal systems. Biochemical Society Transactions, 39(6), 1832–1837. https://doi.org/10.1042/BST20110717

Chen, H. J., Pan, S. C., & Shaw, G. C. (2009). Identification and characterization of a novel intracellular poly(3-hydroxybutyrate) depolymerase from Bacillus megaterium. Applied and Environmental Microbiology, 75(16), 5290–5299. https://doi.org/10.1128/AEM.00621-09

Chidambarampadmavathy, K., Karthikeyan, O. P., & Heimann, K. (2015). Biopolymers made from methane in bioreactors. Engineering in Life Sciences, 15(7), 689–699. https://doi.org/10.1002/elsc.201400203

Chistoserdova, L. (2011). Modularity of methylotrophy, revisited. In Environmental Microbiology (Vol. 13, Issue 10, pp. 2603–2622). https://doi.org/10.1111/j.1462-

2920.2011.02464.x

Chistoserdova, L. (2015). Methylotrophs in natural habitats: current insights through metagenomics. In Applied Microbiology and Biotechnology (Vol. 99, Issue 14, pp. 5763–5779). Springer Verlag. https://doi.org/10.1007/s00253-015-6713-z

Choi, D.W., Kunz, R.C., Boyd, E.S., Semrau, J.D., Antholine, W.E., Han, J.I., Zahn, J.A., Boyd, J.M., de la Mora, A.M. and DiSpirito, A,A, (2003). The membrane-associated methane monooxygenase (pMMO) and pMMO-NADH: quinine oxidoreductase complex from *Methylococcus capsulatus* Bath. J Bacteriol 185, 5755–5764.

Choi, D.W., Zea,, C.J., Do, Y.S., Semrau, J.D., Antholine, W.E., Hargrove, M.S., et al. (2006). Spectral, kinetic and thermodynamic properties of Cu(I)- and Cu(II)-binding by methanobactin from Methylosinus trichosporium OB3b. Biochemistry 45, 1142–1153.

Chu, F., & Lidstrom, M. E. (2016). XoxF acts as the predominant methanol dehydrogenase in the type I methanotroph Methylomicrobium buryatense. Journal of Bacteriology, 198(8), 1317–1325. https://doi.org/10.1128/JB.00959-15

Clark et al., 2019 reporters. (n.d.).

Colby, J., Stirling, D.I. and Dalton, H. (1977). The soluble methane monooxygenase of Methylococcus capsulatus (Bath). Biochem J 165, 395–402.

Colby, J and Dalton, H. (1978). Resolution of the methane monooxygenase of Methylococcus capsulatus (Bath) into three components. Purification and properties of component C, a flavoprotein. Biochem J 171, 461–468.

Colin Murrell, J., & Jetten, M. S. M. (2009). The microbial methane cycle. In Environmental Microbiology Reports (Vol. 1, Issue 5, pp. 279–284). https://doi.org/10.1111/j.1758-2229.2009.00089.x

Conrad, R. (2009). The global methane cycle: Recent advances in understanding the microbial processes involved. In Environmental Microbiology Reports (Vol. 1, Issue 5, pp. 285–292). https://doi.org/10.1111/j.1758-2229.2009.00038.x

Conrado, R. J., & Gonzalez, R. (2014). Envisioning the bioconversion of methane to liquid fuels. In Science (Vol. 343, Issue 6171, pp. 621–623). American Association for the Advancement of Science. https://doi.org/10.1126/science.1246929

Costa, S., Almeida, A., Castro, A., & Domingues, L. (2014). Fusion tags for protein solubility, purification, and immunogenicity in Escherichia coli: The novel Fh8 system. In Frontiers in Microbiology (Vol. 5, Issue FEB). Frontiers Research Foundation. https://doi.org/10.3389/fmicb.2014.00063

Crowe, S.A., Jones, C., Katsev, S., Magen, C., O'Neill, A.H., Sturm, A., Canfield, D.E., Haffner, G.D., Mucci, A., and Sundby, B. (2008). .Photoferrotrophs thrive in an Archean Ocean analogue. Proc. Natl. Acad. Sci. USA 2008, 105, 15938–15943.

Dalton, H., Prior, S.D., Leak, D.J. and Stanley, S.H. (1984). Regulation and control of methane monooxygenase. Microbial Growth on C1 Compounds (Crawford RL & Hanson RS, eds), 75–82.

Dam, B., Dam, S., Kim, Y., & Liesack, W. (2014). Ammonium induces differential expression of methane and nitrogen metabolism-related genes in Methylocystis sp. strain SC2. Environmental Microbiology, 16(10), 3115–3127. https://doi.org/10.1111/1462-2920.12367

de Koning, G. J. M., & Lemstra, P. J. (1992). The amorphous state of bacterial poly[(R)-3-hydroxyalkanoate]in vivo. Polymer, 33(15), 3292–3294. https://doi.org/10.1016/0032-3861(92)90249-V

de Souza Pinto Lemgruber, R., Valgepea, K., Tappel, R., Behrendorff, J,B., William, R.,

Plan, M.P.,. Hodson, M.P., Simpson, S.D., Nielsen, L.K., Köpke, M. and Marcellin, E. (2019). Systems-level engineering and characterization of Clostridium autoethanogenum through heterologous production of poly-3-hydroxybutyrate (PHB). Metabolic Engineering, https://doi.org/10.1016/j.ymben.2019.01.003.

Dedysh, S.N., Liesack, W., Khmelenina, V.N., Suzina, N.E., Trotsenko, Y.A., Semrau, J.D., Bares, A.M., Panikov, N.S. and Tiedje ,J.M.. (2000). Methylocella palustris gen. nov., a new methane-oxidizing acidophilic bacterium from peat bogs, representing a novel subtype of serine pathway methanotrophs. International Journal of Systematic and Evolutionary Microbiology 50, 955–969.

Dedysh,S.N., Khmelenina,V.N., Suzina,N.E., Trotsenko,Y.A.,Semrau, J.D., Liesack, W. and Tiedje, J.M. (2002). Methylocapsa acidiphila gen. nov., sp. nov., a novel methane-oxidizing and dinitrogen-fixing acidophilic bacterium from Sphagnum bog. International Journal of Systematic and Evolutionary Microbiology 52, 251–261.

Dedysh, S.N., Berestovskaya, Y.Y., Vasylieva, L.V., Belova, S.E., Khmelenina, V.N., Suzina, N.E., Trotsenko, Y.A., Liesack, W. and Zavarzin, G.A. (2004). Methylocella tundrae sp. nov., a novel methanotrophic bacterium from acidic tundra peatlands. International Journal of Systematic and Evolutionary Microbiology 54, 151–156.

Dedysh, S.N., Knief., C. and Dunfield, P.F. (2005). Methylocella species are facultatively methanotrophic. Journal of Bacteriology 187, 4665–4670.

Doi, Y. (1992). Microbial Synthesis and Properties of Polyhydroxy-alkanoates. *MRS Bulletin, 17*(11), 39-42. doi:10.1557/S0883769400046649

Downs, J., and Harrison, 1 D. E. F. (1974). Studies on the production of pink pigment in Pseudomonas extorquens NCIB 9399 growing in continuous culture. J. Appl. Bacteriol. 37, 65-74.

Drummond, D, Smith, S. and Dalton, H. (1989). Solubilization of methane monooxygenase from Methylococcus capsulatus (Bath). European Journal of Biochemistry 182, 667–671.

Duc Nguyen, A., Hoang Trung Chau, T., & Yeol Lee, E. (2021). Methanotrophic microbialcell factory platform for simultaneous conversion of methane and xylose to value-added chemicals. Chemical Engineering Journal, 420. https://doi.org/10.1016/j.cej.2020.127632

Dunfield, P.F., Khmelenina, V.N., Suzina, N.E., Trotsenko, Y. and Dedsyh, S.N. (2003). Methylocella silvestris sp. nov., a novel methanotroph isolated from an acidic forest cambisol. International Journal of Systematic and Evolutionary Microbiology 53, 1231–1239..

Dunfield, P.F., Belova, S.E., Vorobev, A.V., Cornish, S.L. and Dedysh, S.N. (2010). Methylocapsa aurea sp. nov., a facultative methanotroph possessing a particulate methane monooxygenase and emended description of the genus Methylocapsa. International Journal of Systematic and Evolutionary Microbiology 60, 2659–2664.

Dworkin, M. and Foster, J.W. (1956). Studies on Pseudomonas methanica (Sohngen) nov. comb. Journal of Bacteriology 72,646–659.

Eberlein, C., Baumgarten, T., Starke, S., & Heipieper, H. J. (2018). Immediate response mechanisms of Gram-negative solvent-tolerant bacteria to cope with environmental stress: cis-trans isomerization of unsaturated fatty acids and outer membrane vesicle secretion. In Applied Microbiology and Biotechnology (Vol. 102, Issue 6, pp. 2583–2593). Springer Verlag. https://doi.org/10.1007/s00253-018-8832-9

El Ghazouani, A., Baslé, A., Gray, J., Graham, D.W., Firbank, S.J., and Dennison, C. (2012). Variations in methanobactin structure influences copper utilization by methane oxidizing bacteria. Proc Natl Acad Sci USA 109, 8400– 8404.

Elango, N., Radhakrishnan, R., Froland, W.A., Wallar, B.J., Earhart, C.A., Lipscomb, J.D. and Ohlendorf, D.H. (1997). Crystal structure of the hydroxylase component of

methane monooxygenase from Methylosinus trichosporium OB3b. Protein Sci 6, 556–568.

Ensign, S. A., Hyman, M. R., & Arp, D. J. (1993). In Vitro Activation of Ammonia Monooxygenase from Nitrosomonas europaea by Copper. In JOURNAL OF BACTERIOLOGY (Vol. 175, Issue 7). https://journals.asm.org/journal/jb

Erguder, T. H., Boon, N., Wittebolle, L., Marzorati, M., & Verstraete, W. (2009). Environmental factors shaping the ecological niches of ammonia-oxidizing archaea. In FEMS Microbiology Reviews (Vol. 33, Issue 5, pp. 855–869). https://doi.org/10.1111/j.1574-6976.2009.00179.x

Eshinimaev, B.T., Khmelenina, V.N., Sacharovskii, V. G., Suzina, N.E. and Trotsenko, Y.A. (2002). Physiological, biochemical and cytological characteristics of haloalkalitolerant methanotroph grown on methanol. Microbiology 7, 512-518. doi1020594300166.

Ettwig, K. F., Butler, M. K., le Paslier, D., Pelletier, E., Mangenot, S., Kuypers, M. M. M., Schreiber, F., Dutilh, B. E., Zedelius, J., de Beer, D., Gloerich, J., Wessels, H. J. C. T., van Alen, T., Luesken, F., Wu, M. L., van de Pas-Schoonen, K. T., Op Den Camp, H. J. M., Janssen-Megens, E. M., Francoijs, K. J., … Strous, M. (2010). Nitrite-driven anaerobic methane oxidation by oxygenic bacteria. Nature, 464(7288), 543–548. https://doi.org/10.1038/nature08883

Ettwig, K. F., van Alen, T., van de Pas-Schoonen, K. T., Jetten, M. S. M., & Strous, M. (2009). Enrichment and molecular detection of denitrifying methanotrophic bacteria of the NC10 phylum. Applied and Environmental Microbiology, 75(11), 3656–3662. https://doi.org/10.1128/AEM.00067-09

Evans, P. N., Boyd, J. A., Leu, A. O., Woodcroft, B. J., Parks, D. H., Hugenholtz, P., & Tyson, G. W. (2019). An evolving view of methane metabolism in the Archaea. In Nature

Reviews Microbiology (Vol. 17, Issue 4, pp. 219–232). Nature Publishing Group. https://doi.org/10.1038/s41579-018-0136-7

Ezgi Bezirhan Arikan, & Havva Duygu Ozsoy. (2015). A Review: Investigation of Bioplastics. Journal of Civil Engineering and Architecture, 9(2). https://doi.org/10.17265/1934-7359/2015.02.007

Fang, J., Barcelona, M. J., & Semrau, J. D. (2000). Characterization of methanotrophic bacteria on the basis of intact phospholipid profiles. FEMS Microbiology Letters, 189(1), 67–72. https://doi.org/10.1111/j.1574-6968.2000.tb09207.x

Fei, Q., Guarnieri, M. T., Tao, L., Laurens, L. M. L., Dowe, N., & Pienkos, P. T. (2014). Bioconversion of natural gas to liquid fuel: Opportunities and challenges. In Biotechnology Advances (Vol. 32, Issue 3, pp. 596–614). Elsevier Inc. https://doi.org/10.1016/j.biotechadv.2014.03.011

Fiore, A. M., Jacob, D. J., Bey, I., Yantosca, R. M., Field, B. D., Fusco, A. C., & Wilkinson, J. G. (2002). Background ozone over the United States in summer: Origin, trend, and contribution to pollution episodes. Journal of Geophysical Research Atmospheres, 107(15), ACH 11-1-ACH 11-25. https://doi.org/10.1029/2001JD000982

Foster, J. W. and Davis, R.H. (1966). A methane-dependent coccus, with notes on classification and nomenclature of obligate, methane utilizing bacteria. Journal of Bacteriology 91,1924–1931.

Fox, B.G., Froland, W.A., Dege,, J.E. and Lipscomb, J.D. (1989). Methane monooxygenase from Methylosinus trichosporium OB3b: purification and properties of a three-component system with high specific activity from a type II methanotroph. J Biol Chem 264, 10023–10033.

Freynhagen, R., Grond, S., Schüpfer, G., Hagebeuker, A., Schmelz, M., Ziegler, D., von

Giesen, H. J., Junker, U., Wagner, K. J., & Konrad, C. (2007). Efficacy and safety of pregabalin in treatment refractory patients with various neuropathic pain entities in clinicalroutine. International Journal of Clinical Practice, 61(12), 1989–1996. https://doi.org/10.1111/j.1742-1241.2007.01589.x

Fu, Y., He, L., Reeve, J., Beck, D. A. C., & Lidstrom, M. E. (2019). Core metabolism shifts during growth on methanol versus methane in the methanotroph methylomicrobium buryatense 5GB1. mBio, 10(2). https://doi.org/10.1128/mBio.00406-19

Gao, Y., Li, D., & Liu, Y. (2012). Production of single cell protein from soy molasses using Candida tropicalis. Annals of Microbiology, 62(3), 1165–1172. https://doi.org/10.1007/s13213-011-0356-9

Gilman, A., Fu, Y., Hendershott, M., Chu, F., Puri, A. W., Smith, A. L., Pesesky, M., Lieberman, R., Beck, D. A. C., & Lidstrom, M. E. (2017). Oxygen-limited metabolism in the methanotroph Methylomicrobium buryatense 5GB1C. PeerJ, 2017(10). https://doi.org/10.7717/peerj.3945

Godbole, s. (2016). Methods for identification, quantification and characterization of polyhydroxyalkanoates. International Journal of Bioassays 5 (4), 4977-4983.

Govil, T., Wang, J., Samanta, D., David, A., Tripathi, A., Rauniyar, S., Salem, D. R., & Sani, R. K. (2020). Lignocellulosic feedstock: A review of a sustainable platform for cleaner production of nature's plastics. In Journal of Cleaner Production (Vol. 270). Elsevier Ltd. https://doi.org/10.1016/j.jclepro.2020.122521

Graham, D. W., Chaudhary, J. A., Hanson, R. S., & Arnold, R. G. (1993). MICROBIAL ECOLOGY Factors Affecting Competition Between Type I and Type II Methanotrophs in Two-organism, Continuous-flow Reactors. In Microb Ecol (Vol. 25).

Green, J. and Dalton, H. (1985). Protein B of soluble methane monooxygenase from Methylococcus capsulatus (Bath). J Biol Chem 260, 15795–15801.

Hallam, S.J., Putnam, N., Preston, C.M., Detter, J.C., Rokhsar, D., Richardson, P.M. and. DeLong, E.F. (2004). Reverse Methanogenesis: Testing the Hypothesis with Environmental Genomics. Science 305 (5689), 1457-1462. https://www.jstor.org/stable/3837824.

Harding, K. G., Dennis, J. S., von Blottnitz, H., & Harrison, S. T. L. (2007). Environmental analysis of plastic production processes: Comparing petroleum-based polypropylene and polyethylene with biologically-based poly-β-hydroxybutyric acid using life cycle analysis. Journal of Biotechnology, 130(1), 57–66. https://doi.org/10.1016/j.jbiotec.2007.02.012

Haroon, M. F., Hu, S., Shi, Y., Imelfort, M., Keller, J., Hugenholtz, P., Yuan, Z., & Tyson, G. W. (2013). Anaerobic oxidation of methane coupled to nitrate reduction in a novel archaeal lineage. Nature, 500(7464), 567–570. https://doi.org/10.1038/nature12375

Hauf, W., Schlebusch, M., Hüge, J., Kopka, J., Hagemann, M. and Forchhammer, K. (2013).Metabolic Changes in Synechocystis PCC6803 upon Nitrogen-Starvation: Excess NADPH Sustains Polyhydroxybutyrate Accumulation. Metabolites 3(1), 101-18. doi: 10.3390/metabo3010101. PMID: 24957892; PMCID: PMC3901256.

He, Z., Wang, J., Zhang, X., Cai, C., Geng, S., Zheng, P., Xu, X., & Hu, B. (2015). Nitrogen removal from wastewater by anaerobic methane-driven denitrification in a lab-scale reactor: heterotrophic denitrifiers associated with denitrifying methanotrophs. Applied Microbiology and Biotechnology, 99(24), 10853–10860. https://doi.org/10.1007/s00253-015-6939-9

Heider, S. A. E., Peters-Wendisch, P., Wendisch, V. F., Beekwilder, J., & Brautaset, T. (2014). Metabolic engineering for the microbial production of carotenoids and related products with a focus on the rare C50 carotenoids. In Applied Microbiology and Biotechnology (Vol. 98, Issue 10, pp. 4355–4368). Springer Verlag. https://doi.org/10.1007/s00253-014-5693-8

Helm, J., Wendlandt, K. D., Jechorek, M., & Stottmeister, U. (2008). Potassium deficiency results in accumulation of ultra-high molecular weight poly-β-hydroxybutyrate in a methane-utilizing mixed culture. Journal of Applied Microbiology, 105(4), 1054–1061. https://doi.org/10.1111/j.1365-2672.2008.03831.x

Henard, C. A., Smith, H., Dowe, N., Kalyuzhnaya, M. G., Pienkos, P. T., & Guarnieri, M. T. (2016). Bioconversion of methane to lactate by an obligate methanotrophic bacterium. Scientific Reports, 6. https://doi.org/10.1038/srep21585

Hibi, Y., Asai, K., Arafuka, H., Hamajima, M., Iwama, T., & Kawai, K. (2011). Molecular structure of La3+-induced methanol dehydrogenase-like protein in Methylobacterium radiotolerans. Journal of Bioscience and Bioengineering, 111(5), 547–549. https://doi.org/10.1016/j.jbiosc.2010.12.017

Hinrichs, U.K., Hayes, J.M.,. Sylva, S.P., Brewer, P.G. and DeLong, E.F. (1999). Methane-consuming archaebacteria in marine sediments. Nature 398, 802-805.

Hill, E.A., Chrisler, W.B., Beliaev, A.S. and Bernstein, H.C. (2017). A flexible microbial co-culture platform for simultaneous utilization of methane and carbon dioxide from gas feedstocks. Bioresource Technology 228, 250–256. http://dx.doi.org/10.1016/j.biortech.2016.12.111.

Hoehler, T. M., Alperin, M. J., Albert, D. B., & Martens, C. S. (1994). Field and laboratory studies of methane oxidation in an anoxic marine sediment' Evidence for a methanogen-sulfate reducer consortium. In GLOBAL BIOGEOCHEMICAL CYCLES (Vol. 8, Issue 4).

Holmes, P.A. 1988. Applications of PHB-a microbially produced biodegradable thermoplastic. Physics in Technology 16 (32).

Home About Biodegradable Packaging The Pros and Cons of Bioplastics The Pros and Cons of Bioplastics. (n.d.). https://greenhome.co.za/the-pros-and-cons-of-bioplastics/

https://www.metabolon.com/

http://www.methanotroph.org/wiki/metabolic-pathways/.

https://web.expasy.org/cgi-bin/protparam/protparam

https://www.investopedia.com/terms/r/r-squared.asp

https://www.mangomaterials.com/

https://www.newlight.com/

https://youmatter.world/en/definition/biodegradable-plastic

https://www.spine-health.com/glossary/biocompatibility

https://www.merriam-webster.com/dictionary/thermoplastic

Iguchi, H., Yurimoto, H., & Sakai, Y. (2010). Soluble and particulate methane monooxygenase gene clusters of the type I methanotroph Methylovulum miyakonense HT12. In FEMS Microbiology Letters (Vol. 312, Issue 1, pp. 71–76). https://doi.org/10.1111/j.1574-6968.2010.02101.x

Martinez-Tobon, DI (2019).Biodegradation of Polyhydroxybutyrate by Bacterial Strains, Native Extracellular PHB Depolymerases, and Structural Variants. Doctoral dissertation, University of Alberta.

Islam, T., Jensen, S., Reigstad, L. J., Larsen, Ø., & Birkeland, N.-K. (2008). Methane oxidation at 55 o C and pH 2 by a thermoacidophilic bacterium belonging to the Verrucomicrobia phylum. www.pnas.org/cgi/content/full/

IPCC. (2013). The Physical Science Basis. Contribution of Working.

Jahng, D. and Wood, T. (1996). Metal ions and chloramphenicol inhibition of soluble methane monooxygenase from Methylosinus trichosporium OB3b. Appl. Microbiol. Biotechnol. 45, 744–749.

Jendrossek, D., & Handrick, R. (2002). Microbial degradation of polyhydroxyalkanoates. In Annual Review of Microbiology (Vol. 56, pp. 403–432). https://doi.org/10.1146/annurev.micro.56.012302.160838

Jin, S., Bae, J., Song, Y., Pearcy, N., Shin, J., Kang, S., Minton, N.P., Soucaille, P. and Cho, B.K. (2020). Synthetic Biology on Acetogenic Bacteria for Highly Efficient Conversion of C1 Gases to Biochemicals. International Journal of Molecular Sciences 21, 7639. doi:10.3390/ijms21207639.

Juengert, J.R., Borisova, M., Mayer, C., Wolz, C., Brigham, C.J., Sinskey, A.J. and Jendrossek D. (2017). Absence of ppGpp Leads to Increased Mobilization of Intermediately Accumulated Poly(3-Hydroxybutyrate) in Ralstonia eutropha H16. Appl Environ Microbiol. 83 (13):e00755-17. doi: 10.1128/AEM.00755-17. PMID: 28455332; PMCID: PMC5478976.

Kaiser, J. C., & Heinrichs, D. E. (2018). Branching Out: Alterations in Bacterial Physiology and Virulence Due to Branched-Chain Amino Acid Deprivation. https://doi.org/10

Kalyuzhnaya, M. G., Puri, A. W., & Lidstrom, M. E. (2015). Metabolic engineering in methanotrophic bacteria. Metabolic Engineering, 29, 142–152. https://doi.org/10.1016/j.ymben.2015.03.010

Kalyuzhnaya, M. G., & Xing, X. H. (2018). Methane biocatalysis: Paving the way to sustainability. In Methane Biocatalysis: Paving the Way to Sustainability. Springer International Publishing. https://doi.org/10.1007/978-3-319-74866-5

Kalyuzhnaya, M. G., Yang, S., Rozova, O. N., Smalley, N. E., Clubb, J., Lamb, A., Gowda, G. A. N., Raftery, D., Fu, Y., Bringel, F., Vuilleumier, S., Beck, D. A. C., Trotsenko, Y. A., Khmelenina, V. N., & Lidstrom, M. E. (2013). Highly efficient methane biocatalysis revealed in a methanotrophic bacterium. Nature Communications, 4. https://doi.org/10.1038/ncomms3785

Karamanlioglu, M., Preziosi, R., & Robson, G. D. (2017). Abiotic and biotic environmental degradation of the bioplastic polymer poly(lactic acid): A review. In Polymer Degradation and Stability (Vol. 137, pp. 122–130). Elsevier Ltd. https://doi.org/10.1016/j.polymdegradstab.2017.01.009

Karr, D. B., Waters, J. K., Emerich, D. W., & Evans, H. (1983). Analysis of Poly-,3-Hydroxybutyrate in Rhizobium japonicum Bacteroids by Ion-Exclusion High-Pressure Liquid Chromatography and UV Detectiont. In APPLIED AND ENVIRONMENTAL MICROBIOLOGY.

Kerr, E. D., & Schulz, B. L. (2016). Vegemite Beer: Yeast extract spreads as nutrient supplements to promote fermentation. PeerJ, 2016(10). https://doi.org/10.7717/PEERJ.2271

Khadem, A. F., van Teeseling, M. C. F., van Niftrik, L., Jetten, M. S. M., Op Den Camp, H. J. M., & Pol, A. (2012). Genomic and physiological analysis of carbon storage in the verrucomicrobial methanotroph "Ca. Methylacidiphilum fumariolicum" SolV. Frontiers in Microbiology, 3(SEP). https://doi.org/10.3389/fmicb.2012.00345

Khmelenina, V. N., Rozova, O. N., But, S. Y., Mustakhimov, I. I., Reshetnikov, A. S., Beschastnyi, A. P., & Trotsenko, Y. A. (2015). Biosynthesis of secondary metabolites in methanotrophs: Biochemical and genetic aspects (review). Applied Biochemistry and Microbiology, 51(2), 150–158. https://doi.org/10.1134/S0003683815020088

Khosravi-Darani, K., Mokhtari, Z. B., Amai, T., & Tanaka, K. (2013). Microbial production of poly(hydroxybutyrate) from C1 carbon sources. In Applied Microbiology and Biotechnology (Vol. 97, Issue 4, pp. 1407–1424). Springer Verlag. https://doi.org/10.1007/s00253-012-4649-0

Kim, H., Graham, D., DiSpirito, AA., Alterman, M., Galeva, N., Asunskis, D., Sherwood, P. and Larive, C. (2004). Methanobactin, a copper-acquisition compound in methane-

oxidizing bacteria. Science 305, 1612–1615.

King, G.M. and Schnel. (1993). Ammonium and Nitrite Inhibition of Methane Oxidation by Methylobacter albus BG8 and Methylosinus trichosporium OB3b at Low Methane Concentrations. Applied and Environmental Microbiology 60 (10), 3508-3513.

Kirschke, S., Bousquet, P., Ciais, P., Saunois, M., Canadell, J. G., Dlugokencky, E. J., Bergamaschi, P., Bergmann, D., Blake, D. R., Bruhwiler, L., Cameron-Smith, P., Castaldi, S., Chevallier, F., Feng, L., Fraser, A., Heimann, M., Hodson, E. L., Houweling, S., Josse, B., … Zeng, G. (2013). Three decades of global methane sources and sinks. In Nature Geoscience (Vol. 6, Issue 10, pp. 813–823). https://doi.org/10.1038/ngeo1955

Kits, K. D., Klotz, M. G., & Stein, L. Y. (2015). Methane oxidation coupled to nitrate reduction under hypoxia by the Gammaproteobacterium Methylomonas denitrificans, sp. nov. type strain FJG1. Environmental Microbiology, 17(9), 3219–3232. https://doi.org/10.1111/1462-2920.12772

Klotz, M. G., & Stein, L. Y. (2008). Nitrifier genomics and evolution of the nitrogen cycle. In FEMS Microbiology Letters (Vol. 278, Issue 2, pp. 146–156). https://doi.org/10.1111/j.1574-6968.2007.00970.x

Knapp, C.W., Fowle, D.A., Kulczycki, E., Roberts, J.A., and Graham, D.W. (2007). Methane monooxygenase gene expression mediated by methanobactin in the presence of mineral copper sources. Proc Natl Acad Sci USA 104, 12040–12045.

Koffas, M, Odom, J.M. and Square, K. (2003) *High growth methanotrophic bacterial strain*. US Patent 6 689 601. Jul. 29.2004.

Kosiur, D.R. and Warford, A.L. (1979). Methane production and oxidation in Santa Barbara Basin sediments. Estuarine Coastal Marine Science 8, 379.

Kung, S. S., Chuang, Y. C., Chen, C. H., & Chien, C. C. (2007). Isolation of polyhydroxyalkanoates-producing bacteria using a combination of phenotypic and genotypic approach. Letters in Applied Microbiology, 44(4), 364–371. https://doi.org/10.1111/j.1472-765X.2006.02090.x

Lan, X., Nisbet, E. G., Dlugokencky, E. J., & Michel, S. E. (2021). What do we know about the global methane budget? Results from four decades of atmospheric CH 4 observations and the way forward. In Philosophical Transactions of the Royal Society A: Mathematical, Physical and Engineering Sciences (Vol. 379, Issue 2210). Royal Society Publishing. https://doi.org/10.1098/rsta.2020.0440

Lazic, M., Gudneppanavar, R., Whiddon, K., Sauvageau, D., Stein, L. Y., & Konopka, M. (2022). In vivo quantification of polyhydroxybutyrate (PHB) in the alphaproteobacterial methanotroph, Methylocystis sp. Rockwell. Applied Microbiology and Biotechnology, 106(2), 811–819. https://doi.org/10.1007/s00253-021-11732-x

Lazic, M., Sugden, S., Sauvageau, D., & Stein, L. Y. (2021). Metabolome profiles of the alphaproteobacterial methanotroph Methylocystis sp. Rockwell in response to carbon and nitrogen source. FEMS Microbiology Letters, 368(2). https://doi.org/10.1093/femsle/fnaa219

Leak, D. J., & Dalton, H. (1986). Growth yields of methanotrophs* I. Effect o f copper on the energetics of methane oxidation. In Appl Microbiol Biotechnol (Vol. 23).

Lee, J., Yasin, M., Park, S., Chang, I. S., Ha, K. S., Lee, E. Y., Lee, J., & Kim, C. (2015). Gas-liquid mass transfer coefficient of methane in bubble column reactor. Korean Journal of Chemical Engineering, 32(6), 1060–1063. https://doi.org/10.1007/s11814-014-0341-7

Lee, O. K., Hur, D. H., Nguyen, D. T. N., & Lee, E. Y. (2016). Metabolic engineering of methanotrophs and its application to production of chemicals and biofuels from methane. In Biofuels, Bioproducts and Biorefining (Vol. 10, Issue 6, pp. 848–863). John Wiley and Sons

Ltd. https://doi.org/10.1002/bbb.1678

Li, M., Karu, E., Brenninkmeijer, C., Fischer, H., Lelieveld, J., & Williams, J. (2018). Tropospheric OH and stratospheric OH and Cl concentrations determined from CH4, CH3Cl, and SF6 measurements. Npj Climate and Atmospheric Science, 1(1). https://doi.org/10.1038/s41612-018-0041-9

Li, M., & Wilkins, M. (2020). Flow cytometry for quantitation of polyhydroxybutyrate production by Cupriavidus necator using alkaline pretreated liquor from corn stover. Bioresource Technology, 295. https://doi.org/10.1016/j.biortech.2019.122254

Li, Q., Du, W., & Liu, D. (2008). Perspectives of microbial oils for biodiesel production. In Applied Microbiology and Biotechnology (Vol. 80, Issue 5, pp. 749–756). https://doi.org/10.1007/s00253-008-1625-9

Lieberman, R. L., Shrestha, D. B., Doan, P. E., Hoffman, B. M., Stemmler, T. L., & Rosenzweig, A. C. (n.d.). Purified particulate methane monooxygenase from Methylococcus capsulatus (Bath) is a dimer with both mononuclear copper and a copper-containing cluster. www.pnas.orgcgidoi10.1073pnas.0536703100

Liew, E.F., Tong, D., Coleman, N.V. and Holmes, A.J. (2014). Mutagenesis of the hydrocarbon monooxygenase indicates a metal centre in subunit-C, and not subunit-B, is essential for copper-containing membrane monooxygenase activity. Microbiology 160, 1267–1277.

Lipscomb, J.D. (1994). Biochemistry of the soluble methane monooxygenase. Annu Rev Microbiol 48, 371–399.

Liu, L. Y., Xie, G. J., Xing, D. F., Liu, B. F., Ding, J., & Ren, N. Q. (2020). Biological conversion of methane to polyhydroxyalkanoates: Current advances, challenges, and

perspectives. In Environmental Science and Ecotechnology (Vol. 2). Elsevier B.V. https://doi.org/10.1016/j.ese.2020.100029

Löbler, M., Saß, M., Schmitz, K.P. and Hopt, U.T. (2003). Biomaterial implants induce the inflammation marker CRP at the site of implantation. J. Biomed. Mater. Res. 61, 165-167.

Mansour, A. A., Saad, G. R., & Hamed, A. H. (n.d.). II. Dielectric investigation of cold crystallization of poly(3-hydroxybutyrate) and poly(3-hydroxybutyrate-co-3-hydroxyvalerate).

Martens, C. S., & Berner, R. A. (n.d.). Interstitial water chemistry of anoxic Lbng Island Sound sediments. 1. Dissolved gases1.

Martinez, V., & Henary, M. (2016). & Photostable Organic Dyes Nile Red andNile Blue:A pplications and Syntheses of Structural Analogues. In Chem. Eur.J (Vol. 22). www.chemeurj.org

Martínez-Tobón, D. I., Waters, B., Elias, A. L., & Sauvageau, D. (2020a). Streamlined production, purification, and fcharacterization of recombinant extracellular polyhydroxybutyrate depolymerases. MicrobiologyOpen, 9(4). https://doi.org/10.1002/mbo3.1001

Martínez-Tobón, D. I., Waters, B., Elias, A. L., & Sauvageau, D. (2020b). Streamlined production, purification, and characterization of recombinant extracellular polyhydroxybutyrate depolymerases. MicrobiologyOpen, 9(4). https://doi.org/10.1002/mbo3.1001

Matsen, J. B., Yang, S., Stein, L. Y., Beck, D., & Kalyuzhnaya, M. G. (2013). Global molecular analyses of methane metabolism in Methanotrophic alphaproteobacterium, methylosinus trichosporium OB3b. Part I: Transcriptomic study. Frontiers in Microbiology, 4(APR). https://doi.org/10.3389/fmicb.2013.00040

Matsumoto, K., & Taguchi, S. (2013). Biosynthetic polyesters consisting of 2-hydroxyalkanoic acids: Current challenges and unresolved questions. In Applied Microbiology and Biotechnology (Vol. 97, Issue 18, pp. 8011–8021). https://doi.org/10.1007/s00253-013-5120-6

McAdam, B., Fournet, M. B., McDonald, P., & Mojicevic, M. (2020). Production of polyhydroxybutyrate (PHB) and factors impacting its chemical and mechanical characteristics. In Polymers (Vol. 12, Issue 12, pp. 1–20). MDPI AG. https://doi.org/10.3390/polym12122908

Mcdonald, I. R., Kenna, E. M., & Murrell, J. C. (1995). Detection of Methanotrophic Bacteria in Environmental Samples with the PCR. In APPLIED AND ENVIRONMENTAL MICROBIOLOGY (Vol. 61, Issue 1). https://journals.asm.org/journal/aem

McGlynn, S. E. (2017). Energy metabolism during anaerobic methane oxidation in ANME archaea. In Microbes and Environments (Vol. 32, Issue 1, pp. 5–13). Japanese Society of Microbial Ecology. https://doi.org/10.1264/jsme2.ME16166

Merrick, J. M., & Doudoroff, M. (1964). Intracellular Enzyme System. In Journal of Bacteriology 88 (1).

Miiller, H.-M., & Seebach, D. (1993). Poly(hydroxya1kanoates) : A Fifth Class of Physiologically Important Organic Biopolymers?" *.

Milucka, J., Ferdelman, T. G., Polerecky, L., Franzke, D., Wegener, G., Schmid, M., Lieberwirth, I., Wagner, M., Widdel, F., & Kuypers, M. M. M. (2012). Zero-valent sulphur is a key intermediate in marine methane oxidation. Nature, 491(7425), 541–546. https://doi.org/10.1038/nature11656

Mitra, R., Xu, T., Chen, G. Q., Xiang, H., & Han, J. (2022). An updated overview on the regulatory circuits of polyhydroxyalkanoates synthesis. In Microbial Biotechnology (Vol. 15,

Issue 5, pp. 1446–1470). John Wiley and Sons Ltd. https://doi.org/10.1111/1751-7915.13915

Mitsui, R., Kusano, Y., Yurimoto, H., Sakai, Y., Kato, N., & Tanaka, M. (2003). Formaldehyde Fixation Contributes to Detoxification for Growth of a Nonmethylotroph, Burkholderia cepacia TM1, on Vanillic Acid. Applied and Environmental Microbiology, 69(10), 6128–6132. https://doi.org/10.1128/AEM.69.10.6128-6132.2003

Miyahara, Y., Yamamoto, M., Thorbecke, R., Mizuno. M. and Tsuge, T. (2020). Autotrophic biosynthesis of polyhydroxyalkanoate by Ralstonia eutropha from non-combustible gas mixture with low hydrogen content. Biotechnology Letters 42, 1655–1662. https://doi.org/10.1007/s10529-020-02876-3

Müller, H., Hellgren, L. I., Olsen, E., & Skrede, A. (2004). Lipids Rich in Phosphatidylethanolamine from Natural Gas-Utilizing Bacteria Reduce Plasma Cholesterol and Classes of Phospholipids: A Comparison with Soybean Oil. In Lipids (Vol. 39, Issue 9).

Mustakhimov, I. I., Reshetnikov, A. S., Glukhov, A. S., Khmelenina, V. N., Kalyuzhnaya, M. G., & Trotsenko, Y. A. (2010). Identification and characterization of EctR1, a new transcriptional regulator of the ectoine biosynthesis genes in the halotolerant methanotroph Methylomicrobium alcaliphilum 20Z. Journal of Bacteriology, 192(2), 410–417. https://doi.org/10.1128/JB.00553-09

Nakagawa, T., Mitsui, R., Tani, A., Sasa, K., Tashiro, S., Iwama, T., Hayakawa, T., & Kawai, K. (2012). A Catalytic Role of XoxF1 as La3+-Dependent Methanol Dehydrogenase in Methylobacterium extorquens Strain AM1. PLoS ONE, 7(11). https://doi.org/10.1371/journal.pone.0050480

Nakajima, T., Hiroo U.-I., Yagi, T. O., Nakahara, T. (1992). Purification and properties of a soluble methane monooxygenase from Methylocystis sp. M. Biosci. Biotechnol. Biochem. 56, 736–740.

Nazaries, L., Murrell, J. C., Millard, P., Baggs, L., & Singh, B. K. (2013). Methane, microbes and models: Fundamental understanding of the soil methane cycle for future predictions. In Environmental Microbiology (Vol. 15, Issue 9, pp. 2395–2417). https://doi.org/10.1111/1462-2920.12149

Nguyen, H., Shiemke, A. K., Jacobs, S. J., Hales, B. J. et al. (1994). The nature of the copper ions in the membranes containing the particulate methane monooxygenase from Methylococcus capsulatus (Bath). J. Biol. Chem. 269, 14995–15005.

Nicole, E., Nozzi, N.E., Oliver, J.W.K., and Atsumi, S. (2013). Cyanobacteria as a platform for biofuel production. Frontiers in Bioengineering and Biotechnology - Synthetic Biology 1. doi: 10.3389/fbioe.2013.00007.

Nomura, C. T., & Taguchi, S. (2007). PHA synthase engineering toward superbiocatalysts for custom-made biopolymers. In Applied Microbiology and Biotechnology (Vol. 73, Issue 5, pp. 969–979). Springer Verlag. https://doi.org/10.1007/s00253-006-0566-4

Nyerges, G., Han, S. K., & Stein, L. Y. (2010). Effects of ammonium and nitrite on growth and competitive fitness of cultivated methanotrophic bacteria. Applied and Environmental Microbiology, 76(16), 5648–5651. https://doi.org/10.1128/AEM.00747-10

Nyerges, G., & Stein, L. Y. (2009). Ammonia cometabolism and product inhibition vary considerably among species of methanotrophic bacteria. FEMS Microbiology Letters, 297(1), 131–136. https://doi.org/10.1111/j.1574-6968.2009.01674.x

Oehmen, A., Keller-Lehmann, B., Zeng, R. J., Yuan, Z., & Keller, J. (2005). Optimisation of poly-β-hydroxyalkanoate analysis using gas chromatography for enhanced biological phosphorus removal systems. Journal of Chromatography A, 1070(1–2), 131–136. https://doi.org/10.1016/j.chroma.2005.02.020

Oksanen O, B. F. (2016). Community Ecology. https://cran.r-project.org, https://github.com/vegandevs/vegan

Olivera, E., Arcos, M., Carrasco, G. and Luengo, J. (2009). Unusual PHA Biosynthesis. Plastics from Bacteria, Springer: Berlin/Heidelberg, Germany 14, 133–186.

Op den Camp, H.J.M., Islam, T., Stott, M.B., Harhangi, H.R., Hynes, A., Schouten, S., Jetten, M.S.M., Birkeland, N.K., Pol, A. and Dunfield, P.F. (2009). Environmental, genomic and taxonomic perspectives on methanotrophic Verrucomicrobia. Environ Microbiol Rep 1, 293–306.

Oshiki, M., Onuki, M., Satoh, H., & Mino, T. (2008). PHA-accumulating microorganisms in full-scale wastewater treatment plants. Water Science and Technology, 58(1), 13–20. https://doi.org/10.2166/wst.2008.652

Ostle, A. G., & Holt, J. G. (1982). Nile Blue A as a Fluorescent Stain for Poly-3-Hydroxybutyrate. In APPLIED AND ENVIRONMENTAL MICROBIOLOGY (Vol. 44, Issue 1).

Pan, H., Feng, J., He, G. X., Cerniglia, C. E., & Chen, H. (2012). Evaluation of impact of exposure of Sudan azo dyes and their metabolites on human intestinal bacteria. Anaerobe, 18(4), 445–453. https://doi.org/10.1016/j.anaerobe.2012.05.002

Panganiban, A.T., Patt, .E., Hart, W. and Hanson, S. (1979). Oxidation of Methane in the Absence of Oxygen in Lake Water Samples. Applied and Environmental Microbiology 37 (2), 303-309.

Patt, T.E., Cole, G.C., Bland, J. and Hanson, R.S. (1974). Isolation and characterization of bacteria that grow on methane and organic compounds as sole sources of carbon and energy. Journal of Bacteriology 120, 955–964.

Pawan, G. L. S., & Semple, S. J. G. (n.d.). EFFECT OF 3-HYDROXYBUTYRATE IN OBESE SUBJECTS ON VERY-LOW-ENERGY DIETS AND DURING THERAPEUTIC STARVATION.

Peel, D., and J. R. Quayle. (1961). Microbial growth on C1 compounds. 1. Isolation and characterization of Pseudomonas AM1. Biochem. J. 81, 465-469

Penkhrue, W., Jendrossek, D., Khanongnuch, C., Pathomareeid, W., Aizawa, T., Behrens, R. L., & Lumyongid, S. (2020). Response surface method for polyhydroxybutyrate (PHB) bioplastic accumulation in Bacillus drentensis BP17 using pineapple peel. PLoS ONE, 15(3). https://doi.org/10.1371/journal.pone.0230443

Diep Ngoc Pham, A. D. (2022.). Outlook on engineering biocatalysts for one-carbon-based industrial. unpublished.

Pieja, A. J., Morse, M. C., & Cal, A. J. (2017). Methane to bioproducts: the future of the bioeconomy? In Current Opinion in Chemical Biology (Vol. 41, pp. 123–131). Elsevier Ltd. https://doi.org/10.1016/j.cbpa.2017.10.024

Pieja, A. J., Rostkowski, K. H., & Criddle, C. S. (2011). Distribution and Selection of Poly-3-Hydroxybutyrate Production Capacity in Methanotrophic Proteobacteria. Microbial Ecology, 62(3), 564–573. https://doi.org/10.1007/s00248-011-9873-0

Pieja, A. J., Sundstrom, E. R., & Criddle, C. S. (2011). Poly-3-hydroxybutyrate metabolism in the type II Methanotroph Methylocystis parvus OBBP. Applied and Environmental Microbiology, 77(17), 6012–6019. https://doi.org/10.1128/AEM.00509-11

Pilkington, S.J. and Dalton, H. (1990). Soluble methane monooxygenase from Methylococcus capsulatus Bath. Method Enzymol 188, 181–190.

Pol, A., Barends, T. R. M., Dietl, A., Khadem, A. F., Eygensteyn, J., Jetten, M. S. M., & Op

den Camp, H. J. M. (2014). Rare earth metals are essential for methanotrophic life in volcanic mudpots. Environmental Microbiology, 16(1), 255–264. https://doi.org/10.1111/1462-2920.12249

Poulton, T.A., Gallagher, A., Pott, C. and Swansonbeckd, J. (1988). Changes in activation markers and cell membrane receptors on human peripheral blood T lymphocytes during cell cycle progression after PHA stimulation. Immunology 64, 419-425.

Potera. (2005). Making succinate more successful. Environ. Health Perspect. https://doi.org/10.1289/ehp.113-a832

Qu, X.H., Wu, Q., Zhang, K.Y., Chen, G. Q. (2006). In vivo studies of poly(3 hydroxybutyrate-co -3-hydroxyhexanoate) based polymer: biodegradation and tissue reactions. Biomaterials. 27, 3540-3548.

Reeburgh, W.S. (1980). Anaerobic methane oxidation: rate depth distributions in Skan Bay by sediments. Earth and Planetary Science Letters, 47, 345-352.

Ritala, A., Häkkinen, S. T., Toivari, M., & Wiebe, M. G. (2017). Single cell protein-state-of-the-art, industrial landscape and patents 2001-2016. In Frontiers in Microbiology (Vol. 8, Issue OCT). Frontiers Media S.A. https://doi.org/10.3389/fmicb.2017.02009

Ritchie, H., & Roser, M. (n.d.). Plastic Pollution-Our World in Data https://ourworldindata.org/plastic-pollution. https://ourworldindata.org/plastic-pollution

Ro, S. Y.; Schachner, L. F.; Koo, C. W.; Purohit, R.; Remis, J. P.; Kenney, G. E.; Liauw, B. W.; Thomas, P. M.; Patrie, S. M.; Kelleher, N. L.; Rosenzweig, A. C. (2019). Native top-down mass spectrometry provides insights into the copper centers of membrane-bound methane monooxygenase. Nat. Commun. , 10, 2675.

Rosenzweig, A.C., Frederick, C.A., Lippard, S.J. and Nordlund, P. (1993). Crystal structure of a bacterial non-haem iron hydroxylase that catalyses the biological oxidation of methane. Nature 366, 537–543.

Ross, M. O., MacMillan, F., Wang, J., Nisthal,, A., Lawton, T. J., Olafson, B. D., Mayo, S. L., Rosenzweig, A. C. and Hoffman, B. M. (2019). Particulate methane monooxygenase contains only monocopper centers. Science 364, 566-570.

Rostkowski, K. H., Pfluger, A. R., & Criddle, C. S. (2013). Stoichiometry and kinetics of the PHB-producing Type II methanotrophs Methylosinus trichosporium OB3b and Methylocystis parvus OBBP. Bioresource Technology, 132, 71–77. https://doi.org/10.1016/j.biortech.2012.12.129

Sanderson, M. (2007). Climate change, methane and ozone. https://www.envchemgroup.com/climate-change-methane-and-ozone.html

Saunois, M., R. Stavert, A., Poulter, B., Bousquet, P., G. Canadell, J., B. Jackson, R., A. Raymond, P., J. Dlugokencky, E., Houweling, S., K. Patra, P., Ciais, P., K. Arora, V., Bastviken, D., Bergamaschi, P., R. Blake, D., Brailsford, G., Bruhwiler, L., M. Carlson, K., Carrol, M., … Zhuang, Q. (2020). The global methane budget 2000-2017. Earth System Science Data, 12(3), 1561–1623. https://doi.org/10.5194/essd-12-1561-2020

Schnell, S., & King, G. M. (1996). Responses of Methanotrophic Activity in Soils and Cultures to Water Stress †. In APPLIED AND ENVIRONMENTAL MICROBIOLOGY (Vol. 62, Issue 9).

Schwibbert, K., Marin-Sanguino, A., Bagyan, I., Heidrich, G., Lentzen, G., Seitz, H., Rampp, M., Schuster, S. C., Klenk, H. P., Pfeiffer, F., Oesterhelt, D., & Kunte, H. J. (2011). A blueprint of ectoine metabolism from the genome of the industrial producer Halomonas elongata DSM 2581 T. Environmental Microbiology, 13(8), 1973–1994. https://doi.org/10.1111/j.1462-2920.2010.02336.x

Semrau, J. D., Dispirito, A. A., & Yoon, S. (2010). Methanotrophs and copper. In FEMS Microbiology Reviews (Vol. 34, Issue 4, pp. 496–531). Blackwell Publishing Ltd. https://doi.org/10.1111/j.1574-6976.2010.00212.x

Semrau, J.D., DiSpirito, A.S. and Vuilleumier, S. (2011). Facultative methanotrophy: false leads, true results, and suggestions for future research. FEMS Microbiology Letters 323, 1–12.

Semrau, J. D., Jagadevan, S., Dispirito, A. A., Khalifa, A., Scanlan, J., Bergman, B. H., Freemeier, B. C., Baral, B. S., Bandow, N. L., Vorobev, A., Haft, D. H., Vuilleumier, S., & Murrell, C. J. (2013). Methanobactin and MmoD work in concert to act as the "copper-switch" in methanotrophs. Environmental Microbiology, 15(11), 3077–3086. https://doi.org/10.1111/1462-2920.12150

Shah, N. N., Leslie Hanna,', M., & Taylo+" ', R. T. (n.d.). Batch Cultivation of Methylosinus trichosporium OB3 b : V. C h a racte r iza t i o n of Poly-P-Hydroxybutyrate Production Under Methane-Dependent Growth Conditions.

Shosuke Yoshida, K. H. (2016). A bacterium that degrades and assimilates poly(ethylene terephthalate). Science (351) 6278, 1196-1199.

Sharma, H., Sauvageau, D., & Stein, L. (2022.).unpublished.

Sirajuddin S et al. (2014). Effects of zinc on particulate methane monooxygenase activity and structure J. Biol. Chem 289, 21782–21794.

Sirohi, R., Prakash Pandey, J., Kumar Gaur, V., Gnansounou, E., & Sindhu, R. (2020). Critical overview of biomass feedstocks as sustainable substrates for the production of polyhydroxybutyrate (PHB). In Bioresource Technology (Vol. 311). Elsevier Ltd. https://doi.org/10.1016/j.biortech.2020.123536

Stein, L.Y., Yoon, S., Semrau, J.D., DiSpirito, A.A., Crombie, A., Murrell, J.C., et al. (2010) Genome sequence of the obligate methanotroph Methylosinus trichosporium strain OB3b. J Bacteriol 192, 6497–6498.

Stein, L. Y., Bringel, F., DiSpirito, A. A., Han, S., Jetten, M. S. M., Kalyuzhnaya, M. G., Kits, K. D., Klotz, M. G., Op den Camp, H. J. M., Semrau, J. D., Vuilleumier, S., Bruce, D. C., Cheng, J. F., Davenport, K. W., Goodwin, L., Han, S., Hauser, L., Lajus, A., Land, M. L., … Woyke, T. (2011). Genome sequence of the methanotrophic alphaproteobacterium Methylocystis sp. Strain Rockwell (ATCC 49242). In Journal of Bacteriology (Vol. 193, Issue 10, pp. 2668–2669). https://doi.org/10.1128/JB.00278-11

Stein, L. Y. (2019). Methane Oxidation. In Encyclopedia of Astrobiology (pp. 1–4). Springer Berlin Heidelberg. https://doi.org/10.1007/978-3-642-27833-4_5405-1Stein, L. (2018). Proteobacterial Methanotrophs, Methylotrophs, and Nitrogen. In M. Xin-Hui XinG, Methane Biocatalysis: Paving the Way to Sustainability (pp. 57-67).

Strong, P. J., Kalyuzhnaya, M., Silverman, J., & Clarke, W. P. (2016). A methanotroph-based biorefinery: Potential scenarios for generating multiple products from a single fermentation. In Bioresource Technology (Vol. 215, pp. 314–323). Elsevier Ltd. https://doi.org/10.1016/j.biortech.2016.04.099

Strong, P. J., Xie, S., & Clarke, W. P. (2015). Methane as a resource: Can the methanotrophs add value? In Environmental Science and Technology (Vol. 49, Issue 7, pp. 4001–4018). American Chemical Society. https://doi.org/10.1021/es504242n

Sudesh, K., & Abe, H. (Hideki). (2010). Practical guide to microbial polyhydroxyalkanoates. ISmithers.

Sugden, S., Lazic, M., Sauvageau, D., & Stein, L. Y. (2021). Transcriptomic and

Metabolomic Responses to Carbon and Nitrogen Sources in Methylomicrobium album BG8. Applied and Environmental Microbiology, 87(13). https://doi.org/10.1128/AEM.00385-21

Suk Ahn, W., Jae Park, S., & Yup Lee, S. (2000). Production of Poly(3-Hydroxybutyrate) by Fed-Batch Culture of Recombinant Escherichia coli with a Highly Concentrated Whey Solution Fermentation strategies for the production of poly(3-hydroxybutyrate) (PHB) from whey by recombinant. In APPLIED AND ENVIRONMENTAL MICROBIOLOGY (Vol. 66, Issue 8).

Sundstrom, E. R., & Criddle, C. S. (2015). Optimization of methanotrophic growth and production of poly(3-hydroxybutyrate) in a high-throughput microbioreactor system. Applied and Environmental Microbiology, 81(14), 4767–4773. https://doi.org/10.1128/AEM.00025-15

Sznajder, A., & Jendrossek, D. (2011). Biochemical characterization of a new type of intracellular PHB depolymerase from Rhodospirillum rubrum with high hydrolytic activity on native PHB granules. Applied Microbiology and Biotechnology, 89(5), 1487–1495. https://doi.org/10.1007/s00253-011-3096-7

Tays, C. (2019). Growth Characterization and Transcriptomics of Methanotrophic Bacteria as Effected by Carbon and Nitrogen Sources. Doctoral dissertation, University of Alberta.

Tays, C., Guarnieri, M. T., Sauvageau, D., & Stein, L. Y. (2018). Combined effects of carbon and nitrogen source to optimize growth of proteobacterial methanotrophs. Frontiers in Microbiology, 9(SEP). https://doi.org/10.3389/fmicb.2018.02239

Tian, J., He, A., Lawrence, A. G., Liu, P., Watson, N., Sinskey, A. J., & Stubbe, J. A. (2005). Analysis of transient polyhydroxybutyrate production in Wautersia eutropha H16 by quantitative Western analysis and transmission electron microscopy. Journal of Bacteriology, 187(11), 3825–3832. https://doi.org/10.1128/JB.187.11.3825-3832.2005

Tokiwa, Y., & Calabia, B. P. (2006). Biodegradability and biodegradation of poly(lactide). In Applied Microbiology and Biotechnology (Vol. 72, Issue 2, pp. 244–251). https://doi.org/10.1007/s00253-006-0488-1

Topp, E., Pattey, E., Topp, E., & Pattey, E. (n.d.). Soils as sources and sinks for atmospheric methane.

Toukdariant, A. E., & Lidstromt, M. E. (1984). Molecular Construction and Characterization of nif Mutants of the Obligate Methanotroph Methylosinus sp. Strain 6. In JOURNAL OF BACTERIOLOGY (Vol. 157, Issue 3). https://journals.asm.org/journal/jb

Trakunjae, C., Boondaeng, A., Apiwatanapiwat, W., Kosugi, A., Arai, T., Sudesh, K., & Vaithanomsat, P. (2021). Enhanced polyhydroxybutyrate (PHB) production by newly isolatedrare actinomycetes Rhodococcus sp. strain BSRT1-1 using response surface methodology.
Scientific Reports, 11(1). https://doi.org/10.1038/s41598-021-81386-2

Trotsenko, Y. A., & Murrell, J. C. (2008). Metabolic Aspects of Aerobic Obligate Methanotrophy{star, open}. In Advances in Applied Microbiology (Vol. 63, pp. 183–229). https://doi.org/10.1016/S0065-2164(07)00005-6

Tsien, H.-C., & Hanson, R. S. (1992). Soluble Methane Monooxygenase Component B Gene Probe for Identification of Methanotrophs That Rapidly Degrade Trichloroethylene. In APPLIED AND ENVIRONMENTAL MICROBIOLOGY. https://journals.asm.org/journal/aem

Uchino, K., Saito, T., Gebauer, B., & Jendrossek, D. (2007). Isolated poly(3-hydroxybutyrate) (PHB) granules are complex bacterial organelles catalyzing formation of PHB from acetyl coenzyme A (CoA) and degradation of PHB to acetyl-CoA. Journal of Bacteriology, 189(22), 8250–8256. https://doi.org/10.1128/JB.00752-07

Unverdorben, M., Spielberger, A., Schywalsky, M. et al. (2002). A polyhydroxybutyrate biodegradable stent: preliminary experience in the rabbit. Cardiovasc. Intervent. Radiol. 25, 127-132.

Valappil, S.P., Misra, S.K., , Boccaccini, A.R. and Roy, I. (2006). Biomedical applications of polyhydroxyalkanoates, an overview of animal testing and in vivo responses, Expert Review of Medical Devices 6, 853-868, DOI: 10.1586/17434440.3.6.853.

Van Dien, S.J., Marx, C.J., O'Brien, B.N., Lidstrom, M.E. (2003). Genetic characterization of the carotenoid biosynthetic pathway in Methylobacterium extorquens AM1 and isolation of a colorless mutant. Appl Environ Microbiol. 69(12), 7563-6. doi: 10.1128/AEM.69.12.7563-7566.2003. PMID: 14660416; PMCID: PMC310018.

Verma, R., Vinoda, K. S., Papireddy, M., & Gowda, A. N. S. (2016). Toxic Pollutants from Plastic Waste- A Review. Procedia Environmental Sciences, 35, 701–708. https://doi.org/10.1016/j.proenv.2016.07.069

Volova, T. G., Gladyshev, M. I., Trusova, M. Y., & Zhila, N. O. (2006). Degradation of polyhydroxyalkanoates and the composition of microbial destructors under natural conditions. Microbiology, 75(5), 593–598. https://doi.org/10.1134/S0026261706050092

Vorobev, A., Jagadevan, S., Jain, S., Anantharaman, K., Dick, G. J., Vuilleumier, S., & Semraua, J. D. (2014). Genomic and transcriptomic analyses of the facultative methanotroph methylocystis sp. strain SB2 grown on methane or ethanol. Applied and Environmental Microbiology, 80(10), 3044–3052. https://doi.org/10.1128/AEM.00218-14

Wallar, B.J. and Lipscomb, J.D. (1996). Dioxygen activation by enzymes containing binuclear non-heme iron clusters. Chem Rev 96, 2625–2657.

Wallar, B.J. and Lipscomb, J.D. (2001). Methane monooxygenase component B mutants alter the kinetics of steps throughout the catalytic cycle. Biochemistry 40, 2220–2233.

Wang, B., Sharma-Shivappa, R. R., Olson, J. W., & Khan, S. A. (2012). Upstream process optimization of polyhydroxybutyrate (PHB) by Alcaligenes latus using two-stage batch and fed-batch fermentation strategies. Bioprocess and Biosystems Engineering, 35(9), 1591–1602. https://doi.org/10.1007/s00449-012-0749-6

Wendlandt, K. D., Stottmeister, U., Helm, J., Soltmann, B. et al. (2010). The potential of methane-oxidizing bacteria for applications in environmental biotechnology. Eng. Life Sci., 10, 87–102.

Whittenbury, R., & Wilkinson, J. F. (1970). Enrichment, Isolation and Some Properties of Me thane-utilizing Bacteria. In Journal of General Microbiology (Vol. 61).

Widyastuti, G. (n.d.). Genetic Engineered Ideonella sakaiensis Bacteria: A Solution of the Legendary Plastic Waste Problem.

Williams, S.F. and Martin, D.P. (2005). Applications of PHAs in medicine and pharmacy In: Biopolymers for Medical and Pharmaceutical Applications (1). Steinbuchel A, Marchessault RH (Eds). Wiley-VCH, Weinheim, Germany, 89-125.

World leaders set sights on plastic pollution. (https://www.unep.org/news-and-stories/story/world-leaders-set-sights-plastic-pollution)

Woodland, M.P. and Dalton, H. (1984). Purification and characterization of component A of the methane monooxygenase from Methylococcus capsulatus (Bath). J Biol Chem 259, 53–60.

Yang, S., Matsen, J. B., Konopka, M., Green-Saxena, A., Clubb, J., Sadilek, M., Orphan, V. J., Beck, D., & Kalyuzhnaya, M. G. (2013). Global molecular analyses of methane metabolism in methanotrophic alphaproteobacterium, methylosinus trichosporium OB3b.

Part II. metabolomics and 13C-labeling study. Frontiers in Microbiology, 4(APR). https://doi.org/10.3389/fmicb.2013.00070

Yang, H., Yu, S. and Lu, H. (2021). Iron-Coupled Anaerobic Oxidation of Methane in Marine Sediments: A Review. Journal of Marine Science and Engineering 9, 875. https://doi.org/10.3390/jmse9080875.

Yasueda, H., Kawahara, Y., & Sugimoto, S. (1999). Bacillus subtilis yckG and yckF Encode Two Key Enzymes of the Ribulose Monophosphate Pathway Used by Methylotrophs, and yckH Is Required for Their Expression. In JOURNAL OF BACTERIOLOGY (Vol. 181, Issue 23).

Ye, R. W., Yao, H., Stead, K., Wang, T., Tao, L., Cheng, Q., Sharpe, P. L., Suh, W., Nagel, E., Arcilla, D., Dragotta, D., & Miller, E. S. (2007). Construction of the astaxanthin biosynthetic pathway in a methanotrophic bacterium Methylomonas sp. strain 16a. Journal of Industrial Microbiology and Biotechnology, 34(4), 289–299. https://doi.org/10.1007/s10295-006-0197-x

Yu, S. S.-F., Chen, K. H.-C., Tseng, M. Y.-H.,Wang, Y.-S. et al. (2003). Production of high-quality particulate methane monooxygenase in high yields from Methylococcus capsulatus (Bath) with a hollow-fiber membrane bioreactor. J. Bacteriol. 185, 5915–5924.

Zahn, J. A., Bergmann, D. J., Boyd, J. M., Kunz, R. C., & DiSpirito, A. A. (2001). Membrane-associated quinoprotein formaldehyde dehydrogenase from Methylococcus capsulatus Bath. Journal of Bacteriology, 183(23), 6832–6840. https://doi.org/10.1128/JB.183.23.6832-6840.2001

Zaldívar Carrillo, J. A., Stein, L. Y., & Sauvageau, D. (2018). Defining Nutrient Combinations for Optimal Growth and Polyhydroxybutyrate Production by Methylosinus trichosporium OB3b Using Response Surface Methodology. Frontiers in Microbiology, 9.

https://doi.org/10.3389/fmicb.2018.01513

Zehnder, A. J. B., & Brock, T. D. (1979). Methane Formation and Methane Oxidation by Methanogenic Bacteria. In JouRNAL OF BACTERIOLOGY. https://journals.asm.org/journal/jb

Zhang, T., Zhou, J., Wang, X., & Zhang, Y. (2017). Coupled effects of methane monooxygenase and nitrogen source on growth and poly-β-hydroxybutyrate (PHB) production of Methylosinus trichosporium OB3b. Journal of Environmental Sciences (China), 52, 49–57. https://doi.org/10.1016/j.jes.2016.03.001

Zhang, Y., Xin, J., Chen, L., Song, H., & Xia, C. (2008). Biosynthesis of poly-3-hydroxybutyrate with a high molecular weight by methanotroph from methane and methanol. Journal of Natural Gas Chemistry, 17(1), 103–109. https://doi.org/10.1016/S1003-9953(08)60034-1

Zhao, J., Fujita, K., & Sakai, K. (2007). Reactive oxygen species, nitric oxide, and their interactions play different roles in Cupressus lusitanica cell death and phytoalexin biosynthesis. New Phytologist, 175(2), 215–229. https://doi.org/10.1111/j.1469-8137.2007.02109.x

Zúñiga, C., Morales, M., le Borgne, S., & Revah, S. (2011). Production of poly-β-hydroxybutyrate (PHB) by Methylobacterium organophilum isolated from a methanotrophic consortium in a two-phase partition bioreactor. Journal of Hazardous Materials, 190(1–3), 876–882. https://doi.org/10.1016/j.jhazmat.2011.04.011

# Appendices

Appendix 1 (supplementary data for chapter 3, excel sheet)

Appendix 2 (Sugden et al., 2021)

Appendix 3 (supplementary data for chapter 6, the list of primers used in sfGFP-SBD design and cloning)

## APPENDIX 1

| | Scaled Sample Means | | | | | | | | Tukey's Honestly Significant Different post hoc test - p values | | | | | |
|---|---|---|---|---|---|---|---|---|---|---|---|---|---|---|
| | | | | | | | | | $CH_4$ | $CH_3OH$ | AMS | NMS | $CH_3OH$:NMS | $CH_3OH$:AMS |
| BIOCHEMICAL | $CH_4$+AMS | $CH_3OH$+AMS | $CH_4$+NMS | $CH_3OH$+NMS | F | num_df | p | q | AMS-NMS | AMS-NMS | $CH_4$-$CH_3OH$ | $CH_4$-$CH_3OH$ | $CH_4$:AMS | $CH_4$:NMS |
| (N(1) + N(8))-acetylspermidine | 0.952 | 0.735 | 1.098 | 3.61 | 63.77270062 | 3 | 3.24E-05 | 0 | 0.8002 | 0 | 0.5538 | 0 | 0 | 0.1637 |
| agmatine | 1.142 | 0.085 | 0.085 | 0.092 | | 3 | | | 0 | 0.9976 | 0 | 0.9976 | 0 | 1 |
| putrescine | 9.768 | 1.13 | 0.298 | 0.91 | 3958.754702 | 3 | 2.93E-10 | 0 | 0 | 0.0561 | 0 | 0 | 0 | 0 |
| spermidine | 0.592 | 0.556 | 0.46 | 2.461 | | 3 | | | 0.9911 | 0.006 | 0.9998 | 0.0042 | 0.0069 | 0.9965 |
| 3-(4-hydroxyphenyl)lactate (HPLA) | 0.791 | 1.01 | 0.791 | 0.791 | | 3 | | | 1 | 0.0517 | 0.0517 | 1 | 1 | 0.0517 |
| 3-dehydroshikimate | 2.218 | 0.607 | 1.006 | 0.708 | | 3 | | | 0 | 0.8795 | 0 | 0.1849 | 0 | 0.0548 |
| 3-formylindole | 0.949 | 0.398 | 1.048 | 2.073 | 401.7907491 | 3 | 1.63E-06 | 0 | 0.2926 | 0 | 0 | 0 | 0 | 0 |
| 4-hydroxyphenylpyruvate | 0.485 | 3.036 | 1.123 | 0.907 | 12.97655339 | 3 | 0.004598 | 0.006 | 0.3037 | 0.0003 | 0 | 0.9233 | 0.6287 | 0.0007 |
| anthranilate | 1.38 | 0.181 | 1.001 | 0.726 | 184.2362314 | 3 | 8.46E-06 | 0 | 0.6502 | 0.3674 | 0.0132 | 0.8274 | 0.2292 | 0.1016 |
| kynurenate | 0.519 | 1.089 | 1.065 | 0.919 | | 3 | | | 0.0172 | 0.6908 | 0.0132 | 0.7755 | 0.0902 | 0.9987 |
| kynurenine | 0.845 | 0.903 | 1.23 | 1.332 | 10.78292829 | 3 | 0.007158 | 0.009 | 0.0068 | 0.0031 | 0.9257 | 0.7065 | 0.0011 | 0.0199 |
| N-acetylphenylalanine | 1.149 | 0.501 | 3.169 | 0.856 | 53.02575266 | 3 | 9.91E-05 | 0 | 0 | 0.1677 | 0.0072 | 0 | 0.3015 | 0 |
| N-acetyltyrosine | 0.474 | 2.347 | 0.932 | 0.474 | | 3 | | | 0.0006 | 0 | 0 | 0.0006 | 1 | 0 |
| N-formylanthranilic acid | 1.485 | 0.228 | 1.118 | 0.968 | 245.5924243 | 3 | 8.35E-07 | 0 | 0.0018 | 0 | 0 | 0.2382 | 0.0001 | 0 |
| N-formylphenylalanine | 0.757 | 2.524 | 1.036 | 0.689 | 22.96397453 | 3 | 0.00212 | 0.003 | 0.6086 | 0 | 0 | 0.4389 | 0.99 | 0.0001 |
| o-Tyrosine | 0.334 | 1.594 | 1.087 | 0.836 | 191.984024 | 3 | 8.68E-06 | 0 | 0 | 0 | 0 | 0.0675 | 0.0006 | 0.0005 |
| p-cresol sulfate | 0.765 | 0.454 | 0.6 | 0.454 | | 3 | | | 0.7606 | 1 | 0.2943 | 0.8173 | 0.2943 | 0.8173 |
| phenethylamine | 0.941 | 0.373 | 1.419 | 1.066 | 58.27239857 | 3 | 4.22E-05 | 0 | 0.0002 | 0 | 0 | 0.0029 | 0.3963 | 0 |
| phenylalanine | 1.041 | 0.782 | 1.089 | 1.016 | 6.337781401 | 3 | 0.023721 | 0.027 | 0.8824 | 0.0173 | 0.0091 | 0.6959 | 0.9821 | 0.0026 |
| phenyllactate (PLA) | 0.789 | 0.459 | 1.196 | 0.848 | 24.20600898 | 3 | 0.001753 | 0.002 | 0.0605 | 0.0746 | 0.1477 | 0.1213 | 0.9749 | 0.0011 |
| phenylpyruvate | 0.399 | 1.468 | 0.756 | 1.255 | 4.694375946 | 3 | 0.045785 | 0.05 | 0.7236 | 0.9206 | 0.0364 | 0.4832 | 0.1064 | 0.2079 |
| prephenic acid | 0.376 | 0.332 | 1.924 | 0.332 | | 3 | | | 0 | 1 | 0.9563 | 0 | 0.9563 | 0 |
| tryptamine | 0.628 | 0.395 | 1.388 | 1.443 | 137.9696025 | 3 | 3.76E-06 | 0 | 0 | 0 | 0.012 | 0.8102 | 0 | 0 |
| tryptophan | 0.632 | 0.802 | 1.211 | 1.145 | 26.69870341 | 3 | 0.000553 | 0.001 | 0.0001 | 0.0052 | 0.2069 | 0.8422 | 0.0002 | 0.0013 |
| tyrosine | 0.403 | 2.804 | 1.097 | 0.864 | 175.4138502 | 3 | 2.65E-06 | 0 | 0.0055 | 0 | 0 | 0.5106 | 0.0647 | 0 |
| 2-methylcitrate/homocitrate | 0.764 | 1.209 | 0.885 | 0.939 | 1.805652223 | 3 | 0.238657 | 0.25 | 0.9063 | 0.4666 | 0.116 | 0.9902 | 0.769 | 0.3198 |
| 5-methylthioadenosine (MTA) | 0.538 | 0.753 | 1.295 | 1.221 | 242.6619682 | 3 | 1.69E-06 | 0 | 0 | 0 | 0.0035 | 0.4407 | 0 | 0 |
| alanine | 1.447 | 1.06 | 0.93 | 0.822 | 38.61645164 | 3 | 0.000146 | 0 | 0 | 0.0145 | 0.0003 | 0.3794 | 0 | 0.2389 |
| asparagine | 0.988 | 1.356 | 0.92 | 0.97 | 9.251696253 | 3 | 0.010944 | 0.013 | 0.6794 | 0.0002 | 0.0003 | 0.8355 | 0.991 | 0.0001 |
| aspartate | 1.54 | 0.179 | 1.119 | 0.862 | 679.281655 | 3 | 3.85E-08 | 0 | 0 | 0 | 0 | 0.0001 | 0 | 0 |
| diaminopimelate | 2.897 | 0.495 | 1.645 | 0.295 | 193.0979227 | 3 | 3.5E-06 | 0 | 0 | 0.2998 | 0 | 0 | 0 | 0 |
| lysine | 0.923 | 1.155 | 0.807 | 2.763 | 342.0880344 | 3 | 2.52E-07 | 0 | 0.2497 | 0 | 0.0092 | 0 | 0 | 0.0004 |
| methionine | 0.944 | 1.122 | 0.925 | 1.542 | 21.26561035 | 3 | 0.001148 | 0.002 | 0.995 | 0.0012 | 0.183 | 0 | 0 | 0.1256 |
| methionine sulfoxide | 0.972 | 0.916 | 0.909 | 1.455 | 17.6766036 | 3 | 0.001485 | 0.002 | 0.89 | 0.0003 | 0.9168 | 0.0002 | 0.0007 | 0.9999 |
| N2-acetyl,N6-methyllysine | 1.033 | 0.772 | 0.683 | 1.03 | 72.86275267 | 3 | 3.88E-05 | 0 | 0.0144 | 0.0787 | 0.0737 | 0.0154 | 1 | 0.7849 |
| N2-acetyllysine | 0.44 | 1.646 | 0.335 | 4.24 | 273.519943 | 3 | 6.28E-07 | 0 | 0.7996 | 0 | 0 | 0 | 0 | 0 |
| N6,N6,N6-trimethyllysine | 0.833 | 0.473 | 1.217 | 4.821 | 295.2179422 | 3 | 4.12E-07 | 0 | 0.0146 | 0 | 0.0215 | 0 | 0 | 0.0001 |
| N6,N6-dimethyllysine | 1.264 | 0.282 | 0.946 | 1.041 | 509.8673342 | 3 | 4.77E-08 | 0 | 0 | 0 | 0 | 0.1034 | 0.0003 | 0 |
| N6-acetyllysine | 0.717 | 1.733 | 0.717 | 0.767 | | 3 | | | 1 | 0.0006 | 0.0004 | 0.9914 | 0.9914 | 0.0004 |
| N6-formyllysine | 0.722 | 2.834 | 0.886 | 1.082 | 28.15409456 | 3 | 0.000459 | 0.001 | 0.8036 | 0 | 0 | 0.7062 | 0.2463 | 0 |
| N6-methyllysine | 1.2 | 0.145 | 1.089 | 0.914 | 533.5337957 | 3 | 1.54E-07 | 0 | 0.0731 | 0 | 0 | 0.0045 | 0.0001 | 0 |
| N-acetylalanine | 0.581 | 0.507 | 2.139 | 0.948 | | 3 | | | 0 | 0.0032 | 0.8662 | 0 | 0.0119 | 0 |
| N-acetylasparagine | 0.308 | 1.54 | 0.419 | 0.308 | | 3 | | | 0.4562 | 0 | 0 | 0.4562 | 1 | 0 |
| N-acetylaspartate (NAA) | 1.115 | 1.137 | 0.689 | 0.942 | 13.87301929 | 3 | 0.003524 | 0.005 | 0.0016 | 0.1602 | 0.9943 | 0.0526 | 0.2341 | 0.0011 |
| N-acetylmethionine | 0.59 | 1.359 | 0.823 | 0.872 | 3.077824897 | 3 | 0.106309 | 0.114 | 0.8234 | 0.3186 | 0.0617 | 0.9978 | 0.7283 | 0.2472 |
| N-acetylthreonine | 0.917 | 1.409 | 0.715 | 1.078 | 13.80546093 | 3 | 0.003367 | 0.004 | 0.6923 | 0.3124 | 0.0795 | 0.2457 | 0.815 | 0.0116 |
| N-formylmethionine | 0.538 | 1.781 | 1.197 | 0.887 | 16.91903261 | 3 | 0.001989 | 0.003 | 0.0071 | 0.0006 | 0 | 0.2684 | 0.1885 | 0.016 |
| pipecolate | 0.508 | 0.444 | 1.25 | 9.89 | 147.9861525 | 3 | 4.57E-06 | 0 | 0.1493 | 0 | 0.997 | 0 | 0 | 0.1081 |
| S-adenosylhomocysteine (SAH) | 2.334 | 1.13 | 0.967 | 0.91 | 21.65793251 | 3 | 0.001169 | 0.002 | 0 | 0.4724 | 0 | 0.9794 | 0 | 0.6944 |
| S-adenosylmethionine (SAM) | 0.666 | 0.693 | 1.286 | 1.938 | 51.82413294 | 3 | 0.000314 | 0.001 | 0.0004 | 0 | 0.994 | 0.0003 | 0 | 0.0006 |
| threonine | 0.973 | 0.671 | 1.121 | 1.153 | 21.98915175 | 3 | 0.00137 | 0.002 | 0.0654 | 0 | 0.0004 | 0.9258 | 0.0225 | 0 |
| isoleucine | 0.808 | 1.175 | 1.814 | 0.953 | 49.83684979 | 3 | 9.19E-05 | 0 | 0 | 0.0651 | 0.0027 | 0 | 0.3052 | 0 |
| 2,3-dihydroxyisovalerate | 0.829 | 1.103 | 1.862 | 0.932 | 89.47426212 | 3 | 1.86E-05 | 0 | 0 | 0.326 | 0.0603 | 0 | 0.7113 | 0 |
| 2-isopropylmalate | 0.768 | 7.256 | 0.69 | 1.61 | 29.87335209 | 3 | 0.000478 | 0.001 | 0.9988 | 0 | 0 | 0.3462 | 0.4181 | 0 |
| 3-methyl-2-oxobutyrate | 0.576 | 0.655 | 1.622 | 1.19 | 45.78683562 | 3 | 0.000202 | 0 | 0 | 0.0021 | 0.8905 | 0.01 | 0.0006 | 0 |
| 3-methyl-2-oxovalerate | 0.421 | 1.697 | 0.837 | 1.126 | 5.660689811 | 3 | 0.030501 | 0.034 | 0.5052 | 0.2542 | 0.0042 | 0.7565 | 0.1252 | 0.0511 |
| 4-methyl-2-oxopentanoate | 0.556 | 1.462 | 0.926 | 1.211 | 2.725323611 | 3 | 0.129758 | 0.138 | 0.6359 | 0.8448 | 0.052 | 0.7931 | 0.1994 | 0.3458 |
| alpha-hydroxyisovalerate | 0.541 | 0.446 | 0.645 | 1.188 | | 3 | | | 0.8163 | 0.0002 | 0.8502 | 0.003 | 0.0007 | 0.3728 |
| beta-hydroxyisovalerate | 0.943 | 0.66 | 0.85 | 3.616 | | 3 | | | 0.8129 | 0 | 0.0801 | 0 | 0 | 0.3162 |
| isovalerylcarnitine (C5) | 0.929 | 1.045 | 1.126 | 0.98 | 0.94042466 | 3 | 0.478004 | 0.494 | 0.696 | 0.9826 | 0.914 | 0.8457 | 0.9916 | 0.968 |
| leucine | 0.73 | 0.941 | 1.042 | 1.45 | 44.82405295 | 3 | 0.000112 | 0 | 0.0052 | 0.0001 | 0.0587 | 0.0006 | 0 | 0.5295 |
| methylmalonate (MMA) | 1.453 | 0.686 | 1.165 | 0.929 | 5.860539465 | 3 | 0.032328 | 0.036 | 0.3001 | 0.4361 | 0.0017 | 0.4587 | 0.0252 | 0.0417 |
| methylsuccinate | 3.022 | 1.14 | 0.388 | 0.986 | 767.8979774 | 3 | 4.26E-08 | 0 | 0 | 0.2634 | 0 | 0 | 0 | 0 |
| N-acetylisoleucine | 0.306 | 0.868 | 2.397 | 0.987 | 56.64247349 | 3 | 5.26E-05 | 0 | 0 | 0.859 | 0.0134 | 0 | 0.0034 | 0 |
| N-acetylleucine | 0.291 | 0.707 | 2.616 | 1.044 | 95.31636359 | 3 | 1.18E-05 | 0 | 0 | 0.0578 | 0.0178 | 0 | 0.0002 | 0 |
| N-acetylvaline | 0.532 | 0.555 | 1.784 | 0.956 | | 3 | | | 0 | 0.0003 | 0.9864 | 0 | 0.0002 | 0 |
| valine | 0.572 | 0.805 | 1.813 | 1.087 | 78.59395936 | 3 | 6.32E-05 | 0 | 0 | 0.0293 | 0.0786 | 0 | 0.0003 | 0 |
| 2-oxoarginine* | 0.925 | 0.158 | 1.151 | 1.58 | 322.8643249 | 3 | 4.04E-07 | 0 | 0.0123 | 0 | 0 | 0.0001 | 0 | 0 |
| 4-guanidinobutanoate | 0.83 | 0.248 | 1.387 | 2.154 | 175.6037075 | 3 | 3.05E-06 | 0 | 0.0004 | 0 | 0.0002 | 0 | 0 | 0 |
| 4-hydroxy-2-oxoglutaric acid | 1.033 | 0.226 | 1.239 | 0.97 | 277.4880384 | 3 | 2.45E-07 | 0 | 0.0007 | 0 | 0 | 0.0001 | 0.3782 | 0 |
| 4-imidazoleacetate | 0.97 | 0.688 | 1.021 | 3.007 | 70.81696269 | 3 | 5.84E-05 | 0 | 0.9758 | 0 | 0.1588 | 0 | 0 | 0.0814 |
| argininate* | 1.183 | 0.329 | 0.999 | 0.351 | | 3 | | | 0.0288 | 0.9783 | 0 | 0 | 0 | 0 |
| arginine | 0.46 | 1.37 | 0.685 | 1.53 | 216.2001122 | 3 | 5.06E-06 | 0 | 0.0058 | 0.0481 | 0 | 0 | 0 | 0 |
| argininosuccinate | 1.187 | 0.435 | 1.62 | 1.999 | 5.692696144 | 3 | 0.031886 | 0.036 | 0.8918 | 0.1004 | 0.6213 | 0.9238 | 0.5636 | 0.2639 |
| citrulline | 0.723 | 2.537 | 1.037 | 0.969 | 104.0624733 | 3 | 1.35E-05 | 0 | 0.0094 | 0 | 0 | 0.8313 | 0.0412 | 0 |
| dimethylarginine (ADMA + SDMA) | 1.222 | 0.592 | 0.498 | 2.398 | 74.97294381 | 3 | 2.17E-05 | 0 | 0.0003 | 0 | 0.0011 | 0 | 0 | 0.8654 |
| formiminoglutamate | 1.392 | 0.211 | 1.056 | 0.713 | 129.7042315 | 3 | 5.2E-06 | 0 | 0.0072 | 0.0003 | 0 | 0.0062 | 0 | 0 |
| glutamate | 2.511 | 0.423 | 1.57 | 0.56 | 1099.62188 | 3 | 1.9E-08 | 0 | 0 | 0.0637 | 0 | 0 | 0 | 0 |
| glutamate, gamma-methyl ester | 3.004 | 0.09 | 1.664 | 0.449 | 119.1515411 | 3 | 4.03E-05 | 0 | 0 | 0.19 | 0 | 0 | 0 | 0 |
| glutamine | 1.03 | 0.966 | 1.227 | 0.573 | 55.39800332 | 3 | 6.62E-05 | 0 | 0.0748 | 0.0007 | 0.8093 | 0 | 0.0002 | 0.0159 |
| histidine | 0.634 | 0.998 | 0.988 | 1.94 | 76.60165063 | 3 | 3.5E-05 | 0 | 0.0098 | 0 | 0.0081 | 0 | 0 | 0.9995 |
| histidinol | 0.71 | 0.884 | 0.71 | 1.092 | | 3 | | | 1 | 0.1039 | 0.198 | 0.0026 | 0.0026 | 0.198 |
| homoarginine | 0.921 | 0.026 | 1.133 | 7.738 | 794.8208913 | 3 | 3.8E-07 | 0 | 0.7828 | 0 | 0.0087 | 0 | 0 | 0.0018 |
| homocitrulline | 1.511 | 0.491 | 0.406 | 1.183 | | 3 | | | 0.0014 | 0.0359 | 0.0027 | 0.0181 | 0.4683 | 0.9788 |
| imidazole lactate | 0.433 | 0.101 | 2.879 | 1.661 | 820.517042 | 3 | 2.44E-08 | 0 | 0 | 0 | 0.0004 | 0 | 0 | 0 |
| N-acetylarginine | 0.378 | 0.537 | 1.515 | 5.207 | 419.0289712 | 3 | 8.72E-07 | 0 | 0 | 0 | 0.4957 | 0 | 0 | 0 |
| N-acetylglutamate | 2.205 | 0.728 | 1.091 | 0.325 | 1639.947192 | 3 | 5.63E-09 | 0 | 0 | 0.0006 | 0 | 0 | 0 | 0.0015 |
| N-acetylglutamine | 0.978 | 1.883 | 0.966 | 0.368 | 42.82868623 | 3 | 0.000139 | 0 | 0.9998 | 0 | 0.0001 | 0.0034 | 0.0029 | 0.0001 |
| N-acetylhistidine | 0.22 | 0.124 | 1.903 | 3.94 | 1271.367848 | 3 | 1.05E-08 | 0 | 0 | 0 | 0.3984 | 0 | 0 | 0 |
| N-alpha-acetylornithine | 1.324 | 0.566 | 0.882 | 1.424 | 53.98645549 | 3 | 0.000246 | 0 | 0.0018 | 0 | 0 | 0.0003 | 0.6948 | 0.0195 |
| N-delta-acetylornithine | 1.254 | 0.909 | 2.53 | 0.587 | 13.93397103 | 3 | 0.004124 | 0.005 | 0.002 | 0.6274 | 0.5782 | 0 | 0.1066 | 0.0003 |
| N-methylglutamate | 0.428 | 2.961 | 0.186 | 1.693 | 425.3334514 | 3 | 2E-07 | 0 | 0.0866 | 0 | 0 | 0 | 0 | 0 |
| ornithine | 0.882 | 0.144 | 1.061 | 1.408 | 783.4516363 | 3 | 2.29E-07 | 0 | 0.1341 | 0 | 0 | 0.0029 | 0.0001 | 0 |
| proline | 1.01 | 1.035 | 1.691 | 0.644 | 165.5893488 | 3 | 3.63E-06 | 0 | 0 | 0.0001 | 0.9702 | 0 | 0.0001 | 0 |
| pyroglutamine* | 1.169 | 0.298 | 1.268 | 0.836 | 97.88788846 | 3 | 1.75E-05 | 0 | 0.5939 | 0.0001 | 0 | 0.0006 | 0.005 | 0 |
| succinylglutamine | 0.976 | 0.032 | 1.013 | 0.038 | | 3 | | | 0.9986 | 1 | 0.0102 | 0.0082 | 0.0107 | 0.0078 |
| 5-oxoproline | 1.096 | 0.727 | 1.048 | 0.424 | 128.4663149 | 3 | 5.31E-06 | 0 | 0.9372 | 0.0154 | 0.004 | 0 | 0 | 0.0109 |
| cysteine-glutathione disulfide | 1.047 | 0.455 | 1.384 | 0.957 | 37.75124446 | 3 | 0.000153 | 0 | 0.0153 | 0.0008 | 0.0002 | 0.0028 | 0.7639 | 0 |
| gamma-glutamylalanine | 1.428 | 0.639 | 1.423 | 0.176 | 315.4771792 | 3 | 2.87E-06 | 0 | 0.9999 | 0 | 0 | 0 | 0 | 0 |
| gamma-glutamyl-alpha-lysine | 0.603 | 0.463 | 1.108 | 1.171 | | 3 | | | 0.0092 | 0.0007 | 0.7033 | 0.9598 | 0.0039 | 0.0015 |
| gamma-glutamyl-epsilon-lysine | 0.272 | 3.535 | 0.39 | 1.794 | 102.7220203 | 3 | 5.65E-05 | 0 | 0.9112 | 0 | 0 | 0 | 0 | 0 |
| gamma-glutamylglutamate | 0.94 | 0.706 | 1.216 | 0.883 | | 3 | | | 0.0351 | 0.231 | 0.0818 | 0.0112 | 0.9131 | 0.0004 |
| gamma-glutamylglutamine | 9.549 | 0.82 | 0.732 | 0.491 | | 3 | | | 0 | 0.3929 | 0 | 0.6361 | 0 | 0.9705 |
| gamma-glutamylglycine | 1.267 | 0.16 | 2.405 | 0.715 | 381.2189293 | 3 | 5.68E-07 | 0 | 0 | 0.0001 | 0 | 0 | 0.0001 | 0 |
| gamma-glutamylisoleucine* | 1.338 | 0.27 | 1.589 | 0.68 | 604.3069439 | 3 | 4.44E-08 | 0 | 0.002 | 0 | 0 | 0 | 0 | 0 |
| gamma-glutamylleucine | 1.101 | 0.29 | 2.157 | 0.92 | 268.2120486 | 3 | 1.03E-06 | 0 | 0 | 0 | 0 | 0 | 0.1024 | 0 |
| gamma-glutamylmethionine | 1.881 | 0.188 | 0.772 | 1.278 | 183.1938114 | 3 | 4.03E-06 | 0 | 0 | 0 | 0 | 0.001 | 0.0002 | 0.0003 |
| gamma-glutamylphenylalanine | 0.892 | 0.095 | 1.871 | 1.059 | 352.8673676 | 3 | 2.53E-06 | 0 | 0 | 0 | 0 | 0 | 0.1181 | 0 |
| gamma-glutamylserine | 0.506 | 1.557 | 1.67 | 0.609 | 182.2252555 | 3 | 2.67E-06 | 0 | 0 | 0 | 0 | 0 | 0.7655 | 0.7149 |
| gamma-glutamylthreonine | 1.166 | 0.11 | 2.769 | 0.849 | 442.1313176 | 3 | 3.39E-07 | 0 | 0 | 0 | 0 | 0 | 0.0366 | 0 |
| gamma-glutamyltryptophan | 0.517 | 0.019 | 1.713 | 1.52 | 282.2491696 | 3 | 5.29E-06 | 0 | 0 | 0 | 0.0003 | 0.1448 | 0 | 0 |
| gamma-glutamyltyrosine | 0.851 | 0.122 | 3.068 | 1.124 | 1862.86307 | 3 | 2.73E-08 | 0 | 0 | 0 | 0 | 0 | 0.0013 | 0 |
| gamma-glutamylvaline | 1.235 | 0.082 | 1.574 | 0.742 | 551.435099 | 3 | 6.94E-07 | 0 | 0.0002 | 0 | 0 | 0 | 0 | 0 |
| glutathione, oxidized (GSSG) | 2.193 | 0.027 | 1.776 | 0.32 | 196.5899549 | 3 | 8.71E-06 | 0 | 0.0187 | 0.1138 | 0 | 0 | 0 | 0 |
| glutathione, reduced (GSH) | 1.375 | 0.887 | 1.013 | 0.566 | 23.93416833 | 3 | 0.001322 | 0.002 | 0.0643 | 0.109 | 0.0115 | 0.0199 | 0.0002 | 0.7591 |
| ophthalmate | 1.887 | 0.371 | 0.834 | 1.212 | | 3 | | | 0.1095 | 0.2408 | 0.0164 | 0.8056 | 0.4114 | 0.695 |
| 2-methylserine | 1.02 | 30.138 | 0.907 | 0.475 | 109.3501501 | 3 | 1.04E-05 | 0 | 0.9995 | 0 | 0 | 0.9764 | 0.9544 | 0 |
| allo-threonine | 0.983 | 0.239 | 0.951 | 2.565 | 935.6929542 | 3 | 2.71E-07 | 0 | 0.965 | 0 | 0 | 0 | 0 | 0 |

| | | | | | | | | | | | | | | |
|---|---|---|---|---|---|---|---|---|---|---|---|---|---|---|
| cystine | 0.143 | 1.065 | 0.81 | 3.127 | 148.1226257 | 3 | 2.63E-05 | 0 | 0.002 | 0 | 0.0001 | 0 | 0 | 0.296 |
| glycine | 0.881 | 0.157 | 1.175 | 1.372 | 612.4018767 | 3 | 1.09E-07 | 0 | 0.0001 | 0 | 0 | 0.0023 | 0 | 0 |
| N-acetylglycine | 0.654 | 0.646 | 1.065 | 1.139 | 3.77640227 | 3 | 0.074259 | 0.08 | 0.218 | 0.1149 | 1 | 0.982 | 0.1224 | 0.2057 |
| N-acetylserine | 0.793 | 5.15 | 0.906 | 0.982 | 157.2498709 | 3 | 2.03E-06 | 0 | 0.8679 | 0 | 0 | 0.9539 | 0.5908 | 0 |
| serine | 0.328 | 2.78 | 0.453 | 1.542 | 842.979746 | 3 | 1.42E-07 | 0 | 0.7038 | 0 | 0 | 0 | 0 | 0 |
| sulfate* | 1.253 | 0.674 | 1.089 | 1.083 | 5.946312709 | 3 | 0.027863 | 0.032 | 0.767 | 0.1224 | 0.0217 | 1 | 0.7469 | 0.1153 |
| taurine | 0.418 | 0.418 | 1.519 | 0.475 | | 3 | | | 0 | 0.1258 | 1 | 0 | 0.1258 | 0 |
| adenosine-5'-diphosphoglucose | 1.204 | 0.506 | 0.77 | 0.989 | | 3 | | | 0.0165 | 0.0081 | 0.0004 | 0.3106 | 0.3277 | 0.1808 |
| deoxythymidine diphosphate-l-rhamnose | 1.87 | 0.199 | 1.62 | 0.458 | 335.3685355 | 3 | 3.23E-07 | 0 | 0.0072 | 0.0055 | 0 | 0 | 0 | 0 |
| erythronate* | 1.253 | 0.662 | 1.232 | 0.732 | 46.50294041 | 3 | 0.000121 | 0 | 0.9922 | 0.8063 | 0 | 0.0002 | 0.0001 | 0 |
| N-acetyl-glucosamine 1-phosphate | 2.283 | 0.376 | 1.737 | 0.366 | 130.7233685 | 3 | 8.64E-06 | 0 | 0.0032 | 0.9998 | 0 | 0 | 0 | 0 |
| N-acetylglucosamine/N-acetylgalactosami | 1.687 | 0.941 | 1.073 | 0.712 | 39.04964666 | 3 | 0.000167 | 0 | 0 | 0.0603 | 0 | 0.0035 | 0 | 0.394 |
| N-acetylmuramate | 1.531 | 1.252 | 0.84 | 0.788 | 16.32457257 | 3 | 0.002612 | 0.003 | 0.0002 | 0.0052 | 0.098 | 0.9636 | 0.0001 | 0.0118 |
| ribonate (ribonolactone) | 0.768 | 0.724 | 1.212 | 0.724 | | 3 | | | 0 | 1 | 0.5288 | 0 | 0.5288 | 0 |
| ribulose/xylulose | 1.067 | 0.854 | 0.901 | 1.015 | | 3 | | | 0.1002 | 0.114 | 0.0292 | 0.3371 | 0.8539 | 0.8874 |
| UDP-galactose | 0.651 | 1.094 | 0.956 | 1.54 | 68.22683843 | 3 | 3.52E-05 | 0 | 0.0221 | 0.0015 | 0.0016 | 0.0001 | 0 | 0.4413 |
| UDP-glucose | 0.711 | 1.129 | 0.986 | 1.637 | 63.86576238 | 3 | 3.43E-05 | 0 | 0.0497 | 0.0007 | 0.0034 | 0.0001 | 0 | 0.442 |
| UDP-glucuronate | 1.007 | 0.661 | 0.776 | 1.252 | | 3 | | | 0.0079 | 0 | 0.0003 | 0 | 0.0052 | 0.2364 |
| UDP-N-acetylglucosamine/galactosamine | 0.652 | 0.045 | 1.497 | 1.037 | | 3 | | | 0 | 0 | 0 | 0 | 0 | 0 |
| 3-phosphoglycerate | 1.495 | 0.078 | 1.539 | 0.952 | | 3 | | | 0.9998 | 0.4605 | 0.1192 | 0.743 | 0.784 | 0.1053 |
| dihydroxyacetone phosphate (DHAP) | 0.961 | 0.618 | 1.069 | 1.138 | 22.83260187 | 3 | 0.000974 | 0.001 | 0.2942 | 0 | 0.0004 | 0.6466 | 0.0437 | 0 |
| sedoheptulose-7-phosphate | 1.447 | 0.454 | 1.3 | 0.927 | 33.42376066 | 3 | 0.000646 | 0.001 | 0.7007 | 0.0191 | 0 | 0.0693 | 0.0104 | 0.0002 |
| glucose | 0.932 | 1.247 | 0.909 | 1.674 | 4.498273745 | 3 | 0.053887 | 0.059 | 0.9999 | 0.7359 | 0.8714 | 0.3019 | 0.325 | 0.8475 |
| glucose 6-phosphate | 1.579 | 0.227 | 1.27 | 0.801 | 83.31320191 | 3 | 2.38E-05 | 0 | 0.079 | 0.0015 | 0 | 0.0069 | 0.0001 | 0 |
| lactate | 1.123 | 1.141 | 1.24 | 1.34 | 0.070904123 | 3 | 0.97347 | 0.973 | 0.9951 | 0.9772 | 1 | 0.9969 | 0.9707 | 0.997 |
| phosphoenolpyruvate (PEP) | 1.59 | 0.127 | 1.56 | 1.152 | 54.25302016 | 3 | 0.000293 | 0 | 0.9999 | 0.2719 | 0.0746 | 0.8701 | 0.8448 | 0.0821 |
| pyruvate | 2.024 | 0.29 | 1.354 | 0.736 | 331.8923158 | 3 | 1.8E-07 | 0 | 0 | 0 | 0 | 0 | 0 | 0 |
| glycerate | 0.991 | 0.096 | 1.198 | 0.945 | 338.4494353 | 3 | 2.89E-06 | 0 | 0.0249 | 0 | 0 | 0.0066 | 0.8719 | 0 |
| 3-deoxyoctulosonate | 0.89 | 0.854 | 0.91 | 0.854 | | 3 | | | 0.9736 | 1 | 0.8679 | 0.6451 | 0.8679 | 0.6451 |
| fructose | 1.16 | 0.283 | 1.182 | 0.466 | | 3 | | | 0.9993 | 0.7468 | 0.002 | 0.009 | 0.0112 | 0.0016 |
| gluconate | 0.598 | 0.598 | 0.928 | 0.598 | | 3 | | | 0.0084 | 1 | 1 | 0.0084 | 1 | 0.0084 |
| mannitol/sorbitol | 0.746 | 0.817 | 0.802 | 1.29 | | 3 | | | 0.9989 | 0.6302 | 0.9978 | 0.6088 | 0.5254 | 1 |
| aconitate [cis or trans] | 0.895 | 1.367 | 1.374 | 0.809 | 2.350925926 | 3 | 0.167963 | 0.178 | 0.3514 | 0.2361 | 0.3631 | 0.2276 | 0.9892 | 1 |
| alpha-ketoglutarate | 3.345 | 0.474 | 1.533 | 0.653 | 129.4304622 | 3 | 6.71E-06 | 0 | 0 | 0.4948 | 0 | 0.0001 | 0 | 0 |
| citrate | 0.844 | 0.685 | 1.164 | 1.642 | 16.564459 | 3 | 0.002003 | 0.003 | 0.1213 | 0 | 0.6331 | 0.0151 | 0.0003 | 0.0152 |
| fumarate | 1.058 | 0.238 | 1.188 | 0.939 | 336.5441506 | 3 | 1.57E-07 | 0 | 0.0158 | 0 | 0 | 0.0001 | 0.0261 | 0 |
| malate | 1.034 | 0.226 | 1.157 | 0.993 | 348.779364 | 3 | 1.4E-07 | 0 | 0.0196 | 0 | 0 | 0.0027 | 0.6679 | 0 |
| maleate | 1.35 | 0.221 | 1.279 | 0.954 | 97.84167394 | 3 | 1.95E-05 | 0 | 0.9845 | 0.0174 | 0.0007 | 0.4226 | 0.2651 | 0.0012 |
| succinate | 1.092 | 0.148 | 1.721 | 0.864 | 392.2151589 | 3 | 1.34E-06 | 0 | 0.0002 | 0 | 0 | 0 | 0.144 | 0 |
| threonate | 0.92 | 0.92 | 0.96 | 0.92 | | 3 | | | 0.5146 | 1 | 1 | 0.5146 | 1 | 0.5146 |
| pantothenate (Vitamin B5) | 2.425 | 0.843 | 1.139 | 0.671 | 1145.215907 | 3 | 7.35E-08 | 0 | 0 | 0.0328 | 0 | 0 | 0 | 0.0006 |
| pterin | 1.5 | 0.494 | 1.061 | 0.979 | 40.5894365 | 3 | 0.000149 | 0 | 0.0162 | 0.0084 | 0 | 0.9035 | 0.005 | 0.0026 |
| adenosine 5'-diphosphoribose (ADP-ribo | 2.308 | 0.414 | 0.808 | 0.491 | | 3 | | | 0 | 0.9232 | 0 | 0.0998 | 0 | 0.0345 |
| NAD+ | 1.079 | 0.921 | 0.921 | 0.921 | | 3 | | | 0.2113 | 1 | 0.2113 | 1 | 0.2113 | 1 |
| nicotinamide | 1.278 | 0.171 | 0.906 | 1.085 | 811.7663206 | 3 | 9.26E-08 | 0 | 0 | 0 | 0 | 0.0009 | 0.0005 | 0 |
| nicotinamide ribonucleotide (NMN) | 0.91 | 0.482 | 1.967 | 0.586 | | 3 | | | 0 | 0.8277 | 0.0187 | 0 | 0.0821 | 0 |
| nicotinamide riboside | 2.084 | 0.396 | 0.421 | 1.131 | 181.5686678 | 3 | 9.51E-07 | 0 | 0 | 0 | 0 | 0 | 0 | 0.9848 |
| nicotinate | 0.964 | 0.226 | 1.036 | 2.126 | 1004.76878 | 3 | 5.12E-09 | 0 | 0.1424 | 0 | 0 | 0 | 0 | 0 |
| nicotinate ribonucleoside | 1.847 | 0.177 | 0.142 | 0.142 | | 3 | | | 0 | 0.7254 | 0 | 1 | 0 | 0.7254 |
| nicotinic acid mononucleotide (NaMN) | 3.11 | 2.047 | 0.291 | 0.159 | 188.2277966 | 3 | 2.18E-06 | 0 | 0 | 0 | 0.0001 | 0.8452 | 0 | 0 |
| acetylphosphate | 1.061 | 0.95 | 1.036 | 0.948 | 0.395972815 | 3 | 0.760839 | 0.769 | 0.9968 | 1 | 0.807 | 0.8912 | 0.7973 | 0.8985 |
| methylphosphate | 0.775 | 0.075 | 1.318 | 1.271 | 399.7024902 | 3 | 1.54E-06 | 0 | 0.0001 | 0 | 0 | 0.9263 | 0.0001 | 0 |
| phosphate | 1.051 | 0.541 | 1.016 | 1.048 | 53.00587102 | 3 | 6.26E-05 | 0 | 0.9168 | 0 | 0 | 0.9354 | 0.9999 | 0 |
| FAD | 1.269 | 0.632 | 0.918 | 1.02 | 15.89486624 | 3 | 0.004442 | 0.006 | 0.0017 | 0.0008 | 0 | 0.5078 | 0.0201 | 0.0081 |
| FMN | 0.939 | 0.984 | 1.057 | 0.94 | 0.504826366 | 3 | 0.694088 | 0.71 | 0.8901 | 0.9931 | 0.9925 | 0.8927 | 1 | 0.9703 |
| thiamin monophosphate | 3.261 | 0.401 | 0.996 | 0.462 | | 3 | | | 0 | 0.9778 | 0 | 0.0197 | 0 | 0.0099 |
| pyridoxal phosphate | 1.831 | 0.087 | 1.128 | 0.884 | 180.7722085 | 3 | 9.57E-06 | 0 | 0.0001 | 0 | 0 | 0.1299 | 0 | 0 |
| pyridoxamine | 1.086 | 0.472 | 1.502 | 0.945 | 121.5456822 | 3 | 4.59E-06 | 0 | 0.0001 | 0 | 0 | 0 | 0.1727 | 0 |
| pyridoxamine phosphate | 1.444 | 0.38 | 0.91 | 1.145 | 100.2904419 | 3 | 8.89E-06 | 0 | 0 | 0 | 0 | 0.0149 | 0.0027 | 0 |
| pyridoxate | 1.869 | 0.188 | 2.163 | 0.136 | 387.0281553 | 3 | 1.57E-06 | 0 | 0.0555 | 0.9543 | 0 | 0 | 0 | 0 |
| indole-3-carboxylate | 2.364 | 0.085 | 1.321 | 0.744 | 419.6388396 | 3 | 2.03E-07 | 0 | 0 | 0.0009 | 0 | 0.0028 | 0 | 0 |
| 2-dimethylaminoethanol | 1.154 | 0.744 | 0.453 | 1.077 | 65.13168024 | 3 | 6.2E-05 | 0 | 0 | 0.0082 | 0.0017 | 0 | 0.7905 | 0.0199 |
| choline | 1.043 | 0.807 | 0.966 | 1.308 | 76.27943585 | 3 | 2.88E-05 | 0 | 0.2524 | 0 | 0.0003 | 0 | 0.0001 | 0.008 |
| diethanolamine | 0.634 | 10.442 | 1.991 | 0.604 | 0.964236318 | 3 | 0.469353 | 0.487 | 0.9895 | 0.1732 | 0.1751 | 0.9888 | 1 | 0.2761 |
| phosphocholine | 0.116 | 0.059 | 2.002 | 3.871 | 392.3480512 | 3 | 3.1E-07 | 0 | 0 | 0 | 0.9924 | 0 | 0 | 0 |
| palmitamide (16:0) | 0.771 | 1.195 | 0.891 | 1.054 | 17.44929151 | 3 | 0.001691 | 0.002 | 0.4993 | 0.3637 | 0.0013 | 0.255 | 0.0235 | 0.0148 |
| palmitoleoyl ethanolamide* | 0.673 | 0.478 | 1.032 | 0.934 | 0.90759363 | 3 | 0.488826 | 0.504 | 0.7979 | 0.6608 | 0.9584 | 0.9943 | 0.9082 | 0.5167 |
| palmitoyl ethanolamide | 0.567 | 1.283 | 0.91 | 1.22 | 37.92398964 | 3 | 0.000392 | 0.001 | 0.0072 | 0.8774 | 0 | 0.0146 | 0 | 0.004 |
| myristoyl sulfate | 0.566 | 0.993 | 1.036 | 1.889 | 12.08181386 | 3 | 0.006157 | 0.008 | 0.3578 | 0.0295 | 0.435 | 0.0387 | 0.002 | 0.9986 |
| (14 or 15)-methylpalmitate (a17:0 or i17:0 | 1.028 | 0.366 | 0.954 | 15.321 | 12.98620487 | 3 | 0.004297 | 0.006 | 1 | 0.0001 | 0.9901 | 0.0001 | 0.0002 | 0.993 |
| ethylmalonate | 4.808 | 0.192 | 1.131 | 0.477 | 269.0420271 | 3 | 1.27E-06 | 0 | 0 | 0.242 | 0 | 0.003 | 0 | 0.0001 |
| 2-aminoheptanoate | 2.182 | 0.216 | 1.27 | 0.788 | 147.989989 | 3 | 3.17E-06 | 0 | 0 | 0.0002 | 0 | 0.0009 | 0 | 0 |
| 2-aminooctanoate | 1.767 | 0.248 | 1.216 | 0.818 | 92.21563159 | 3 | 1.75E-05 | 0 | 0.0122 | 0.0097 | 0 | 0.0759 | 0.0001 | 0.0001 |
| N,N,N-trimethyl-5-aminovalerate | 0.939 | 0.734 | 0.757 | 0.661 | | 3 | | | 0.612 | 0.9569 | 0.5203 | 0.9095 | 0.2759 | 0.9985 |
| adipate | 1.181 | 0.271 | 0.941 | 1.04 | 60.39410414 | 3 | 4.39E-05 | 0 | 0.0307 | 0 | 0 | 0.5625 | 0.2713 | 0 |
| azelate (nonanedioate; C9) | 1.394 | 0.277 | 1.128 | 0.901 | 96.53029788 | 3 | 2.85E-05 | 0 | 0.0042 | 0 | 0 | 0.0126 | 0 | 0 |
| dodecanedioate (C12) | 0.729 | 0.664 | 1.051 | 2.172 | 20.84093455 | 3 | 0.001442 | 0.002 | 0.7378 | 0.0021 | 0.9967 | 0.0172 | 0.0029 | 0.619 |
| dodecenedioate (C12:1-DC)* | 2.573 | 0.134 | 1.7 | 0.575 | 35.44052554 | 3 | 0.000568 | 0.001 | 0.0699 | 0.5207 | 0 | 0.0173 | 0.0002 | 0.0016 |
| glutarate (C5-DC) | 1.118 | 0.267 | 0.957 | 1.179 | 106.0791125 | 3 | 7.64E-06 | 0 | 0.4111 | 0 | 0 | 0.1762 | 0.9297 | 0.0001 |
| malonate | 1.048 | 0.521 | 1.032 | 1.135 | 20.13337667 | 3 | 0.001139 | 0.002 | 0.9987 | 0.0004 | 0.0014 | 0.76 | 0.8376 | 0.0017 |
| pimelate (C7-DC) | 1.386 | 0.35 | 1.12 | 0.99 | 41.06170733 | 3 | 0.000132 | 0 | 0.117 | 0.0003 | 0 | 0.6326 | 0.0146 | 0.0001 |
| sebacate (C10-DC) | 1.64 | 0.174 | 1.127 | 0.924 | 133.5381304 | 3 | 6.59E-06 | 0 | 0.0005 | 0 | 0 | 0.1578 | 0 | 0 |
| suberate (C8-DC) | 1.296 | 0.326 | 1.218 | 0.944 | 45.45502061 | 3 | 0.00016 | 0 | 0.743 | 0 | 0 | 0.0164 | 0.0028 | 0 |
| undecanedioate (C11-DC) | 2.123 | 0.216 | 1.283 | 0.822 | 115.1042945 | 3 | 1.12E-05 | 0 | 0.0001 | 0.0014 | 0 | 0.011 | 0 | 0 |
| undecenedioate (C11:1-DC)* | 1.583 | 0.112 | 1.521 | 0.587 | 286.241446 | 3 | 4.43E-07 | 0 | 0.7903 | 0.0001 | 0 | 0 | 0 | 0 |
| 2,3-dihydroxy-2-methylbutyrate | 1.211 | 0.705 | 0.668 | 0.64 | | 3 | | | 0 | 0.7081 | 0 | 0.9666 | 0 | 0.9235 |
| 2-hydroxybutyrate/2-hydroxyisobutyrate | 1.091 | 0.465 | 0.602 | 1.115 | | 3 | | | 0.6193 | 0.3948 | 0.4254 | 0.5841 | 0.9999 | 0.9851 |
| 2-hydroxyglutarate | 1.023 | 0.331 | 1.565 | 0.406 | | 3 | | | 0.0017 | 0.9001 | 0.0002 | 0 | 0.0006 | 0 |
| 2-hydroxyheptanoate* | 1.979 | 0.134 | 1.121 | 0.954 | 188.1129705 | 3 | 2.12E-06 | 0 | 0 | 0 | 0 | 0.4376 | 0 | 0 |
| 2-hydroxymyristate | 0.144 | 0.704 | 0.178 | 2.746 | | 3 | | | 0.9991 | 0 | 0.1718 | 0 | 0 | 0.2109 |
| 2-hydroxyoctanoate | 1.525 | 0.113 | 1.044 | 0.984 | 236.9051617 | 3 | 6.99E-07 | 0 | 0 | 0 | 0 | 0.7715 | 0 | 0 |
| 2-hydroxysebacate | 1.41 | 0.171 | 0.943 | 1.035 | 94.83693821 | 3 | 2.06E-05 | 0 | 0.0011 | 0 | 0 | 0.7397 | 0.0059 | 0 |
| 2R,3R-dihydroxybutyrate | 0.484 | 0.283 | 2.162 | 1.467 | 363.4779759 | 3 | 1.24E-07 | 0 | 0 | 0 | 0.0322 | 0 | 0 | 0 |
| 2S,3R-dihydroxybutyrate | 0.131 | 1.534 | 0.518 | 1.108 | 38.19158843 | 3 | 0.000155 | 0 | 0.0371 | 0.0214 | 0 | 0.0022 | 0 | 0 |
| 3-hydroxybutyrate (BHBA) | 1.69 | 0.426 | 0.528 | 3.009 | 132.1487353 | 3 | 1.31E-05 | 0 | 0 | 0 | 0 | 0 | 0 | 0.842 |
| 3-hydroxydecanoate | 0.687 | 1.622 | 0.827 | 1.053 | 15.04954134 | 3 | 0.003614 | 0.005 | 0.7716 | 0.0093 | 0.0002 | 0.4318 | 0.105 | 0.0007 |
| 3-hydroxydodecanedioate* | 1.478 | 0.424 | 0.995 | 0.992 | 32.35654451 | 3 | 0.000371 | 0.001 | 0.0002 | 0 | 0 | 1 | 0.0002 | 0 |
| 3-hydroxyhexanoate | 0.772 | 3.796 | 0.881 | 0.904 | 9.553250887 | 3 | 0.011121 | 0.013 | 0.991 | 0 | 0 | 0.9999 | 0.9844 | 0 |
| 3-hydroxylaurate | 0.689 | 1.514 | 0.513 | 1.303 | 32.91863045 | 3 | 0.000276 | 0 | 0.5596 | 0.4127 | 0.0002 | 0.0003 | 0.0026 | 0 |
| 3-hydroxymyristate | 0.576 | 1.594 | 0.531 | 4.39 | 67.48132869 | 3 | 0.000104 | 0 | 0.9972 | 0 | 0.0038 | 0 | 0 | 0.0028 |
| 3-hydroxyoctanoate | 0.917 | 1.193 | 0.905 | 0.984 | 1.194583034 | 3 | 0.397619 | 0.414 | 0.9996 | 0.3436 | 0.1506 | 0.91 | 0.9416 | 0.1286 |
| 3-hydroxyoleate* | 0.732 | 1.755 | 0.769 | 4.036 | 6.80112685 | 3 | 0.02261 | 0.026 | 0.9999 | 0.0153 | 0.3975 | 0.0011 | 0.001 | 0.4272 |
| 3-hydroxypalmitate | 0.499 | 1.811 | 0.471 | 6.146 | 15.17701297 | 3 | 0.004331 | 0.006 | 1 | 0.0023 | 0.5006 | 0.0002 | 0.0002 | 0.4836 |
| 8-hydroxyoctanoate | 1.114 | 0.824 | 0.784 | 0.931 | 0.833430272 | 3 | 0.523021 | 0.537 | 0.5056 | 0.9663 | 0.6055 | 0.9191 | 0.8548 | 0.998 |
| alpha-hydroxycaproate | 1.392 | 0.421 | 0.646 | 0.943 | | 3 | | | 0.0015 | 0.0197 | 0.0001 | 0.2427 | 0.0466 | 0.464 |
| (12 or 13)-methylmyristate (a15:0 or i15: | 0.984 | 0.471 | 1.012 | 8.612 | 12.75899451 | 3 | 0.004227 | 0.005 | 1 | 0.0001 | 0.9748 | 0.0002 | 0.0002 | 0.9706 |
| (16 or 17)-methylstearate (a19:0 or i19:0) | 1 | 0.214 | 0.988 | 5.593 | 23.0616606 | 3 | 0.001295 | 0.002 | 1 | 0.0001 | 0.7618 | 0.0005 | 0.0005 | 0.77 |
| 10-undecenoate (11:1n1) | 0.752 | 0.7 | 1.44 | 1.525 | 11.59507551 | 3 | 0.006064 | 0.008 | 0.0064 | 0.0016 | 0.9888 | 0.9545 | 0.0027 | 0.0037 |
| 2-nonenoate (9:1n7) | 1.945 | 0.121 | 1.353 | 0.693 | 227.2141752 | 3 | 1.36E-06 | 0 | 0.0001 | 0.0001 | 0 | 0 | 0 | 0 |
| 5-dodecenoate (12:1n7) | 0.647 | 4.812 | 0.782 | 1.035 | 25.79029448 | 3 | 0.000624 | 0.001 | 0.9833 | 0 | 0 | 0.9039 | 0.732 | 0 |
| arachidate (20:0) | 1.172 | 0.655 | 0.885 | 2.417 | 7.827040278 | 3 | 0.014925 | 0.018 | 0.7372 | 0.0002 | 0.2998 | 0.0007 | 0.0038 | 0.8441 |
| caprate (10:0) | 1.017 | 1.515 | 0.874 | 0.872 | 6.81803015 | 3 | 0.020101 | 0.023 | 0.6288 | 0.0007 | 0.0054 | 1 | 0.6168 | 0.0007 |
| caproate (6:0) | 0.734 | 3.669 | 0.846 | 1.052 | 11.7882902 | 3 | 0.005348 | 0.007 | 0.9896 | 0.0001 | 0 | 0.9407 | 0.8199 | 0 |
| caprylate (8:0) | 0.719 | 1.522 | 0.979 | 0.972 | 10.73838309 | 3 | 0.006404 | 0.008 | 0.1575 | 0.002 | 0.0001 | 0.9999 | 0.173 | 0.0022 |
| eicosenoate (20:1n9 or 1n11) | 1.195 | 0.581 | 0.853 | 2.496 | 5.22261219 | 3 | 0.038327 | 0.042 | 0.8382 | 0.0026 | 0.4692 | 0.0082 | 0.0352 | 0.9086 |
| erucate (22:1n9) | 0.925 | 0.622 | 0.955 | 2.773 | 4.128000369 | 3 | 0.062063 | 0.067 | 0.9999 | 0.0012 | 0.8846 | 0.0044 | 0.0039 | 0.8534 |
| heptanoate (7:0) | 0.93 | 1.14 | 1.35 | 0.846 | 2.000693296 | 3 | 0.218759 | 0.23 | 0.3234 | 0.607 | 0.8073 | 0.1927 | 0.9835 | 0.8069 |
| laurate (12:0) | 0.709 | 1.19 | 0.92 | 1.04 | 4.384479606 | 3 | 0.053939 | 0.059 | 0.3624 | 0.6338 | 0.0101 | 0.7685 | 0.0824 | 0.1846 |
| linoleate (18:2n6) | 1.255 | 0.735 | 0.683 | 2.617 | 7.576956929 | 3 | 0.018774 | 0.022 | 0.4398 | 0.0013 | 0.5168 | 0.001 | 0.0139 | 0.9989 |
| linolenate (18:3n3 or 3n6) | 1.17 | 0.771 | 0.605 | 2.771 | 8.261991475 | 3 | 0.017557 | 0.021 | 0.5003 | 0.0013 | 0.7442 | 0.0007 | 0.0072 | 0.9731 |
| margarate (17:0) | 1.178 | 0.465 | 0.881 | 2.68 | 8.641658479 | 3 | 0.011617 | 0.014 | 0.8903 | 0.0009 | 0.3598 | 0.0047 | 0.0163 | 0.7527 |
| myristate (14:0) | 1.066 | 0.811 | 0.783 | 2.474 | 6.124641258 | 3 | 0.031852 | 0.036 | 0.8127 | 0.0011 | 0.8544 | 0.0009 | 0.004 | 0.9997 |
| myristoleate (14:1n5) | 0.365 | 2.456 | 0.55 | 1.506 | 71.37267888 | 3 | 2.4E-05 | 0 | 0.8158 | 0.0034 | 0 | 0.0033 | 0.0008 | 0 |

| | | | | | | | | | | | | | | |
|---|---|---|---|---|---|---|---|---|---|---|---|---|---|---|
| nonadecanoate (19:0) | 1.08 | 0.459 | 0.893 | 2.26 | 9.223961626 | 3 | 0.009665 | 0.012 | 0.9352 | 0.0005 | 0.2627 | 0.0051 | 0.014 | 0.5468 |
| oleate/vaccenate (18:1) | 1.126 | 0.709 | 0.859 | 1.819 | 5.323163266 | 3 | 0.037452 | 0.041 | 0.65 | 0.0018 | 0.2997 | 0.0054 | 0.0422 | 0.9073 |
| palmitate (16:0) | 1.059 | 0.595 | 0.91 | 2.436 | 9.473923582 | 3 | 0.009066 | 0.011 | 0.9461 | 0.0001 | 0.3645 | 0.0006 | 0.0014 | 0.6637 |
| palmitoleate (16:1n7) | 1.274 | 0.771 | 0.72 | 2.561 | 6.42518743 | 3 | 0.026616 | 0.03 | 0.4845 | 0.0023 | 0.5606 | 0.0018 | 0.0231 | 0.9991 |
| pelargonate (9:0) | 1.16 | 0.463 | 1.15 | 0.972 | 34.99887239 | 3 | 0.000195 | 0 | 0.999 | 0.0001 | 0 | 0.1339 | 0.1066 | 0 |
| pentadecanoate (15:0) | 1.016 | 0.555 | 0.953 | 1.789 | 5.766580154 | 3 | 0.03136 | 0.035 | 0.9989 | 0.0694 | 0.7316 | 0.2859 | 0.3464 | 0.8068 |
| stearate (18:0) | 1.048 | 0.714 | 0.935 | 2.83 | 4.212088191 | 3 | 0.060963 | 0.066 | 0.9946 | 0.0031 | 0.8869 | 0.007 | 0.0107 | 0.963 |
| glycerol | 0.706 | 0.554 | 0.917 | 1.881 | 15.14155194 | 3 | 0.003486 | 0.005 | 0.6436 | 0 | 0.8267 | 0.0007 | 0.0001 | 0.2249 |
| 1-linoleoyl-GPC (18:2) | 2.001 | 0.539 | 0.858 | 1.316 | 22.03736183 | 3 | 0.001034 | 0.002 | 0.0001 | 0.0022 | 0 | 0.0643 | 0.0056 | 0.2531 |
| 1-oleoyl-GPC (18:1) | 1.431 | 0.441 | 1.121 | 0.964 | 18.5397206 | 3 | 0.002488 | 0.003 | 0.0504 | 0.0015 | 0 | 0.4642 | 0.0037 | 0.0001 |
| 1-oleoyl-GPE (18:1) | 1.062 | 0.336 | 0.903 | 0.869 | 7.22870179 | 3 | 0.026457 | 0.03 | 0.9165 | 0.1955 | 0.0547 | 0.9991 | 0.8639 | 0.1587 |
| 1-oleoyl-GPG (18:1)* | 2.249 | 0.135 | 1.233 | 0.824 | 145.7725658 | 3 | 4.61E-06 | 0 | 0.0001 | 0.0039 | 0 | 0.0886 | 0 | 0.0001 |
| 1-palmitoleoyl-GPC* (16:1)* | 1.904 | 0.155 | 0.917 | 1.086 | 574.6835357 | 3 | 4.14E-08 | 0 | 0 | 0 | 0 | 0.093 | 0 | 0 |
| 1-palmitoyl-GPC (16:0) | 2.487 | 0.372 | 1.172 | 0.893 | | 3 | | | 0.621 | 0.9604 | 0.2491 | 0.9935 | 0.4724 | 0.8757 |
| 1-palmitoyl-GPG (16:0)* | 0.957 | 0.446 | 0.545 | 2.622 | | 3 | | | 0.7518 | 0.001 | 0.6143 | 0.0014 | 0.0077 | 0.9949 |
| 1-stearoyl-GPC (18:0) | 0.798 | 0.942 | 1.013 | 0.841 | | 3 | | | 0.4228 | 0.8796 | 0.7186 | 0.6022 | 0.9879 | 0.9519 |
| 1-stearoyl-GPG (18:0) | 0.942 | 0.211 | 0.446 | 2.161 | | 3 | | | 0.4364 | 0.0003 | 0.1533 | 0.0008 | 0.0111 | 0.8795 |
| 2-palmitoleoyl-GPC* (16:1)* | 1.145 | 0.188 | 0.984 | 1.054 | 102.1238065 | 3 | 1.39E-05 | 0 | 0.2442 | 0 | 0 | 0.8194 | 0.6848 | 0 |
| glycerol 3-phosphate | 0.982 | 0.544 | 1.028 | 1.396 | 68.39086499 | 3 | 3.55E-05 | 0 | 0.7154 | 0 | 0 | 0 | 0 | 0 |
| glycerophosphoethanolamine | 1.367 | 0.994 | 1.019 | 0.686 | 79.87705225 | 3 | 6.86E-05 | 0 | 0.0003 | 0.001 | 0.0002 | 0.0005 | 0 | 0.9727 |
| glycerophosphoglycerol | 1.285 | 0.772 | 0.9 | 1.089 | 28.52066147 | 3 | 0.000399 | 0.001 | 0 | 0.0002 | 0 | 0.0121 | 0.0094 | 0.0971 |
| glycerophosphorylcholine (GPC) | 1.035 | 0.931 | 0.848 | 1.092 | 40.81904121 | 3 | 0.000158 | 0 | 0.0002 | 0.0009 | 0.0215 | 0 | 0.2885 | 0.0703 |
| glycerophosphoserine* | 0.249 | 0.249 | 0.249 | 0.962 | | 3 | | | 1 | 0 | 1 | 0 | 0 | 1 |
| 1,2-dioleoyl-GPC (18:1/18:1) | 1.067 | 0.507 | 1.079 | 0.972 | 36.9881338 | 3 | 0.000184 | 0 | 0.9926 | 0 | 0 | 0.1247 | 0.1917 | 0 |
| 1,2-dioleoyl-GPE (18:1/18:1) | 1.534 | 0.405 | 1.892 | 0.638 | 102.0398078 | 3 | 4.36E-05 | 0 | 0.0102 | 0.1058 | 0 | 0 | 0 | 0 |
| 1,2-dioleoyl-GPG (18:1/18:1) | 1.008 | 0.584 | 1.167 | 1.074 | 11.51884799 | 3 | 0.006173 | 0.008 | 0.6979 | 0.0244 | 0.0541 | 0.9173 | 0.9668 | 0.008 |
| 1,2-dipalmitelaidoyl-GPC (tr16:1/tr16:1) | 1.42 | 0.534 | 0.732 | 1.307 | 38.44257145 | 3 | 0.00021 | 0 | 0 | 0 | 0 | 0.0002 | 0.6195 | 0.1934 |
| 1,2-dipalmitoleoyl-GPE (16:1/16:1)* | 0.857 | 0.741 | 1.003 | 1.423 | 2.791529833 | 3 | 0.128963 | 0.137 | 0.8998 | 0.0328 | 0.9463 | 0.2483 | 0.0836 | 0.6195 |
| 1,2-dipalmitoleoyl-GPG (16:1/16:1)* | 0.753 | 0.943 | 0.946 | 1.087 | 0.324123264 | 3 | 0.808602 | 0.815 | 0.915 | 0.9619 | 0.9188 | 0.9643 | 0.6873 | 1 |
| 1,2-dipalmitoyl-GPE (16:0/16:0)* | 2.052 | 0.401 | 0.935 | 1.542 | 25.07916077 | 3 | 0.00093 | 0.001 | 0.0012 | 0.001 | 0 | 0.0668 | 0.141 | 0.1184 |
| 1-palmitoleoyl-2-oleoyl-GPC (16:1/18:1) | 1.29 | 0.294 | 1.119 | 0.879 | 43.84815651 | 3 | 0.0001 | 0 | 0.3207 | 0.0002 | 0 | 0.1038 | 0.0046 | 0 |
| 1-palmitoleoyl-2-oleoyl-GPE (16:1/18:1) | 2.029 | 0.564 | 0.996 | 0.982 | 36.7250719 | 3 | 0.000286 | 0 | 0.0001 | 0.0744 | 0 | 0.9997 | 0.0001 | 0.0634 |
| 1-palmitoyl-2-alpha-linolenoyl-GPC (16: | 1.478 | 0.359 | 0.981 | 0.97 | 41.12446958 | 3 | 0.000175 | 0 | 0.0008 | 0.0001 | 0 | 0.9992 | 0.0006 | 0.0001 |
| 1-palmitoyl-2-linoleoyl-GPC (16:0/18:2) | 0.763 | 1.075 | 0.763 | 0.763 | | 3 | | | 1 | 0.0872 | 0.0872 | 1 | 1 | 0.0872 |
| 1-palmitoyl-2-oleoyl-GPC (16:0/18:1) | 1.131 | 0.695 | 0.879 | 1.393 | 146.4203883 | 3 | 2.99E-06 | 0 | 0.0012 | 0 | 0 | 0 | 0.0009 | 0.0128 |
| 1-palmitoyl-2-oleoyl-GPE (16:0/18:1) | 1.094 | 0.343 | 1.525 | 0.98 | 20.13946761 | 3 | 0.001039 | 0.002 | 0.0389 | 0.0029 | 0.0008 | 0.0092 | 0.8424 | 0 |
| 1-palmitoyl-2-oleoyl-GPG (16:0/18:1) | 1.144 | 0.301 | 0.943 | 2.26 | 153.8357687 | 3 | 1.78E-06 | 0 | 0.1268 | 0 | 0 | 0 | 0 | 0 |
| 1-palmitoyl-2-palmitoleoyl-GPC (16:0/16 | 1.24 | 0.481 | 0.877 | 1.584 | 16.88962421 | 3 | 0.002865 | 0.004 | 0.0766 | 0 | 0.0005 | 0.0009 | 0.0981 | 0.051 |
| 1-stearoyl-2-oleoyl-GPC (18:0/18:1) | 1.008 | 0.8 | 1.007 | 1.76 | 150.5216475 | 3 | 2.1E-05 | 0 | 1 | 0 | 0.0515 | 0 | 0 | 0.0527 |
| palmitoyl sphingomyelin (d18:1/16:0) | 1.198 | 1.026 | 0.842 | 1.033 | 0.395794341 | 3 | 0.760658 | 0.769 | 0.833 | 1 | 0.9759 | 0.9677 | 0.9789 | 0.9713 |
| phytosphingosine | 0.413 | 0.486 | 0.413 | 1.098 | | 3 | | | 1 | 0 | 0.7368 | 0 | 0 | 0.7368 |
| sphinganine | 0.474 | 0.511 | 0.474 | 1.071 | | 3 | | | 1 | 0 | 0.8365 | 0 | 0 | 0.8365 |
| cholesterol | 2.562 | 0.652 | 1.146 | 0.975 | 6.206246113 | 3 | 0.027553 | 0.031 | 0.3973 | 0.9814 | 0.177 | 0.9971 | 0.3063 | 0.9389 |
| 2'-AMP | 1.247 | 0.322 | 1.068 | 0.603 | | 3 | | | 0.6492 | 0.2939 | 0.0003 | 0.0409 | 0.0052 | 0.0017 |
| 2'-deoxyadenosine | 1.082 | 0.427 | 0.937 | 1.025 | 37.0779779 | 3 | 0.000461 | 0.001 | 0.1706 | 0 | 0 | 0.5518 | 0.8152 | 0 |
| 2'-deoxyadenosine 5'-monophosphate | 2.189 | 0.431 | 0.659 | 1.429 | 60.75680739 | 3 | 6.47E-05 | 0 | 0 | 0.0012 | 0 | 0.0085 | 0.0094 | 0.65 |
| 2'-deoxyguanosine | 3.915 | 0.141 | 0.722 | 0.148 | | 3 | | | 0 | 1 | 0 | 0.4064 | 0 | 0.3979 |
| 2'-deoxyguanosine 5'-monophosphate (d | 3.092 | 0.185 | 0.82 | 1.316 | 98.32508854 | 3 | 3.41E-05 | 0 | 0 | 0.0021 | 0 | 0.2055 | 0 | 0.0785 |
| 2'-deoxyinosine | 2.018 | 0.113 | 0.233 | 0.113 | | 3 | | | 0 | 1 | 0 | 0.8902 | 0 | 0.8902 |
| 3'-AMP | 1.919 | 0.306 | 0.845 | 1.121 | 20.85581326 | 3 | 0.001329 | 0.002 | 0.0203 | 0.0871 | 0.001 | 0.808 | 0.095 | 0.3424 |
| 5'- GMP | 1.297 | 0.628 | 0.869 | 1.166 | 31.3521049 | 3 | 0.000306 | 0 | 0.0005 | 0.0001 | 0 | 0.0094 | 0.3506 | 0.0349 |
| 7-methylguanine | 0.842 | 0.762 | 1.254 | 1.036 | | 3 | | | 0.4291 | 0.7287 | 0.9897 | 0.8378 | 0.8797 | 0.2881 |
| adenine | 0.632 | 0.344 | 1.57 | 2.376 | 10.27409007 | 3 | 0.011903 | 0.014 | 0.1506 | 0.0015 | 0.8916 | 0.2468 | 0.005 | 0.046 |
| adenosine | 1.197 | 2.202 | 0.862 | 0.696 | 24.53188132 | 3 | 0.0009 | 0.001 | 0.2139 | 0 | 0.0002 | 0.7347 | 0.039 | 0 |
| adenosine-2',3'-cyclic monophosphate | 2.258 | 0.413 | 1.506 | 0.906 | | 3 | | | 0.6776 | 0.8779 | 0.0691 | 0.8025 | 0.2282 | 0.3904 |
| AMP | 1.415 | 0.473 | 0.917 | 1.054 | 264.9460255 | 3 | 3.85E-07 | 0 | 0 | 0 | 0 | 0.0073 | 0 | 0 |
| guanine | 1.032 | 0.884 | 0.491 | 5.402 | 170.4798083 | 3 | 1.53E-05 | 0 | 0.028 | 0 | 0.8042 | 0 | 0 | 0.13 |
| guanosine | 3.433 | 0.021 | 1.071 | 0.073 | | 3 | | | 0 | 0.9963 | 0 | 0.0067 | 0 | 0.0046 |
| guanosine-2',3'-cyclic monophosphate | 1.921 | 0.452 | 0.982 | 0.641 | | 3 | | | 0.1423 | 0.964 | 0.0148 | 0.8283 | 0.0337 | 0.5661 |
| hypoxanthine | 0.526 | 0.526 | 0.526 | 0.971 | | 3 | | | 1 | 0.0215 | 1 | 0.0215 | 0.0215 | 1 |
| inosine | 3.51 | 0.006 | 1.149 | 0.045 | | 3 | | | 0 | 0.9983 | 0 | 0.0028 | 0 | 0.0021 |
| urate | 3.625 | 0.934 | 2.736 | 0.41 | 2.045783954 | 3 | 0.213199 | 0.225 | 0.9437 | 0.9874 | 0.3762 | 0.4947 | 0.2399 | 0.6829 |
| xanthosine | 1.606 | 1.219 | 1.583 | 0.552 | 8.888218773 | 3 | 0.015886 | 0.019 | 1 | 0.643 | 0.898 | 0.3019 | 0.2847 | 0.9135 |
| 2'-deoxycytidine | 1.095 | 0.404 | 0.8 | 1.35 | 63.41137781 | 3 | 6.78E-05 | 0 | 0.0064 | 0 | 0 | 0 | 0.0172 | 0.0006 |
| 2'-deoxyuridine | 0.912 | 0.912 | 0.912 | 0.998 | | 3 | | | 1 | 0.0235 | 1 | 0.0235 | 0.0235 | 1 |
| 5,6-dihydrouridine | 1.906 | 0.537 | 0.639 | 1.076 | 7.367062579 | 3 | 0.017421 | 0.021 | 0.0034 | 0.2689 | 0.0018 | 0.4347 | 0.0506 | 0.9828 |
| CMP | 0.796 | 1.257 | 0.421 | 2.142 | 118.3076116 | 3 | 2.58E-05 | 0 | 0.0106 | 0 | 0.0023 | 0 | 0 | 0 |
| cytidine | 0.792 | 1.259 | 0.442 | 2.202 | 166.9364795 | 3 | 6.68E-06 | 0 | 0.0076 | 0 | 0.0008 | 0 | 0 | 0 |
| cytidine 2',3'-cyclic monophosphate | 0.909 | 0.173 | 0.91 | 2.232 | 113.3432239 | 3 | 1.31E-05 | 0 | 1 | 0 | 0.0017 | 0 | 0 | 0.0017 |
| cytidine diphosphate | 0.643 | 0.829 | 0.749 | 4.647 | 43.61883841 | 3 | 0.000129 | 0 | 0.9799 | 0 | 0.9042 | 0 | 0 | 0.9908 |
| cytosine | 0.876 | 1.187 | 0.792 | 2.499 | 29.06673704 | 3 | 0.000419 | 0.001 | 0.9299 | 0 | 0.1685 | 0 | 0 | 0.0627 |
| dCMP | 2.467 | 0.214 | 0.656 | 1.296 | 453.0580992 | 3 | 2.25E-07 | 0 | 0 | 0.0002 | 0 | 0.0154 | 0.0001 | 0.1084 |
| dihydroorotate | 0.943 | 0.943 | 0.943 | 0.996 | | 3 | | | 1 | 0.0183 | 1 | 0.0183 | 0.0183 | 1 |
| hydroxymethylpyrimidine | 0.831 | 0.739 | 1.291 | 0.739 | | 3 | | | 0 | 1 | 0.3004 | 0 | 0.3004 | 0 |
| orotate | 0.05 | 0.056 | 0.05 | 2.183 | | 3 | | | 1 | 0 | 1 | 0 | 0 | 1 |
| pseudouridine | 1.035 | 0.553 | 0.748 | 1.335 | | 3 | | | 0.1452 | 0.0002 | 0.0095 | 0.0022 | 0.1203 | 0.4205 |
| thymidine | 0.355 | 0.355 | 0.355 | 1.053 | | 3 | | | 1 | 0 | 1 | 0 | 0 | 1 |
| thymine | 1.197 | 1.04 | 1.14 | 0.899 | 0.454732368 | 3 | 0.72347 | 0.737 | 0.9987 | 0.9811 | 0.974 | 0.9161 | 0.8551 | 0.993 |
| TMP | 1.593 | 0.424 | 0.73 | 1.457 | 233.7071028 | 3 | 1.62E-06 | 0 | 0.0001 | 0 | 0 | 0.0004 | 0.7038 | 0.1219 |
| UMP | 1.133 | 0.505 | 0.879 | 2.046 | 155.2409622 | 3 | 3.62E-06 | 0 | 0.0057 | 0 | 0 | 0 | 0 | 0.0002 |
| uracil | 0.54 | 0.596 | 0.748 | 3.317 | | 3 | | | 0.6199 | 0 | 0.9866 | 0 | 0 | 0.8057 |
| uridine | 1.646 | 0.711 | 0.871 | 1.137 | 20.12592245 | 3 | 0.001336 | 0.002 | 0.0001 | 0.0108 | 0 | 0.1297 | 0.0029 | 0.4967 |
| uridine 3'-monophosphate (3'-UMP) | 1.374 | 0.219 | 0.846 | 1.113 | | 3 | | | 0.0361 | 0.0009 | 0.0001 | 0.4183 | 0.4335 | 0.0131 |
| uridine 5'-diphosphate (UDP) | 0.531 | 0.229 | 1.491 | 4.592 | 77.73268124 | 3 | 0.000115 | 0 | 0.1745 | 0 | 0.897 | 0.0001 | 0 | 0.0554 |
| uridine-2',3'-cyclic monophosphate | 1.165 | 0.348 | 0.821 | 1.415 | 60.0021412 | 3 | 3.73E-05 | 0 | 0.0141 | 0 | 0 | 0.0002 | 0.0799 | 0.0013 |
| alanylleucine | 1.133 | 0.13 | 0.969 | 1.437 | 384.12826 | 3 | 6.91E-07 | 0 | 0.2369 | 0 | 0 | 0.0005 | 0.013 | 0 |
| glycylisoleucine | 0.941 | 0.604 | 1.274 | 0.746 | | 3 | | | 0.0294 | 0.5272 | 0.0283 | 0.0011 | 0.2766 | 0.0001 |
| glycylleucine | 1.059 | 0.253 | 0.964 | 1.359 | 170.7487325 | 3 | 1.97E-06 | 0 | 0.494 | 0 | 0 | 0.0003 | 0.003 | 0 |
| glycylvaline | 0.589 | 0.231 | 1.508 | 1.588 | 135.5618745 | 3 | 8.7E-06 | 0 | 0 | 0 | 0.0105 | 0.8219 | 0 | 0 |
| histidylalanine | 1.155 | 0.803 | 0.817 | 1.023 | | 3 | | | 0.0008 | 0.0197 | 0.0006 | 0.0291 | 0.2083 | 0.9958 |
| isoleucylglycine | 1.438 | 0.063 | 1.174 | 0.785 | | 3 | | | 0.3738 | 0.003 | 0 | 0.1156 | 0.0063 | 0.0001 |
| leucylalanine | 0.931 | 0.144 | 1.116 | 1.063 | 778.1655402 | 3 | 1.34E-07 | 0 | 0.0033 | 0 | 0 | 0.5829 | 0.0315 | 0 |
| leucylglutamine* | 1.668 | 0.129 | 0.973 | 1.068 | 441.9376253 | 3 | 1.23E-06 | 0 | 0.0003 | 0 | 0 | 0.8421 | 0.001 | 0 |
| leucylglycine | 0.902 | 0.107 | 1.122 | 1.12 | 300.2310143 | 3 | 3.06E-06 | 0 | 0.0133 | 0 | 0 | 1 | 0.0143 | 0 |
| lysylleucine | 1.309 | 0.184 | 0.866 | 1.302 | 146.2784626 | 3 | 5.01E-06 | 0 | 0.004 | 0 | 0 | 0.0045 | 0.9999 | 0.0001 |
| phenylalanylalanine | 1.529 | 0.09 | 1.042 | 1.001 | 421.1385077 | 3 | 1.29E-06 | 0 | 0 | 0 | 0 | 0.9108 | 0 | 0 |
| phenylalanylglycine | 1.227 | 0.239 | 1.02 | 1.027 | 221.1087745 | 3 | 3.84E-06 | 0 | 0.0382 | 0 | 0 | 0.9996 | 0.0457 | 0 |
| prolylglycine | 0.877 | 0.179 | 1.101 | 1.034 | 120.8560406 | 3 | 6.94E-06 | 0 | 0.1777 | 0 | 0.0001 | 0.9083 | 0.447 | 0 |
| threonylphenylalanine | 0.732 | 0.096 | 1.273 | 2.118 | 212.4827119 | 3 | 3.47E-06 | 0 | 0.0031 | 0 | 0.0008 | 0.0001 | 0 | 0 |
| tryptophylglycine | 1.145 | 0.129 | 0.986 | 1.105 | 206.2894814 | 3 | 3.22E-06 | 0 | 0.1702 | 0 | 0 | 0.3838 | 0.9395 | 0 |
| tyrosylglycine | 0.889 | 0.63 | 1.281 | 0.95 | | 3 | | | 0.0007 | 0.0037 | 0.016 | 0.0028 | 0.83 | 0 |
| valylglutamine | 1.243 | 0.099 | 0.929 | 1.146 | 348.6318891 | 3 | 1.25E-06 | 0 | 0.0012 | 0 | 0 | 0.0176 | 0.4198 | 0 |
| valylglycine | 0.99 | 0.172 | 0.994 | 1.335 | 187.4013257 | 3 | 5.63E-06 | 0 | 1 | 0 | 0 | 0.0069 | 0.0063 | 0 |
| valylleucine | 1.792 | 0.067 | 0.983 | 1.081 | 271.5437427 | 3 | 5.17E-06 | 0 | 0 | 0 | 0 | 0.8025 | 0.0001 | 0 |
| alanyl-glutamyl-meso-diaminopimelate | 0.743 | 0.743 | 0.996 | 0.79 | | 3 | | | 0.2086 | 0.9782 | 1 | 0.3637 | 0.9782 | 0.2086 |
| glutamyl-meso-diaminopimelate | 2.001 | 0.542 | 0.913 | 2.176 | 6.541594694 | 3 | 0.025802 | 0.03 | 0.2978 | 0.0689 | 0.1133 | 0.1928 | 0.9904 | 0.9196 |
| 4-hydroxybenzoate | 0.654 | 0.192 | 1.453 | 1.053 | | 3 | | | 0 | 0 | 0.0001 | 0.0002 | 0.0002 | 0 |
| benzoate | 1.146 | 0.858 | 1.061 | 1.258 | | 3 | | | 0.9873 | 0.4478 | 0.6934 | 0.8716 | 0.972 | 0.8628 |
| p-toluic acid | 0.862 | 0.888 | 0.944 | 0.809 | 0.080226766 | 3 | 0.968539 | 0.972 | 0.9926 | 0.9936 | 0.9998 | 0.9694 | 0.998 | 0.9976 |
| salicylate | 1.009 | 1.002 | 0.72 | 1.025 | 24.44393618 | 3 | 0.000745 | 0.001 | 0.0122 | 0.9899 | 0.9996 | 0.0086 | 0.997 | 0.0146 |
| syringic acid | 1.305 | 0.213 | 1.043 | 0.923 | | 3 | | | 0.2755 | 0.0012 | 0 | 0.8189 | 0.0691 | 0.0003 |
| 3-hydroxy-3-methylglutarate | 1.134 | 0.657 | 0.844 | 2.05 | | 3 | | | 0.496 | 0.0001 | 0.1337 | 0.0003 | 0.0031 | 0.7869 |
| succinimide | 0.844 | 0.636 | 1.138 | 1.117 | | 3 | | | 0.1354 | 0.0103 | 0.3777 | 0.9981 | 0.1779 | 0.0076 |
| thioproline | 0.007 | 2.148 | 0.007 | 0.017 | | 3 | | | 1 | 0 | 0 | 0.9993 | 0.9993 | 0 |
| PHB | 0.5 | 1.7 | 0.64 | 1.16 | 11.68 | 3 | 0.004 | | 0.934 | 0.138 | 0.006 | 0.007 | 0.105 | 0.161 |

AMERICAN SOCIETY FOR MICROBIOLOGY | Applied and Environmental Microbiology®

ENVIRONMENTAL MICROBIOLOGY

# Transcriptomic and Metabolomic Responses to Carbon and Nitrogen Sources in *Methylomicrobium album* BG8

Scott Sugden,[a] Marina Lazic,[a] Dominic Sauvageau,[b] Lisa Y. Stein[a]

[a]Department of Biological Sciences, University of Alberta, Edmonton, Alberta, Canada
[b]Department of Chemical and Materials Engineering, University of Alberta, Edmonton, Alberta, Canada

ABSTRACT Methanotrophs use methane as their sole carbon and energy source and represent an attractive platform for converting single-carbon feedstocks into value-added compounds. Optimizing these species for biotechnological applications involves choosing an optimal growth substrate based on an understanding of cellular responses to different nutrients. Although many studies of methanotrophs have examined growth rate, yield, and central carbon flux in cultures grown with different carbon and nitrogen sources, few studies have examined more global cellular responses to different media. Here, we evaluated global transcriptomic and metabolomic profiles of *Methylomicrobium album* BG8 when grown with methane or methanol as the carbon source and nitrate or ammonium as the nitrogen source. We identified five key physiological changes during growth on methanol: *M. album* BG8 cultures upregulated transcripts for the Entner-Doudoroff and pentose phosphate pathways for sugar catabolism, produced more ribosomes, remodeled the phospholipid membrane, activated various stress response systems, and upregulated glutathione-dependent formaldehyde detoxification. When using ammonium, *M. album* BG8 upregulated hydroxylamine dehydrogenase (*haoAB*) and overall central metabolic activity, whereas when using nitrate, cultures upregulated genes for nitrate assimilation and conversion. Overall, we identified several nutrient source-specific responses that could provide a valuable basis for future research on the biotechnological optimization of these species.

IMPORTANCE Methanotrophs are gaining increasing interest for their biotechnological potential to convert single-carbon compounds into value-added products such as industrial chemicals, fuels, and bioplastics. Optimizing these species for biotechnological applications requires a detailed understanding of how cellular activity and metabolism vary across different growth substrates. Although each of the two most commonly used carbon sources (methane or methanol) and nitrogen sources (ammonium or nitrate) in methanotroph growth media have well-described advantages and disadvantages in an industrial context, their effects on global cellular activity remain poorly characterized. Here, we comprehensively describe the transcriptomic and metabolomic changes that characterize the growth of an industrially promising methanotroph strain on multiple combinations of carbon and nitrogen sources. Our results represent a more holistic evaluation of cellular activity than previous studies of core metabolic pathways and provide a valuable basis for the future biotechnological optimization of these species.

KEYWORDS methanotroph, methane, methanol, *Methylomicrobium album* BG8, nitrate, ammonium, transcriptome, metabolome

Methanotrophs are a taxonomically diverse group of bacteria capable of using methane ($CH_4$) and other one-carbon molecules as their sole source of energy and carbon (1). All aerobic methanotrophs share the same initial steps of their methane utilization pathway: methane is oxidized to methanol by methane monooxygenase

Citation Sugden S, Lazic M, Sauvageau D, Stein LY. 2021. Transcriptomic and metabolomic responses to carbon and nitrogen sources in *Methylomicrobium album* BG8. Appl Environ Microbiol 87:e00385-21. https://doi.org/10.1128/AEM.00385-21.

Editor Rebecca E. Parales, University of California, Davis



Address correspondence to Lisa Y. Stein, stein1@ualberta.ca.

Received 22 February 2021
Accepted 21 April 2021
Accepted manuscript posted online 23 April 2021
Published 11 June 2021

(MMO), and methanol is then converted to formaldehyde by methanol dehydrogenase (MDH) (1). The metabolic pathways downstream from formaldehyde vary among species and growth conditions: formaldehyde can be incorporated into cell biomass via either the serine cycle in alphaproteobacterial methanotrophs or the ribulose monophosphate (RuMP) cycle in gammaproteobacterial methanotrophs, or else formaldehyde is further oxidized to formate using either the tetrahydromethanopterin pathway or formaldehyde dehydrogenase (2). Formate is then oxidized to $CO_2$ by formate dehydrogenase. In gammaproteobacterial methanotrophs, the RuMP pathway feeds fructose-6-phosphate into the Embden-Meyerhof-Parnas (EMP), Entner-Doudoroff (ED), or pentose phosphate (PP) pathways (2), the last of which can be divided into oxidative (NADPH-generating) and nonoxidative (carbon-rearranging) phases.

Although methane is considered the primary carbon substrate for methanotrophs, many culture-based studies addressing the biotechnological applications of these species have explored the use of alternative growth substrates such as methanol (3–6). In some cases, alternative carbon sources may be desirable because they are cost-efficient, easier to upscale, or the target of bioremediation programs (7). Alternative growth sources may also affect growth rates or increase the yield of value-added compounds, which are the target of ongoing bioindustrial research (4, 8). Methanol has been one of the most widely studied carbon sources aside from methane because it is easier to use in continuous-culture systems (9), can be inexpensively synthesized from $CO_2$ or $CH_4$ (10), and avoids gas-liquid mass transfer issues associated with insoluble gases such as methane (11).

Many alphaproteobacterial methanotrophs exhibit a longer lag phase, lower growth rate, and lower final yield when grown on methanol, but several gammaproteobacterial methanotrophs exhibit robust growth on this substrate (3, 12, 13). Previous studies of gammaproteobacterial growth in methanol have focused largely on growth rate, yield, or flux through central carbon pathways (3, 5, 6, 14–16). For example, both *Methylotuvimicrobium alcaliphilum* 20Z and *Methylomonas* sp. DH-1 were shown to upregulate the EMP pathway during growth on methanol (5, 17), whereas *Methylotuvimicrobium buryatense* 5GB1 favored the ED pathway, which appears to be essential to this species (18), along with an incomplete tricarboxylic acid (TCA) cycle (6). Because most of the electrons required by MMO are provided by the MDH cofactor pyrroloquinoline-quinone (PQQ) (11), growth on methanol has been proposed to free MDH-derived electrons for use in ATP production, although this hypothesis has not been widely tested outside of *M. buryatense* 5GB1 (6). Although these targeted carbon flux studies are valuable, there is limited information on cellular responses and adaptations of methanotrophs to growth on methanol outside of changes in their central carbon pathways.

Nitrogen source is another important consideration for the growth of methanotrophs, as it also has the potential to influence growth rate and other aspects of cellular physiology. Methanotrophs possess a diverse suite of genes for importing and metabolizing nitrogen, and some are capable of nitrification or denitrification activities (19–21). Ammonium may be a more bioenergetically favorable nitrogen source because it can be directly incorporated into cell biomass, but it can also be oxidized by MMO, competitively inhibiting methane oxidation and causing the formation of toxic intermediates like hydroxylamine (22). Because of competitive inhibition by ammonium, nitrate has been used in the typical growth medium for culture-based studies of methanotrophs (3), even though some species grow better on ammonium and are able to detoxify hydroxylamine (3, 22, 23).

Recent studies of methanotrophic growth have begun to identify strain-specific preferences based on different combinations of carbon-nitrogen sources that also affect metabolite pools (3–5, 13, 23). These studies have also shown that the effects of methanol toxicity exceed the effects of nitrogen source for cultures grown on methane. In this study, we used global transcriptomic and metabolomic analyses to holistically evaluate the metabolism and physiology of *M. album* BG8 grown with different

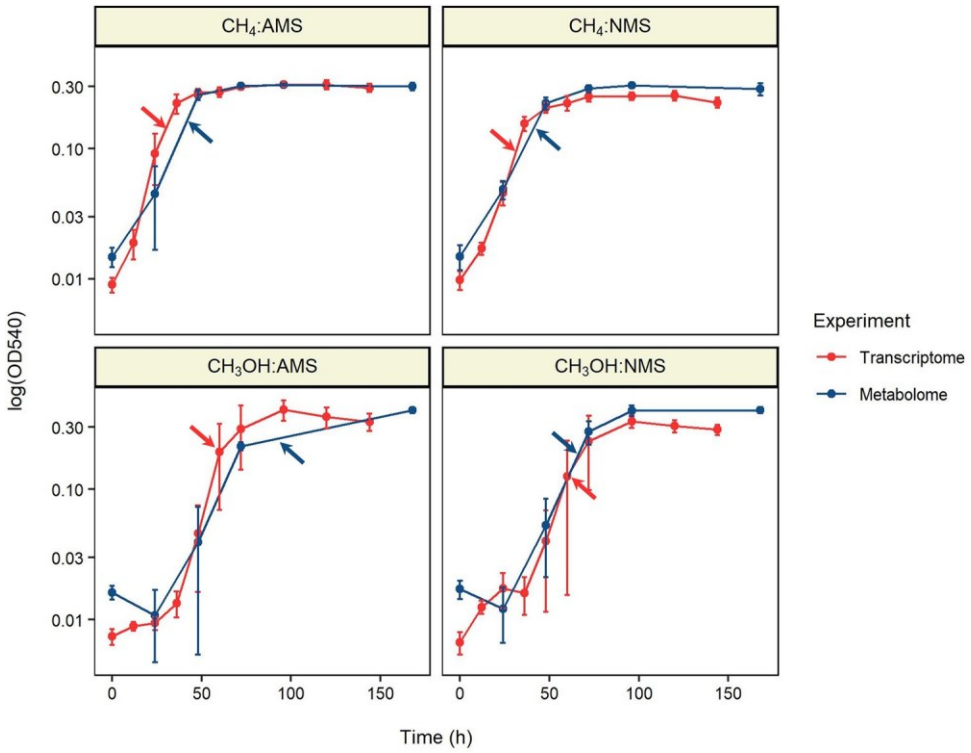


FIG 1 Growth curves for *Methylomicrobium album* BG8 under different medium conditions. Growth was measured as the optical density at 540 nm (OD540) of cultures of *M. album* BG8. Cultures were provided with either methane or methanol as the carbon source and either ammonium (AMS) or nitrate (NMS) as the nitrogen source. Arrows indicate when cultures were harvested for transcriptomic (red) or metabolomic (blue) analysis.

combinations of carbon-nitrogen sources. *M. album* BG8 was recently classified into a separate genus from *M. buryatense* and *M. alcaliphilum* (24), grows to its highest optical density on methanol rather than methane (3), and prefers growth on nitrate rather than ammonium (3, 23). We first evaluated the strategies adopted by *M. album* BG8 to maintain equal growth rates in either methane or methanol, and we assessed whether these strategies differ depending on whether the culture is provided with nitrate or ammonium. To determine if methanol alters nitrogen source preference, we additionally compared the nitrogen source response in methanol to the nitrogen source response in methane. Our results provide quantitative information on how *M. album* BG8 responds to different nutrient environments; this information can be used in genome-scale metabolic models and other biotechnological frameworks designed to optimize cultivation strategies for commercial scale-up and to direct metabolism toward the production of value-added compounds.

## RESULTS

We harvested *M. album* BG8 cultures grown under four different growth conditions derived from the combinations of two carbon sources (methane or methanol) and two nitrogen sources (ammonium or nitrate). All cultures exhibited similar growth rates and yields, regardless of the carbon-nitrogen source combination (Fig. 1). Transcriptome sequencing (RNA-seq) analysis from the cultures yielded 176,337,841 reads across 12 samples (triplicate samples of each carbon-nitrogen combination), representing 3,772 of the 3,794 annotated sequences in the published *M. album* BG8 genome (see Table S1 in the supplemental material). Of these genes, 567 transcripts comprising 7.81% of all reads were not annotated in the Clusters of Orthologous Groups (COG) database, leaving 3,205 meaningfully classified genes that were used for downstream overrepresentation

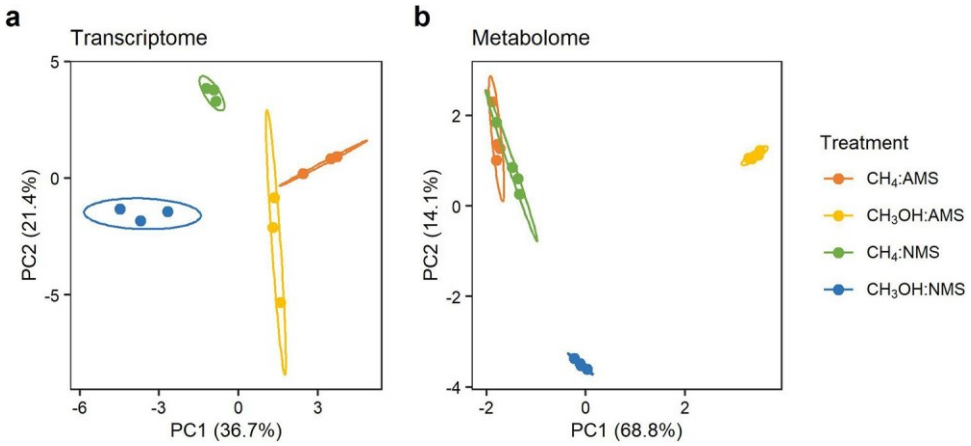


FIG 2 Principal-component analysis. Principal-component analysis was performed on natural log-transformed transcript RPKM (reads per kilobase per million) values (a) and on natural log-transformed median-scaled metabolite abundances (b). Ellipses indicate 95% confidence intervals.

analyses. Genes for particulate methane monooxygenase (*pmoCAB*) were among the most abundant transcripts regardless of carbon or nitrogen source. Metabolome analysis yielded 341 metabolites across 16 samples (quadruplicate samples of each carbon-nitrogen combination) (Table S2). There were no significant differences in transcript detection among treatments, but significantly fewer metabolites were detected in the methanol-ammonium cultures (Fig. S1). Both supervised and unsupervised clustering approaches confirmed that the treatments exhibited distinct transcriptome and metabolome profiles that were largely consistent among biological replicates (Fig. 2; Fig. S2).

Carbon source effects when using nitrate. To determine how *M. album* BG8 maintains equivalent growth in methane and methanol, we first compared transcriptomic and metabolomic responses between methane and methanol when cultures were grown using nitrate. In total, 257 genes were significantly differentially expressed between treatments (Fig. 3a), and the number of up- and downregulated genes was equally distributed between methane ($n$ = 128) and methanol ($n$ = 129). Notably, over 50% of the genes upregulated in methanol had no functional annotation (Table S1). Hypergeometric test-based overrepresentation analysis showed that methanol samples were enriched only for "translation" (J) (Fig. 3b; Table S3), with almost all ribosomal proteins showing moderate to significant upregulation in methanol. The stress response sigma factor *rpoE*, carbon storage regulator *csrA*, and other oxidative stress response genes were also upregulated in methanol (Table S1). Cells grown on methane were enriched for "cell motility" (N), "inorganic ion transport" (P), and "secondary metabolite biosynthesis" (Q) (Fig. 3b; Table S3); representative upregulated genes in these categories included those encoding flagellar proteins, metal transporters, and nonribosomal peptide synthases, respectively (Table S1). Genes involved in oxidative phosphorylation, including those encoding cytochrome *c* oxidase and NADH ubiquinone oxidoreductase, were also consistently more abundant in methane cultures, though not all these differences were significant (Table S1).

Metabolite production was highly favored in methane cultures versus methanol: of the 105 differentially abundant metabolites (DAMs) distinguishing methane-nitrate and methanol-nitrate cultures, 90 DAMs were more abundant in methane (Fig. 3a). These metabolites were distributed relatively equally among amino acids, carbohydrates, and cofactors, although only carbohydrates were significantly overrepresented (Fig. 3c; Table S4). No metabolite superfamilies or subfamilies were significantly overrepresented in methanol cultures (Fig. 3c; Tables S4 and S5); the few metabolites that were significantly more abundant during growth on methanol included select fatty acids, phospholipids, lyso-phospholipids, aromatic amino acids, and branched-chain

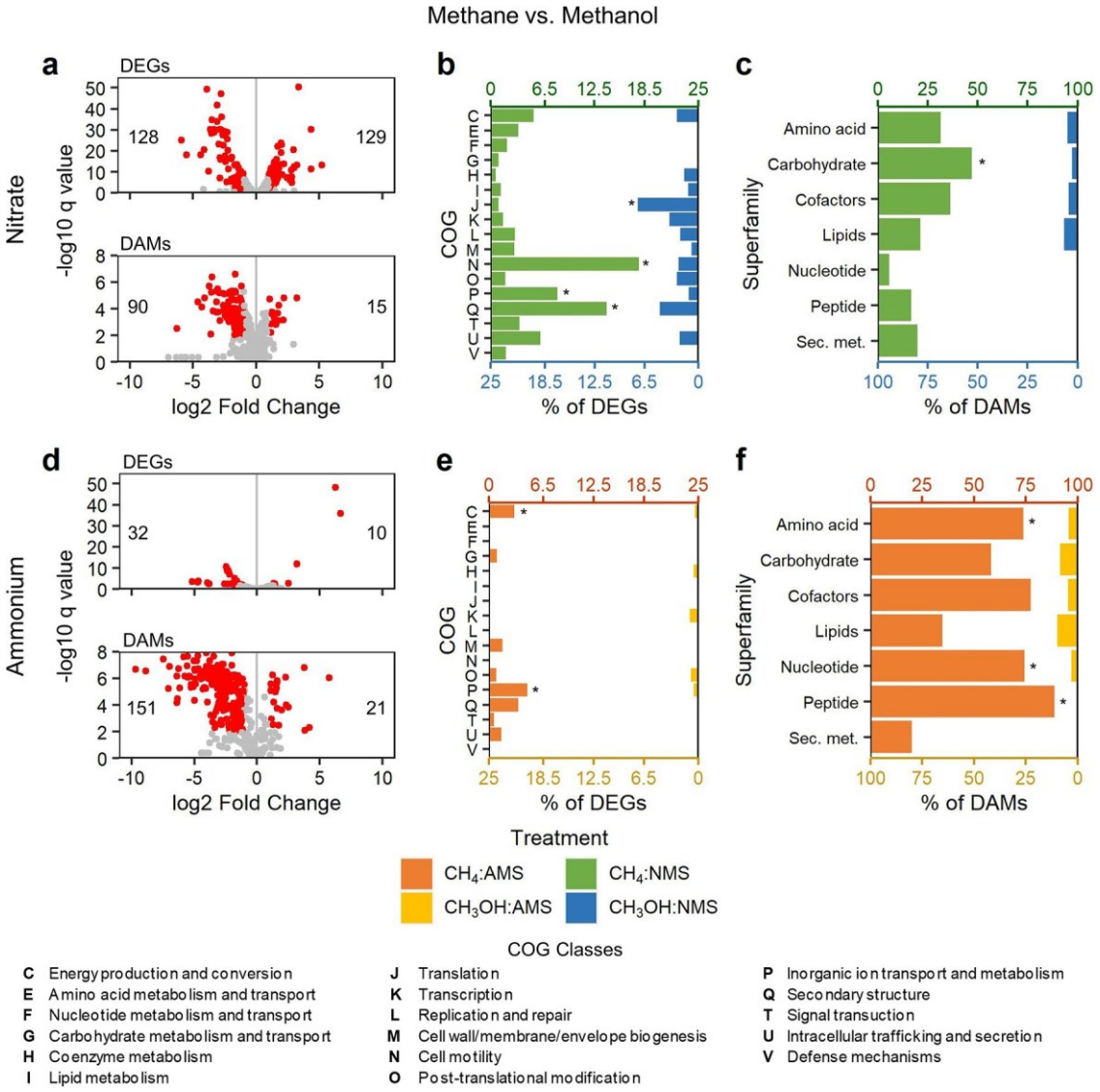


FIG 3 Transcriptomic and metabolomic responses between methane and methanol. Transcriptomic and metabolomic responses to methanol are shown for either nitrate (top panels) or ammonium (bottom panels) as a nitrogen source. (a, d) Volcano plots for differentially expressed genes (DEGs) and differentially abundant metabolites (DAMs) between methane and methanol, using methane as a reference. Numbers indicate the number of DEGs or DAMs that were upregulated (on right) and downregulated (on left) when cultures were grown on methanol rather than methane. (b, e) DEGs were categorized based on the Clusters of Orthologous Groups (COG) database. For each COG, the number of DEGs is expressed as a percentage of the total number of detected genes in that COG. Significantly overrepresented COGs ($P$ , 0.05) are indicated by asterisks. (c, f) DAMs were similarlycategorized according to their superfamily classification and expressed as a percentage of the total number of detected metabolites in that superfamily. Significant overrepresentation ($P$ ¸ 0.05) is indicated by asterisks.

amino acids, as well as histidine and histidinol (Table S2). Several additional phospholipids were more abundant in methanol cultures, but the fold changes between treatments did not meet our significance criterion (Table S2).

The differentially expressed genes (DEGs) and DAMs between methane-nitrate and methanol-nitrate cultures were used for KEGG pathway enrichment analysis to test for differences in general metabolic activity. Significantly affected pathways among the DEGs included flagellar assembly, which was more abundant in methane cultures, and ribosomal biosynthesis, which was more abundant in methanol cultures (Table S5). Among the DAMs, significantly overrepresented KEGG pathways included select amino acid biosynthesis pathways, which were largely implicated by the increased abundances of glutamate, glutamine, pyruvate, and TCA cycle intermediates in methane

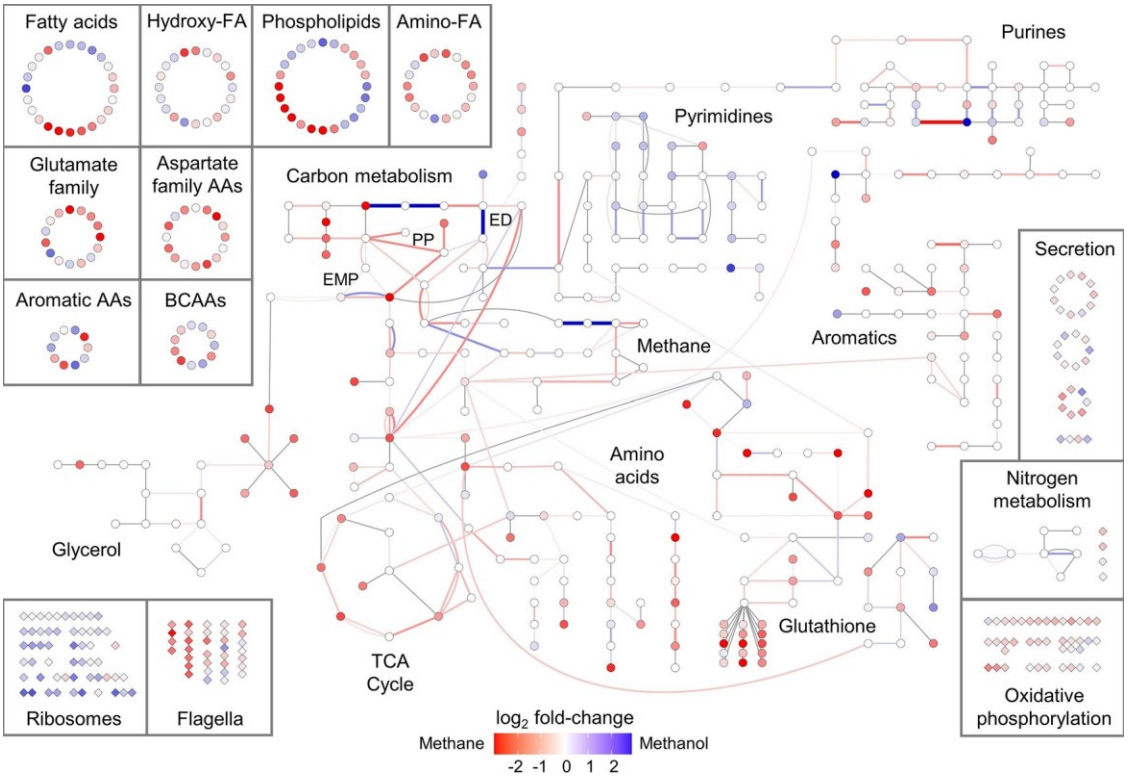


FIG 4 Pathway-level responses to methane and methanol. Central metabolic pathways are presented in the center of the figure. Additional metabolites not involved in central metabolic pathways are shown in the top left, and additional transcripts are shown in the bottom left and right. Transcripts (connections) and metabolites (nodes) are colored based on their $\log_2$-transformed fold change between methane and methanol for cultures grown in nitrate; red and blue indicate upregulation in methane and methanol, respectively. See Fig. S3 in the supplemental material for the same figure reproduced for cultures grown on ammonium. Abbreviations: FA, fatty acids; AAs, amino acids; BCAAs, branched-chain amino acids; ED, Entner-Doudoroff; EMP, Embden-Meyerhof-Parnas; PP, pentose phosphate; TCA, tricarboxylic acid.

cultures (Table S5). However, many of the DAMs, including phospholipids and branched-chain and aromatic amino acids, were not assigned to any KEGG pathways, limiting the utility of this test.

We manually inspected other pathways and noted that genes encoding glucose-6-phosphate 1-dehydrogenase and 6-phosphogluconate dehydrogenase, two key enzymes shared by the ED and oxidative PP pathways, were among the most highly upregulated DEGs in methanol cultures (Fig. 4; Table S1); intermediate metabolites in these pathways were not detected on our metabolomics platform. In contrast, several of the enzymes and metabolites involved in the EMP glycolytic pathway and the TCA cycle were upregulated in methane cultures (Fig. 4; Table S1). Genes encoding glutathione-dependent formaldehyde detoxification to $CO_2$ via S-hydroxymethylglutathione, S-formylglutathione, and formate were also upregulated in methanol cultures (Fig. 4; Table S1), whereas all detected gamma-glutamyl amino acids, which are products of glutathione degradation, were either slightly or significantly more abundant in methane cultures (Table S2). Figure 4 provides an integrated visual representation of the transcriptomic and metabolomic differences between methane-nitrate and methanol-nitrate cultures in the context of their biological pathways and functions.

Carbon source effects when using ammonium. We then tested whether the observed transcriptomic and metabolomic responses to growth on methane versus methanol were consistent when ammonium was substituted for nitrate as the nitrogen source. The broad trends in the transcriptome were largely the same, with methanol-grown cultures showing upregulation of all ribosomal proteins and methane-grown cultures showing upregulation of genes encoding flagellar proteins, oxidative phosphorylation enzymes,

metal transporters, and, to a lesser extent, stress response proteins (Table S1). However, the effect size of many of these differences between treatments was smaller in ammonium: only 42 genes were identified as DEGs based on our criteria for significance, 6-fold fewer than in nitrate (Fig. 3d), and the genes encoding the stress response proteins RpoE, superoxide dismutase, and thioredoxin were not differentially expressed. Oxidative phosphorylation enzymes were an exception to this trend; the genes encoding these enzymes were more highly upregulated in methane than in methanol cultures grown with ammonium, resulting in significant overrepresentation at both the COG (Fig. 3e; Table S3) and KEGG (Table S5) levels. The preferred pathway for sugar catabolism was also less clear in ammonium, as several genes from the EMP and nonoxidative PP pathways were nonsignificantly upregulated in methanol (Table S1 and Fig. S3).

In contrast to the transcriptomic results, the effect size of metabolomic differences was 2-fold larger in ammonium than nitrate (Fig. 3d and f), even when excluding metabolites that were not detected in methanol-ammonium cultures. The broad trends remained similar, however, with the 21 methanol-enriched DAMs encompassing select fatty acids, phospholipids, branched-chain amino acids, and histidinol. One notable difference between carbon source effects in ammonium and nitrate was that sedoheptulose-7-phosphate, a key intermediate of the nonoxidative PP pathway, was significantly more abundant in methanol-ammonium cultures than in methane-ammonium cultures (Table S2). Physiological responses to methane and methanol for cultures grown with ammonium are visually represented in Fig. S3.

Nitrogen source effects. Lastly, we evaluated how *M. album* BG8 responds to nitrate and ammonium and whether these results were consistent during growth on either methane or methanol. In methane cultures, there were 106 DEGs and 25 DAMs between ammonium and nitrate treatments (Fig. 5a). Nitrate-grown cultures were significantly enriched for genes associated with "inorganic ion transport and metabolism" (COG P) (Fig. 5b) and the KEGG pathway "nitrogen metabolism" (Table S5). These genes included primarily ABC transporters involved in acquiring extracellular nitrate as well as the nitrate and nitrite reductase genes responsible for converting nitrate into bioavailable ammonium (Table S1). Glutamine, glutamine synthetase, select sphingolipids and genes for iron transport were also upregulated in nitrate cultures (Tables S1 and S2). In contrast, ammonium-grown cultures were enriched for "energy production and conversion" (COG C) and the KEGG pathway "oxidative phosphorylation" (Fig. 5b; Table S5) and generally exhibited higher levels of transcripts and metabolites associated with basic metabolism, including the TCA cycle and nucleotide biosynthesis (Fig. 6). Transcripts for hydroxylamine dehydrogenase (*haoAB*) and several efflux pumps were also upregulated in ammonium cultures (Table S1).

The nitrogen source response was stronger in methanol cultures, with 2-fold more DEGs ($n = 198$) and 6-fold more DAMs ($n = 147$) than in methane cultures (Fig. 5). Nitrate assimilation and conversion genes were significantly upregulated in nitrate cul- tures, whereas *haoAB* was significantly upregulated in ammonium cultures (Table S1 and Fig. S4), as before. Many other trends became less clear for cells grown on metha-nol, even when considering only the metabolites that were detected in both treat- ments. General transcriptional regulators (COG K) were significantly overrepresented in nitrate cultures, as were dipeptides, whereas drug efflux pumps (COGs P and V) were significantly overrepresented in ammonium cultures (Fig. 5e and f). Basic metabolic activity appeared to be higher in nitrate than in ammonium, with most nucleotides and amino acids accumulating at higher abundances in nitrate-grown cultures (Fig. S4). Central carbon pathways were the only exception to this trend, with ammonium-grown cultures showing general upregulation of the genes and metabolites involved in central carbon metabolism.

## DISCUSSION

An understanding of the growth and physiology of specific methanotroph strains in response to carbon-nitrogen source combinations is important for scaling up their

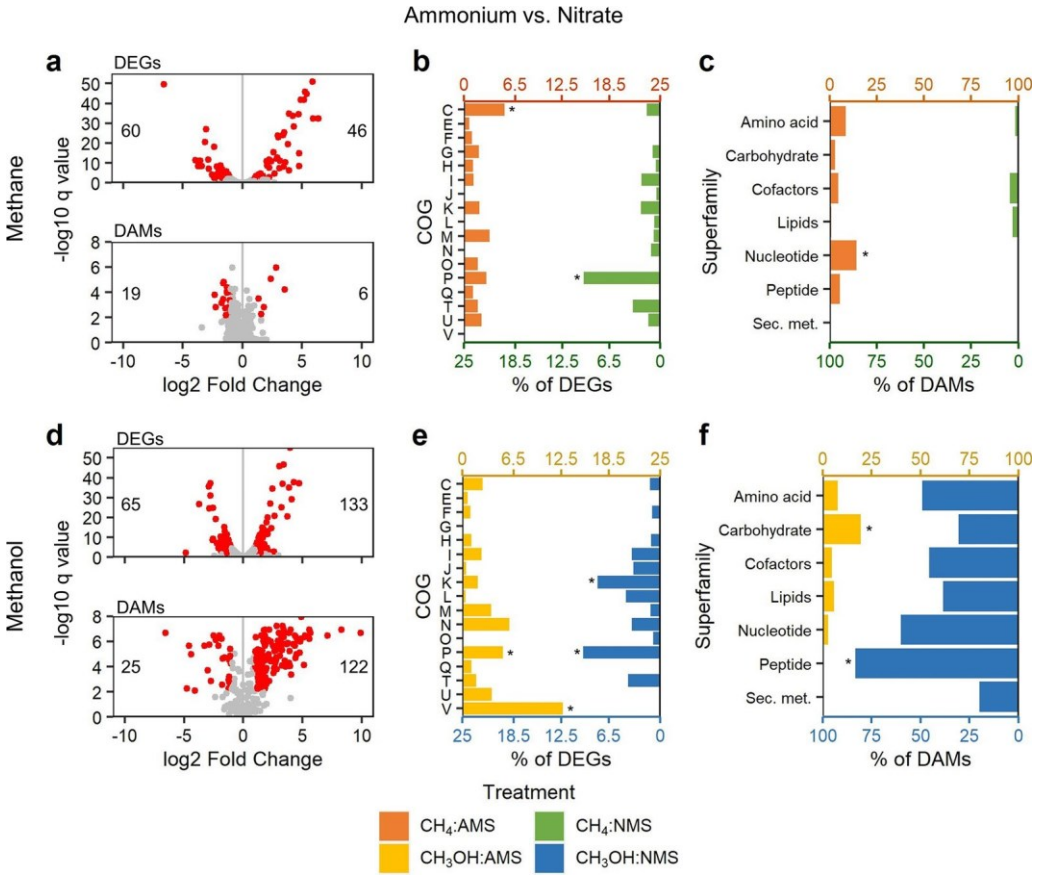


FIG 5 Transcriptomic and metabolomic responses between ammonium and nitrate. Transcriptomic and metabolomic responses to nitrogen source are shown for either methane (top panels) or methanol (bottom panels) as a carbon source. See Fig. 3 and its legend for a complete description of the panels and for the list of COG categories. Fold changes are expressed relative to nitrate, so that numbers in panels a and d indicate the numbers of DEGs or DAMs that were upregulated (on right) and downregulated (on left) when cultures were grown on ammonium rather than nitrate.

growth in an industrial context and parameterizing genome-scale metabolic models for predictive applications. Using a global transcriptomic and metabolomic approach, we evaluated how *M. album* BG8 maintains equivalent growth rates when growing on either methane or methanol and whether its responses to either ammonium or nitrate are consistent between the two carbon sources. Several of the physiological responses we observed could be detected only by using the global multiomics approach used here and have not been described in previous studies of central metabolic pathways in other gammaproteobacterial methanotrophs (5, 6, 12, 15).

Our results implicate five major differences distinguishing growth on methanol from growth on methane, most of which presumably stem from the effects of methanol on redox chemistry and the general cellular stress of growing on an organic solvent. First, methanol-grown *M. album* BG8 appeared to prefer the ED and oxidative PP pathways for sugar catabolism. In *M. buryatense* 5GB1, the ED pathway is essential for cellular growth, although the reasons for its importance remain unclear (18). Increased carbon flux through the ED pathway for *M. buryatense* 5GB1 growing on methanol has been attributed to the lower rate of ATP production from this pathway, as the ATP production power when growing on methanol can instead be provided by MDH-derived electrons that are not needed for methane oxidation (6). Our observation that the NADH oxidoreductases are downregulated in methanol cultures provides further support for this hypothesis; in methanol, MDH-derived electrons can be directly transferred to cytochromes to fuel the electron transport chain (25), reducing the need for the electron-harvesting

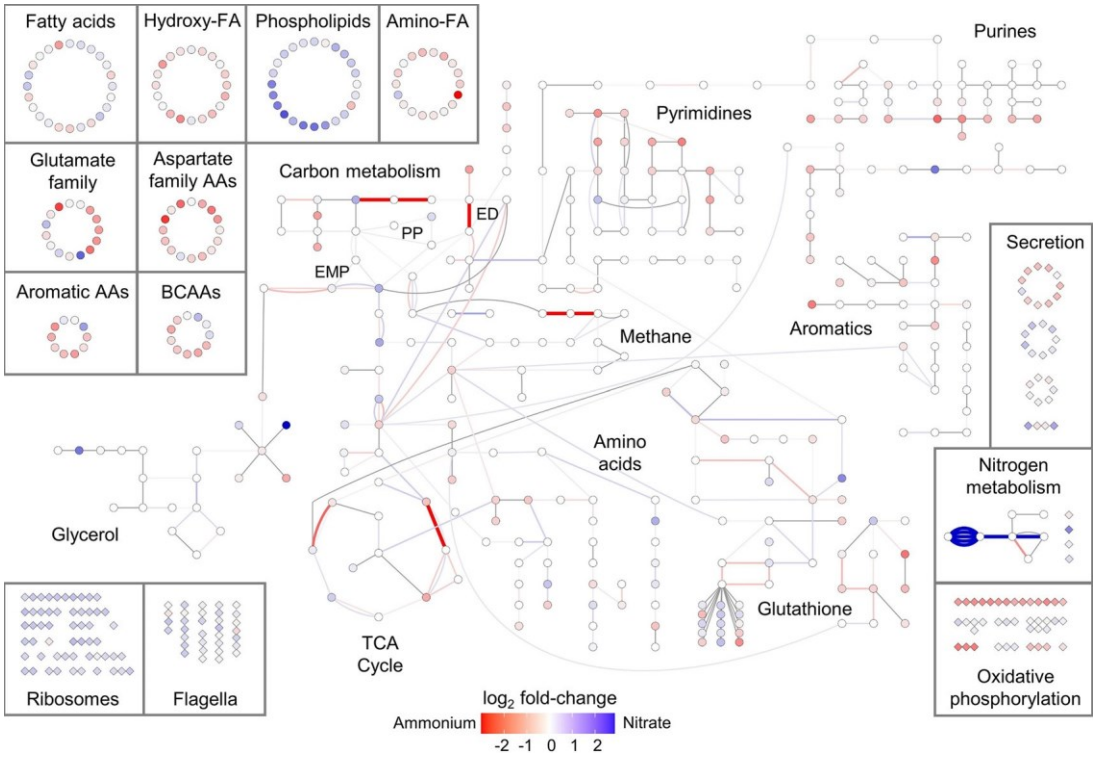


FIG 6 Pathway-level responses to ammonium and nitrate. Central metabolic pathways are presented in the center of the figure. Additional metabolites not involved in central metabolic pathways are shown in the top left, and additional transcripts are shown in the bottom left and right. Transcripts (connections) and metabolites (nodes) are colored based on their $log_2$- transformed fold change between ammonium and nitrate for cultures grown in methane; red and blue indicate upregulationin ammonium and nitrate, respectively. See Fig. S4 in the supplemental material for the same figure reproduced for cultures grown in methanol. Abbreviations: FA, fatty acids; AAs, amino acids; BCAAs, branched-chain amino acids; ED, Entner-Doudoroff; EMP, Embden-Meyerhof-Parnas; PP, pentose phosphate; TCA, tricarboxylic acid.

NADH oxidoreductase complex to power ATP production. There is less evidence for the importance of the PP pathway in methanotrophs, although increased flux through the oxidative PP pathway has been shown to satisfy the higher demand for NADPH production in response to oxidative stress in *M. alcaliphilum* 20Z (26). Other gammaproteobacterial methanotrophs do not show the same preference for the ED or PP pathways when growing on methanol (5, 17), suggesting that some methanol adaptations may be strain specific, but further investigation of sugar catabolism pathway flux using more targeted analysis will be needed to confirm carbon pathway preferences in *M. album* BG8.

Second, we found that growth on methanol induced dramatic and consistent upregulation of translational machinery, including all ribosomal proteins. Bacterial growth is controlled by the rate of protein synthesis, which is in turn dictated by the number of actively translating ribosomes and the translational elongation rate (27). Previous studies have shown that *Escherichia coli* responds to stressors that lower the translation elongation rate, such as reactive oxygen species, by increasing ribosome production, while the opposite is true for stressors that reduce ribosome production (27). Because ribosomes are rate limited (28), the production of additional ribosomes by methanol-grown *M. album* BG8 may therefore be a strategy for maintaining the same growth rate while growing on a toxic substrate. We hypothesize that the longer lag phase described for methanol-grown methanotrophs, which was also observed for *M. album* BG8, may be caused by this requirement for additional ribosomes to be produced when growing on methanol, as cultures cannot begin logarithmic growth until they have produced a sufficient number of ribosomes (28–30).

Third, we observed significant alterations in fatty acid and phospholipid production that may reflect membrane adaptation to growth on methanol, an organic solvent.

Organic solvents are generally toxic to bacteria because they compromise cell membrane integrity (31); however, several species of Gram-negative bacteria are able to thrive in the presence of solvents by altering cell membrane composition (32), upregulating solvent efflux pumps in the outer membrane (33), and increasing the rate of solvent biotransformation (34). We did not find evidence for the latter two mechanisms acting in *M. album* BG8 growing on methanol, but the significant differences in fatty acid and phospholipid abundances that we observed likely indicate some degree of membrane remodeling. Although we expected unsaturated fatty acids to be more abundant in methanol cultures, reflecting the increased membrane fluidity required to uptake methanol from the culture media (35), there were no clear trends in the abundances of saturated or unsaturated lipids. We hypothesize that this is driven by the need to balance methanol assimilation with the need to ensure membrane integrity when exposed to a solvent, although further work will be needed to test this hypothesis. Growth on methanol has also been shown to decrease fatty acid methyl ester abundance in *M. album* BG8 due to the reduced need to synthesize intracytoplasmic membranes for methane oxidation (13). The metabolomics approach used in this study did not allow us to quantify lipid abundances, but our results nonetheless provide evidence for alterations in lipid composition as a mechanism for methanol tolerance.

Fourth, we observed other general responses that indicated that the presence of methanol created a more stressful environment for the cells. Methanol-grown cultures had 2-fold-higher abundances of the envelope stress response sigma factor *rpoE* and the carbon storage regulator *csrA*, which are required for maintaining periplasmic and outer membrane integrity (36) and adjusting central carbon metabolism to stress conditions (37), respectively. We also observed the upregulation of several oxidative stress responses described for *Methylomonas* sp. DH-1 grown on methanol (17), including hopanoid biosynthesis, peroxiredoxin, superoxide dismutase, and thioredoxin, although we did not observe the corresponding changes in the *oxyR* or *soxS* regulons. Select branched-chain and aromatic amino acids which are associated with adaptation to nutrient limitation (4, 38) were also upregulated in methanol cultures. Aside from these few exceptions, most central metabolic pathways were downregulated in the presence of methanol: methanol-grown *M. album* BG8 accumulated fewer carbohydrates, TCA cycle intermediates, and nucleotides and downregulated several of the genes involved in those pathways. These results align with the well-established observation that stress reduces global metabolic activity (39), as energy stores are overwhelmingly directed toward growth, leaving little room for the production of other metabolites or energy-intensive cellular accessories such as flagella (40, 41).

Finally, *M. album* BG8 cultures produced significantly fewer gamma-glutamyl amino acids, 5-oxoproline, and glutamate when grown on methanol, indicating the upregulation of glutathione (GSH)-dependent formaldehyde detoxification in methanol cultures. During this response, GSH is condensed with formaldehyde either spontaneously or via formaldehyde-activated enzyme to yield *S*-hydroxymethylglutathione, which is subsequently converted to formate through a multistep reaction that releases GSH. The regenerated GSH can then be used to detoxify another formaldehyde molecule (42). We noted that several of the genes involved in these reactions were upregulated in methanol cultures. However, in the absence of formaldehyde toxicity, unused GSH can be degraded by gamma-glutamyl transferase, which transfers the gamma-glutamyl group in GSH to an amino acid. In later steps, these gamma-glutamyl acids can be used to produce glutamic acid via 5-oxoproline (43). The methanol-induced upregulation of genes involved in GSH-dependent formaldehyde detoxification and the lower abundance of the byproducts of GSH degradation collectively suggest that *M. album* BG8 cultures grown in methanol upregulate the GSH-dependent formaldehyde detoxification system to overcome formaldehyde toxicity. *M. album* BG8 can also use a partial serine cycle to fuel tetrahydrofolate-based formaldehyde detoxification (3, 42), but no serine cycle metabolites or genes were upregulated in methanol-nitrate relative to methane-nitrate, suggesting that the use of this additional detoxification mechanism is limited.

These five adaptations to methanol (altered carbon flux, ribosomal biogenesis, phospholipid replacement, stress responses, and formaldehyde detoxification) were largely conserved when cultures were grown in ammonium: methanol-grown cultures again exhibited significant upregulation of translation machinery, downregulation of oxidative phosphorylation enzymes, upregulation of formaldehyde detoxification, and decreased general metabolic activity. However, the accumulation of sedoheptulose-7-phosphate and slight upregulation of EMP, nonoxidative PP pathway, and serine cycle genes suggested that carbon flux in methanol-ammonium was different from that in methanol-nitrate and less focused toward the ED pathway. It is possible that this result reflects the fact that methanol-ammonium may be less stressful than methanol-nitrate, as evidenced by the fact that fewer stress response genes were upregulated with methanol-ammonium. More detailed carbon flux analysis is needed to confirm the pathways that process carbon for cells grown on methanol-ammonium. Trends in metabolite production were also less clear when ammonium was the nitrogen source, partially due to the low rate of metabolite detection in methanol-ammonium cultures, but we noted that several phospholipids were still significantly differentially abundant between methane and methanol, again suggesting some degree of membrane remodeling. Methanol-ammonium cultures were harvested slightly later than the other treatments (Fig. 1), which may explain some of this variation in metabolite detection.

We additionally examined whether growth on methanol alters the response to nitrogen source, as competitive inhibition of MMO by ammonium would presumably not play a role when the bacteria are not actively oxidizing methane. Although the magnitude of the nitrogen source response was notably larger in methanol cultures, overall trends were largely consistent with previous studies that indicate a hydroxylamine detoxification response in ammonium (20, 22). In both methane and methanol cultures, growth with nitrate expectedly led to the consistent upregulation of all nitrate assimilation and ammonification genes, which would be required to convert nitrogen into bioavailable ammonium. In contrast, the hydroxylamine dehydrogenase genes *haoAB* were upregulated in ammonium cultures, which would allow *M. album* BG8 to rapidly metabolize the hydroxylamine produced by ammonia oxidation by MMO (22). This ammonia-induced upregulation of *haoAB* was preserved during growth on methanol. Nitrate also led to increased production of lipids, ribosomes, and flagella, whereas ammonium led to the upregulation of oxidative phosphorylation, central carbon pathways, and the TCA cycle. This focus on central metabolic activities in ammonium may explain why ammonium often enriches for gammaproteobacterial methanotrophs (44, 45).

As shown in this study, a global transcriptomic and metabolomic approach provides information on physiological adaptations to nutrient sources that cannot be detected by the use of more focused approaches like $^{13}C$ tracer analysis, which is better for quantifying metabolic flux through specific pathways. It has also been argued that methanotrophs exhibit little in the form of transcriptomic responses and that the proteome or metabolome are therefore a better indicator of substrate-based metabolic responses (6); however, several foci of transcriptional regulation in this study, including ribosome biogenesis, flagellar synthesis, and oxidative phosphorylation enzymes, do not produce detectable metabolites and would not have been identified in a metabolomic study alone. Our results are admittedly limited by the low detection of metabolites in methanol-ammonium cultures and the inability to quantify metabolite abundances in a global metabolomics analysis. Even so, our results implicate several nutrient-based response strategies that have not previously been described for methanotrophs grown with different carbon-nitrogen combinations. These response strategies represent valuable directions for future research on methanotroph physiology and are important considerations in computational models designed for the biotechnological optimization of these species.

## MATERIALS AND METHODS

Culture growth. We used a two-by-two factorial design, with four different growth conditions derived from the combinations of two carbon sources (methane or methanol) and two nitrogen sources (ammonium

or nitrate). Separate cultures of *M. album* BG8 were grown for transcriptomic and metabolomic analyses, and cultures were passaged at least once under experimental conditions before being grown for each experiment. All cultures were grown in 250-ml Wheaton medium bottles filled with 100 ml of medium and closed with butyl-rubber septa caps. Cultures were grown in either ammonium mineral salts (AMS) or nitrate mineral salts (NMS) medium (46) buffered to pH 6.8 using 1.5 ml phosphate buffer.

For cultures grown with methane, 50 ml of gas headspace was removed from the culture bottle and 2.5 mmol of methane was injected through a 0.22-*m*m filter-fitted syringe. For cultures grown on methanol, pure high-performance liquid chromatography (HPLC)-grade methanol was added to the culture medium to final amounts of 2.5 mmol for the transcriptome cultures and 1 mmol for the metabolome cultures. *M. album* BG8 exhibits similar growth rates at both 1 mmol and 2.5 mmol methanol (3) (Fig. 1), so we expected comparable results between the transcriptome and metabolome experiments. Cultures designated for transcriptome analysis were grown in triplicate, and cultures for metabolome analysis were grown in quadruplicate. All cultures were incubated at 30°C with shaking at 150 rpm.

Culture growth was monitored by measuring the optical density of the medium at 540 nm using a 48-well microplate reader (Multiskan Spectrum, Thermo Scientific). Culture purity was assessed via phase-contrast microscopy and plating on Trypticase soy agar (TSA)/nutrient agar, where colony growth would indicate contamination. Cultures were harvested during logarithmic growth after at least three doublings had occurred (Fig. 1), with metabolome cultures harvested slightly later than transcriptome cultures. The delayed metabolite sampling allowed for the effects of transcriptional regulation to be observed at the metabolomic level while still ensuring that all samples were collected during logarithmic growth.

Transcriptome analysis. Total RNA was extracted from harvested cultures using a Masterpure complete DNA and RNA kit (Lucigen Corporation, Middleton, WI). RNA was subsequently purified using a Zymo RNA Clean & Concentrator kit (Zymo Research, Irvine, CA). We assessed the quality and purity of extracted RNA samples using NanoDrop spectrophotometry and an Agilent 2100 bioanalyzer. High-quality RNA was sent to the Centre d'Expertise et de Services at Génome Québec (Montreal, Québec, Canada) for library preparation and sequencing. rRNA was depleted from 250 ng of total RNA using a QIAseq FastSelect kit (Qiagen). RNA was then reverse transcribed using NEBNext RNA first-strand synthe- sis and NEBNext Ultra directional RNA second-strand synthesis modules (New England BioLabs). The remaining steps of library preparation were done using an NEBNExt Ultra II DNA library prep kit for Illumina (New England BioLabs). Sequencing was performed on an Illumina HiSeq 4000 with 100-bp paired-end reads.

Raw paired-end RNA-seq reads were quality filtered using the default filtering parameters in Trimmomatic 0.39 (47). High-quality reads were mapped to the published *M. album* BG8 genome (48) using BowTie2 2.4.1 (49), and the number of reads mapped to each gene was calculated using HTSeq 0.11.1 (50). To facilitate downstream analyses of functional differences among treatments, we mapped each transcript to functional identifiers in the Clusters of Orthologous Groups (COG) and Kyoto Encyclopedia of Genes and Genomes (KEGG) databases using eggNOG (51) and blastKOALA (52), respectively. For downstream analyses requiring normalized count data, we converted raw HTSeq counts to transcripts per million (TPM).

Metabolome analysis. Frozen cell pellets were processed by Metabolon, Inc. (Durham, NC, USA), for global metabolomics analysis using the Metabolon HD4 platform. In brief, metabolites were extracted using methanol with vigorous shaking and then recovered by centrifugation. Methanol was removed using a TurboVap (Zymark). The resulting extracts were stored under nitrogen overnight before being analyzed using the following four independent procedures: (i) reverse-phase ultra-high-performance liquid chromatography-tandem mass spectroscopy (RP/UPLC-MS/MS) with positive-ion-mode electrospray ionization (ESI), chromatographically optimized for hydrophilic compounds; (ii) the same procedure as described in (i) but optimized for hydrophobic compounds; (iii) RP/UPLC-MS/MS with negative-ion-mode ESI; and (iv) hydrophilic interaction chromatography (HILIC)/UPLC-MS/MS with negative-ion-mode ESI. All analysis procedures were performed alongside multiple quality control samples as outlined in Metabolon's standard protocol (Metabolon, Inc., Durham, NC).

Metabolites were identified by comparing the retention time, mass-to-charge ratio, and chromatographic data for each compound to a database of known standards. This process additionally classified metabolites into seven main superfamilies based on their molecular structures (amino acids, carbohydrates, cofactors and electron carriers, lipids, nucleotides, peptides, and secondary metabolites). Metabolite abundances were quantified as area-under-the-curve detector ion counts. If a metabolite was detected in some samples, but not all, missing values were assumed to be lower than the detection threshold for the analysis platform and were therefore imputed as one-half the lowest detected abundance of that metabolite. For downstream analyses requiring normalized data, we divided raw area-under-the-curve values by the median value for each metabolite prior to minimum value imputation.

Statistical analysis. All downstream analyses were performed in R 3.6.2 (53). For both transcriptome and metabolome data, we first tested for broad differences among treatments by performing principal-component analysis (PCA) and sparse partial least-squares discriminant analysis (sPLS-DA). These analyses were performed on natural log-transformed transcripts per million (TPM) values and natural log-transformed median-scaled metabolite abundances using the "rda" function in the R package vegan (54) and the "splsda" function in the package mixOmics (55). We used an analysis of variance (ANOVA) with Tukey's *post hoc* test to evaluate if there were differences in transcript or metabolite detection rates among treatments.

We then evaluated the effects of carbon and nitrogen sources on metabolic activity in *M. album* BG8 by testing for differentially expressed genes (DEGs) and differentially abundant metabolites (DAMs).

DEGs and DAMs were identified for each of the four pairwise comparisons in our two-by-two design. All differential abundance analyses were performed on raw counts or abundances using edgeR (56) for transcriptome data and the Student's *t* test for metabolome data. *P* values were adjusted using the Benjamini-Hochberg (false discovery rate [FDR]) correction, and transcripts or metabolites with a $\log_2$-transformed fold change of ≥1 and an FDR of ≤0.01 were considered significant. Due to the significantly lower metabolite detection rate in methanol-ammonium (see Results and Fig. S1 in the supplemental material), we chose to remove undetected metabolites from all pairwise DAM comparisons that included this treatment, which resolved the large number of interaction effects originally observed in the metabolome data. We additionally confirmed the differential abundance results for this treatment by comparison to results obtained using a separate procedure in which within-sample metabolite abundances were normalized prior to differential abundance testing (see Supplemental Methods).

To determine whether any physiological functions or metabolic pathways were preferentially enriched in the DEGs and DAMs associated with each treatment comparison, we categorized DEGs and DAMs based on COGs and metabolite superfamilies, respectively. We tested for significant overrepresentation of COGs and of metabolite superfamilies and subfamilies using Fisher's exact test, with a significance threshold of an FDR-adjusted *P* of ≤0.05. Overrepresentation analyses were repeated at the pathway level after assignment of transcripts and metabolites to their corresponding pathways in the KEGG pathway database. We used the package clusterProfiler (57) to test for pathway overrepresentation in the transcriptome data and MetaboAnalyst (58) for the metabolome data, with a significance threshold of an FDR-adjusted *P* of ≤0.05. Transcripts and metabolites that did not have a corresponding KEGG identifier were excluded from overrepresentation analyses.

Data availability. Raw transcriptome reads have been deposited in the NCBI database under accession number PRJNA698057. Metabolome data, along with the R code and workspace required to reproduce all analyses, can be found in the GitHub repository at https://github.com/sasugden/BG8_multi_omics.

## SUPPLEMENTAL MATERIAL

Supplemental material is available online only.

SUPPLEMENTAL FILE 1, PDF file, 1.2 MB.

SUPPLEMENTAL FILE 2, XLSX file, 0.8 MB.

## ACKNOWLEDGMENTS

We thank Phillip Sun, Melissa Harrison, and Mariah Hermary for technical assistance with culturing and RNA extraction. Danny Alexander and Metabolon assisted with the analysis and interpretation of the metabolomics data.

We declare no conflicts of interest.

Funding for this study was provided by the Canada First Research Excellence Fund2Future Energy Systems Program (CFREF, FES), the Natural Sciences and Engineering Research Council of Canada (NSERC)2Discovery Program, the Alberta Innovates BioSolutions2Biofuture Program, and the Climate Change Innovation and Technology Framework2Clean Technology Development Program (CCITF, CTD).

Author contributions were as follows: conceptualization, S.S., M.L., D.S., and L.Y.S.; data curation, S.S.; formal analysis, S.S.; funding acquisition, D.S. and L.Y.S.; investigation, S.S. and M.L.; project administration, D.S. and L.Y.S.; resources, D.S. and L.Y.S.; software, S.S.; supervision, L.Y.S.; visualization, S.S.; writing—original draft preparation, S.S.; writing—review and editing, S.S., M.L., D.S., and L.Y.S. All authors have read and agreed to the published version of the manuscript.

## REFERENCES

1. Trotsenko YA, Murrell JC. 2008. Metabolic aspects of aerobic obligate methanotrophy. Adv Appl Microbiol 63:183–229. https://doi.org/10.1016/S0065-2164(07)00005-6.
2. Khmelenina VN, Colin Murrell J, Smith TJ, Trotsenko YA. 2018. Physiology and biochemistry of the aerobic methanotrophs, p 1–25. *In* Rojo F (ed), Aerobic utilization of hydrocarbons, oils and lipids. Springer International Publishing, Cham, Switzerland.
3. Tays C, Guarnieri MT, Sauvageau D, Stein LY. 2018. Combined effects of carbon and nitrogen source to optimize growth of proteobacterial methanotrophs. Front Microbiol 9:2239. https://doi.org/10.3389/fmicb.2018.02239.
4. Lazic M, Sugden S, Sauvageau D, Stein LY. 2021. Metabolome profiles of the alphaproteobacterial methanotroph *Methylocystis* sp. Rockwell in response to carbon and nitrogen source. FEMS Microbiol Lett 368:fnaa219. https://doi.org/10.1093/femsle/fnaa219.
5. Nguyen AD, Park JY, Hwang IY, Hamilton R, Kalyuzhnaya MG, Kim D, Lee EY. 2020. Genome-scale evaluation of core one-carbon metabolism in gammaproteobacterial methanotrophs grown on methane and methanol. Metab Eng 57:1–12. https://doi.org/10.1016/j.ymben.2019.10.004.
6. Fu Y, He L, Reeve J, Beck DAC, Lidstrom ME. 2019. Core metabolism shifts during growth on methanol versus methane in the methanotroph *Methylomicrobium buryatense*. mBio 10:e00406-19. https://doi.org/10.1128/mBio.00406-19.
7. Jiang H, Chen Y, Murrell JC, Jiang P, Zhang C, Xing X-H, Smith TJ. 2011. Methanotrophs: multifunctional bacteria with promising applications in environmental bioengineering, p 249–262. In Moo-Young MB (ed),

Comprehensive biotechnology, 2nd ed. Elsevier, Amsterdam, The Netherlands.
8. Strong PJ, Xie S, Clarke WP. 2015. Methane as a resource: can the methanotrophs add value? Environ Sci Technol 49:4001–4018. https://doi.org/10.1021/es504242n.
9. Belkhelfa S, Roche D, Dubois I, Berger A, Delmas VA, Cattolico L, Perret A, Labadie K, Perdereau AC, Darii E, Pateau E, De Berardinis V, Salanoubat M, Bouzon M, Döring V. 2019. Continuous culture adaptation of *Methylobacterium extorquens* AM1 and TK 0001 to very high methanol concentrations. Front Microbiol 10:1313. https://doi.org/10.3389/fmicb.2019.01313.
10. Schrader J, Schilling M, Holtmann D, Sell D, Filho MV, Marx A, Vorholt JA. 2009. Methanol-based industrial biotechnology: current status and future perspectives of methylotrophic bacteria. Trends Biotechnol 27:107–115. https://doi.org/10.1016/j.tibtech.2008.10.009.
11. Bjorck CE, Dobson PD, Pandhal J. 2018. Biotechnological conversion of methane to methanol: evaluation of progress and potential. AIMS Bioeng 5:1–38. https://doi.org/10.3934/bioeng.2018.1.1.
12. Akberdin IR, Thompson M, Hamilton R, Desai N, Alexander D, Henard CA, Guarnieri MT, Kalyuzhnaya MG. 2018. Methane utilization in *Methylomicrobium alcaliphilum* 20ZR: a systems approach. Sci Rep 8:2512. https://doi.org/10.1038/s41598-018-20574-z.
13. Gilman A, Laurens LM, Puri AW, Chu F, Pienkos PT, Lidstrom ME. 2015. Bioreactor performance parameters for an industrially-promising methanotroph *Methylomicrobium buryatense* 5GB1. Microb Cell Fact 14:182. https://doi.org/10.1186/s12934-015-0372-8.
14. Kalyuzhnaya MG, Yang S, Rozova ON, Smalley NE, Clubb J, Lamb A, Gowda GAN, Raftery D, Fu Y, Bringel F, Vuilleumier S, Beck DAC, Trotsenko YA, Khmelenina VN, Lidstrom ME. 2013. Highly efficient methane biocatalysis revealed in a methanotrophic bacterium. Nat Commun 4:2785. https://doi.org/10.1038/ncomms3785.
15. He L, Fu Y, Lidstrom ME. 2019. Quantifying methane and methanol metabolism of "Methylotuvimicrobium buryatense" 5GB1C under substrate limitation. mSystems 4:e00748-19. https://doi.org/10.1128/mSystems.00748-19.
16. Yang S, Matsen JB, Konopka M, Green-Saxena A, Clubb J, Sadilek M, Orphan VJ, Beck D, Kalyuzhnaya MG. 2013. Global molecular analyses of methane metabolism in methanotrophic alphaproteobacterium, *Methylosinus trichosporium* OB3b. Part II. Metabolomics and 13C-labeling study. Front Microbiol 4:70. https://doi.org/10.3389/fmicb.2013.00070.
17. Nguyen AD, Kim D, Lee EY. 2019. A comparative transcriptome analysis of the novel obligate methanotroph *Methylomonas* sp. DH-1 reveals key differences in transcriptional responses in C1 and secondary metabolite pathways during growth on methane and methanol. BMC Genomics 20:130. https://doi.org/10.1186/s12864-019-5487-6.
18. He L, Groom JD, Lidstrom ME. 2020. The Entner-Doudoroff pathway is an essential metabolic route for *Methylotuvimicrobium buryatense* 5GB1C. Appl Environ Microbiol 87:e02481-20. https://doi.org/10.1128/AEM.02481-20.
19. Stein LY, Klotz MG. 2011. Nitrifying and denitrifying pathways of methanotrophic bacteria. Biochem Soc Trans 39:1826–1831. https://doi.org/10.1042/BST20110712.
20. Nyerges G, Stein LY. 2009. Ammonia cometabolism and product inhibition vary considerably among species of methanotrophic bacteria. FEMS Microbiol Lett 297:131–136. https://doi.org/10.1111/j.1574-6968.2009.01674.x.
21. Kits KD, Klotz MG, Stein LY. 2015. Methane oxidation coupled to nitrate reduction under hypoxia by the Gammaproteobacterium *Methylomonas denitrificans*, sp. nov. type strain FJG1. Environ Microbiol 17:3219–3232. https://doi.org/10.1111/1462-2920.12772.
22. Campbell MA, Nyerges G, Kozlowski JA, Poret-Peterson AT, Stein LY, Klotz MG. 2011. Model of the molecular basis for hydroxylamine oxidation and nitrous oxide production in methanotrophic bacteria. FEMS Microbiol Lett 322:82–89. https://doi.org/10.1111/j.1574-6968.2011.02340.x.
23. Nyerges G, Han SK, Stein LY. 2010. Effects of ammonium and nitrite on growth and competitive fitness of cultivated methanotrophic bacteria. Appl Environ Microbiol 76:5648–5651. https://doi.org/10.1128/AEM.00747-10.
24. Orata FD, Meier-Kolthoff JP, Sauvageau D, Stein LY. 2018. Phylogenomic analysis of the gammaproteobacterial methanotrophs (order *Methylococcales*) calls for the reclassification of members at the genus and species levels. Front Microbiol 9:3162. https://doi.org/10.3389/fmicb.2018.03162.
25. Davidson VL. 2004. Electron transfer in quinoproteins. Arch Biochem Biophys 428:32–40. https://doi.org/10.1016/j.abb.2004.03.022.
26. Bordel S, Pérez R, Rodríguez E, Cantera S, Fernández-González N, Martínez MA, Muñoz R. 2020. Halotolerance mechanisms of the methanotroph *Methylomicrobium alcaliphilum*. Biotechnol Bioeng 117:3459–3474. https://doi.org/10.1002/bit.27506.
27. Zhu M, Dai X. 2020. Bacterial stress defense: the crucial role of ribosome speed. Cell Mol Life Sci 77:853–858. https://doi.org/10.1007/s00018-019-03304-0.
28. Levin BR, McCall IC, Perrot V, Weiss H, Ovesepian A, Baquero F. 2017. A numbers game: ribosome densities, bacterial growth, and antibiotic-mediated stasis and death. mBio 8:e02253-16. https://doi.org/10.1128/mBio.02253-16.
29. Rolfe MD, Rice CJ, Lucchini S, Pin C, Thompson A, Cameron ADS, Alston M, Stringer MF, Betts RP, Baranyi J, Peck MW, Hinton JCD. 2012. Lag phaseis a distinct growth phase that prepares bacteria for exponential growth and involves transient metal accumulation. J Bacteriol 194:686–701. https://doi.org/10.1128/JB.06112-11.
30. Bertrand RL. 2019. Lag phase is a dynamic, organized, adaptive, and evolvable period that prepares bacteria for cell division. J Bacteriol 201:e00697-18. https://doi.org/10.1128/JB.00697-18.
31. Torres S, Pandey A, Castro GR. 2011. Organic solvent adaptation of Gram positive bacteria: applications and biotechnological potentials. Biotechnol Adv 29:442–452. https://doi.org/10.1016/j.biotechadv.2011.04.002.
32. Eberlein C, Baumgarten T, Starke S, Heipieper HJ. 2018. Immediate response mechanisms of Gram-negative solvent-tolerant bacteria to cope with environmental stress: cis-trans isomerization of unsaturated fatty acids and outer membrane vesicle secretion. Appl Microbiol Biotechnol 102:2583–2593. https://doi.org/10.1007/s00253-018-8832-9.
33. Fernandes P, Sommer FB, Sampaio CJ. 2003. Solvent tolerance in bacteria: role of efflux pumps and cross-resistance with antibiotics. Int J Antimicrob Agents 22:211–216. https://doi.org/10.1016/S0924-8579(03)00209-7.
34. Vangnai AS, Sayavedra-Soto LA, Arp DJ. 2002. Roles for the two 1-butanol dehydrogenases of *Pseudomonas butanovora* in butane and 1-butanol metabolism. J Bacteriol 184:4343–4350. https://doi.org/10.1128/jb.184.16.4343-4350.2002.
35. Dyrda G, Boniewska-Bernacka E, Man D, Barchiewicz K, Słota R. 2019. The effect of organic solvents on selected microorganisms and model liposome membrane. Mol Biol Rep 46:3225–3232. https://doi.org/10.1007/s11033-019-04782-y.
36. Egler M, Grosse C, Grass G, Nies DH. 2005. Role of the extracytoplasmic function protein family sigma factor RpoE in metal resistance of *Escherichia coli*. J Bacteriol 187:2297–2307. https://doi.org/10.1128/JB.187.7.2297-2307.2005.
37. Romeo T, Vakulskas CA, Babitzke P. 2013. Post-transcriptional regulation on a global scale: form and function of Csr/Rsm systems. Environ Microbiol 15:313–324. https://doi.org/10.1111/j.1462-2920.2012.02794.x.
38. Kaiser JC, Heinrichs DE. 2018. Branching out: alterations in bacterial physiology and virulence due to branched-chain amino acid deprivation. mBio 9:e01188-18. https://doi.org/10.1128/mBio.01188-18.
39. Shimizu K. 2013. Regulation systems of bacteria such as *Escherichia coli* in response to nutrient limitation and environmental stresses. Metabolites 4:1–35. https://doi.org/10.3390/metabo4010001.
40. Spöring I, Felgner S, Preuße M, Eckweiler D, Rohde M, Häussler S, Weiss S, Erhardt M. 2018. Regulation of flagellum biosynthesis in response to cell envelope stress in *Salmonella enterica* serovar Typhimurium. mBio 9:e00736-17. https://doi.org/10.1128/mBio.00736-17.
41. Maurer LM, Yohannes E, Bondurant SS, Radmacher M, Slonczewski JL. 2005. pH regulates genes for flagellar motility, catabolism, and oxidative stress in *Escherichia coli* K-12. J Bacteriol 187:304–319. https://doi.org/10.1128/JB.187.1.304-319.2005.
42. Chen NH, Djoko KY, Veyrier FJ, McEwan AG. 2016. Formaldehyde stress responses in bacterial pathogens. Front Microbiol 7:257. https://doi.org/10.3389/fmicb.2016.00257.
43. Bachhawat AK, Yadav S. 2018. The glutathione cycle: glutathione metabolism beyond the *g*-glutamyl cycle. IUBMB Life 70:585–592. https://doi.org/10.1002/iub.1756.
44. He D, Zhang L, Dumont MG, He JS, Ren L, Chu H. 2019. The response of methanotrophs to additions of either ammonium, nitrate or urea in alpine swamp meadow soil as revealed by stable isotope probing. FEMS Microbiol Ecol 95:fiz077. https://doi.org/10.1093/femsec/fiz077.
45. Hu A, Lu Y. 2015. The differential effects of ammonium and nitrate on methanotrophs in rice field soil. Soil Biol Biochem 85:31–38. https://doi.org/10.1016/j.soilbio.2015.02.033.

46. Whittenbury R, Phillips K, Wilkinson J. 1970. Enrichment, isolation and some properties of methane-utilizing bacteria. J Gen Microbiol 61:205–218. https://doi.org/10.1099/00221287-61-2-205.
47. Bolger AM, Lohse M, Usadel B. 2014. Trimmomatic: a flexible trimmer for Illumina sequence data. Bioinformatics 30:2114–2120. https://doi.org/10.1093/bioinformatics/btu170.
48. Kits KD, Kalyuzhnaya MG, Klotz MG, Jetten MSM, Op den Camp HJM, Vuilleumier S, Bringel F, DiSpirito AA, Murrell JC, Bruce D, Cheng J-F, Copeland A, Goodwin L, Hauser L, Lajus A, Land ML, Lapidus A, Lucas S, Médigue C, Pitluck S, Woyke T, Zeytun A, Stein LY. 2013. Genome sequence of the obligate gammaproteobacterial methanotroph *Methylomicrobium album* strain BG8. Genome Announc 1:e00170-13. https://doi.org/10.1128/genomeA.00170-13.
49. Langmead B, Salzberg SL. 2012. Fast gapped-read alignment with Bowtie 2. Nat Methods 9:357–360. https://doi.org/10.1038/nmeth.1923.
50. Anders S, Pyl PT, Huber W. 2015. HTSeq: a Python framework to work with high-throughput sequencing data. Bioinformatics 31:166–169. https://doi.org/10.1093/bioinformatics/btu638.
51. Huerta-Cepas J, Szklarczyk D, Heller D, Hernandez-Plaza A, Forslund SK, Cook H, Mende DR, Letunic I, Rattei T, Jensen LJ, Von Mering C, Bork P. 2019. eggNOG 5.0: a hierarchical, functionally and phylogenetically annotated orthology resource based on 5090 organisms and 2502 viruses. Nucleic Acids Res 47:D309–D314. https://doi.org/10.1093/nar/gky1085.
52. Kanehisa M, Sato Y, Morishima K. 2016. BlastKOALA and GhostKOALA: KEGG tools for functional characterization of genome and metagenome sequences. J Mol Biol 428:726–731. https://doi.org/10.1016/j.jmb.2015.11.006.
53. R Core Team. 2019. R: A language and environment for statistical computing. R Foundation for Statistical Computing, Vienna, Austria.
54. Oksanen J, Blanchet FG, Friendly M, Kindt R, Legendre P, McGlinn D, Minchin PR, O'Hara RB, Simpson GL, Solymos P, Stevens MHH, Szoecs E, Wagner H. 2018. vegan: community ecology package. https://cran.r-project.org/web/packages/vegan/index.html.
55. Rohart F, Gautier B, Singh A, Le Cao K-A. 2017. mixOmics: an R package for 'omics feature selection and multiple data integration. PLoS Comput Biol 13:e1005752. https://doi.org/10.1371/journal.pcbi.1005752.
56. McCarthy DJ, Chen Y, Smyth GK. 2012. Differential expression analysis of multifactor RNA-Seq experiments with respect to biological variation. Nucleic Acids Res 40:4288–4297. https://doi.org/10.1093/nar/gks042.
57. Yu G, Wang L-G, Han Y, He Q-Y. 2012. clusterProfiler: an R package for comparing biological themes among gene clusters. Omi A. J Integr Biol 16:284–287. https://doi.org/10.1089/omi.2011.0118.
58. Pang Z, Chong J, Li S, Xia J. 2020. MetaboAnalystR 3.0: toward an optimized workflow for global metabolomics. Metabolites 10:186. https://doi.org/10.3390/metabo10050186.